MODELING AND DESIGN OF RELOAD LWR CORES FOR AN ULTRA-LONG OPERATING CYCLE

by

Michael Vincent McMahon

B.S., Systems Engineering
United States Naval Academy, 1988

M.S., Nuclear Engineering
Massachusetts Institute of Technology, 1990

SUBMITTED TO THE DEPARTMENT OF NUCLEAR ENGINEERING IN PARTIAL FULFILLMENT OF THE REQUIREMENTS FOR THE DEGREE OF

DOCTOR OF PHILOSOPHY IN NUCLEAR ENGINEERING

at the

MASSACHUSETTS INSTITUTE OF TECHNOLOGY

February 1998

Signature of the Author _____
Department of Nuclear Engineering
12 September 1997

Certified by _____
Michael J. Driscoll
Professor of Nuclear Engineering, Emeritus
Thesis Supervisor

Certified by _____
Neil E. Todreas
KEPCO Professor of Nuclear Engineering
Professor of Nuclear Engineering and Mechanical Engineering
Thesis Supervisor

Certified by _____
John E. Meyer
Professor of Nuclear Engineering
Thesis Reader

Accepted by _____
Lawrence M. Lidsky
Chairman, Department Committee on Graduate Students

Modeling and Design of Reload LWR Cores for an Ultra-Long Operating Cycle

by

Michael Vincent McMahon

Submitted to the Department of Nuclear Engineering on September 12, 1997
in Partial Fulfillment of the Requirements for the Degree of
Doctor of Philosophy in Nuclear Engineering

ABSTRACT

The purpose of this research was to use state-of-the-art nuclear and fuel performance design packages to develop extended cycle cores for existing Light Water Reactor (LWR) designs which respect current fuel burnup limits while considering the full range of practical design and economic considerations. The driving force behind this research was the desire to make nuclear power more economically competitive with fossil fuel options by permitting higher plant capacity factors.

In this thesis, reference cores for a 38.8 Effective Full Power Month (EFPM) PWR cycle and a 45 EFPM BWR cycle were developed and evaluated. To achieve these cycle lengths the designs use a single batch reloading strategy and contain fuel with enrichments as high as $7.4^{w}/_{o}$ U^{235} (exceeding the current licensing limit of $5^{w}/_{o}$). The PWR design uses gadolinium oxide (Gd_2O_3) and IFBA (Integral Fuel Burnable Absorbers - a thin fuel pellet surface coating of ZrB_2) as burnable poisons to hold down excess reactivity and to control power peaking. The BWR employs only Gd_2O_3. Both core designs require higher worth control rods in order to meet shutdown safety requirements.

Fuel performance issues were also investigated. The presence of high burnup fuel assemblies in areas of greater-than core-average power leads to fuel performance concerns which must be carefully addressed. The effects of waterside corrosion, increased fission gas pressure, and intensified cladding strain in these assemblies must be carefully quantified. Steady state-analyses of fuel pin internal pressure performed on the PWR design show acceptable fuel pin performance. Fuel performance areas requiring further research were highlighted.

Economic calculations show that extended cycle, single batch loaded cores have a fuel cost that is $13 million to $17 million per year more expensive than an optimized multi-batch strategy. This deficit would have to be made up from the net benefits of a higher capacity factor (e.g., less replacement energy, fewer refueling outages) levelized over plant lifetime.

Thesis Supervisor: Michael J. Driscoll
Title: Professor of Nuclear Engineering, Emeritus

Thesis Supervisor: Neil E. Todreas
Title: KEPCO Professor of Nuclear Engineering
Professor of Nuclear Engineering and Mechanical Engineering

Thesis Reader: John E. Meyer
Title: Professor of Nuclear Engineering

Acknowledgments

I would like to express my sincere gratitude to my thesis advisors, Professor Michael Driscoll and Professor Neil Todreas, for all of the support and guidance that they have given me throughout this endeavor. I have learned so much from both of you, and it has truly been a privilege for me to be able to work with you.

I also greatly appreciate my thesis reader Professor John Meyer for his insight and aide, and for the time he has spent reviewing this work.

This work has benefited immeasurably from the input and hard work of my fellow graduate students in the Extended Cycle Project Core Design Group; Chris Handwerk, Heather MacLean, and Luis Garcia-Delgado. I am grateful for all the help that you have given me.

Many thanks are also due to our industry collaborators for their input into this project. I would especially like to extend a very personal thank you to Ken Walters of Siemens Power Corporation, Dr. Kord Smith, Lorne Covington, and Dr. Tamer Bahadir of STUDSVIK of America, and Kevin St. John, Richard Weader, and Dr. Ed Pilat of the Yankee Atomic Electric Company for their invaluable assistance.

This project has been funded by the INEEL University Research Consortium. The INEEL is managed by Lockheed Martin Idaho Technologies Company for the U.S. Department of Energy, Idaho Operations Office, under Contract No. DE-AC07-94ID13223.

Most of all, I wish to extend a very special thank you to my wife, Janice, for her love, patience, and companionship. This would not have been possible without you.

Finally, I would be remiss if I did not extend an "extra-special" thank you to my daughter, Sarah, for her very earnest and well-intentioned attempts to help me type this on the computer. You are a joy, *niñita*, and you bring much happiness into my life.

Table of Contents

List of Tables

List of Figures

CHAPTER 1

Introduction

Incentives to reduce the cost of electricity by increasing reactor capacity factor have motivated lengthening operating cycles in the United States to 18-24 months. Extending the operating cycle length beyond 24 months offers a further opportunity to improve nuclear plant economic performance by raising capacity factors and by reducing the number of costly refueling operations required during a given period of time. The objective of this project is to establish the feasibility of an ultra-long fuel cycle in currently operating light water reactor (LWR) designs while respecting current fuel burnup limits. This research, sponsored by the INEEL University Research Consortium, examines the currently contemplatable upper limit of 48 months as part of a project of wider scope, which also considers how and whether plants could be operated at power for periods this long [D-1].

The primary focus of this research has been the design and evaluation of an extended cycle core for a currently operating pressurized water reactor (PWR) plant. Following the completion of the work on the PWR core, the design for a neutronically more complex boiling water reactor (BWR) was also developed. Accordingly, this report focuses primarily on the development and evaluation of the PWR extended cycle core design, with the BWR design presented as an extension of the established PWR framework.

1.1 Background

In a scoping study of the 48 month PWR cycle performed by Ayoub and Driscoll, 1995, elementary burnup reactivity models immediately demonstrated that only a single-batch reloading strategy might permit ≥40-month cycles, while respecting current fuel burnup limits [A-1]. Preliminary economic estimates from this study also suggested that a 48-month cycle single-batch loaded core has a steady-state fuel cost that is about 3.0 mills/kWhre (~25 million $/year) more expensive than an optimized multi-batch strategy. This deficit would have to be made up from the net benefits of a higher capacity factor (e.g., less replacement energy, fewer refueling outages) levelized over plant lifetime.

In the Ayoub report, the plausibility of a generic 48 month PWR core design was established using the computer code RPM (**R**eload **P**ower **M**apping). RPM is a 1 1/2 group nodal program that characterizes fuel assemblies by their reactivity, linear slope of reactivity as a function of burnup, and idealized burnable poison reactivity at beginning of cycle (BOC). The purpose of the present research is to use state-of-the-art nuclear and fuel performance design packages to evaluate the feasibility of a 48 calendar month core in existing LWR designs, considering the full range of practical design and economic considerations.

It must be emphasized that this research effort is directed at establishing the feasibility of a core design that can be used in *currently operating* LWRs. Accordingly, the following guidelines constrain and focus the scope of the project:

- The core must be able to be retrofit into current designs
- Fuel burnup must be maintained at or below current licensing limits
- For the PWR, a capacity factor of 87% is targeted, in which case a 48 calendar month core requires ~42 effective full power months (EFPM) of operation. A capacity factor of 87% corresponds to a likely U.S. industry target goal for the year 2000.
- Single batch loading will be used

The desire to retrofit and the selection of a uni-batch reload scheme place severe restraints on the design of the core. The single batch design in particular deprives the fuel manager of much needed flexibility by eliminating the ability to "coddle" highly burned fuel by shuffling high burnup assemblies into areas of low power peaking or to even out fluence gradients by assembly

rotation. However, the single batch reload scheme is essential in order to prevent exceeding current fuel burnup licensing limits.

The importance of single batch loading to the achievement of a feasible extended cycle core design cannot be over-emphasized. The following section contains a more detailed discussion of the single batch reload scheme and its impact on the design of the extended cycle core.

1.2 Single Batch Reload Design

1.2.1 Justification

In a "conventional" PWR core with three-batch fuel loading, incremental extensions of fuel cycle length (from 18 months to 24 months) lead to predictable increases in required fuel enrichment, assembly in-core residence time, and assembly discharge burnup. Three-batch loading allows core designers to drive fuel assemblies to higher discharge exposures, thereby maximizing fuel utilization. The decreased reactivity of highly burned fuel can be compensated for by the addition of fresh fuel at the beginning of each cycle. Additionally, three-batch loading gives fuel managers greater flexibility by enabling them to shuffle highly burned assemblies into areas with high power peaking tendencies. This flexibility aids managers in ensuring that fuel thermal performance criteria are met.

However, for a radical increase in fuel cycle length, conventional three-batch management creates many problems. Three-batch fuel management in a PWR core with a 4 year cycle length produces lead pin discharge exposures well in excess of 100,000 MWD/MTU (clearly violating the current licensing limit of 60,000 MWD/MTU) [A-1]. In addition, the increases in required fuel enrichment (to $>10^{w}/_{o}\ U^{235}$), and assembly in-core residence times create a host of regulatory and fuel performance difficulties. Clearly, a 48 calendar month core design requires an *unconventional* solution.

The extended cycle core designs in this project use a single batch fuel loading scheme. This scheme maintains peak fuel rod discharge burnup within the current licensing limit of 60,000 MWD/MTU and reduces the initial fuel enrichment required with respect to a three-batch core with a similar cycle length from $>10^{w}/_{o}\ U^{235}$ to about $7^{w}/_{o}\ U^{235}$. Furthermore, assembly in-core residence times are actually less than those currently achieved by three-batch cores operating today

(48 months vs. 54 months for an 18 month cycle). Weighing against these advantages, uranium utilization decreases since some fuel is discharged with significantly high fissile content. Therefore, as stated earlier, an economic benefit to the plant can only be achieved if the cost penalty of the extended cycle core can be offset by the gains from improved plant operational availability.

1.2.2 Relationships Between Burnup, Cycle Length, and Enrichment

Using the "linear reactivity model" of LWR core behavior, it is relatively straightforward to establish the following [D-2]:

For a core having n-batch fuel management, (i.e., $1/n^{th}$ of the core refueled per cycle), batch average discharge burnup (B_d) and cycle burnup (B_c) are related by the following good approximation:

$$B_d\left(\frac{MWD}{MTU}\right) \approx n \cdot B_c\left(\frac{MWD}{MTU}\right) \tag{1.1}$$

Cycle burnup can also be expressed in terms of a uniform burnup rate, $\dot{B}$, and the cycle length, T_c: With $\dot{B}$ given in terms of MWD/MTU per Effective Full Power Day [EFPD], and T_c given in EFPD, the following equation can be written:

$$B_c\left(\frac{MWD}{MTU}\right) = \dot{B}\left(\frac{MWD/MTU}{EFPD}\right) \cdot T_c(EFPD) \tag{1.2a}$$

If cycle length is expressed in the more convenient units of calendar months, then this relationship becomes:

$$B_c\left(\frac{MWD}{MTU}\right) = \dot{B}\left(\frac{MWD/MTU}{month}\right) \cdot T_c(months) \tag{1.2b}$$

For a given LWR, the burnup rate is calculated from the core specific power, Q_{sp} (kW_{th}/kgU or MWD/MTU per EFPD). With the cycle length given in units of EFPD, the relationship between burnup rate and core specific power is simply:

$$\dot{B}\left(\frac{MWD/MTU}{EFPD}\right) = Q_{sp}\left(\frac{MWD/MTU}{EFPD}\right) \tag{1.3a}$$

However, for a cycle length given in calendar months, calculation of the burnup rate requires a knowledge of the plant capacity factor, L. Defining the plant capacity factor for a given period as the ratio of EFPD to calendar days, the burnup rate in MWD/MTU per calendar month becomes:

$$\dot{B}\left(\frac{MWD/MTU}{month}\right) = Q_{sp}\left(\frac{MWD/MTU}{EFPD}\right)L\left(\frac{EFPD}{day}\right)\left(\frac{30.44\text{days}}{1\text{month}}\right) \tag{1.3b}$$

Note that a "month" is defined as 1/12 of a year, or 30.44 days. Consequently, using equations (1.1), (1.2b), and (1.3b), the batch average discharge burnup for a cycle length given in units of calendar months is

$$B_d\left(\frac{MWD}{MTU}\right) = n \cdot Q_{sp}\left(\frac{MWD/MTU}{EFPD}\right)L\left(\frac{EFPD}{day}\right)\left(\frac{30.44\text{days}}{1\text{month}}\right) \cdot T_c(months) \tag{1.4a}$$

which for the highly rated PWR in this study (Q_{sp} = 38.7 kW_{th}/kgU = 38.7 MWD/MTU per EFPD) operating at the target capacity factor of L = 87% yields:

$$B_d\left(\frac{MWD}{MTU}\right) = n \cdot 1025\left(\frac{MWD/MTU}{month}\right) \cdot T_c(months) \tag{1.4b}$$

Additionally, in the range of practical interest, an approximate linear fit of plant enrichment and discharge burnup data is given by the following equation[1]:

$$B_d\left(\frac{MWD}{MTU}\right) \approx \left[7392 \cdot \left(\frac{2 \cdot n}{n+1}\right) \cdot (X_p(\%) + 0.1072)\right]\left(\frac{MWD}{MTU}\right) \tag{1.5}$$

where X_p is the weight percent enrichment of nuclear fuel.

The Burnup-Cycle Length Map of Figure 1 is based on equation (1.4b). We also desire to explicitly show enrichments on Figure 1. Therefore we seek an expression for B_d as a function of X_p and T_c. This can be obtained by multiplying both sides of equation (1.5) by $(n + 1)$ and substituting the expression for B_d from equation (1.4b) as follows:

$$B_d\left(\frac{MWD}{MTU}\right)(n+1) \approx [14{,}784 \cdot n \cdot (X_p(\%) + 0.1072)]\left(\frac{MWD}{MTU}\right)$$

$$B_d\left(\frac{MWD}{MTU}\right)n \approx [14{,}784 \cdot n \cdot (X_p(\%) + 0.1072)]\left(\frac{MWD}{MTU}\right) - B_d\left(\frac{MWD}{MTU}\right)$$

1. A more accurate quadratic fit is introduced later in Chapter 8, "Economic Aspects of Ultra-Long Operating Cycles"

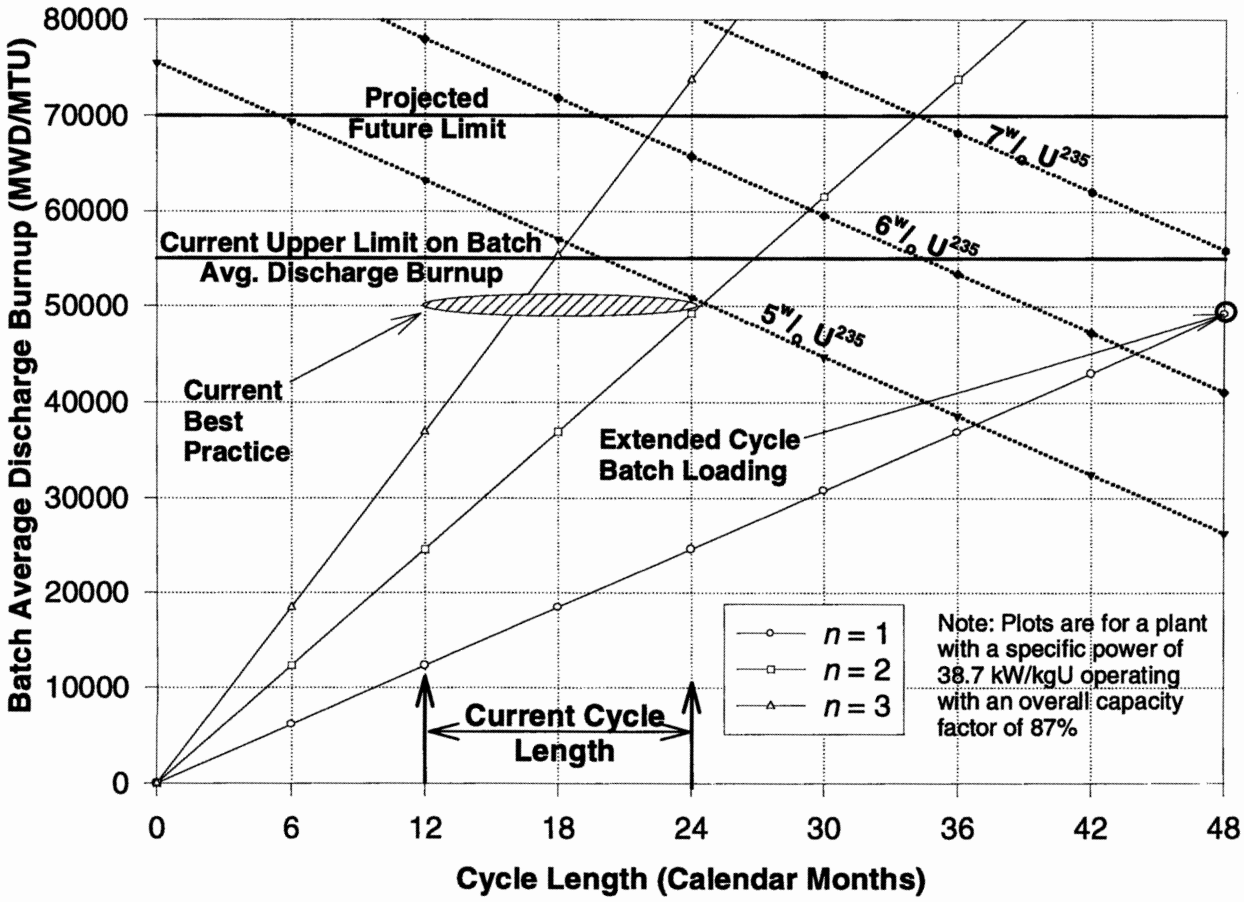

Figure 1: Burnup-Cycle Length Map for a Representative PWR

$$B_d\left(\frac{MWD}{MTU}\right)n \approx [14{,}784 \cdot n \cdot (X_p(\%) + 0.1072)]\left(\frac{MWD}{MTU}\right) - n \cdot 1025\left(\frac{MWD/MTU}{month}\right) \cdot T_c(months)$$

$$B_d\left(\frac{MWD}{MTU}\right) \approx [14{,}784 \cdot (X_p(\%) + 0.1072)]\left(\frac{MWD}{MTU}\right) - 1025\left(\frac{MWD/MTU}{month}\right) \cdot T_c(months) \quad (1.6)$$

Equation (1.4a) and equation (1.6) are both plotted on Figure 1 for $n = 1$, 2, and 3 and $X_p = 5^{w}/_{o}$, $6^{w}/_{o}$, and $7^{w}/_{o}$ U^{235}. Note that:

1. Discharge burnup increases linearly with cycle length and exhibits a positive slope that is directly proportional to n [from equation (1.4b)]
2. The effect of enrichment can be illustrated by eliminating n in the B_d-T_c relationship of equation (1.4b) in favor of X_p. This produces curves with a negative slope (equal to -1025 MWD/MTU) with intercepts on the B_d axis that increase with increasing enrichment [from equation (1.6)].

The map demonstrates that extended cycle lengths can be achieved by two principal strategies:

1. For a given number of fuel batches (i.e, n fixed) cycle length can be increased by increasing the reload enrichment, with a concurrently higher discharge fuel burnup (i.e., move up the "fixed n" lines shown on the map), or alternatively
2. For a fixed discharge burnup (i.e, B_d fixed) decrease the number of batches (i.e., move horizontally along the map).

For the second strategy, decreasing the number of batches results in higher enrichments of unburned U^{235} in the discharged fuel and therefore leads to an increased fuel cost penalty when this enriched fuel is "thrown away" at the end of the cycle. Nevertheless, it is only through this strategy that the goal of an extended operating cycle which does not exceed current burnup constraints can be reached.

Next it is desired to illustrate the relationship between cycle length, burnup, and the mass of fuel loaded into the core. Substituting equation (1.3a) into equation (1.2a) yields:

$$B_c\left(\frac{MWD}{MTU}\right) = Q_{sp}\left(\frac{MWD/MTU}{EFPD}\right) \cdot T_c(EFPD) \tag{1.7}$$

Expressing Q_{sp} as the ratio of core thermal power, Q, and the mass of fuel in the core, M, and solving for T_c leads to the following equation:

$$T_c(EFPD) = \frac{B_c\left(\frac{MWD}{MTU}\right) \cdot M(MTU)}{Q(MW)} \tag{1.8}$$

Equation (1.8) shows that for a given core thermal power, cycle length depends on the total amount of energy produced by the reactor (i.e., the product of B_c and M) and not simply on B_c. Conventional core designs focus on optimizing fuel utilization by maximizing fuel discharge burnup for a given cycle length. However, calculations using CASMO-3 show that maximizing the achievable end of cycle (EOC) burnup for a core using $7^{w}/_{o}$ U^{235} enriched fuel actually requires a reduction in the amount of fuel loaded into the core in order to make the lattice "wetter" (i.e., to increase the water-to-fuel ratio in the core). Since achieving a wetter lattice involves reducing M, equation (1.8) shows that this can actually lead to a *decrease* in the achievable cycle length. For the extended cycle design, which seeks the maximum achievable T_c, it is therefore not desirable to alter the lattice configuration to a wetter arrangement (i.e., increase rod pitch or decrease fuel pin diameter) in order to optimize achievable core discharge burnup. Thus the extended cycle design

has the same lattice configuration (i.e., the same total number of fuel pins, arranged in the same geometry) as a conventional, multi-batch core. With the lattice constrained in this way, M for the extended cycle core can only be varied by design changes which alter fuel pellet effective density, such as the use of annular fuel.

A simple thought experiment also shows that the fuel assemblies should have as uniform an enrichment as possible, since the EOC poison-free reactivity will be the highest for a core having the highest total residual fissile content. This also argues for reactivity and power shape control using burnable poison. The preceding line of reasoning agrees with the approach taken by ABB/CE in their design of a single-batch-loaded, erbium-poisoned core for the disposition of weapons-grade plutonium [R-1]. However, while the total time in core for the ABB/CE design was also four years, annual shutdowns were assumed, during which assemblies were to be shuffled in order to adjust assembly discharge isotopics.

1.3 Report Structure

Chapter 2 of this report describes in detail the PWR plant model used in this design effort. Chapter 3 discusses the neutronic design goals of the PWR design and the basis for each of these goals. In Chapter 4, the modeling codes used to evaluate the extended cycle core designs are described. Chapter 5 contains a detailed description of the PWR extended cycle core design, and Chapter 6 evaluates its neutronic performance. Chapter 7 examines the thermal and mechanical behavior of the fuel in the extended cycle PWR core design. Chapter 8 compares the economic performance of the extended cycle PWR core to that of more conventional designs. Chapter 9 presents the BWR extended cycle core design and outlines the key differences between the PWR and BWR. Chapter 10 evaluates the performance of the BWR design. Chapter 11 summarizes the overall conclusions and proposes areas for future work.

CHAPTER 2

PWR Model Description

The PWR plant used in this study is a Westinghouse 4-loop 1150 MW_e Pressurized Water Reactor. The Westinghouse 4-loop PWR was selected as the target plant for this study because of its widespread use and because its high specific power makes it a challenging target for an extended cycle core design. A design strategy which produces an extended cycle core for this type of PWR can be confidently applied to the vast majority of the currently operating commercial PWR plants in the United States.

2.1 Plant Description

The operating parameters for this plant were provided by the Yankee Atomic Electric Company. Yankee Atomic performs core reload analyses for the North Atlantic Energy Services Company's Seabrook Nuclear Station in Seabrook, New Hampshire. These operating parameters are listed in the table below [W-1], [Y-1]. All dimensions given are cold dimensions.

Figure A.1 and Figure A.2 in Appendix A show the rod cluster control assembly pattern and the fuel assembly cross sections for the 17×17 fuel arrays used in this study [P-1]. All dimensions shown in the figures are cold dimensions and are given in inches.

The challenge of achieving an extended cycle length with the Westinghouse 4-loop PWR while still respecting current fuel discharge burnup limits can be illustrated by recalling equation (1.7) from Chapter 1. The specific power, or burnup rate, in equation (1.7) measures how quickly the

Table 1: Operating Parameters for a Westinghouse 4-Loop Pressurized Water Reactor

	Operating Parameter	Value
1.	Plant	
	Number of primary loops	4
	Total heat output of the core (MW_{th})	3411
	Total plant thermal efficiency (%)	34
	Electrical output of plant (MW_e)	1150
	Energy deposited in the fuel (%)	97.4
	Energy deposited in the moderator (%)	2.6
2.	Core	
	Core barrel inside diameter/outside diameter (m)	3.76/3.87
	Mass of fuel as UO_2 (MT)	101.0
	Mass of fuel as U (MTU)	88.2
	Mass of cladding material (MT)	23.1
	Rated power density (kW/L)	104.5
	Specific power (kW/kgU)	38.7
	Average linear heat generation rate (kW/ft)	5.6
	Core volume (m^3)	32.6
	Design axial enthalpy rise ($F_{\Delta H}$)	1.65
	Allowable core total peaking factor (F_Q)	2.5
3.	Primary Coolant	
	System pressure (MPa)	15.51
	Total core flow rate (Mg/sec)	18.63
	Rated coolant mass flux (kg/m^2-sec)	2087.6
	Core inlet temperature (^oC)	292.7
4.	Fuel Rods	
	Total number	50,952
	Fuel density (% of theoretical)	94

Table 1: Operating Parameters for a Westinghouse 4-Loop Pressurized Water Reactor

	Operating Parameter	Value
	Pellet diameter (mm)	8.19
	Pellet height (mm)	13.4
	Fuel-clad radial gap width (μm)	82
	Cladding material	Zircaloy-4
	Cladding thickness (mm)	0.57
	Clad outer diameter (mm)	9.5
	Total fuel height (m)	3.66
5.	Fuel Assemblies	
	Number of assemblies	193
	Number of fuel rods per assembly	264
	Number of grids per assembly	7
	Rod pitch (mm)	12.6
	Overall dimensions (mm×mm)	214×214
6.	Rod Cluster Control Assemblies	
	Neutron absorbing material	Ag-In-Cd
	Cladding material	Type 304 SS
	Cladding thickness (mm)	0.46
	Number of clusters Full/Part length	53/8
	Number of absorber rods per cluster	24
	Assembly array	17×17
	Array geometry	square

reactor consumes fuel. Reactors with high specific power (and thus high burnup rates) consume fuel more rapidly than reactors with lower specific powers. Equation (1.7) shows that for a fixed cycle length, a reactor with a larger burnup rate produces a higher discharge fuel burnup at the end of an operating cycle.

The PWR modeled in this study has a nominal burnup rate of 38.7 MWD/MTU per EFPD, or 14.1 GWD/MTU per Effective Full Power Year (EFPY). A reactor operating for 48 calendar months at the target capacity factor of 87% will therefore accrue 41.76 Effective Full Power Months (EFPM) of operation. The discharge burnup for this reactor at the end of four years of operation can be calculated by rearranging equation (1.8) in the following manner:

$$B_c = T_c \cdot Q/M \tag{2.1}$$

$$B_c = 41.76\ EFPM \cdot \left(\frac{1 EFPY}{12\ EFPM}\right) \cdot 14.1\ \frac{GWD}{MTU} \cdot \frac{1}{EFPY} \tag{2.2}$$

$$B_c = 49.1\ \frac{GWD}{MTU} \tag{2.3}$$

where: B_c = ***Core average*** discharge burnup for a Westinghouse 4-loop PWR running on a 48-month, uni-batch loaded cycle

This burnup is at the upper limit of current widespread practice in the U.S., but well within the worldwide experience base. Nevertheless, problems have been experienced with high burnup fuel, and care must be taken that the proposed single batch application does not aggravate any known issues.

2.2 Model Description

The PWR in this project was modeled using 1/8 core symmetry as illustrated in Figure 2. In this study a full three-dimensional model of the core was implemented, with each fuel assembly divided into 24 axial and 4 radial quadrant nodes. The core was modeled for reactor physics design using the CASMO-3/TABLES-3 /SIMULATE-3 reactor analysis suite developed by STUDSVIK NUCLEAR, a division of STUDSVIK AB, Nyköping, Sweden. The codes have been made available to this project through collaboration with STUDSVIK of America, Inc.

The PWR core is analyzed at a condition of steady-state Hot Full Power (HFP) with all control rods fully withdrawn and with reactivity being controlled by soluble poison (boron) within the coolant. The core is initially free of fission product poisons. However, iodine, xenon, promethium, and samarium build up (rapidly) to equilibrium levels as the operating cycle progresses.

A more detailed description of the CASMO-3, TABLES-3, and SIMULATE-3 computer codes used in this study is contained in Chapter 4.

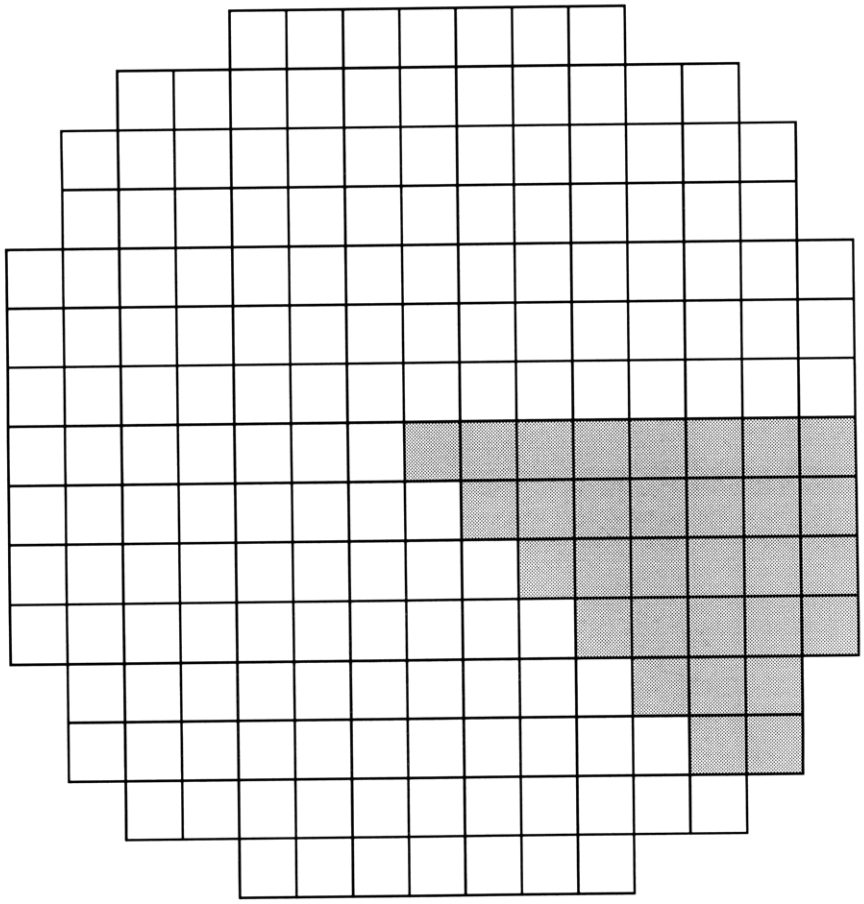

Figure 2: PWR Core Map Showing 1/8 Core Symmetry used in Modeling

CHAPTER 3

PWR Core Design Goals

As stated previously, the purpose of this project was to design reload cores for an extended operating cycle while maintaining existing burnup limits in *currently operating* LWR units. Accordingly, the extended cycle design will not change any of the core flow paths or internal dimensions. Rather, increased cycle length is accomplished by changing the fuel composition itself and by implementing innovative assembly loading patterns. Because of this, a complete licensing analysis of the core need not be performed in order to demonstrate technical feasibility. Rather, technical feasibility of a *reload core* may be reasonably demonstrated if certain carefully selected parameters defining the allowable operating envelope of a currently licensed design can be met. The PWR core performance parameters selected for evaluation in this project are listed in Table 2.

For the PWR extended cycle design, the only performance parameters assigned specific design goal limits are $F_{\Delta H}$, F_Q, and CBC. The remaining parameters in Table 2 are quantified and their impact on core performance is assessed. $F_{\Delta H}$, F_Q, and CBC and their assigned limits are discussed in greater detail in the sections which follows.

3.1 Maximum Enthalpy Rise Hot Channel Factor ($F_{\Delta H}$)

As described in Chapter 1, the framework for the extended cycle PWR core is a single-batch-loaded core of uniformly enriched fuel assemblies. Maintaining the enrichment of the fuel as uniform as possible reduces the peak fuel enrichment required to achieve an extended cycle.

Table 2: Evaluated Performance Parameters for the Extended Cycle PWR Core

Parameter	Significance	Impact of Extended Cycle Design on Parameter
Total peaking factor (F_Q)	• Defined as the maximum local fuel rod linear power density, divided by average fuel rod linear power density • Sets the maximum linear heat generation rate (LHGR) in the core • Affects large break Loss of Coolant Accident (LOCA) analysis • High burnup assemblies are limited to lower LHGR	• Since fuel enrichment is relatively uniform, peaking must be controlled almost completely with burnable poison loading • Cannot shuffle high burnup assemblies into areas of lower power peaking
Maximum Enthalpy Rise Hot Channel Factor ($F_{\Delta H}$)	• Defined as the ratio of the integral of linear power along the rod with the highest integrated power to the average rod power • Limits radial power peaking in the core	• Similar to F_Q above
Core Critical Boron Concentration (CBC)	• High CBC can produce an undesirable positive MTC • High CBC can lower pH, leading to cladding corrosion problems • High CBC can lead to increased lithium concentrations in the coolant (added to raise coolant pH) which can lead to fuel and steam generator corrosion problems	• High initial reactivity required by the extended cycle design can lead to high CBC • Must use burnable poisons to lower CBC
Fuel (Doppler) Temperature Coefficient (FTC)	• A negative FTC is generally required for negative power feedback • Magnitude of FTC affects time constants and core stability during severe transients	• Hardening of the neutron energy spectrum and the increase in fuel enrichment will produce a slightly less negative FTC.

Table 2: Evaluated Performance Parameters for the Extended Cycle PWR Core

Parameter	Significance	Impact of Extended Cycle Design on Parameter
Moderator Temperature Coefficient (MTC)	• A negative MTC is generally required for negative power feedback • MTC magnitude effects the severity of rod withdrawal and ejection accidents, cold water injection accidents, and steam line breaks	• High CBC of the design may produce a positive MTC at certain times in core life • Hardening of the neutron energy spectrum resulting from the increase in fuel and poison enrichment will produce a more negative MTC
Control Rod Worth	• Determines shutdown margin • Affects core performance during control rod withdrawal and ejection accidents	• Hardening of the neutron energy spectrum resulting from the increase in fuel enrichment will reduce control rod worth
Boron Worth	• Affects core performance during a boron dilution accident	• Hardened neutron spectrum will lower the boron worth

Because fuel enrichment zoning is minimized, the extended cycle design must rely heavily on burnable poison loading (instead of extensive enrichment differences) to achieve an acceptable radial power shape. Additionally, the single batch strategy eliminates the possibility of controlling the power shape by shuffling fuel assemblies between cycles.

The $F_{\Delta H}$ limit for a Westinghouse 4-Loop 1150 MW_e PWR is 1.65, excluding uncertainties. Design margins vary throughout the industry, but common practice is to include a 4% margin for analysis uncertainties and 4% for manufacturing tolerances. Applying these factors reduces the design $F_{\Delta H}$ to 1.53. This research project, which seeks to demonstrate the technical feasibility of a new and unconventional core design, targets a value for $F_{\Delta H}$ of 1.56, which lies within 2% of this common industry standard. Further refinements of the extended cycle core design should eliminate the need for this 2% design margin buffer in the future. In the three-dimensional model, SIMULATE-3's pin power reconstruction features are used to calculate the power peaking in individual fuel pins.

3.2 Total Peaking Factor (F_Q)

The total peaking factor (F_Q) is affected by the core's radial and axial power shapes, as well as by the pin-to-pin power peaking within each assembly. Again, because of the unique design features of the extended cycle core, the radial, axial, and intra-assembly power shapes are controlled almost entirely through the use of burnable poison. Maintaining F_Q at or below the Westinghouse design limit of 2.50 without uncertainties reduces the core's vulnerability to a large break LOCA [H-1]. Furthermore, reducing F_Q results in increased fuel mechanical and thermal performance margins, since fuel with a lower peak power density operates at lower temperatures and releases less fission gas into the fuel-clad gap. Applying the standard 8% design margin lowers the allowable F_Q to 2.31. To stay within 2% of this common industry standard, F_Q for the extended cycle core design must be kept below 2.36.

3.3 Core Critical Boron Concentration (CBC)

Pressurized water reactors use boron in the coolant (in the form of boric acid) as a soluble poison to control reactivity within the core. The critical boron concentration (CBC) with all control rods withdrawn is an indicator of the excess reactivity in the core. A high CBC can have adverse effects on two important facets of PWR operation: primary water chemistry control and Moderator Temperature Coefficient.

The concentration of soluble boron directly impacts the chemistry of the primary coolant, influencing both pH and lithium concentration. In most commercial PWRs, LiOH is added to the primary coolant to raise pH to desired levels. High concentrations of boron (in the form of boric acid) require high concentrations of Li (in the form of LiOH) in order to achieve the optimum pH for the plant. The proper coordination of Li/B/pH is important to material corrosion performance and is especially important for a high burnup, extended cycle core design. Concern over proper primary chemistry control stems from the desire to minimize the detrimental effects of Zircaloy corrosion, Inconel 600 primary water stress corrosion cracking (PWSCC), and increased shutdown radiation fields from increased deposition of crud. In order to aid utilities in optimizing plant

performance, the Electric Power Research Institute has developed guidelines for maintaining proper primary chemistry in commercial PWRs [E-1].

EPRI recommendations for maintaining proper Li/B/pH coordinated primary water chemistry are contained in the following generic principles (listed in order of priority):

1. Operate at or above pH = 6.9 to minimize crud deposition on fuel and crud-enhanced Zircaloy corrosion.
2. For operation above 2.2 ppm lithium for extended periods of time (> 3 months) to achieve a pH = 6.9 during an extended fuel cycle, a plant specific fuel and materials review should be performed. Prolonged exposure to elevated concentrations of lithium raises concerns about PWSCC and Zircaloy corrosion.
3. Once lithium has been reduced to 2.2± 0.15 ppm (consistent with 1 and 2 above) either maintain pH constant at 6.9 (Coordinated Chemistry Regime) or maintain Li concentration constant at 2.2± 0.15 ppm {Modified Chemistry Regime) until a specified pH between 6.9 and 7.4 is reached.
4. Maintain selected pH while controlling Li to ± 0.15 ppm until the end of the operating cycle.

These guiding principles are illustrated in Figure 3, which shows an example of the operating chemistry regime for a generic PWR [K-1]. The black bands in the figure show acceptable combinations of Li concentration and pH for various values of soluble boron.

In this study, the maximum permissible concentration of soluble boron was calculated using tabulated correlations from EPRI's "Primary Water Chemistry Guidelines". These correlations relate pH, lithium concentration, boron concentration, and the plant average coolant temperature (T_{ave}) [E-1]. From these calculations, the boron concentration which corresponds to a Li concentration of 2.2 ppm at a pH of 6.9 and a Hot Full Power (HFP) T_{ave} of 312°C is **1780 ppm**. Note that this concentration was calculated using a plant specific T_{ave}, and therefore does not necessarily correlate to the more generic relationships shown in Figure 3. Therefore, 1780 ppm is selected as the maximum allowable value of CBC for the extended cycle core under HFP, equilibrium xenon conditions.

EPRI's guidelines state that prior to commencing extended operations (> 3 months) with Li >2.2 ppm, a complete plant-specific fuel and materials review should be performed in order to assess the plant's susceptibility to PWSCC. If the concentration of lithium in the coolant can be kept ≤2.2 ppm, the likelihood of excessive PWSCC and Zircaloy corrosion can be greatly reduced. Maintaining the CBC below 1780 ppm ensures that the plant can operate in favorable regimes of

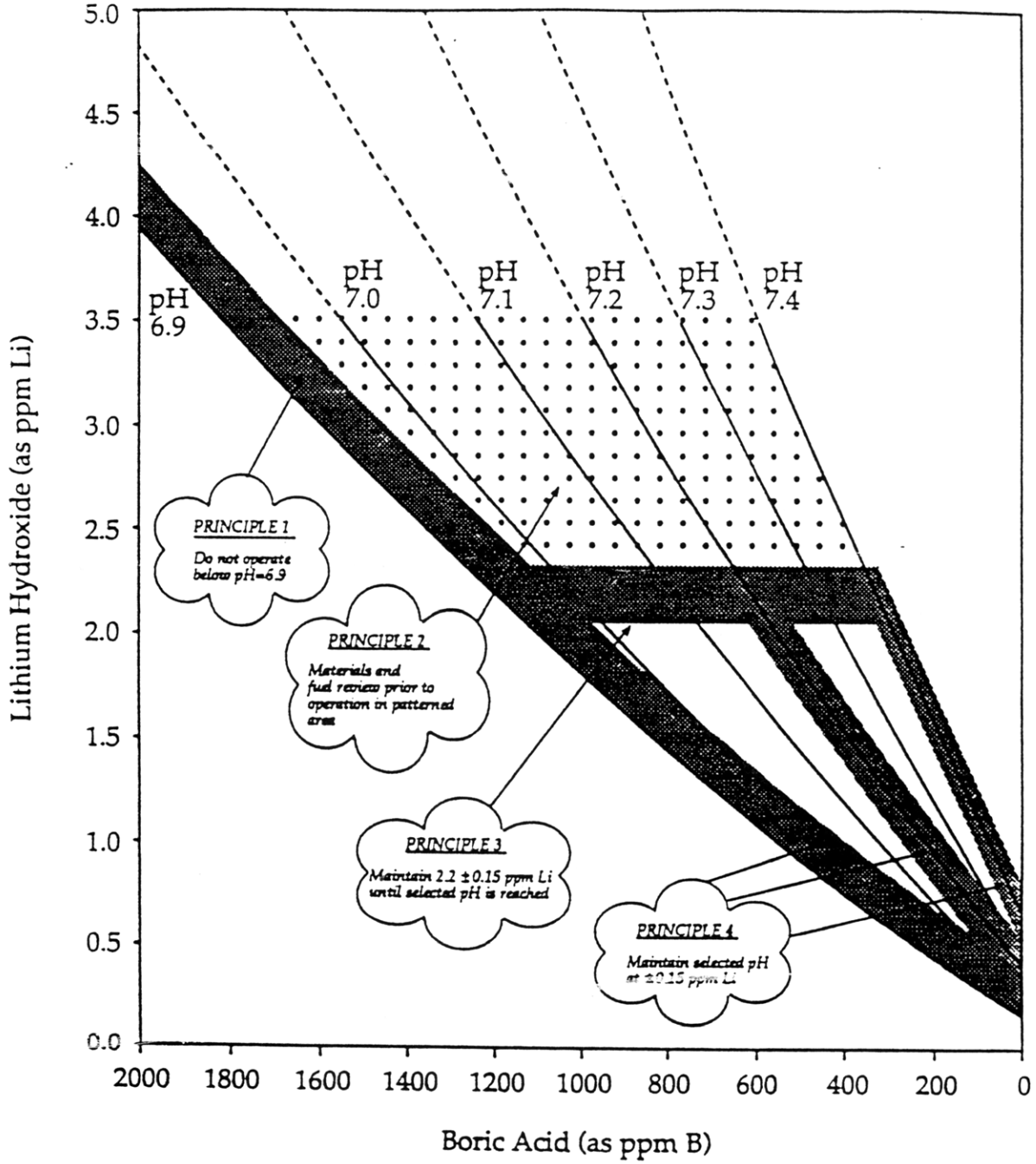

Figure 3: General Regimes for Reactor Coolant pH Control (T_{ave} = 300°C) [K-1]

both pH and lithium concentration throughout core life. In the extended cycle length PWR, reduction of the CBC below the design goal limit is accomplished through the addition of large amounts of burnable poisons, which hold down the excess reactivity of the 7% enriched fuel loaded into the core.

In addition to affecting primary water chemistry, the soluble boron concentration also influences neutronic performance by altering the core's Moderator Temperature Coefficient (MTC). PWRs are typically designed to be undermoderated, so that a decrease in the core water-to-fuel ratio causes an addition of negative reactivity. Lowering the water-to-fuel ratio decreases the effectiveness of the moderator and shifts the neutron energy spectrum away from the thermal region, in which fissions by U^{235} nuclei are much more probable. The decrease in U^{235} fission rate outweighs the slight decrease in parasitic neutron absorptions by the moderator, and net negative reactivity is inserted into the core. During normal operation, changes in the core water-to-fuel ratio stem primarily from changes in the density (and therefore, temperature) of the sub-cooled reactor coolant. In a typical undermoderated PWR core the MTC is negative, since an increase in coolant temperature causes a decrease in coolant density and core water-to-fuel ratio, which results in the insertion of negative reactivity. As indicated in Table 2, a negative MTC is generally desirable because it increases reactor safety and stability by providing a means of limiting the magnitude of a reactor power excursion in the event of a large positive reactivity insertion.

Because soluble boron is dissolved in the moderator, its effectiveness as a neutron poison varies directly with the density of the primary coolant (and *inversely* with its temperature). Soluble boron therefore contributes to a *positive* MTC because an increase in moderator temperature results in a decrease in the dissolved poison density in the core and adds positive reactivity to the core. If the CBC becomes excessively high, an undesirable positive MTC can result. However, the extended cycle reactor design is much less susceptible to a positive MTC than a conventional plant because of the unique neutronic characteristics of the extended cycle core.

Because it contains 7% enriched fuel and large amounts of burnable poisons, the extended cycle core is much "blacker" (i.e., has a larger absorption cross-section) for thermal neutrons than the core of a "conventional" reactor with a multi-batch refueling scheme. This increased propensity for thermal neutron absorption results in a depletion of the thermal neutron population and a shift of the neutron spectrum toward higher energies. With its "hardened" energy spectrum,

the thermal neutron starved extended cycle core experiences a larger negative reactivity addition for a given decrease in moderator efficiency than does a conventional core. As a result, the extended cycle design exhibits a more negative MTC than a design with a shorter cycle length. The unique neutron energy spectrum of the extended cycle core and the fairly conservative 1780 ppm soluble boron limit combine to ensure that a positive MTC will not occur during normal plant operating conditions.

The next section of this report discusses in detail the computer codes used to design and model the extended cycle cores.

CHAPTER 4

Computer Code Description

The computer codes used in this project are the CASMO-3/TABLES-3/SIMULATE-3 reactor analysis suite developed by STUDSVIK. CASMO-3 is a multi-group two-dimensional transport theory code for burnup calculations on PWR and BWR fuel assemblies. SIMULATE-3 is an advanced two group nodal code for PWR and BWR analysis that allows for two-dimensional and three-dimensional full core depletion modeling. The data processing code TABLES-3 connects CASMO-3 and SIMULATE-3. This code uses CASMO-3 output to generate a library of "tables" of two-group cross-sections, discontinuity factors, and kinetics, isotopics, and fission product data in a format that is usable by SIMULATE-3. These powerful, licensing level codes allow the performance of a high quality analysis of the core design.

4.1 CASMO-3

4.1.1 Flow of Calculation

A flow chart of the CASMO-3 calculation process is shown in Figure 4. CASMO-3 begins processing by calculating macroscopic group cross sections for the fuel assembly being modeled based upon the density, composition, geometry, and temperature information provided as input data. These cross sections are prepared using an internal library of either 70 or 40 energy groups, depending on user preference. In this study the 40 energy group library was used in order to reduce overall processing time, while still maintaining accuracy more than sufficient for present purposes.

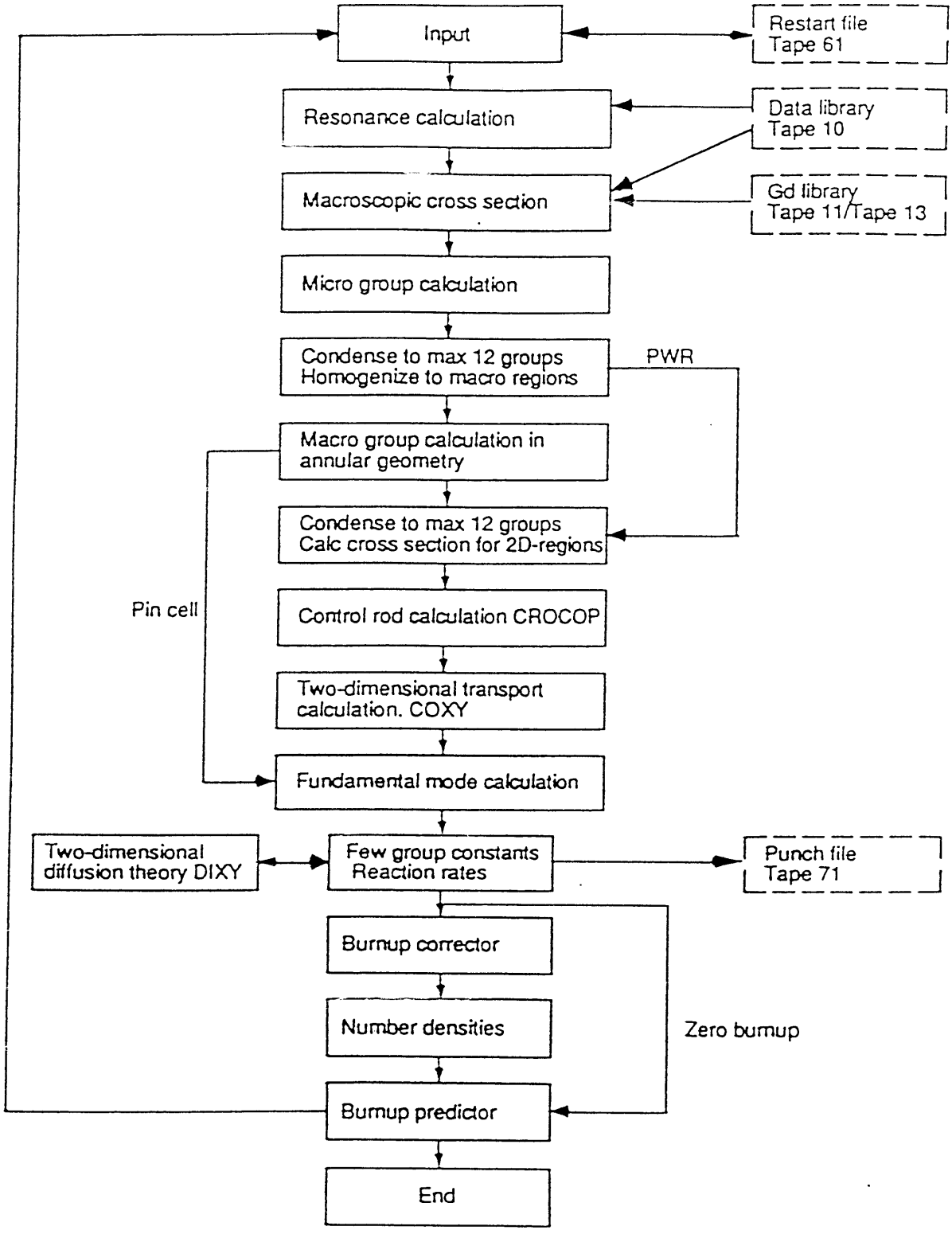

Figure 4: Flow Diagram for CASMO-3 [E-2]

Effective cross sections in the resonance region for important resonance absorbers (U^{235}, U^{236}, U^{238}, and Pu^{239}) are calculated using an equivalence theorem which relates tabulated effective resonance integrals for each resonance absorber in each resonance group to the particular heterogeneous problem being considered [E-2]. The resonance integrals are used to calculated the effective absorption and fission cross sections for these absorbers. The screening effect between different pins is accounted for through the use of Dancoff factors.

The cross sections described above are then used in a series of "micro group" calculations in order to obtain detailed neutron energy spectrum information for the pin cells within the assembly. The micro group calculation is performed for each different type of pin in the assembly in order to obtain information on the spectra for pins with various enrichments or burnable poison loadings. The detailed neutron energy spectra obtained from these calculations are then used to homogenize the pin cells and to collapse the number of energy groups down to a maximum of 12.

Using as many as 12 group cross sections and homogenized pin cells, the code then employs a two-dimensional transmission probability routine (COXY) to obtain the flux distribution throughout the assembly. Leakage is accounted for through the use of a fundamental buckling mode which modifies the COXY output in order to account for leakage effects.

Isotopic depletion due to fuel burnup is calculated for each fuel pin in the assembly and for each burnable region. Burnup chains are linearized and are calculated using 24 separate fission products, 2 "pseudo" fission products, and 17 heavy nuclides. For increased accuracy, CASMO-3 performs two calculations for each depletion point being modeled. One calculation is performed using the neutron energy spectra at the beginning of each step. At the end of the step the calculation is then repeated using the new energy spectra just determined from the first calculation. The average number densities from these two calculations are then used as the start values for the next energy step.

The output of CASMO-3 includes the reactivity (k_∞), pin-to-pin power distribution, reaction rates, material composition, and few group parameters for the assembly, along with discontinuity factors which account for bundle interference and reflector regions. This information can then be used by the advanced nodal code SIMULATE-3 to model overall core performance

4.1.2 Branch Calculations in CASMO-3

In order to obtain an adequate library of cross sections for realistic modeling of core operations, many different CASMO-3 runs must be performed to account for in-core parameters which vary with reactor power or fuel depletion. For the PWR in this study, each different type of fuel assembly in the core was modeled, with the following parameters varied:

Table 3: Varied Parameters in CASMO-3 PWR Runs

	Parameter	Base Value	Branches
1.	Base Case		
	Core Boron Concentration (ppm)	450.0	0, 900, 2000
	Moderator Temperature (°C)	310.0	292.7, 326.9
	Fuel Temperature (°C)	626.9	292.7, 826.9
	Control Rod Position	Fully Withdrawn	Fully Inserted
2.	0 ppm Boron case		
	Core Boron Concentration (ppm)	0.0	450, 900, 2000
	Moderator Temperature (°C)	310.0	-
	Fuel Temperature (°C)	626.9	-
	Control Rod Position	Fully Withdrawn	-
3.	900 ppm Boron case		
	Core Boron Concentration (ppm)	900.0	0, 450, 2000
	Moderator Temperature (°C)	310.0	-
	Fuel Temperature (°C)	626.9	-
	Control Rod Position	Fully Withdrawn	-
4.	2000 ppm Boron case		
	Core Boron Concentration (ppm)	2000.0	0, 450, 900
	Moderator Temperature (°C)	310.0	-
	Fuel Temperature (°C)	626.9	-
	Control Rod Position	Fully Withdrawn	-

Table 3: Varied Parameters in CASMO-3 PWR Runs

	Parameter	Base Value	Branches
5.	Low Moderator Temperature case		
	Core Boron Concentration (ppm)	450.0	-
	Moderator Temperature (°C)	292.7	310.0, 326.9
	Fuel Temperature (°C)	626.9	-
	Control Rod Position	Fully Withdrawn	-

For each depletion point in a modeling case CASMO-3 conducts a Burnup calculation for the parameters listed in the Base Values column of the above table. Following the completion of the last depletion point, CASMO-3 returns to each state point and performs Branch calculations by calculating cross sections for the values listed in the Branches column. Each fuel assembly in the core is modeled to an average burnup of 60 GWD/MTU. The relatively fine mesh of the depletion points and number of Base and Branch cases run ensures that a sufficiently detailed library of cross sections is generated to assure accurate modeling of the extended cycle core design. Following the completion of depletion calculations, CASMO-3 generates an output file of information specified by the user and a card image file which contains cross section information that will be used by the data processing code TABLES-3.

4.2 TABLES-3

TABLES-3 is a data processing code that links CASMO-3 to SIMULATE-3. The code processes the following types of data [S-1]:

- Two-group cross sections
- Discontinuity factors
- Fission product data
- Detector data
- Pin power reconstruction data
- Kinetics data
- Isotopics data

TABLES-3 reads the CASMO-3 card image files and produces a master binary library in the format required by the third code of the suite, SIMULATE-3.

4.3 SIMULATE-3

SIMULATE-3 is an advanced two group nodal code suitable for the analysis of both PWRs and BWRs. The code is based on the QPANDA neutronics model which employs fourth order polynomial representations of the intranodal flux distributions in both the fast and thermal groups [S-2]. SIMULATE-3 cross sections are provided by CASMO-3 and translated into a binary master library by the linkage code TABLES-3.

SIMULATE-3 allows for depletion calculations in two or three dimensions using 1/8, 1/4, 1/2, or full core symmetry modeling and provides a versatile array of options for evaluating core performance. In the two-dimensional model, axial leakage is accounted for through the use of a user input value for axial buckling. In this study the extended cycle PWR core was evaluated using a three-dimensional model employing one-eighth core symmetry and 24 axial nodes. Each fuel assembly was divided into 4 radial nodes to allow for the modeling of asymmetric bundles. For the evaluations performed in this study the PWR core was depleted at Hot Full Power (HFP) to the End of Full Power Life (EOFPL), i.e., until the HFP CBC was reduce to 0 ppm. The PWR core was modeled with all control rods fully withdrawn and with criticality control accomplished by varying the soluble boron concentration in the coolant to compensate for burnup-induced changes in reactivity. The soluble boron concentration for each time step was determined by setting $k_{eff} = 1$ and having SIMULATE-3 iteratively solve for the CBC.

In the next chapter, the PWR extended cycle core design is described in detail.

CHAPTER 5

PWR Core Design Description

Distinctive features of the extended cycle PWR core design include:

- Single batch reload scheme
- Fuel enriched to $>5^{w}/_{o}$ U^{235} (the current licensing limit)
- Unique burnable poison scheme

The single batch concept has been discussed in detail in Chapter 1. The following sections discuss the fuel enrichment and burnable poison aspects of the extended cycle PWR core design.

5.1 Fuel Enrichment

In order to determine the fuel enrichment necessary to achieve an extended cycle PWR core design, CASMO/SIMULATE models of *unpoisoned* PWR cores of various fuel enrichments were developed. The models are of cores having poison-free fuel assemblies that are uniformly enriched to the same weight percentage of U^{235}. Burnable poisons loaded into the core shorten the achievable cycle length, since any incompletely burned residual absorbers impose a negative reactivity penalty on the reactor at EOC. Therefore, the maximum attainable cycle length for a given fuel enrichment can be determined by examining the performance of these unpoisoned cores. The results of the unpoisoned PWR core models are shown in Figure 5. Note that 1 GWD/MTU

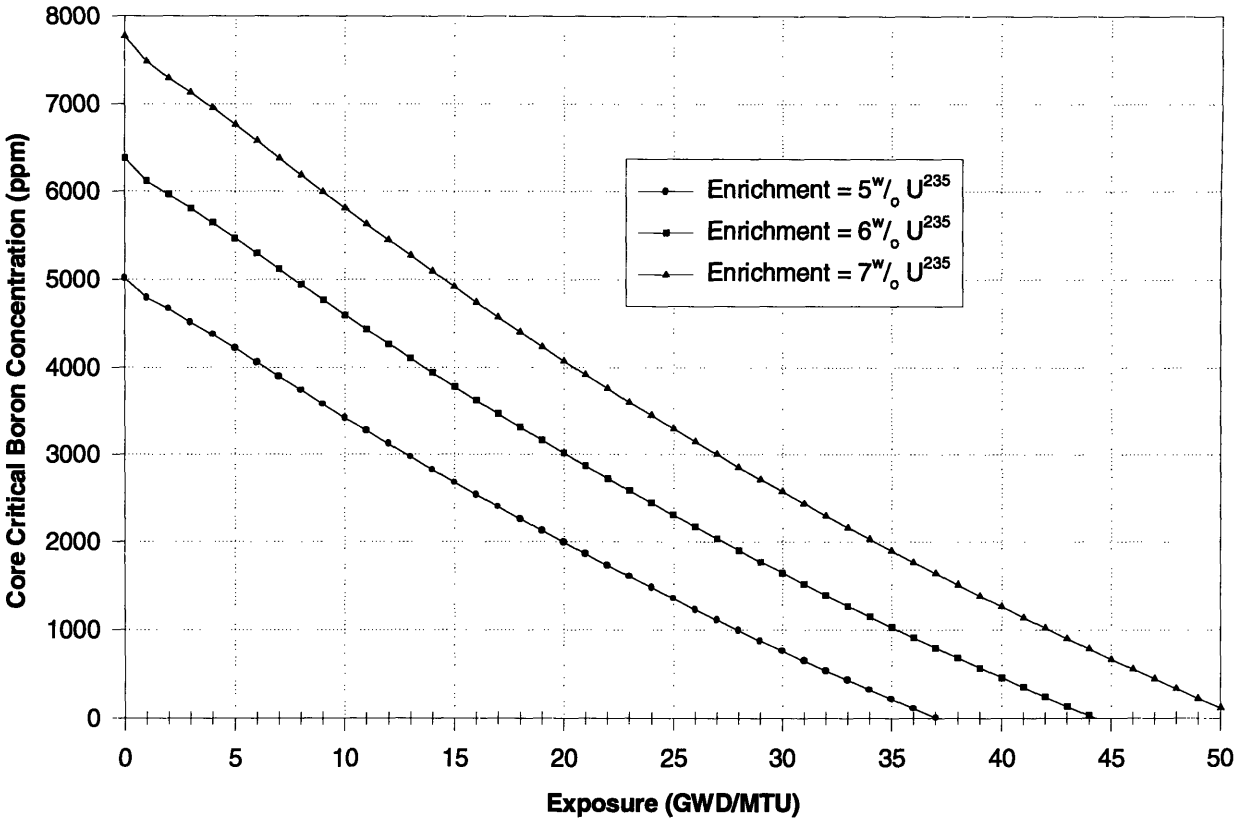

Figure 5: CBC for Unpoisoned Cores of Various Enrichments

of core-average exposure equates to 0.85 EFPM. Also note the extremely high CBC values required.

The results clearly show that even with a single-batch-loaded PWR core, an extended operating cycle is not achievable with fuel enriched to the current licensing limit of $5^{w}/_{o}$ U^{235}. The unpoisoned $5^{w}/_{o}$ U^{235} core shows a maximum achievable EOC core-average burnup of 37 GWD/MTU. From equation (1.8), corresponds to a cycle length of 31.4 EFPM or **36.1 calendar months** at the target capacity factor of 87%. Figure 5 also shows that fuel enriched to 7^{w}/o U^{235} is capable of achieving the required cycle length while still leaving some margin for the residual reactivity of burnable poisons that will be loaded into the core.

5.2 Burnable Poisons

The high fuel loading required in a long-life, single batch PWR core necessitates a corresponding increase in the concentration of burnable poison required to hold down excess reactivity.

Because excess reactivity is normally controlled using a mixture of burnable *and* soluble poisons (usually boron), a high concentration of burnable poison serves to reduce the required soluble boron concentration. The reduction in soluble boron concentration aids in the maintenance of proper primary water chemistry and in the preservation of a negative MTC throughout the cycle. Additionally, the single batch strategy of the extended cycle PWR core necessitates a heavy reliance on burnable poison to control power peaking in the core. Therefore, in an extended cycle PWR core, burnable poisons must fulfill the following dual mission:

- To hold down core excess reactivity in order to keep the coolant soluble boron concentration within acceptable limits, and
- To control the axial and radial core power distributions in order meet design limits on power peaking.

Ideally, a burnable poison used in the PWR extended cycle design would be able to control the core's excess reactivity and power shape while having a minimum impact on the operating cycle length. Unfortunately, the neutronic characteristics of a poison which are desirable for the advancement of one of these missions may be completely unfavorable for the achievement of the others. For example, in order to limit the coolant soluble born concentration, the poison selected should exhibit a large thermal neutron absorption cross-section (Σ). Obviously, the burnable poison must be able to hold down the large magnitude initial excess reactivity of the fresh 7% enriched fuel in the core. However, absorbers with a large Σ are depleted from the core at a high rate. A poison which burns out at a faster rate than the fissile atoms in the core are being depleted will cause the CBC to rise as the fuel cycle progresses. Poisons which burn out too rapidly can lead to an unacceptably high soluble born concentration later in core life.

Rapidly depleting burnable poisons can also cause excessive power peaking within the reactor. A fast burning neutron poison produces large changes in reactivity for a given amount of exposure. Regions of the core which are operating at different powers (i.e., which are accruing exposure at *different rates*) will over time experience large relative changes in reactivity. These reactivity changes can cause undesirable shifts in the power distribution, leading to violations of core design limits. Finally, problems can also arise if the burnable poison is depleted too slowly. If a considerable inventory of the poison remains in the core at EOC, then a substantial negative residual reactivity penalty is incurred. While EOC residual reactivity does not challenge any design limits,

by prematurely ending the operating cycle it diminishes flexibility in achieving desired core lifetime.

The Ayoub report models an "ideal" burnable poison which depletes linearly with burnup and disappears completely at the end of cycle (EOC) [A-1]. For the current study, devising a suitable real burnable poison loading pattern was one of the principal challenges. Solving this challenge for the PWR required the use of two different types of burnable poisons. Gadolinium in the form of gadolinium oxide (Gd_2O_3) is mixed with the UO_2 of selected pins and combined with a zirconium di-boride (ZrB_2) integral fuel burnable absorber (IFBA) coating on the surface of the Gd_2O_3-UO_2 fuel pellets. This "two-stage" poison was developed to reduce the CBC without excessively shortening the cycle length with a large residual reactivity penalty.

5.2.1 Gadolinium

Gadolinium is a rare earth metal (atomic number 64) with seven naturally occurring isotopes. Natural gadolinium has a thermal neutron absorption cross section of 44,000 barns, the largest of any element in the periodic table [H-2]. Gadolinium's large thermal neutron absorption cross section produces a self-shielding effect in the fuel pins in which it is loaded. This self-shielding attenuates the flux seen by the pin and therefore causes the gadolinium to burn out more slowly. The result is a flatter, more linear response of reactivity vs. exposure than for less-self-shielding burnable poisons such as erbium or boron. The time to deplete the poison increases as the weight percent concentration of Gd_2O_3 loaded into a fuel pin increases, so that the reactivity response of a given assembly can be controlled by varying the amount of poison loaded into the fuel [S-3]. Because of its higher thermal neutron absorption cross-section, gadolinium burns out more rapidly than erbium, thus leaving a smaller residual reactivity penalty at EOC. Specific comparative analyses of burnable poisons using CASMO-3 show that gadolinium exhibits much less residual reactivity at EOC than an amount of erbium which produces the same initial reactivity hold-down in a poisoned fuel assembly [T-1].

Gadolinium's moderate burnout rate and relatively low residual reactivity make it an excellent burnable poison candidate for an extended fuel cycle core. At $12^{w}/_{o}$, the concentration of Gd_2O_3 in the fuel pellets slows the burnout rate of the poison enough to produce an allowable CBC without shortening the cycle length significantly. However, further attempts to reduce the peak CBC by increasing the concentration of Gd_2O_3 in the fuel result in large EOC residual reactivity penalties

and unacceptable reductions in cycle length. CASMO/SIMULATE results show that at these high levels of poison loading, increasing the poison concentration by $1^{w}/_{o}$ Gd_2O_3 shortens the PWR cycle length by ~1.3 EFPM, or ~1.5 calendar months of operation at the target capacity factor of 87%. In addition, Gd_2O_3 reduces the thermal conductivity of UO_2, so that increased concentrations will adversely affect the thermal and mechanical performance of the fuel [I-1]. Finally, since the current envelope of large scale industrial experience with gadolinium as a PWR burnable poison only extends to $10^{w}/_{o}$ Gd_2O_3, the use of concentrations much higher than this may introduce unexpected difficulties in the manufacture and performance of the poison bearing fuel pins [H-3]; computer code cross-sections and benchmarking are also lacking for higher poison loadings.

5.2.2 Integral Fuel Burnable Absorbers (IFBA)

Lowering the CBC further without unacceptably reducing the cycle length required the addition of a different type of burnable poison. Achieving the design goals of the PWR extended cycle core requires using a burnable poison "black" enough to hold down the very high initial reactivity of the 7% enriched core, and short lived enough so as not to reduce the fuel cycle length unacceptably. In the PWR design, Integral Fuel Burnable Absorbers (IFBAs) were added in order lower the peak CBC of the gadolinium poisoned core. IFBA was developed by the Westinghouse Electric Corporation and consists of a thin coating of ZrB_2 on the outside of the UO_2 fuel pellets.

The primary reason for incorporating IFBA into the PWR extended cycle core design is its ability to reduce CBC with a corresponding minimal impact on operating cycle length. The thin coating burns out evenly and completely. Since B^{10} produces no neutron absorbing daughters and burns out completely, the EOC residual reactivity penalty is greatly reduced. Additionally, since IFBA is a surface coating and does not displace any fuel or moderating material it offers the best fuel economy of any available PWR burnable absorber [S-4]. IFBA has undergone extensive operational testing and is a key component of advanced Westinghouse PERFORMANCE+ ultra-high burnup fuel [S-5]. In the extended cycle design IFBA was modeled as a 0.015 mm surface coating with an absorber loading of 1.545 mg-B^{10}/inch. This loading corresponds to that of the 1.0X IFBA product line which is currently available from Westinghouse. The addition of 1.0X IFBA to the $12^{w}/_{o}$ Gd_2O_3 poisoned core reduces the peak CBC by over 100 ppm with no reduction in cycle length.

5.2.3 Gadolinium and IFBA Interaction

As described earlier, the thermal absorption cross-section of gadolinium is high, and its burnout rate must be slowed by increasing the concentration at which it is loaded into the fuel. Unfortunately, these higher concentrations of Gd_2O_3 also reduce the achievable cycle length by increasing the core's EOC negative residual reactivity penalty. Conversely, because it burns out rapidly and completely, IFBA has no impact on the extended cycle PWR core's cycle length. However, this high burnout rate also produces a large excess reactivity peak which translates into an unacceptably high soluble boron concentration at mid cycle. The PWR extended cycle core incorporates Gd_2O_3 and IFBA into the same fuel pins in order to synergistically maximize the benefits and minimize the drawbacks of both poisons. By combining gadolinium and IFBA into the same pins to link their depletion behavior, increased flexibility and control is gained over the reactivity vs. exposure response of the core's fuel assemblies.

Figure 6 illustrates the effect of co-locating the two poison types in the same fuel pin. The figure shows CASMO-3 calculations of the infinite medium neutron multiplication factor (k_∞) vs. exposure for Westinghouse 17×17 PWR assemblies containing UO_2 fuel enriched to $7^w/_o$ U^{235}. These CASMO-3 calculations compare the performance of the following three poison schemes:

- Case 1: $12^w/_o$ Gd_2O_3 loaded into 44 of the assembly's 264 fuel pins.
- Case 2: $12^w/_o$ Gd_2O_3 loaded into 44 of the assembly's 264 fuel pins and a 1.545 mg B^{10}/inch IFBA surface coating on 44 additional different fuel pins. The neutron absorbers are placed on separate fuel pins for a total of 88 poisoned pins.
- Case 3: $12^w/_o$ Gd_2O_3 and a 1.545 mg B^{10}/inch IFBA surface coating loaded into the same 44 of the assembly's 264 fuel pins. The amount of poison loaded is identical to that of Case 2, but co-location is implemented so that only 44 fuel pins contain burnable absorbers.

The behavior of an unpoisoned fuel assembly is also shown for reference. Each calculation was made using the "Base Case" parameters listed in Table 3 on page 44 (fuel temperature = 626.9°C, moderator temperature = 310°C, soluble boron concentration = 450 ppm).

Predictably, the initial reactivity of Case 1 exceeds that of Case 2 because the addition of IFBA onto separate fuel pins simply increases the amount of burnable absorber exposed to the available neutron flux. As exposure increases, the rapid burnout of IFBA in Case 2 produces a sharp rise in

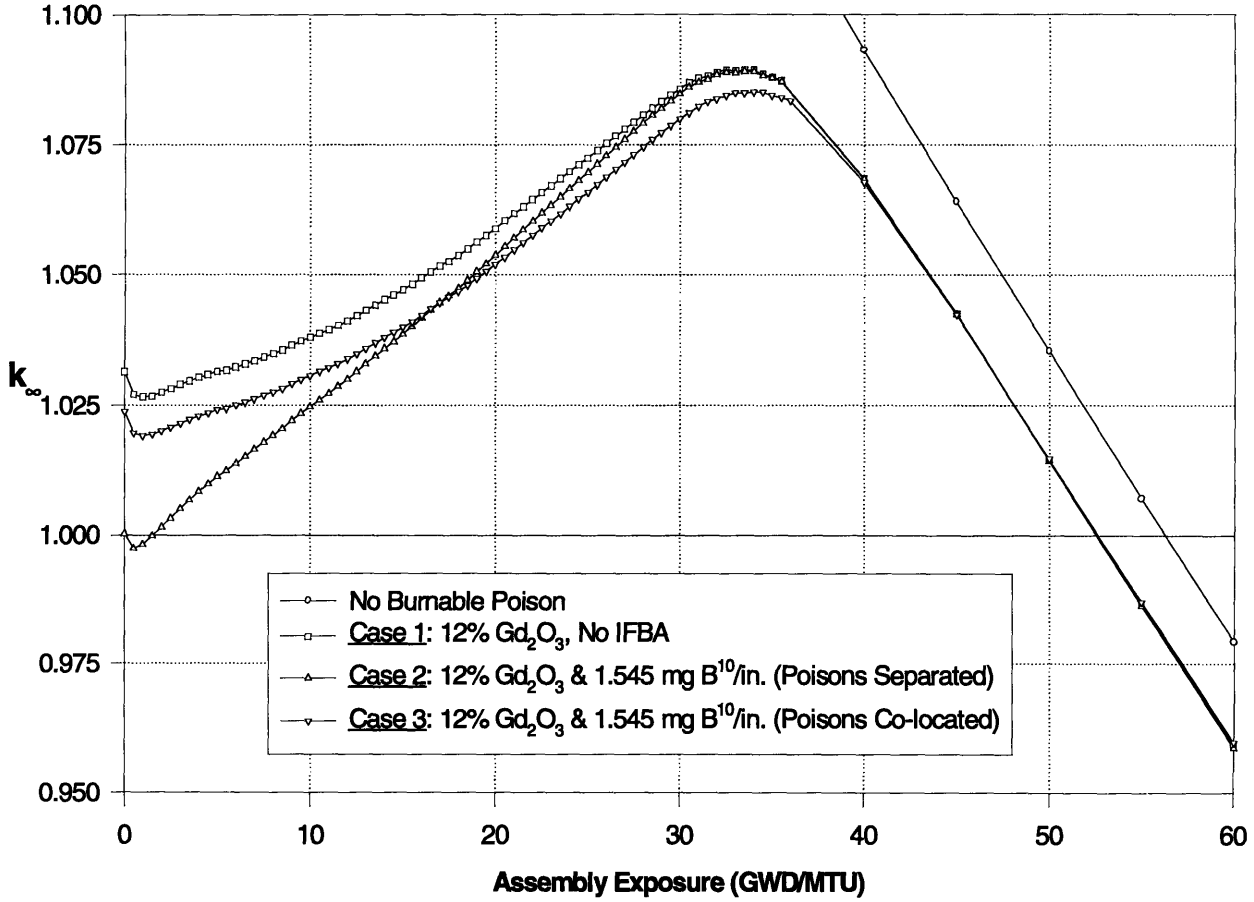

Figure 6: PWR Assembly Reactivity Response to Poison Co-Location

assembly reactivity compared to the other poison schemes. By approximately 30 GWD/MTU, the IFBA in Case 2 has been completely exhausted, so that the depletion behavior of gadolinium controls the reactivity response of the assembly for the remainder of its exposure. Close scrutiny of the figure reveals that at exposures higher than 30 GWD/MTU, the reactivity response of Case 1 and Case 2 are nearly identical. Because the two burnable absorbers were not neutronically "linked" through co-location, once the fast-burning IFBA has been depleted, it has no effect on the high exposure burnup behavior of the gadolinium. Thus, because the peak reactivity of the assembly is not reduced, the addition of IFBA in Case 2 produces no net performance benefits compared to the use of Gd_2O_3 only in Case 1. In actuality, the increased slope of Case 2's reactivity vs. exposure response may degrade overall core performance by introducing large exposure induced shifts in reactivity between regions of the core operating at disparate power levels.

In Case 3, with the neutron absorbers co-located in the same fuel pins, the reactivity response of the assembly becomes much more favorable. The initial reactivity of Case 3 is lower than that of Case 1 because the placement of IFBA onto the Gd_2O_3 loaded fuel pellets increases the "blackness" of the assembly's poisoned pins. More significantly, because the IFBA coating reduces the amount of flux penetrating each poisoned pin's interior, the burnout rate of Gd_2O_3 is noticeably reduced. Consequently, Case 3 exhibits a lower peak reactivity than either of the other two cases. In the full core model, this decrease in assembly peak reactivity translates into the reduction of peak CBC by **115 ppm**. Essentially, the addition of IFBA produces the same "self-shielding" effect as an increase in Gd_2O_3 loading, but without the accompanying rise in the EOC negative residual reactivity penalty and the loss of fuel pellet thermal conductivity characteristic of Gd_2O_3 addition. At exposures near 60 GWD/MTU the reactivity of the Case 3 assembly actually slightly exceeds the reactivity of the other two cases. The co-location of gadolinium and IFBA provides improved performance over "conventional" poison schemes, and is an important and innovative feature of the extended cycle core design.

In addition to improving the neutronic performance of both poisons, the co-location and use of both gadolinium and IFBA allows for greater flexibility in the design of the reactivity vs. exposure response of a given assembly. Figure 7 below demonstrates the effect that various loadings of Gd_2O_3 and IFBA have on assembly neutronic behavior. This plot shows k_∞ against exposure for Westinghouse 17×17 PWR assemblies under the same conditions described for Figure 6 above. For these comparisons, each assembly contains 44 burnable absorber pins, but the poison contained in these pins varies as follows:

- Case 1: $10^w/_o$ Gd_2O_3, no IFBA.
- Case 2: $10^w/_o$ Gd_2O_3 and a 3.09 mg B^{10}/inch IFBA surface coating
- Case 3: $12^w/_o$ Gd_2O_3, no IFBA.
- Case 4: $12^w/_o$ Gd_2O_3 and a 1.545 mg B^{10}/inch IFBA surface coating.

As shown in the plot, the addition of co-located IFBA to gadolinium poisoned fuel decreases both the initial and peak reactivity of the assembly. However, the use of the fast-burning IFBA also increases the slope of the bundle's reactivity vs. exposure response. A comparison of Cases 1 & 2 to Cases 3 & 4 reveals that the changes in reactivity and reactivity slope increase with increased

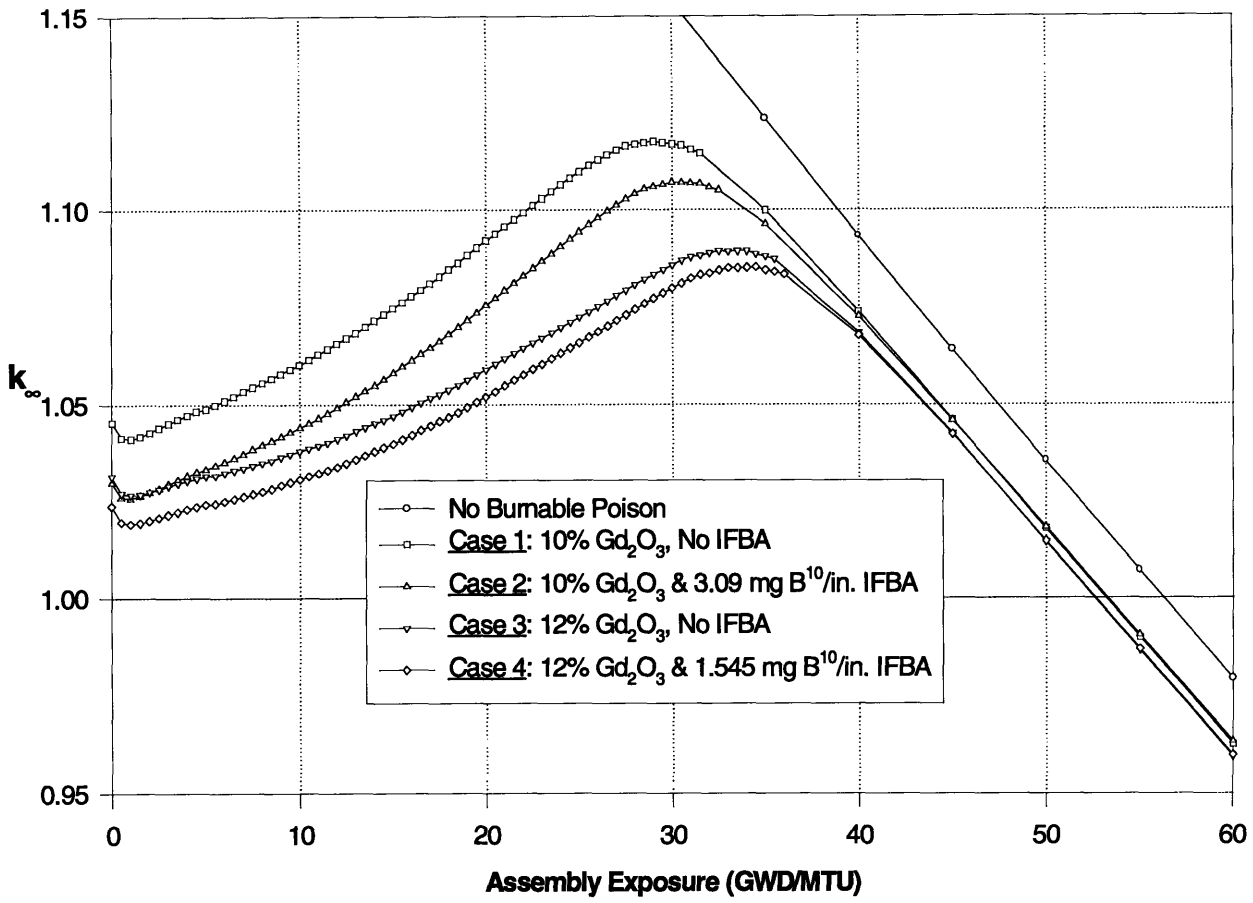

Figure 7: PWR Assembly Reactivity Behavior for Varied Gd_2O_3 & IFBA Loadings

IFBA loading. Raising the Gd_2O_3 loading in the fuel also lowers the initial and peak assembly reactivity, but it lessens the slope of the reactivity response. As noted previously, the higher gadolinium concentration also increases the EOC residual reactivity penalty. Figure 7 shows a reactivity "gap" between the $10^w/_o$ and the $12^w/_o$ Gd_2O_3 cases and between them and the unpoisoned assembly at high exposures. These gaps represent the residual reactivity of the gadolinium and translate into a decrease in the cycle length achievable by a given design. By varying the relative loading of Gd_2O_3 and IFBA within an assembly, the neutronic behavior of the core can be optimized based on the performance parameters of primary importance for a given design. For the extended cycle core design, the $12^w/_o$ Gd_2O_3-1.545 mg B^{10}/inch IFBA poison scheme offers the most promising compromise in the trade-off between peak reactivity, reactivity slope, and achievable cycle length.

5.2.4 Alternative Poisons

Other burnable poison schemes investigated for the PWR included erbium (as erbium oxide, Er_2O_3) and combinations of Er_2O_3 and IFBA. Erbium (atomic number 68) is a rare earth element with six naturally occurring isotopes that is similar in chemical and physical properties to gadolinium. Naturally occurring erbium has a thermal neutron absorption cross-section of 166 barns and a large twin resonance peak at ~0.5 ev [J-1]. Figure 8 compares the total cross-section of Er^{167} (the primary absorber in naturally occurring erbium) and Gd^{157} (the primary absorber in naturally occurring gadolinium) for neutron energies in the thermal range (<1 eV) [R-2]. The fission cross-section for U^{235} is also shown for comparison. The presence of this large resonance peak aids in maintaining a negative MTC within the core. When the neutron energy spectrum hardens due to an increase in moderator temperature, more neutrons become available for absorption in the resonance peak. This contribution to negative MTC is one of the important advantages of using erbium in the long life core design.

Another advantage of erbium stems from its relatively low thermal neutron absorption cross-section. Unlike gadolinium, which requires lumping in order to prevent it from burning out too quickly, erbium, with its lower cross-section, can be uniformly distributed throughout the fuel. The uniform distribution of erbium lowers fuel pin power peaking and reduces the concentration of poison required in each individual fuel rod. This reduction in concentration mitigates the detrimental effects of burnable poison loading on UO_2 thermal conductivity. Er_2O_3 has undergone extensive testing by ABB-Combustion Engineering for use in high burnup PWR fuels. These tests have demonstrated satisfactory performance, and fuel loaded with erbium has been licensed and supplied to operating U.S. plants [J-2]. As mentioned in Chapter 1, ABB-CE's design for a weapons-grade plutonium burning core for their System 80+™ reactor plant uses Er_2O_3 as a distributed burnable poison.

Using evenly distributed Er_2O_3 as a burnable poison in the long-cycle PWR core, a maximum $F_{\Delta H}$ of <1.4 is achievable. However, because of its lower thermal neutron absorption cross-section, erbium depletes more slowly than other poisons, and it therefore exhibits a high negative residual reactivity penalty at EOC. The production of odd isotopes by capture in even isotopes also increases erbium's EOC residual reactivity penalty, as it does for gadolinium. The high residual reactivity of erbium makes it undesirable for use in the PWR extended cycle core design. The

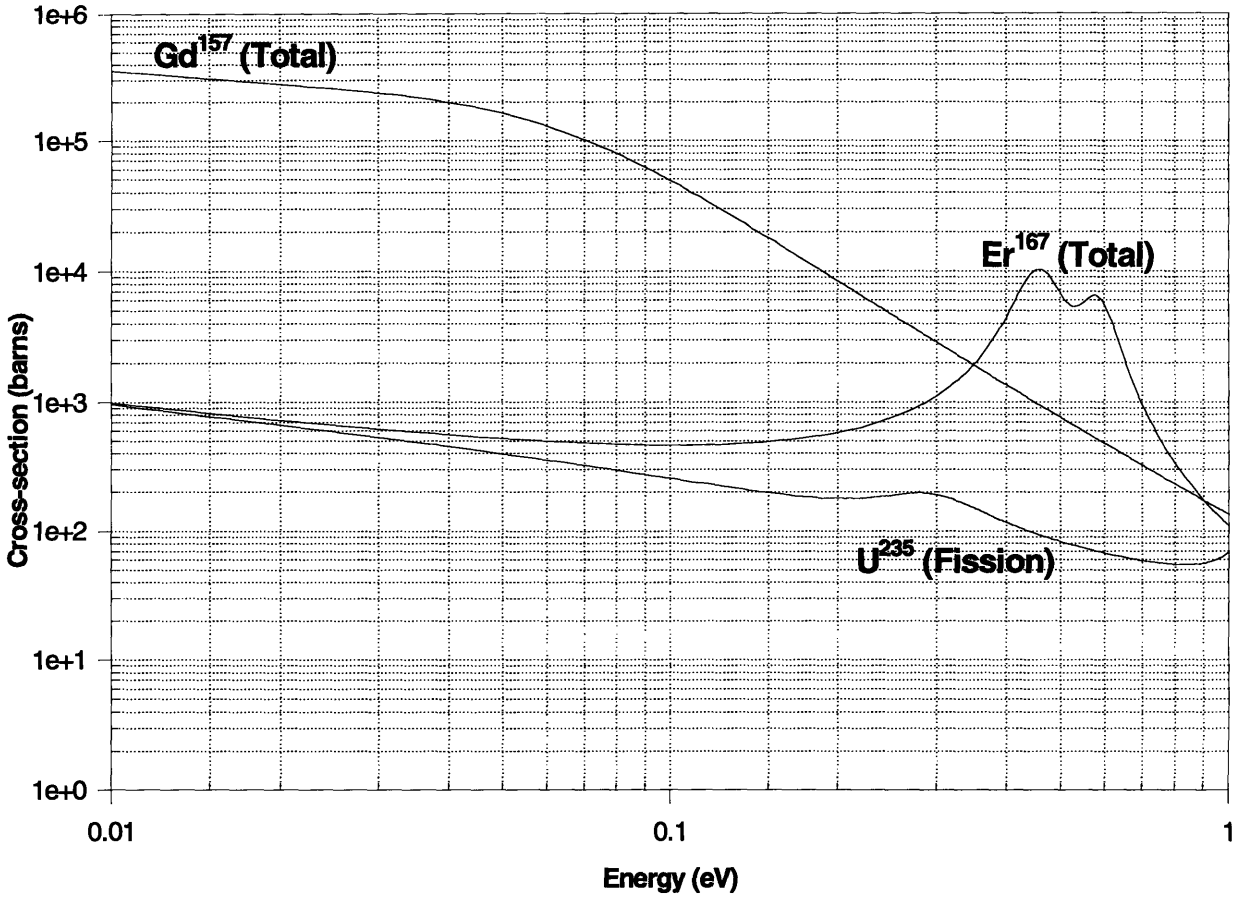

Figure 8: Comparison of Burnable Absorber Cross-sections

large residual reactivity of natural erbium at EOC leads to a decrease in cycle length with increasing initial Er_2O_3 loading. Reducing the initial concentration of Er_2O_3 to extend cycle length results in an unacceptably high CBC. The lowest peak CBC achievable for an erbium poisoned PWR core with a 48 calendar month cycle length was 4366 ppm at a core average exposure of 6 GWD/MTU. Even with the addition of IFBA, a peak CBC of 2726 ppm is reached at 16 GWD/MTU. Increasing the poison concentration to achieve a peak CBC of < 1780 shortens the cycle length to <42 calendar months at the target capacity factor of 87%. Hence erbium was not given further consideration for the present application.

5.3 Interior Assembly Design

5.3.1 Poison Loading Patterns

In a conventional multi-batch operating cycle, fuel managers load assemblies of varying reactivity in complex patterns designed to distribute power evenly throughout the core. Because this fuel is drawn from multiple batches, the reactivity of these assemblies varies due to differences in enrichment, accumulated exposure, and burnable poison loading. For the single batch extended cycle PWR design, only burnable poison loading controls the initial reactivity of the vast majority of the interior (non-peripheral) assemblies in the core. In order to increase cycle length by maximizing the number of fissile atoms loaded into the core, the enrichment of all but 5 of these interior assemblies is a uniform 7% U^{235}. Five of the PWR central fuel assemblies have an enrichment of 6% U^{235} in order to reduce the severity of radial power peaking in the innermost regions of the core. The reactivity of the interior fuel assemblies is varied by changing the number of poisoned pins within each, while maintaining the poison concentration in each pin the same.

Increasing the number of poisoned pins in a fuel bundle exposes more burnable poison to the available neutron flux and thus lowers the assembly's initial reactivity. In the PWR extended cycle design, the core contains five different burnable absorber pin loading patterns. The five different types of assemblies provide the variations in reactivity required to achieve an acceptably uniform power distribution within the core. The number of poisoned pins per assembly varies from 44 in the center of the core to 24 near the core periphery. Figure 9 shows the five burnable absorber loading patterns used in the PWR extended cycle design. These poison patterns maintain octant symmetry and minimize pin-to-pin power peaking within each assembly. Beginning with a given number of poisoned pins (i.e., a desired initial assembly reactivity), each pattern was developed by manually implementing multiple CASMO-3 runs to determine an optimized layout to minimize internal power peaking. In general, the pins containing burnable absorbers are clustered near the assembly guide thimbles in order to reduce the "water-hole peaking" which can result in fuel pins adjacent to empty control rod guide tubes.

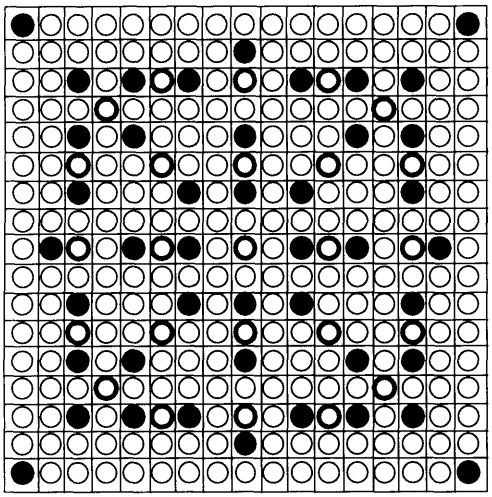

44 Burnable Absorber Pins

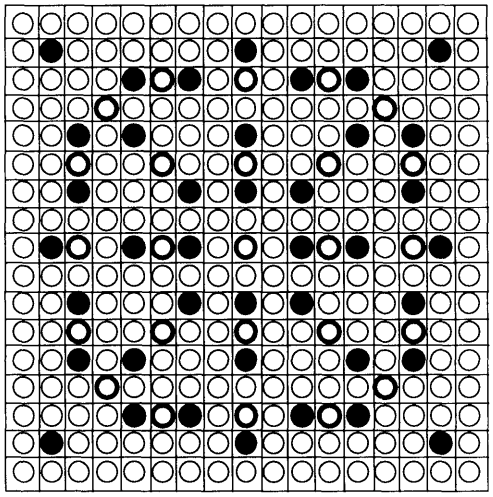

40 Burnable Absorber Pins

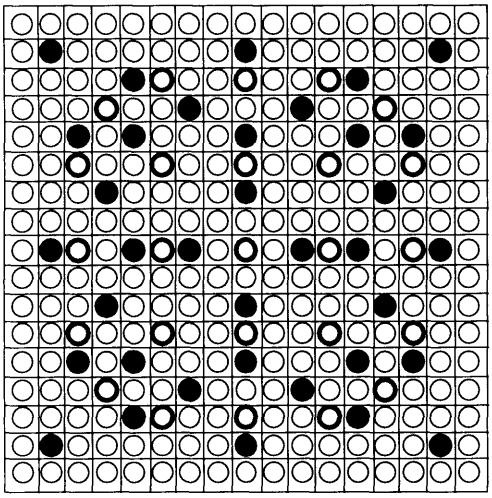

36 Burnable Absorber Pins

Key:

- ○ **7% UO_2 Fuel Pin**
- ● **7% UO_2 Fuel Pin with 12 w/o Gd_2O_3 & IFBA (ZrB_2 Pellet coating)**
- ◎ **Control Rod Guide Tube/ Instrumentation Thimble**

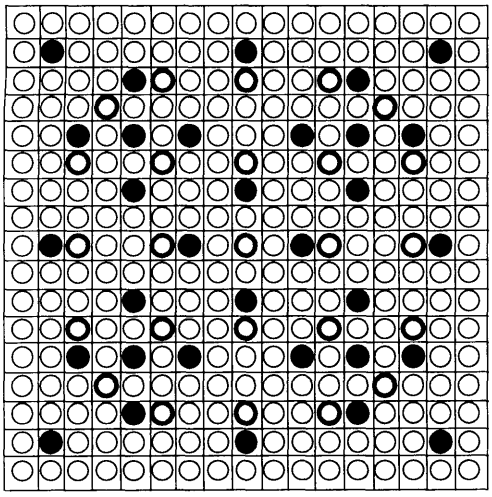

32 Burnable Absorber Pins

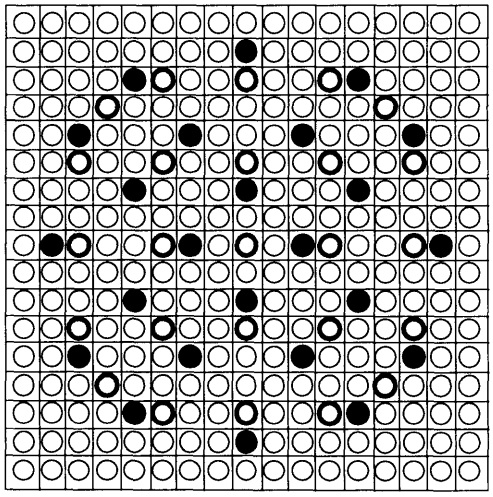

24 Burnable Absorber Pins

Figure 9: Pin Layout for PWR Interior Fuel Assemblies

5.3.2 Poison Pin Structure

As described in earlier sections, the pellets in each burnable absorber pin contain $12^{w}/_{o}$ Gd_2O_3 integrally mixed in with the ceramic UO_2 fuel and a thin surface coating of ZrB_2 (IFBA) with a loading of 1.545 mg B^{10}/in. Because increased concentrations of gadolinium degrade the thermal conductivity of UO_2, $12^{w}/_{o}$ Gd_2O_3 loaded pins will exhibit higher centerline temperatures than unpoisoned pins operating at the same linear heat generation rate. Higher fuel temperatures increase the amount of gaseous fission products released into the fuel-clad gap and can lead to unacceptably high pin internal pressures in Gd_2O_3 loaded fuel rods. To control the peak centerline temperatures in Gd_2O_3 containing pins, standard industry practice has been to load the gadolinium into a UO_2 matrix containing either depleted, natural, or low enriched uranium [D-3]. Typical vendor recommendations for Gd_2O_3 pins limit their enrichment to half of the enrichment assay of the surrounding fuel rods. Reducing the enrichment of the poisoned pins suppresses the power that they generate and thus lowers peak centerline temperature. However, this reduction in enrichment increases assembly pin-to-pin peaking by forcing the distribution of more power into the unpoisoned fuel rods of the assembly. Additionally, lowering the poison pin enrichment removes fissile atoms from the core, thus limiting the achievable cycle length and diminishing the fuel cycle's profitability.

Consequently, in order to maximize cycle energy and improve local power peaking profiles, the Gd_2O_3 pins in the extended cycle PWR core are enriched to same levels as the surrounding unpoisoned fuel rods. To control temperatures, these fully enriched, high Gd_2O_3 loaded pins consist entirely of annular fuel pellets. The ratio of the peak center-to-surface temperature rise of annular to solid fuel pellets having the same diameter and operating at the same linear power can be expressed as [A-1], [T-2]:

$$\frac{\Delta\hat{T}_a}{\Delta\hat{T}_s} = F = 1 - \frac{\ln\left[\left(\frac{d_v}{d_{UO_2}}\right)^2\right]}{\left[\left(\frac{d_v}{d_{UO_2}}\right)^2 - 1\right]} \tag{5.1}$$

where: $\Delta\hat{T}_a$, $\Delta\hat{T}_s$ =Peak center-to-surface temperature rise of annular and solid fuel, respectively

d_{UO_2} = Fuel pellet diameter

d_v = Annular pellet central void diameter

For a void size of 10% pellet volume, (i.e., $(d_v/d_{UO_2})^2 = 0.1$) $F = 0.74$. Thus the temperature rise across a 10% void annular pellet is approximately 25% lower than the rise across a solid fuel pellet generating the same linear power.

The lower temperatures in annular pellets serve to reduce fission gas release and, in conjunction with the increased free volume, reduce internal pressures in the highly poisoned pins [S-6]. The selected void size of 10% pellet volume (void radius = 1.295 mm), as employed in Russian VVÉR-1000 cores, strikes a balance between a large free volume for fission gas expansion and the undesirable rise in assembly peak reactivity resulting from the removal of gadolinium atoms from the fuel as void size increases (a complete discussion of the interaction between core neutronic and fuel performance design goals is contained in Chapter 8). Using CASMO-3, the annular fuel pellets were modeled as solid pellets with a reduced density. The neutronic properties of fuel pellets with internal cavities not containing absorber or moderator are equivalent to those of a solid fuel pellet with an effective fuel density ($\rho^{eff}_{UO_2}$) determined as follows:

$$\rho^{eff}_{UO_2} = \rho^{act}_{UO_2} \cdot \left[1 - \left(\frac{d_v}{d_{UO_2}}\right)^2\right] \tag{5.2}$$

where $\rho^{act}_{UO_2}$ is the actual fuel density of an annular fuel pellet with a diameter d_{UO_2} and a void diameter d_v [P-2].

5.3.3 Assembly Reactivity Behavior

Figure 10 shows the effect of burnup on the reactivity performance of fuel assemblies which are enriched to $7^{w}/_{o}$ U^{235} and which employ the five different poison loading patterns shown in Figure 9. As before, each calculation was made using the "Base Case" parameters listed in Table 3 on page 44 (fuel temperature = 626.9°C, moderator temperature = 310°C, soluble boron concentration = 450 ppm). As expected, the plot shows that for a given fuel enrichment, the initial reactivity of an assembly depends upon the number of burnable absorber pins loaded into it. Increasing the number of burnable poison pins in an assembly augments the amount of burnable poison exposed to the available neutron flux, thus raising the poison's initial reactivity hold-down. For a given fuel enrichment and burnable poison concentration, the initial k_∞ of an assembly varies linearly with the number of burnable poison pins (N_p) that it contains.

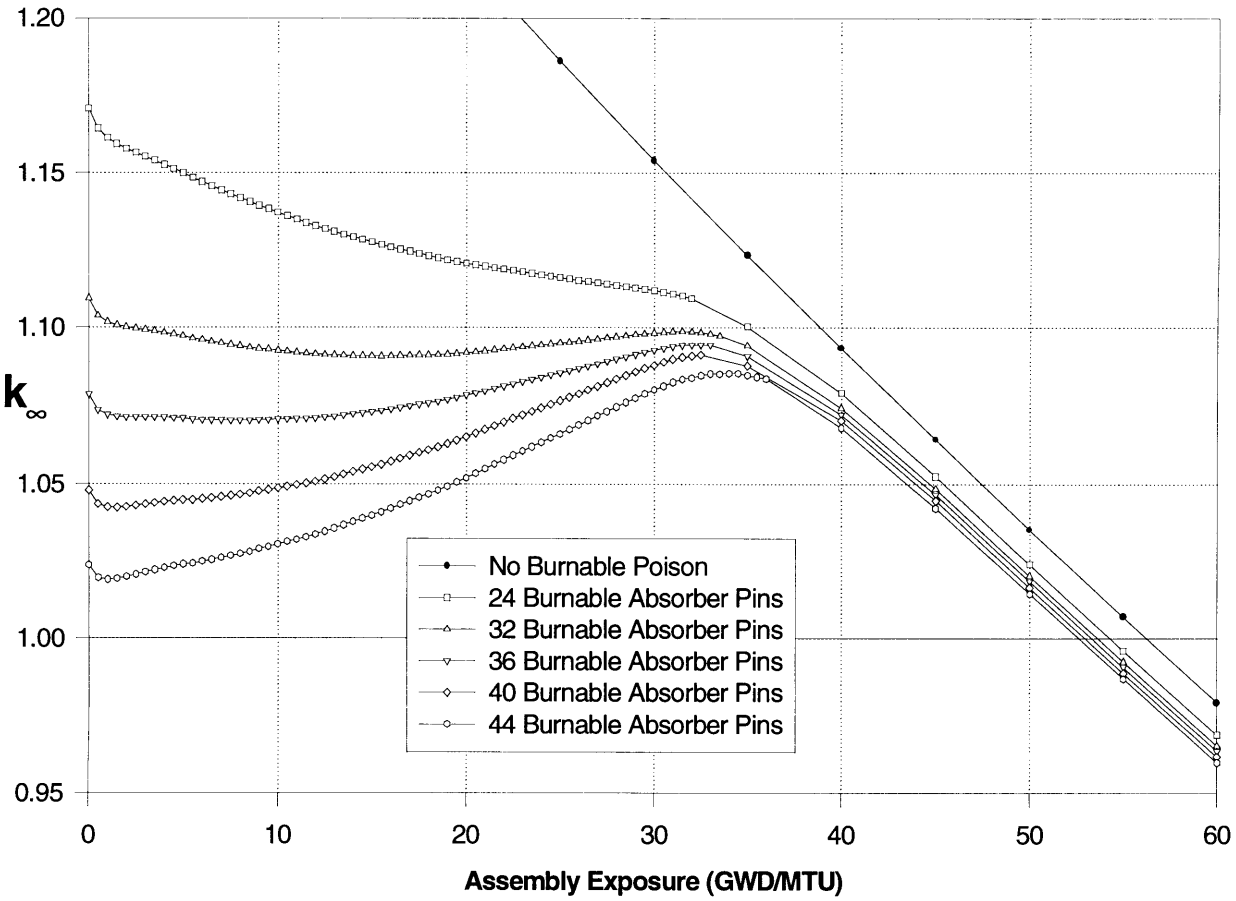

Figure 10: Reactivity Behavior of PWR Interior Fuel Assemblies

This behavior is shown in Figure 11 which plots k_∞ against the number of burnable poison pins for the five assembly types in the extended cycle core containing 7% enriched UO_2. These calculations were made under conditions identical to those described for Figure 10. The fit of data shows the strong linear correlation between initial assembly reactivity (i.e., $\rho = (k-1)/k \approx k-1$) and the number of poisoned pins. Note that for completely "black" poison pins, the initial poison reactivity hold-down is *entirely* a function of the number of burnable absorber pins per fuel assembly and not of the poison concentration in each pin. However, as noted in previous discussions, for the poison concentrations used in the extended cycle core design, the burnable poison pins are not completely black. Figure 12 shows the initial reactivity of a fuel assembly containing 44 burnable absorber pins for increasing concentrations of Gd_2O_3. The concentration of IFBA in each pin is kept the same (1.545 mg B^{10}/in.), and, as before, the CASMO-3 calculations are performed using the Base Case conditions given in Table 3. The figure shows assembly reactivity decreasing with increasing poison concentration (p), with the reactivity

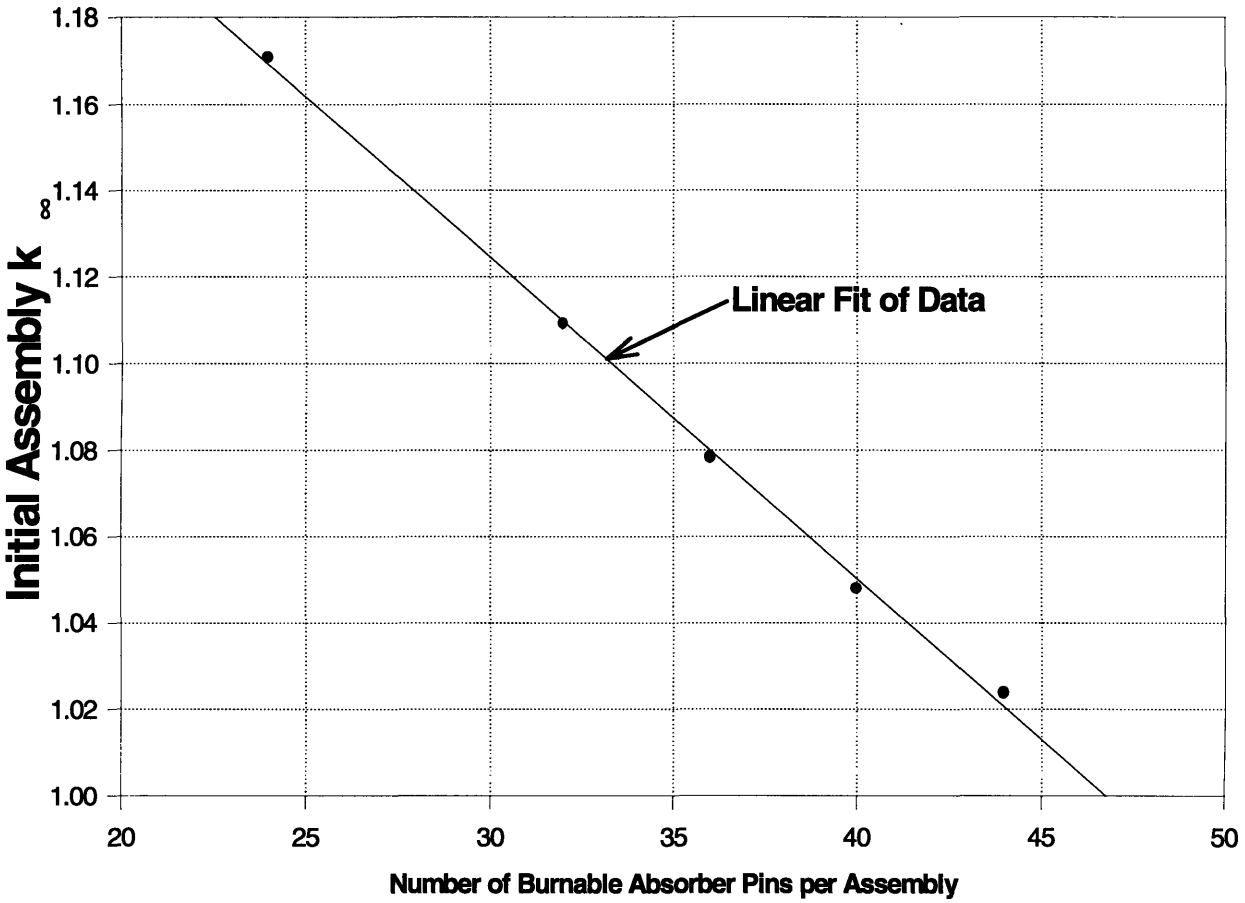

Figure 11: Assembly Initial k_∞ vs. No. of Poisoned Pins

decrement diminishing in magnitude for each addition of Gd_2O_3 to the absorber pins. As the concentration of poison is raised, the attenuation of neutron flux in the burnable absorber pins increases until eventually neutrons are prevented from interacting with the poison in the pin interior. At this point assembly reactivity becomes insensitive to pin poison concentration and must be altered by adding additional burnable absorber pins.

Assembly reactivity behavior with respect to burnup depends upon both poison concentration, p, and the number of poison pins, N_p. The point (time or burnup) at which a neutron poison is depleted depends on its initial concentration. For conditions identical to those described for Figure 12, Figure 13 shows the initial concentration of Gd_2O_3 against the time required to deplete the poison in the assembly for the five poison loading patterns used in the extended cycle core design. In this case, a poison is considered "depleted" when 99.5% of the *original* inventory of Gd^{155} and Gd^{157} have been removed from the fuel, as calculated by CASMO-3. The concentrations of Gd_2O_3

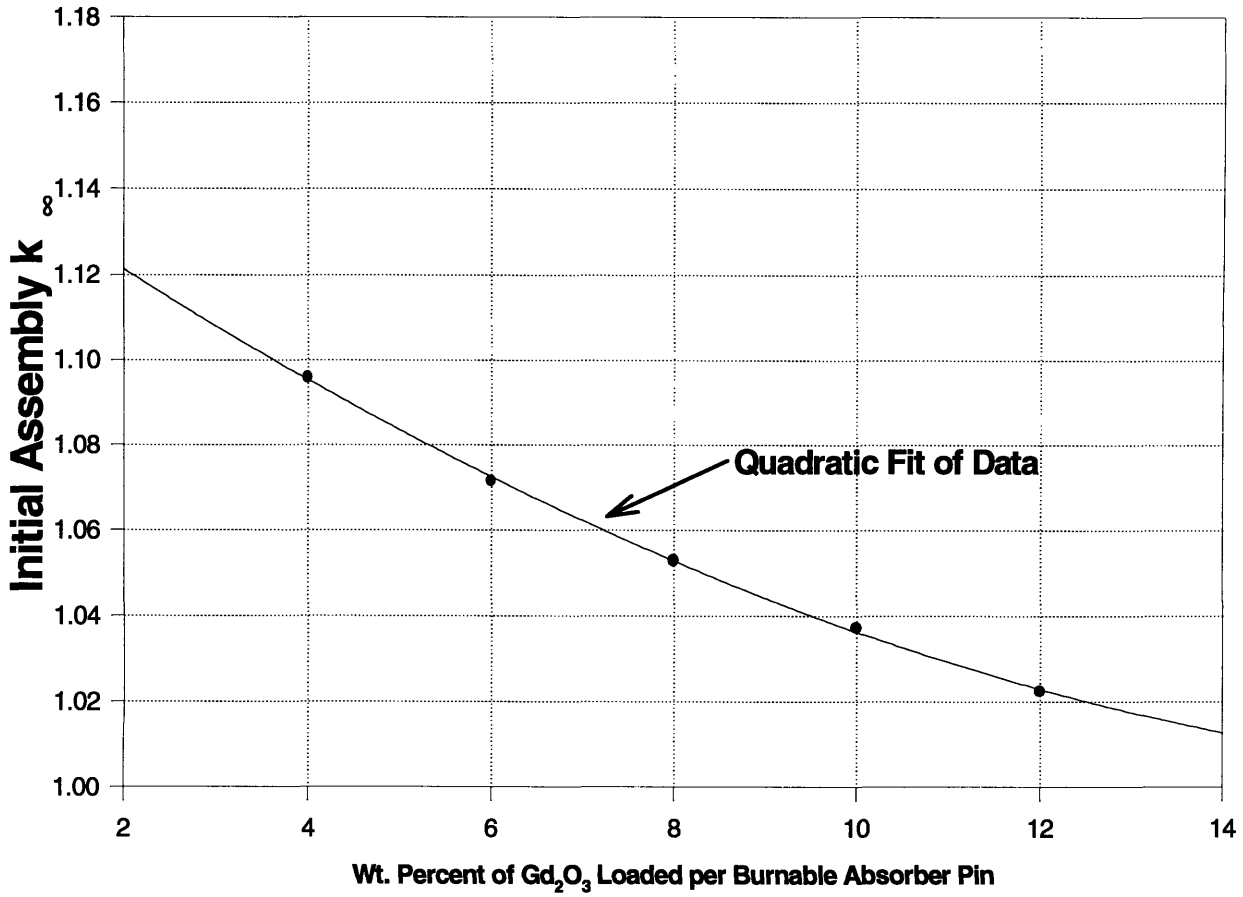

Figure 12: Assembly Initial k_∞ vs. Poison Concentration

analyzed for the plot range from $4^{w}/_{o}$ - $12^{w}/_{o}$. While there is some scattering in the data for the different loading patterns, the figure shows the strong linear correlation between the initial concentration of a poison, p, and its time to depletion. Although the $12^{w}/_{o}$ Gd_2O_3 poisoned fuel bundles in the extended cycle core deplete at roughly the same amount of exposure, the magnitude of the change in reactivity experienced during this time varies widely from assembly to assembly. Increasing N_p in an assembly exposes more poison to the available neutron flux and thus increases the magnitude of the change in poison reactivity for a given amount of exposure. In Figure 10, the slope of the 44 BA pin assembly is initially positive, indicating that the poison is depleting faster than the fissile atoms in the fuel and thus causing an increase in reactivity. As N_p decreases, the initial slope of each assembly's reactivity response lessens in magnitude as less poison is exposed to neutron flux. Eventually, when $N_p = 24$, the initial slope is actually negative, indicating that the fuel is now depleting faster than the burnable neutron absorbers.

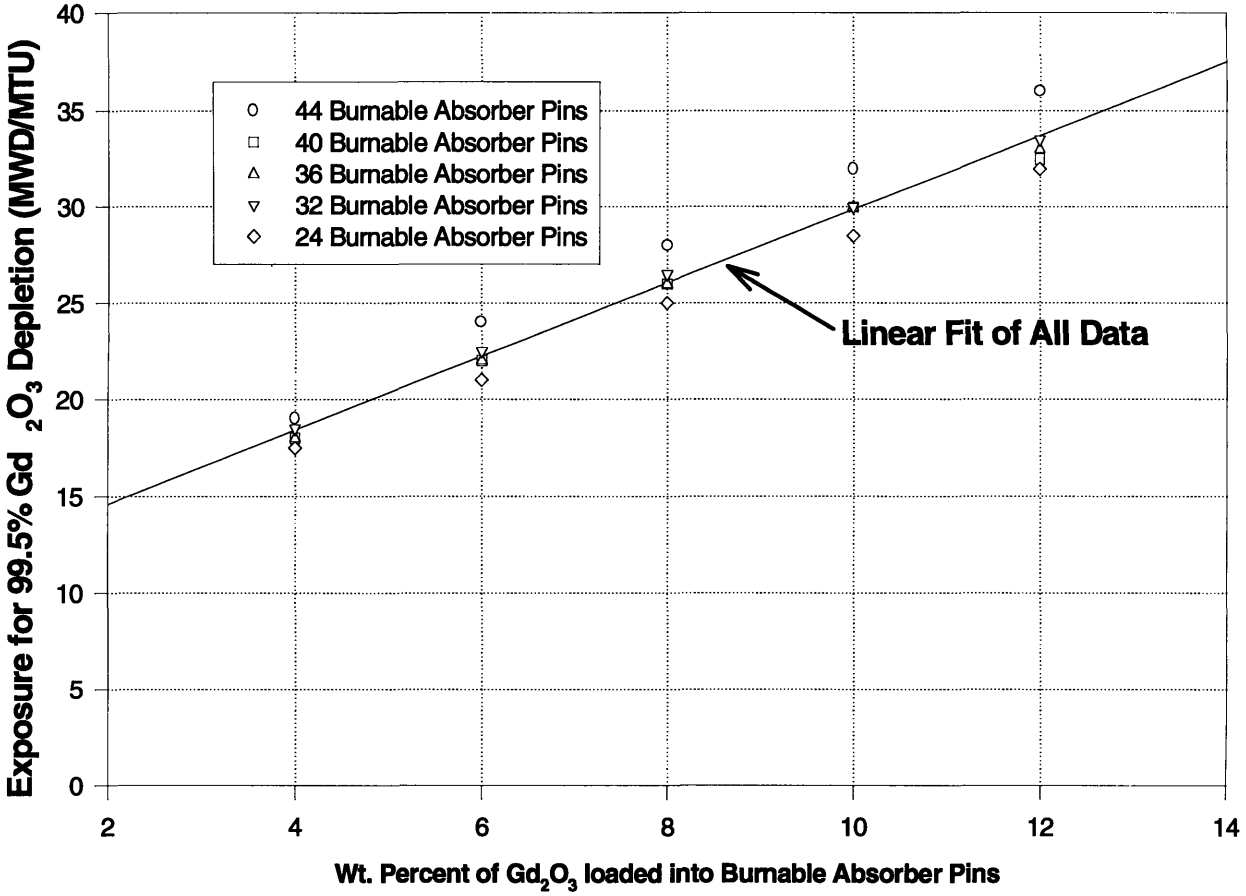

Figure 13: Gd_2O_3 Depletion Exposure vs. Initial Concentration

One final characteristic of each assembly is its EOC residual reactivity penalty compared to the unpoisoned case. Figure 10 shows that this penalty (represented by the vertical distance between the unpoisoned and poisoned cases at high burnup) increases with N_p. The residual reactivity penalty rises with N_p primarily due to the removal of fissile atoms from the assembly when an unpoisoned fuel rod is replaced with a poisoned one. Since poison atoms replace fuel atoms in the pellets, pins containing $12^w/_o$ Gd_2O_3 only hold $88^w/_o$ UO_2. Additionally, since unpoisoned fuel is solid, and poisoned fuel is in 10% central void annular pellets, the number of fissile atoms in a burnable absorber pin is further reduced. Because of this an annular poisoned fuel pin enriched to $7^w/_o$ U^{235} contains the same number of fissile atoms as a solid unpoisoned fuel pin enriched to only $5.6^w/_o$ U^{235}. This reduction in the "effective" enrichment of the poisoned pins causes a decrease in reactivity at EOC. Residual reactivity is also due to the production of new odd atomic number isotopes (e.g., Gd^{157}) by neutron capture in their even precursors (e.g., Gd^{156}).

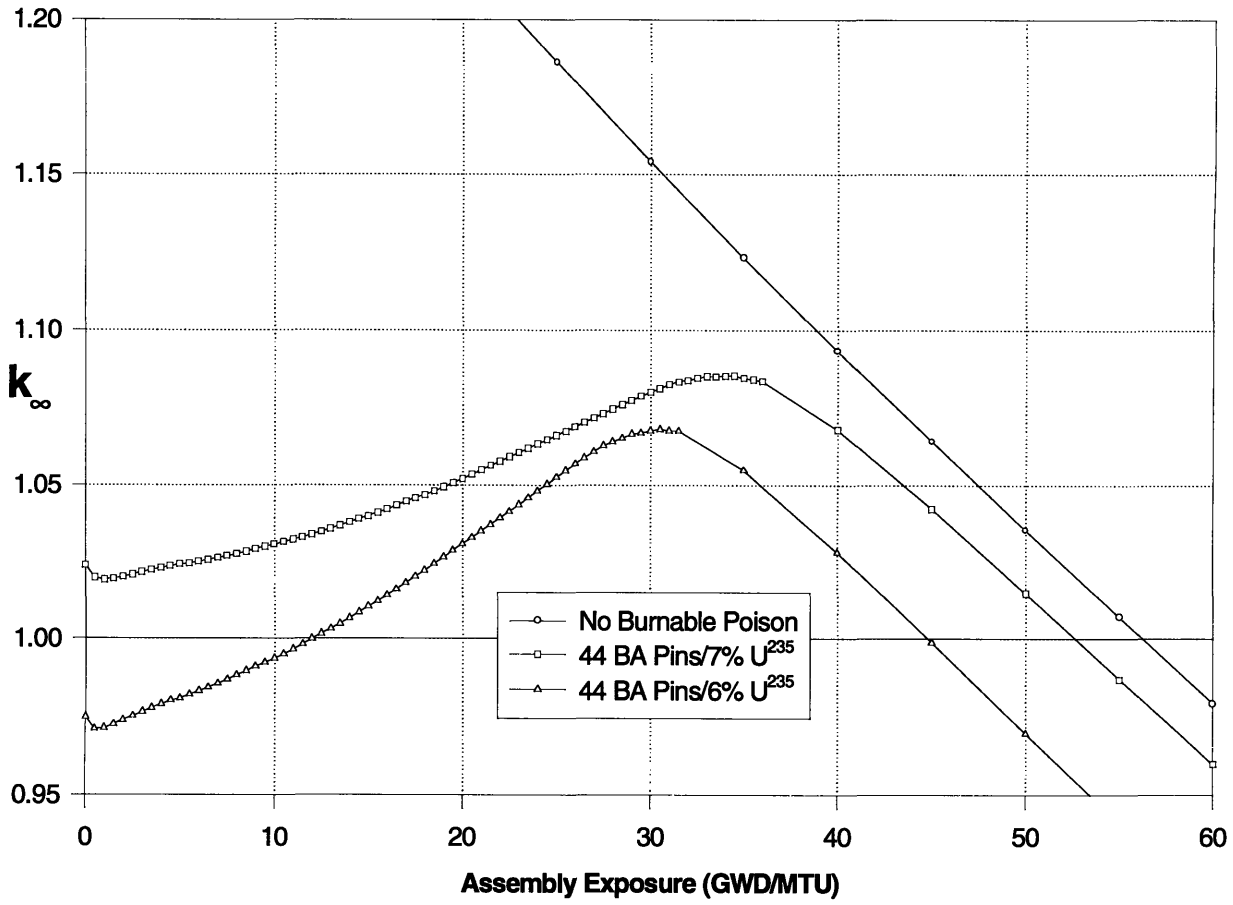

Figure 14: PWR Assembly Reactivity Response to Changes in Fuel Enrichment

The effects of changes in enrichment on assembly reactivity behavior can be seen in Figure 14. This plot compares the reactivity behavior of an assembly with an enrichment of $7^{w}/_{o}$ U^{235} to one enriched to $6^{w}/_{o}$ U^{235}. The PWR extended cycle design uses 5 assemblies enriched to $6^{w}/_{o}$ U^{235} to control power peaking in the most reactive regions of the core. Both types of assemblies shown in Figure 14 contain 44 burnable absorber pins. As shown in the figure, reducing assembly enrichment lowers both initial and peak reactivity in the same manner as an increase in poison concentration (compare Cases 1 & 3 in Figure 7 on page 55). However, unlike an increase in poison concentration, a decrease in enrichment causes assembly peak reactivity to occur earlier rather than later in life. Because neutrons entering a poison pin are attenuated by both poison atoms *and* fissile nuclei, a drop in the fuel enrichment reduces poison pin self-shielding and causes the neutron absorbers in the fuel to burn out more rapidly.

5.3.4 Axial Blankets

In a typical large PWR, approximately 4% of all neutrons are lost due to axial and radial leakage [P-3]. To improve the economic performance of the PWR extended cycle core design, all interior assemblies make use of annular axial fuel blankets. Annular axial blankets are regions of reduced enrichment annular fuel at the top and bottom of each assembly. Reducing the enrichment in these outlying areas drives down the power generated there, thus reducing leakage and improving neutron economy. Since reduced enrichment fuel is less expensive to manufacture, the employment of axial blankets also lowers up-front fuel costs. Additionally, the use of 10% void annular fuel in these blankets offers an increased expansion volume for fission gases released during burnup. This larger volume lowers pin internal pressure and offers a greater margin to fuel mechanical performance limits. Axial blankets create an economic advantage by allowing a reduction in fuel costs without a significant negative impact on cycle length or plant thermal margins. A blanket length of 15.24 cm for the top and bottom of the core was selected for the PWR extended cycle design, based on Westinghouse analyses which show that this length provided the optimum trade-off between reducing leakage and minimizing the volume of low-reactivity blanket material. [S-5], [S-7].

Westinghouse studies also demonstrated that for high burnup cores (such as the PWR extended cycle design) natural uranium blankets do not achieve optimum economic performance. Comparative analyses showed that blankets of higher enrichment were optimal for high discharge burnup applications because (for a central zone enrichment of $4.8^{w}/_{o}$ U^{235}) the Separative Work Unit (SWU) savings in the blanket region were negated by the increased central zone SWU requirements for blanket enrichments below ~$2.5\ ^{w}/_{o}$ U^{235}. For the PWR core design modeled in this study, axial blankets of various enrichments were analyzed in order to determine the economically optimum blanket enrichment for a core with a central zone enrichment of $7.0\ ^{w}/_{o}$ U^{235}. Based on the Westinghouse example of a minimum blanket enrichment approximately equal to one-half of the central zone enrichment, axial blankets of enrichments $3.5^{w}/_{o}$ to $6.5^{w}/_{o}$ U^{235} were modeled and compared. The results of these comparisons are shown in Table 4.

These results illustrate the effects of changes in axial blanket enrichment on cycle length, peak Critical Boron Concentration, maximum enthalpy rise hot channel factor ($F_{\Delta H}$), and total power peaking factor (F_Q). The table shows the change from the base case and indicates the time in core

life (in GWD/MTU of core-average burnup) when these peak values occurred. Figure 15 plots the percentage change of each of these parameters as a function of blanket enrichment; the calculations were performed using SIMULATE-3 to compare the performance of mid-enriched blankets against a base case with a "blanket" enriched to $7^{w}/_{o}$ U^{235}. In each case the blanket region consisted of 15.24 cm of 10% void annular fuel at the top and bottom of each fuel assembly. All burnable poisons were removed from the axial blanket regions to reduce assembly axial power peaking.

Table 4: Comparison of PWR Axial Blanket Enrichments

Axial Blanket Enrichment	ΔCycle Length	ΔPeak CBC (Time of Peak)	$\Delta F_{\Delta H}$ (Time of Peak)	ΔF_{Q} (Time of Peak)
$3.5^{w}/_{o}$ U^{235}	-1.3 EFPM	-95 ppm (23 GWD/MTU)	+1.21% (0 GWD/MTU)	+1.20% (36 GWD/MTU)
$4.5^{w}/_{o}$ U^{235}	-0.9 EFPM	-76 ppm (23 GWD/MTU)	-0.06% (0 GWD/MTU)	+1.03% (36 GWD/MTU)
$4.75^{w}/_{o}$ U^{235}	-0.8 EFPM	-72 ppm (23 GWD/MTU)	-0.38% (0 GWD/MTU)	+1.03% (36 GWD/MTU)
$5.0^{w}/_{o}$ U^{235}	-0.7 EFPM	-68 ppm (24 GWD/MTU)	-0.77% (0 GWD/MTU)	+0.94% (36 GWD/MTU)
$5.25^{w}/_{o}$ U^{235}	-0.6 EFPM	-63 ppm (24 GWD/MTU)	-0.83% (30 GWD/MTU)	+0.86% (36 GWD/MTU)
$5.5^{w}/_{o}$ U^{235}	-0.5 EFPM	-58 ppm (24 GWD/MTU)	-0.70% (30 GWD/MTU)	+0.77% (36 GWD/MTU)
$6.0^{w}/_{o}$ U^{235}	-0.4 EFPM	-42 ppm (0 GWD/MTU)	-0.32% (30 GWD/MTU)	+0.73% (36 GWD/MTU)
$6.5^{w}/_{o}$ U^{235}	-0.2 EFPM	-22 ppm (0 GWD/MTU)	-0.13% (30 GWD/MTU)	+0.73% (36 GWD/MTU)
$7.0^{w}/_{o}$ U^{235}	0.0 EFPM	0 ppm (0 GWD/MTU)	0% (31 GWD/MTU)	0% (36 GWD/MTU)

The figure shows that as axial blanket enrichment is reduced below central zone enrichment, peak CBC drops due to the removal of fissile atoms from the reactor. Lowering blanket enrichment also increases F_Q by driving power into the central regions of the core. As fissile atoms are removed from the ends of the fuel rods, the axial power profile of the pins becomes more peaked in the center. Additionally, decreasing the blanket region enrichment negatively impacts cycle

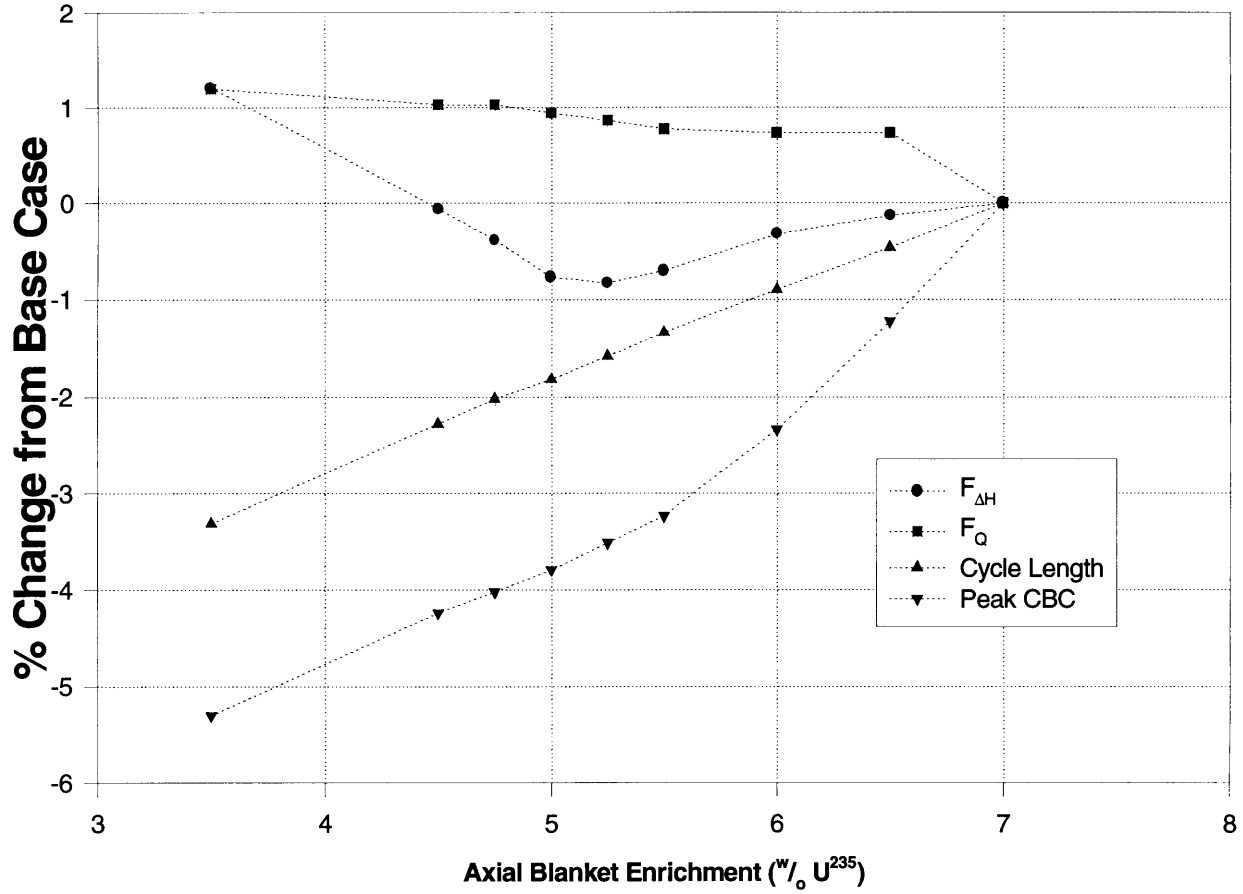

Figure 15: PWR Axial Blanket Enrichment Optimization

length, as the loss of fissile atoms from this area lowers EOC core reactivity. The effect of blanket enrichment on $F_{\Delta H}$ is more complex. Because neutron importance is higher in the center of the core, uniform changes in axial blanket enrichment produce core reactivity changes of greater magnitude in interior assemblies than in peripheral assemblies. Thus for the present core loading, an increase in axial blanket enrichment shifts reactivity (and therefore power) toward the center of the core. For axial blanket enrichments at or below $5^{w}/_{o}$ U^{235} the peak $F_{\Delta H}$ occurs in the core periphery and takes place at BOC. Increasing axial blanket enrichment up to $5^{w}/_{o}$ U^{235} causes a decrease in $F_{\Delta H}$ by shifting reactivity (and power) away from the periphery and into the center of the core. At an axial blanket enrichment of $5.25^{w}/_{o}$ U^{235}, the relative decrease in peripheral reactivity causes $F_{\Delta H}$ to shift to the center of the core and to take place at mid-cycle. Raising axial blanket enrichment higher than $5.25^{w}/_{o}$ U^{235} increases $F_{\Delta H}$ by forcing more power into the core's interior.

Thus, among the cases compared in this study, the $5.25^{w}/_{o}$ U^{235} axial blanket produces the lowest value of $F_{\Delta H}$ while still decreasing core SWU requirements (and thus fuel costs) with a minimal reduction in the operating cycle length. Raising blanket enrichment higher than $5.25^{w}/_{o}$ U^{235} reduces F_Q, but it raises $F_{\Delta H}$ and increases fuel costs. Reducing blanket enrichment below $5.25^{w}/_{o}$ U^{235} lowers fuel costs, but it also decreases cycle length and the margin to core thermal limits by increasing F_Q and $F_{\Delta H}$. Therefore, unpoisoned annular axial blankets with an enrichment of $5.25^{w}/_{o}$ U^{235} were selected for use in the extended cycle PWR core design to reduce fuel costs and $F_{\Delta H}$ at the tolerable expense of increased total power peaking.

5.4 Peripheral Assembly Design

5.4.1 Radial Leakage in PWRs

Reducing the radial leakage in a PWR provides a similar improvement in uranium utilization and decrease in fuel cycle costs as reducing the axial leakage. Moreover, diminishing the radial neutron leakage from the core can extended the effective lifetime of the plant by lowering the rate of neutron embrittlement of the reactor pressure vessel (RPV). Neutron radiation bombarding the reactor pressure vessel changes the crystalline structure of its steel, raising the temperature at which the material makes the transition from being brittle to being ductile. A high transition temperature makes the reactor vessel more susceptible to failure from Pressurized Thermal Shock (PTS). In a PTS failure scenario, a PWR operating at normal temperatures and pressures undergoes a rapid cooldown followed by a primary system repressurization. Rapidly cooling the RPV induces thermal gradients along its inner wall, which produce large tensile stresses. If severe enough, this thermal shock can cause cracking in embrittled welds which hold the RPV together [B-1]. Already, concern over RPV weld embrittlement has forced at least one U.S. utility to plan for an expensive RPV thermal annealing in order to avoid premature shutdown [C-1]. Thermal annealing, which restores ductility to the vessel's steel by gradually raising and lowering its temperature, requires that the reactor be shut down and the RPV emptied and drained. As many U.S. plants approach the end of their license life (and consider license extension), slowing the rate of RPV neutron embrittlement by reducing radial leakage becomes increasingly important economically.

From a fuel management perspective, the simplest method of decreasing radial leakage is to reduce the fraction of core power generated in the peripheral assemblies. In conventional multi-batch fuel management, radial leakage can be controlled by arranging the fuel into a Low Leakage Loading Pattern (L^3P). In this scheme, fresh fuel is placed preferentially in the interior of the core and partially burned fuel is loaded into the periphery. Placing the more reactive fresh fuel in the center of the core draws power away from the periphery, reducing leakage and improving overall neutron economy. Although (as with axial blankets) the use of the L^3P increases total power peaking, the overall advantages of this strategy make it an attractive and popular choice for cost-driven fuel managers.

Obviously, with the batch-loaded extended operating cycle core design, the L^3P strategy cannot be implemented. SIMULATE-3 models of a batch-loaded long cycle PWR core predict an average discharge burnup for the 44 peripheral assemblies of 30.4 GWD/MTU. This corresponds to a cycle average normalized power of 0.65 for these assemblies, compared to a typical value of 0.4 for the peripheral assemblies in L^3P cores [S-8]. As expected, the peripheral assemblies in the batch-loaded design generate a larger fraction of core power than the peripheral assemblies in a conventional 18-month core utilizing the L^3P strategy. This higher peripheral power translates into more neutron leakage, a greater EOC leakage reactivity penalty, and a faster rate of neutron embrittlement for the RPV. Suppressing power in the periphery with increased burnable poison loading reduces radial leakage, but it hampers the core's economic performance by decreasing the fuel utilization in these assemblies.

SIMULATE-3 models show that with the PWR core exterior running at 2/3 of reactor average power, the peripheral assemblies reach an average discharge burnup that is 40% lower than that achieved by the interior fuel bundles (30.4 GWD/MTU vs. 51.8 GWD/MTU respectively, at a core-average discharge burnup of 47 GWD/MTU). From an economic point of view, while the cost of a peripheral assembly is roughly equal to that of an interior assembly, the amount of energy (and therefore revenue) extracted from these assemblies is significantly reduced. Thus the underutilization of the peripheral assemblies has an adverse effect on the economic viability of the extended cycle PWR design. Additionally, these under-burned assemblies will be discharged with a much higher reactivity than the assemblies from the core interior. This increased reactivity raises criti-

cality control concerns in the storage and shipping of spent nuclear fuel. Consequently, a strategy for countering these concerns was devised.

5.4.2 Radial Blanket Assemblies

5.4.2.1 Description

To reduce vessel fluence and to increase the economic viability of the PWR extended cycle design, the concept of a peripheral partial natural uranium Radial Blanket Assembly (RBA) was developed. The RBA concept had previously been explored by Westinghouse as an alternative to loading highly burned fuel assemblies on the core periphery. The RBA developed by Westinghouse consisted of a 17×17 full assembly with 10 rows of enriched uranium and 7 rows natural uranium. Compared to an all natural uranium assembly, this heterogeneous design maximizes leakage reduction while allowing the greater control of radial power peaking. The natural uranium exterior of the RBA effectively attenuates fast flux to the reactor pressure vessel and reduces the SWU requirement and the fuel costs of the core. Westinghouse analyses showed similar reductions in radial leakage and fuel costs for cores using RBAs and for cores implementing a standard L^3P fuel management strategy [P-3]. By using RBAs the benefits of a low leakage core can be achieved, thus mitigating the problems of increased pressure vessel exposure and peripheral assembly underutilization in the uni-batch extended cycle PWR core design.

5.4.2.2 RBA Modeling Using CASMO/SIMULATE

To determine the optimum peripheral assembly design for the higher enrichment extended cycle PWR core, the effects of changing the number of rows of natural uranium pins in the RBAs were analyzed using CASMO and SIMULATE. These comparisons were made using a full core, three-dimensional model in which the only parameter changed from case to case was the number of rows of natural uranium pins in the RBAs. The remaining fuel pins in each RBA consisted primarily of unpoisoned, 10% central void annular fuel pellets enriched to $7^{w}/_{o}$ U^{235}. The enriched pins use annular fuel in order to achieve a wetter lattice and to improve uranium utilization in the RBAs. Note that the enriched pins also have a 15.24 cm annular axial blanket of reduced enrichment fuel at the top and bottom, while the natural uranium pins remain axially uniform. The comparisons were made by varying the number of natural uranium pin rows in each RBA from three to eight. The values of cycle length, CBC, $F_{\Delta H}$, and F_Q for each case were compared to the

base case values of the original Westinghouse design containing seven rows of natural uranium pins. The results of these models are summarized in Table 5. As in the comparison of axial blanket enrichments, the table shows the change from the base case and indicates the time in core life (in GWD/MTU of core-average burnup) when these peak values occurred

Figure 16 shows the percentage change against the base case of the parameters listed as a function of the number of natural uranium pin rows in each RBA. The figure shows that decreasing the number of rows of natural uranium pins from the base case value lengthens the achievable operating cycle and raises the peak CBC. These changes result from the increase in core fissile atom loading caused by the replacement of natural uranium fuel pins with enriched pins. Removing natural uranium pins from the RBAs also causes a reduction in the core total power peaking factor, F_Q. As more enriched fuel is added to the RBAs, a higher fraction of core total power is generated in the periphery. This shift of power to the cores's exterior reduces total peaking through two different mechanisms. First, the shift to the peripheral assemblies simply draws power

Table 5: Comparison of PWR RBA Designs

Natural Uranium Fuel Pin Rows	ΔCycle Length	ΔPeak CBC (Time of Peak)	$\Delta F_{\Delta H}$ (Time of Peak)	ΔF_Q (Time of Peak)
3	+1.5 EFPM	+111 ppm (0 GWD/MTU)	-3.07% (0 GWD/MTU)	+1.30% (37 GWD/MTU)
4	+1.1 EFPM	+27 ppm (24 GWD/MTU)	-6.55% (0 GWD/MTU)	-1.30% (36 GWD/MTU)
5	+0.7 EFPM	+19 ppm (23 GWD/MTU)	-1.92% (0 GWD/MTU)	-1.05% (35 GWD/MTU)
6	+0.4 EFPM	+10 ppm (23 GWD/MTU)	-6.79% (25 GWD/MTU)	-0.63% (35 GWD/MTU)
7	0.0 EFPM	0 ppm (22 GWD/MTU)	0.0% (0 GWD/MTU)	0.0% (34 GWD/MTU)
8	-0.4 EFPM	-13 ppm (22 GWD/MTU)	+1.68% (0 GWD/MTU)	+1.05% (20 GWD/MTU)

away from the center assemblies in which the highest total power peaking occurs. Less obviously, increasing the fraction of power generated in the RBAs also diminishes F_Q by reducing the *axial* power peaking in the core.

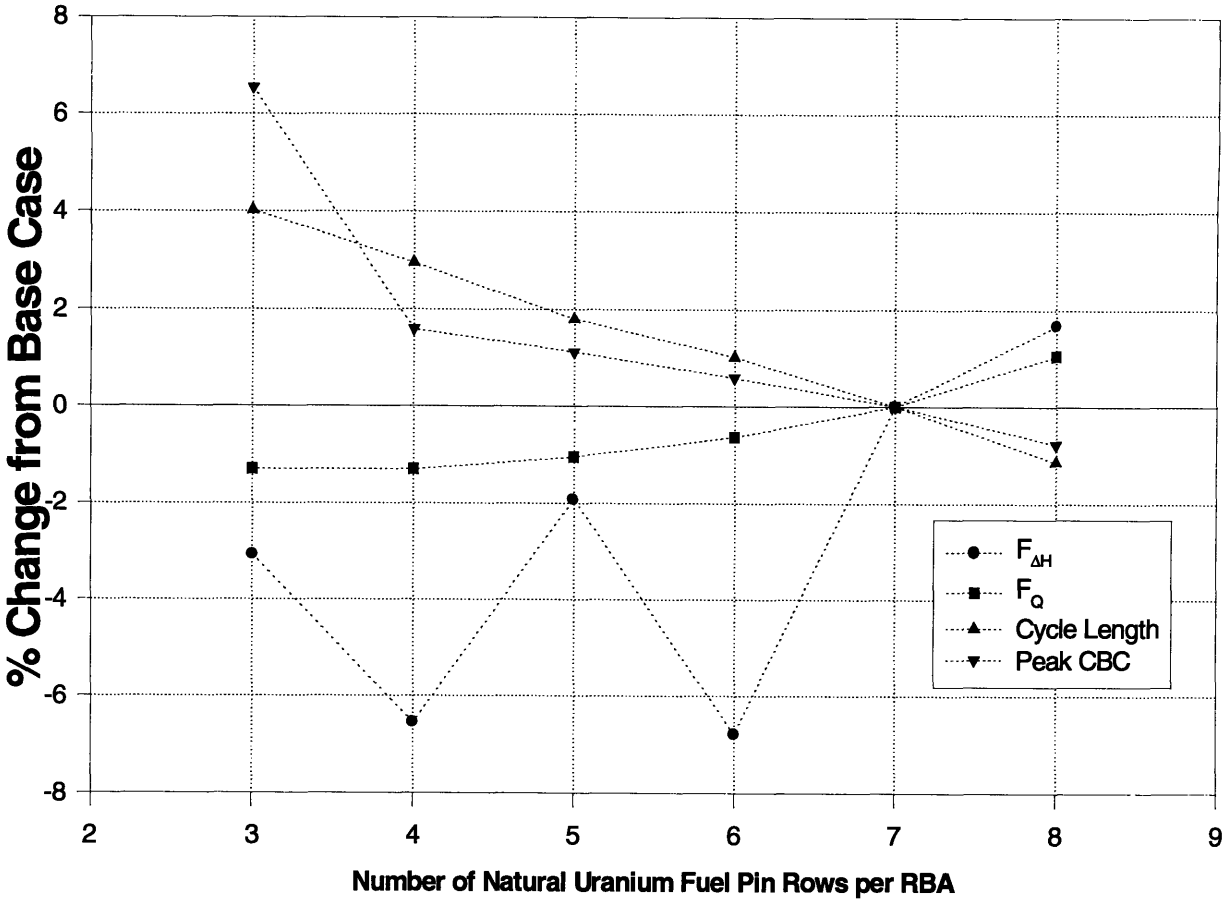

Figure 16: PWR Radial Blanket Assembly Optimization

Figure 17 shows the effect of burnup on the reactivity performance of an RBA containing 4 rows of natural uranium pins and an interior assembly with $7^{w}/_{o}$ U^{235} and 44 burnable poison pins. As before, these CASMO-3 calculations were made using the Base Case parameters given in Table 3. The nearly linear decrease in RBA reactivity in response to burnup contrasts sharply with the initial positive slope of the interior assembly's reactivity curve. This rise in reactivity with burnup increases the severity of axial power peaking in the heavily poisoned interior assemblies of the extended cycle core. At BOC, the axial power distribution in a typical fuel assembly assumes a chopped cosine shape. Power peaks in the center and is depressed at the ends due to leakage and the use of reduced enrichment axial blankets. This power distribution will peak in the bottom half of the core when operating with a negative MTC. In assemblies with a positive reactivity-burnup slope, the faster burning center portions of the assembly gain reactivity more rapidly than the slower burning ends. Increased relative reactivity in the center causes this high power region to burn even more intensely and leads to more severe assembly axial power peaking. Note that since

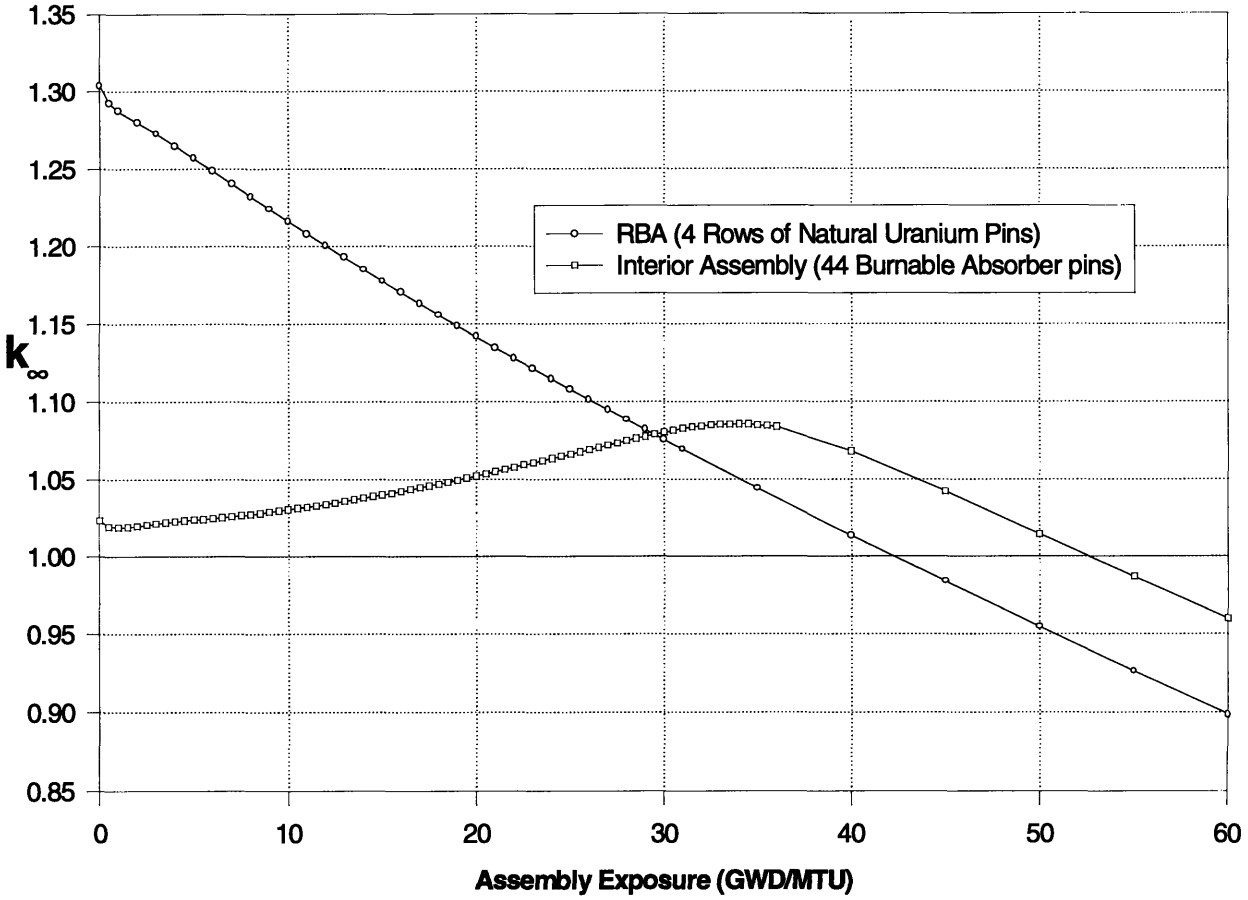

Figure 17: RBA and Interior Assembly Reactivity Behavior

the positive reactivity slope disappears at higher levels of burnup, this effect is strongest in the early portions of the operating cycle. This "positive reactivity feedback" amplifies the normal variations in the assembly power distribution to create exaggerated axial power peaking in the center of the core. In contrast, the unpoisoned RBAs operate in a "negative reactivity feedback" regime in which the regions with the highest initial power peaking lose reactivity and power in response to burnup.

These burnup induced changes in assembly axial power distribution are illustrated in Figure 18 and Figure 19. The figures show SIMULATE-3 calculations of assembly normalized axial power for an interior assembly with 44 burnable absorber pins and for an RBA containing 4 rows of natural uranium pins. Assembly power is calculated both at BOC and at the time when the core-wide axial power distribution first achieves a maximum peak (B_c = 21 GWD/MTU). At this point in the operating cycle the interior assembly and the RBA have accumulated nearly identical

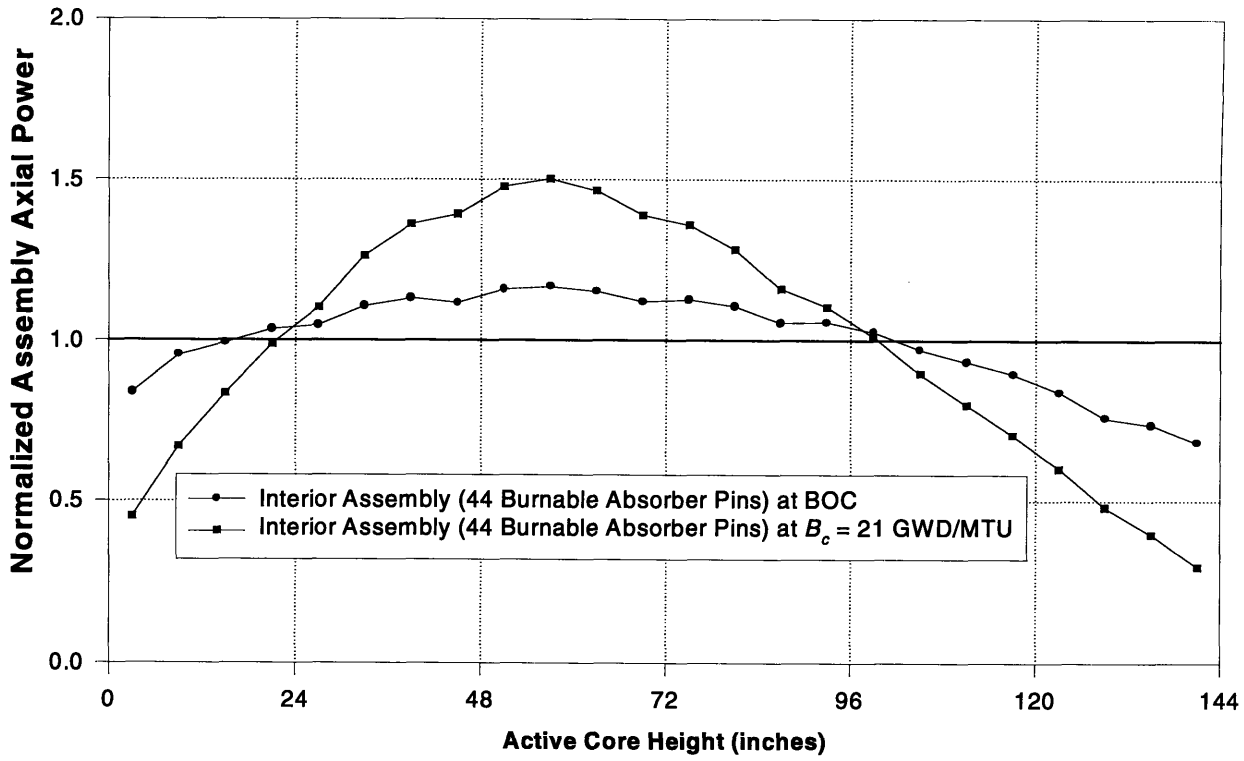

Figure 18: Burnup Induced Changes in PWR Interior Assembly Axial Power

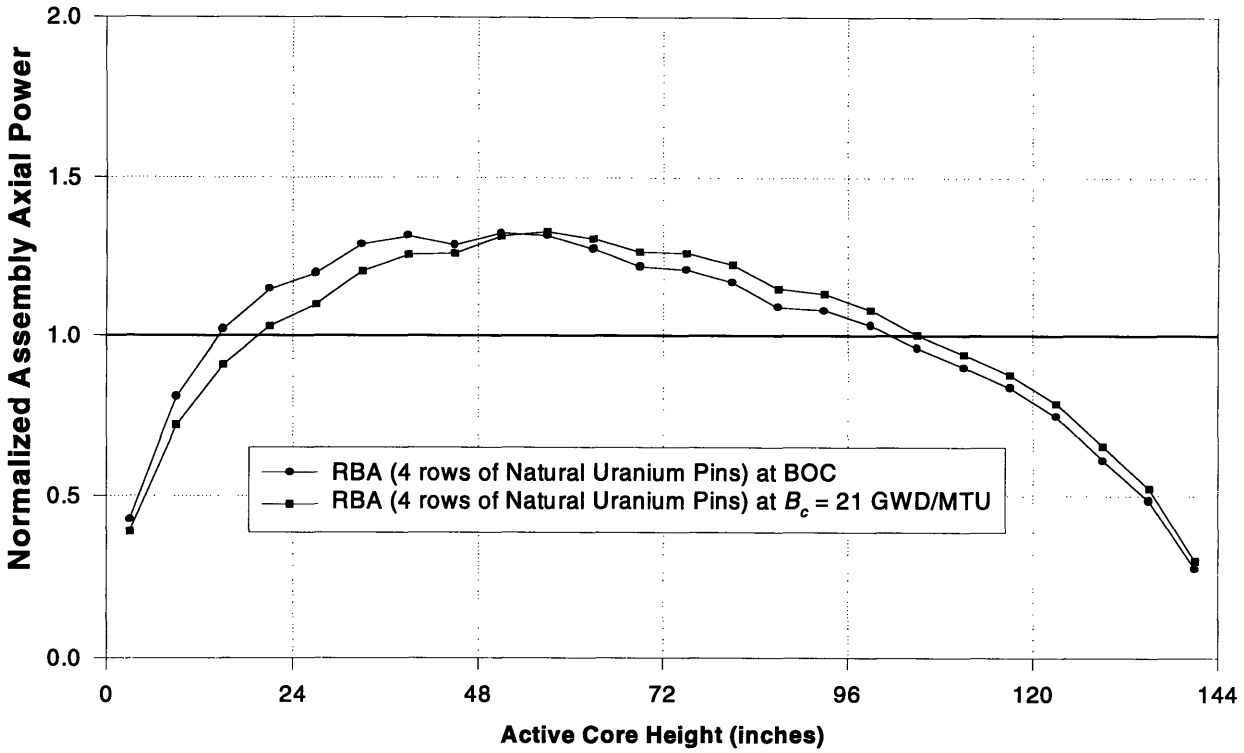

Figure 19: Burnup Induced Changes in PWR RBA Axial Power

amounts of exposure (17.7 GWD/MTU an 17.9 GWD/MTU, respectively). As shown in the figures, the interior assembly begins the operating cycle with a flatter axial power distribution than the RBA. Interior assembly axial power is more uniform because burnable poisons reduce the reactivity in the central enrichment zone of the fuel relative to the reactivity in the unpoisoned annular axial blankets. However, since these burnable poisons deplete most rapidly in the regions of highest power, positive reactivity feedback in the interior assembly eventually causes its axial power peaking to exceed that of the RBA. At the same time in core life, the negative reactivity feedback in the RBA has merely shifted axial power slightly into the less depleted upper regions of the assembly.

Generating a larger fraction of power in the periphery enhances the stabilizing effect of the RBAs on the core-wide axial power distribution. Reducing the number of rows of natural uranium pins in the RBAs draws power out to the periphery and therefore reduces the severity of core-wide axial power peaking. SIMULATE-3 calculations show that lowering the number of natural uranium pin rows from eight to three decreases maximum core axial power peaking in the first part of the operating cycle by ~2.5%. This reduction in core-wide axial power peaking contributes to the decrease in F_Q indicated in Table 5 and Figure 16. Although this decrease improves the margin to core thermal limits, it comes at the cost of increasing CBC unacceptably (i.e., to greater than 1780 ppm) when less than four rows of natural uranium pins are used in the RBA design.

Unlike cycle length, CBC, and F_Q, $F_{\Delta H}$ does not correlate well with the number of natural uranium pin rows in the RBAs. The calculation of $F_{\Delta H}$ depends upon both the global distribution of power within the core and the pin-to-pin peaking within each assembly. Compared to the interior assemblies, the asymmetric RBAs exhibit extremely high pin-to-pin power peaks, especially along the interface between the enriched and unenriched regions. These high pin peaking factors make the RBAs preferential locations for the peak $F_{\Delta H}$ during the cycle. In general, reducing the number of natural uranium pin rows in an RBA raises the amount of power that it generates, while at the same time decreasing the severity of its pin-to-pin peaking. With these two trends working at cross-purposes, $F_{\Delta H}$ does not follow any recognizable correlation with RBA design.

The RBA design with 4 rows of natural uranium pins provides the most favorable overall performance and was therefore selected for use in the 44 peripheral assemblies of the extended

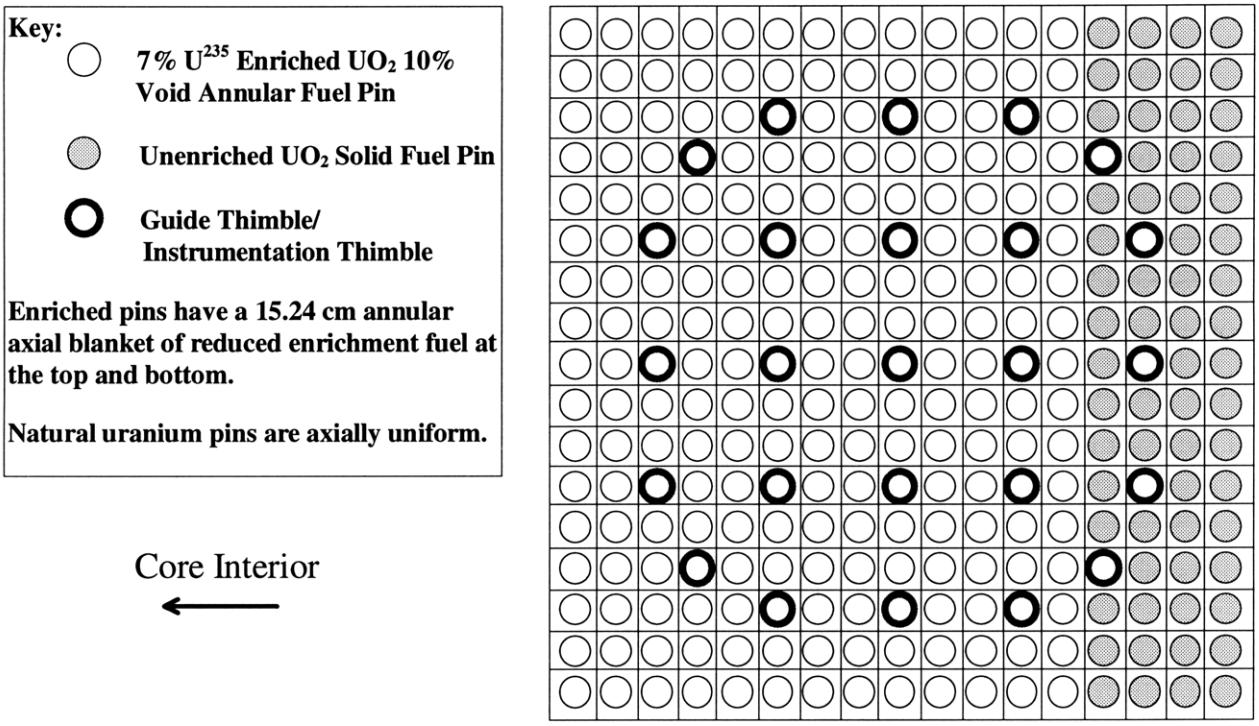

Figure 20: PWR Radial Blanket Assembly Design

cycle PWR core. This design reduces fuel costs and improves neutron economy without causing unacceptable increases in F_Q, $F_{\Delta H}$, or CBC. All other RBA designs exceeded one or more of the limits set for these design goal parameters. A diagram of this assembly is shown in Figure 20. In order to evaluate the effectiveness of the RBAs in reducing the rate of pressure vessel neutron embrittlement, their performance was modeled using the particle transport code MCNP4A (Monte Carlo N-Particle Transport Code System) distributed by the OakRidge National Laboratory [B-2]. The details of this analysis are contained in the following section.

5.4.2.3 RBA Modeling Using MCNP

As discussed earlier, the RBAs must be effective in reducing the rate of neutron embrittlement in the reactor pressure vessel. Ideally the use of RBAs should reduce the embrittlement rate at least as effectively as the use of L^3P fuel management. The two fluence reduction strategies were compared using MCNP4A and a model of a 34 pin linear array of fuel pins and core internals extending outward to the core baffle plate that was developed by Chodak [C-2]. Figure 21 contains two drawings of the same 34 pin model which simulates a single row of pins across two 1×17 assemblies; the upper picture is the full-length 34 pin model and the lower picture is a close-up

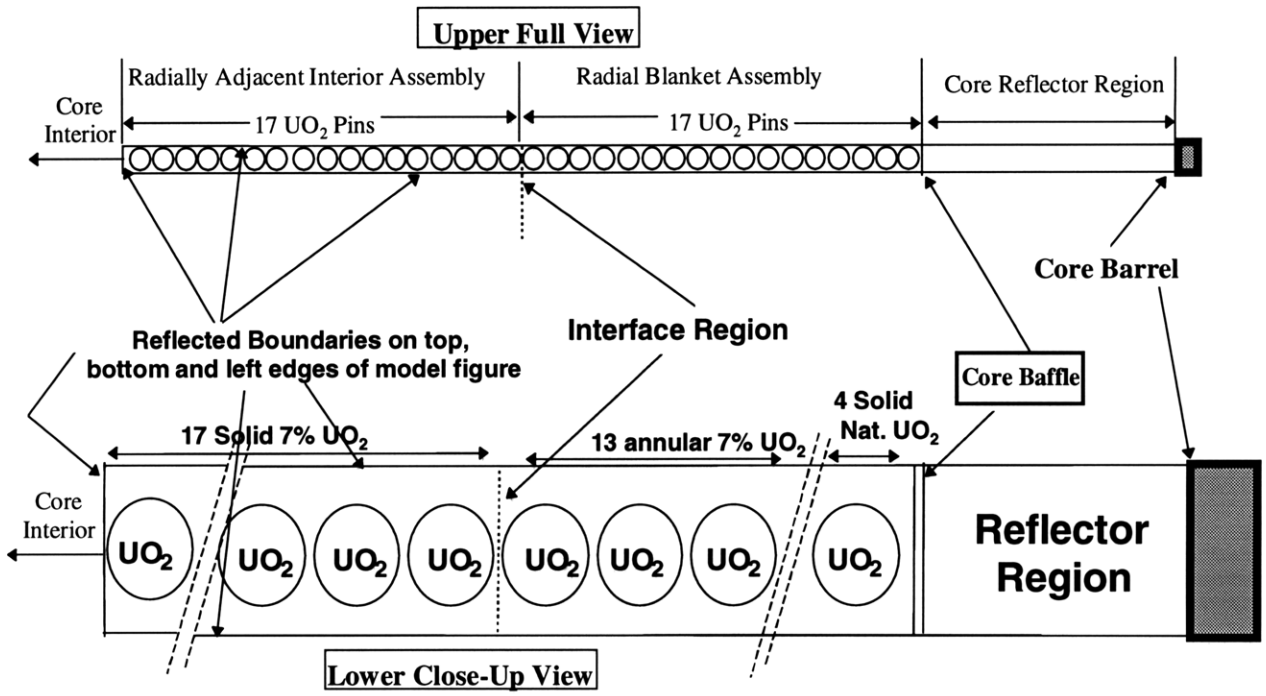

Figure 21: MCNP4A 34 Pin, PWR Two Assembly Model

truncated view. This 34 pin model is used to determine the rate of RPV neutron embrittlement for a given PWR core design. The model simulates the interface between a peripheral assembly and its radially adjacent inboard assembly. The dashed line in the lower close-up view indicates where the row is truncated. The 17 assembly pins adjacent to the core reflector region simulate a peripheral fuel assembly. A reflected boundary condition is imposed on the left-most model surface adjacent to the core interior. Thus, the inner 17 UO_2 pins simulate the rest of the PWR core interior. The assembly dimensions, core baffle plate, reflector region and core barrel are explicitly modeled to simulate the Westinghouse 4-Loop PWR used in this study. The moderator is H_2O with 500 ppm boron. This linear array of fuel pins models the performance of core peripheral assemblies and can be used to evaluate their effectiveness in controlling the rate of RPV neutron embrittlement.

As noted earlier, the steel in the RPV becomes embrittled through the accumulation of neutron fluence. Decreasing the rate of fluence accumulation will therefore slow the rate of neutron embrittlement. Assuming that thermal neutrons exiting the fuel region will not reach the RPV, the rate of fluence accumulation in the RPV will be proportional to the number of fast neutrons per second (per unit area) exiting the core baffle plate in the direction of the RPV. In the 34 pin MCNP4A

model, this value corresponds to the magnitude of the fast neutron current in the positive x direction, J_1^{x+}, tallied at the inner edge of the core baffle plate. In this study, the term 'fast' applies to neutrons with energies >10 ev. The effectiveness of a given fluence reduction strategy is determined by calculating and comparing its "Fluence Reduction Factor" (*FRF*), defined as the ratio of J_1^{x+} for a base case of a uniformly enriched 34-pin array to J_1^{x+} for the case being evaluated (i.e., $FRF = 2$ shows a 50% reduction in the rate of fluence accumulation).

For the evaluation of the extended cycle core RBAs, the following cases were modeled:

- Base Case: The 17 inner pins and 17 outer pins of this model contain unpoisoned, solid UO_2 fuel pellets enriched to $5^w/_o$ U^{235}. This model represents a conventional core with fresh fuel loaded in the interior and on the periphery. Loading the core in this manner shows no concern for reducing RPV flux accumulation.

- Low Leakage Loading Pattern (L^3P) Case: The 17 inner pins contain unpoisoned, solid UO_2 fuel pellets enriched to $5^w/_o$ U^{235}. The 17 outer pins contain unpoisoned, solid UO_2 fuel pellets enriched to $2.5^w/_o$ U^{235}. This model simulates a Low Leakage Loading Pattern with fresh fuel in the core interior and "twice-burned" fuel on the periphery. CASMO-3 calculations show that an enrichment of $2.5^w/_o$ U^{235}corresponds to the fissile loading (U^{235} plus fissile Pu) of a fuel assembly with an initial enrichment of $5^w/_o$ U^{235} that has accumulated 35-40 GWD/MTU of exposure. Exposures in this range are representative of twice-burned fuel assemblies which are loaded onto the periphery of cores employing L^3P fluence reduction strategies [Z-1].
- Radial Blanket Assembly (RBA) Case: The 17 inner pins contain unpoisoned, solid UO_2 fuel pellets enriched to $7^w/_o$ U^{235}. The first 13 of the 17 outer pins contain unpoisoned, 10% void annular UO_2 fuel pellets enriched to $7^w/_o$ U^{235}. The outer 4 fuel pins contain unpoisoned, solid unenriched UO_2 fuel pellets. This model simulates the extended cycle core with RBAs loaded onto the periphery.

In MCNP4A, the value of J_1^{x+} must be calculated from the tallied value given in the code output. This tallied value, T_1^{x+}, is normalized per fission neutron (i.e., a neutron resulting from fission) and is given in the following units:

$$T_1^{x+} = \frac{neutrons}{(cm^2) \cdot (fission\ neutron)} \tag{5.3}$$

To determine the actual value of J_1^{x+}, T_1^{x+} must be multiplied by a "Power Normalization Constant," designated *PN*, which represents the number of fission neutrons generated per second in the reactor at a given core power level, *P* [R-3]. This relationship is illustrated in the following equation:

$$J_1^{x+}\left(\frac{neutrons}{cm^2 \cdot s}\right) = T_1^{x+}\left(\frac{neutrons}{(cm^2) \cdot (fission\ neutron)}\right) \cdot PN\left(\frac{fission\ neutrons}{s}\right) \tag{5.4}$$

To accurately compare the performance of each fluence reduction scheme, the various cases must be evaluated at the same core power level. Thus the value of *PN* used in each case will be the same, and the expression for *FRF* for case *n* can be written as follows:

$$FRF_n = \frac{J_{1Base}^{x+}}{J_{1n}^{x+}} = \frac{T_{1Base}^{x+} \cdot PN_{Base}}{T_{1n}^{x+} \cdot PN_n} = \frac{T_{1Base}^{x+}}{T_{1n}^{x+}} \tag{5.5}$$

The accuracy of this method of analysis was verified by benchmarking the FRF values determined here against those calculated in a Westinghouse Nuclear Fuel Division study using detailed transport calculations [S-8]. Because the Westinghouse study uses a different "Base Case" than the one selected here, *FRF* values must be compared on the basis of the ratio of the fraction of core power in the peripheral assembly for case *n*, PAP_n, to the fraction of core power in the peripheral assembly for the base case, PAP_{Base}. A plot of $1/FRF_n$ against PAP_n/PAP_{Base} for the two analysis methods is shown in Figure 22. The figure shows good agreement between the results of the Westinghouse study and the FRF values calculated using MCNP4A. The values of *PAP* are calculated from the MCNP4A tallies of the power deposited in each of the model's 34 fuel pins. Peripheral assemblies comprise roughly 25% of the total number of assemblies in a core. Thus, the 17 interior fuel pins represent 3/4 and the 17 outer fuel pins represent 1/4 of the total number of pins in the core. The power deposited in each pin is normalized to the core average pin power in order to determine peripheral assembly power as a fraction of core average power. The core average pin power is calculated by:

$$PP_{CA} = \frac{3\sum_{i=1}^{17} PP_i + \sum_{i=18}^{34} PP_i}{68} \tag{5.6}$$

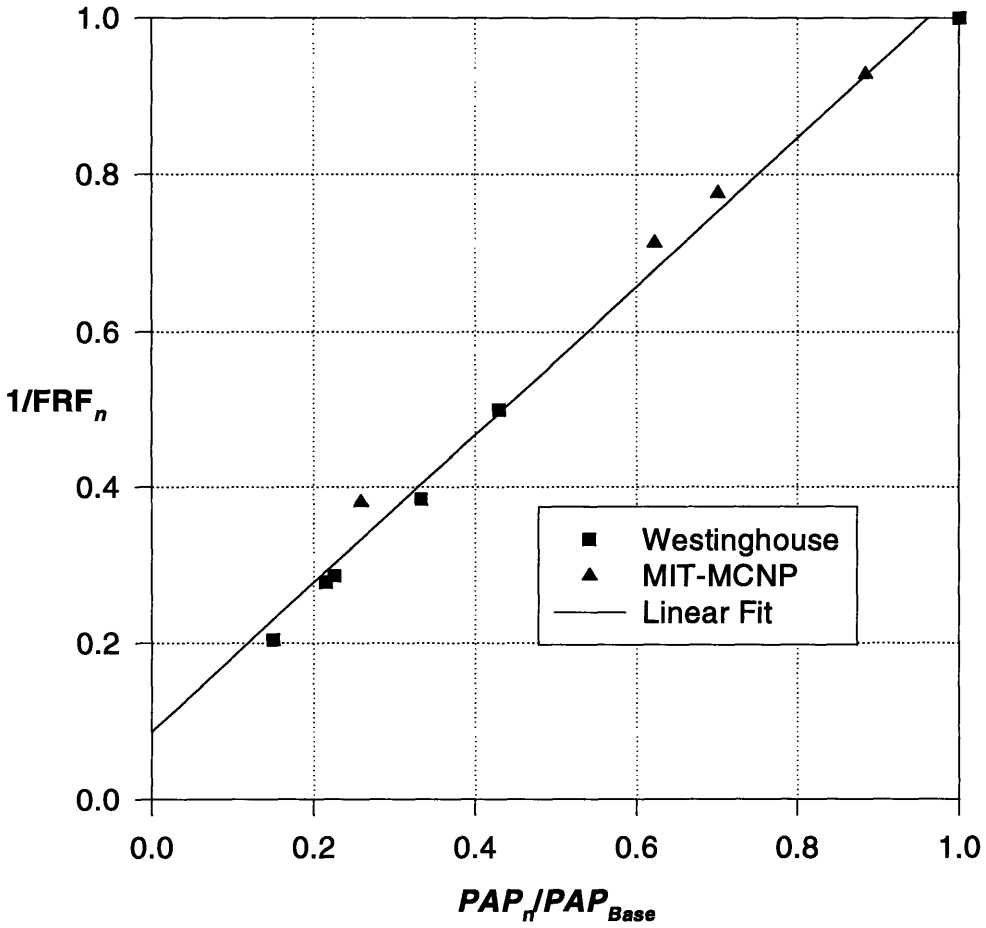

Figure 22: Comparison of *FRF* Calculations

where: PP_{CA} = Core Average Pin Power

PP_i = Power deposited in fuel pin i. Fuel pins are numbered so that $i = 1$ correlates to the left-most fuel pin directly adjacent to the reflected left vertical core interior surface in Figure 21, and $i = 34$ correlates to the right-most pin directly adjacent to the core baffle.

The fraction of core power in the peripheral assembly for case n, PAP_n, can then be calculated by dividing peripheral assembly average pin power by core average pin power, as shown in equation (5.7) below:

$$PAP_n = \frac{\frac{1}{17}\sum_{i=18}^{34}(PP_i)_n}{(PP_{CA})_n} \tag{5.7}$$

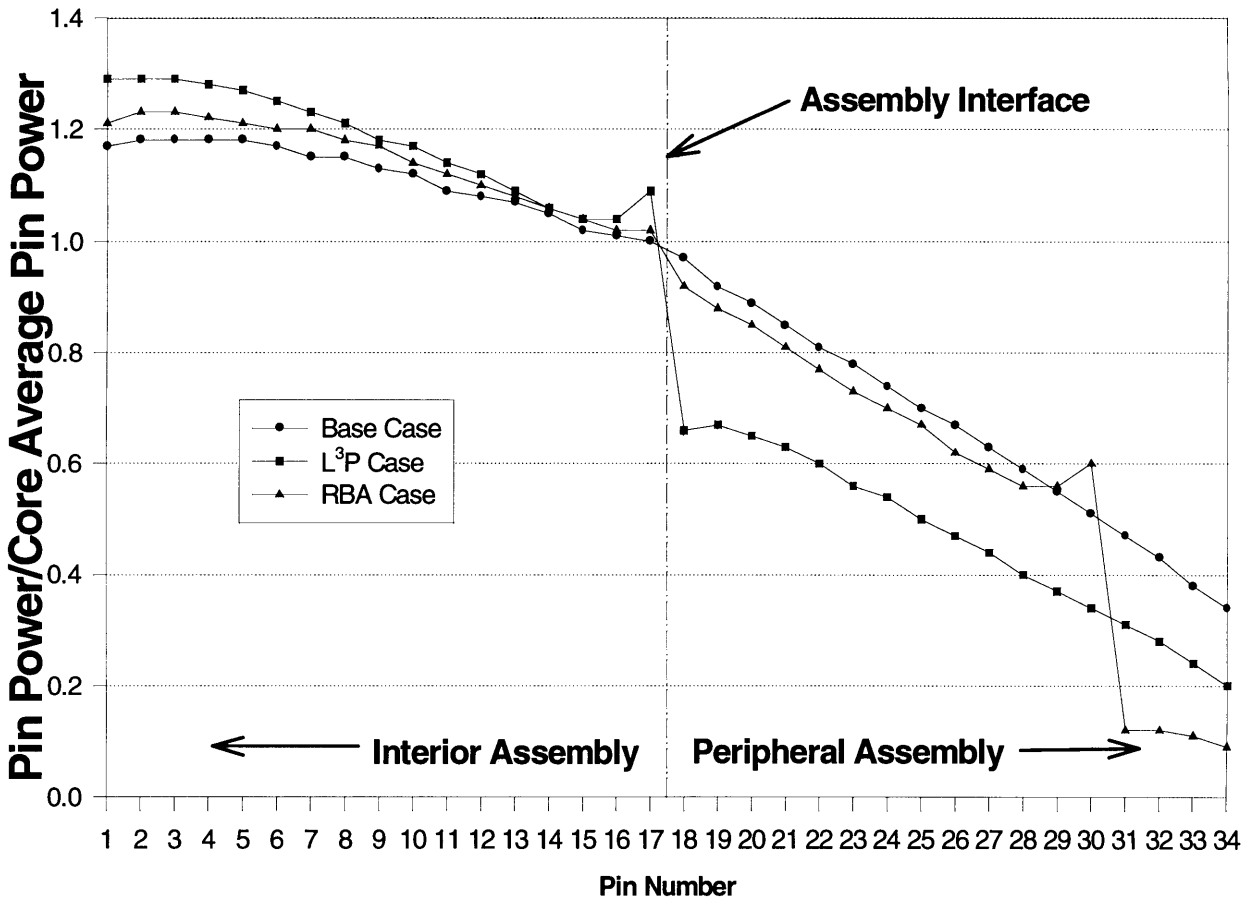

Figure 23: Pin Relative Power from the MCNP4A 34 Pin Model

The MCNP4A calculations of *FRF* and *PAP* for the Base, L^3P, and RBA Cases described earlier are compared in Table 6. Figure 23 shows the radial power profile for each of these strategies. The results in Table 6 demonstrate that the use of RBAs on the periphery of the PWR reduces the

Table 6: Comparison of Flux Reduction Strategies

Case	FRF	PAP
1. Base	-	0.66
2. L^3P	1.29	0.46
3. RBA	1.30	0.57

rate of vessel fluence accumulation at least as effectively as the employment of a typical L^3P strategy. Note also (from the comparison of *PAP* values in the table) that this is accomplished even though the power generated in an RBA is greater than that generated in a peripheral assembly of the L^3P case. Therefore, the extended cycle PWR core with Radial Blanket Assemblies

conveys the same benefit of pressure vessel wall embrittlement arrest as a multi-batch core using Low Leakage fuel management strategies. Additionally, fuel cycle economic studies show that their use lowers the fuel costs of the extended cycle design by approximately $3-4M/year [H-4]. Thus the use of the unique asymmetric RBAs reduces radial neutron leakage and lowers fuel costs without causing unacceptable degradation in core power peaking or in the other design goal parameters of the PWR extended cycle core.

5.5 Core Loading Pattern

The loading pattern of the interior assemblies and Radial Blanket Assemblies in the extended cycle core maximizes operating cycle length while maintaining design goal operating parameters within acceptable limits. Along with balancing the obvious trade-offs between core excess reactivity and achievable cycle length, the loading pattern also determines the spatial and temporal shifts in reactivity which control reactor power peaking throughout core life. In the loading pattern selected for the extended cycle design, the more heavily poisoned, lower reactivity fuel assemblies are placed in the central regions of the core to suppress peaking and flatten the radial power shape. The more lightly poisoned interior assemblies and the unpoisoned RBAs on the exterior also draw power outward from the center. Figure 24 shows a full core map of the assembly loading pattern for the extended cycle design. The assemblies in the figure are shaded to reflect their relative infinite medium reactivity, with darker colors representing a lower BOC k_∞. Additionally, the black banding on the RBAs (marked with an "R" in the figure) indicates the orientation of their four rows of natural uranium fuel pins. The characteristics of these various fuel assemblies are summarized in Table 7.

As noted earlier, the interior assemblies of the extended cycle design are uniformly enriched to $7^w/_o$ U^{235}, with the exception of the five $6^w/_o$ U^{235} enriched assemblies placed in the center of the core to reduce radial power peaking. Without these reduced enrichment assemblies, the design limits set for $F_{\Delta H}$ cannot be met. The final core loading pattern was developed by sequential evaluation and modification of a series of SIMULATE-3 runs to determine an acceptable near-optimum layout for maximizing operating cycle length while still meeting the limits of the core design operating parameters.

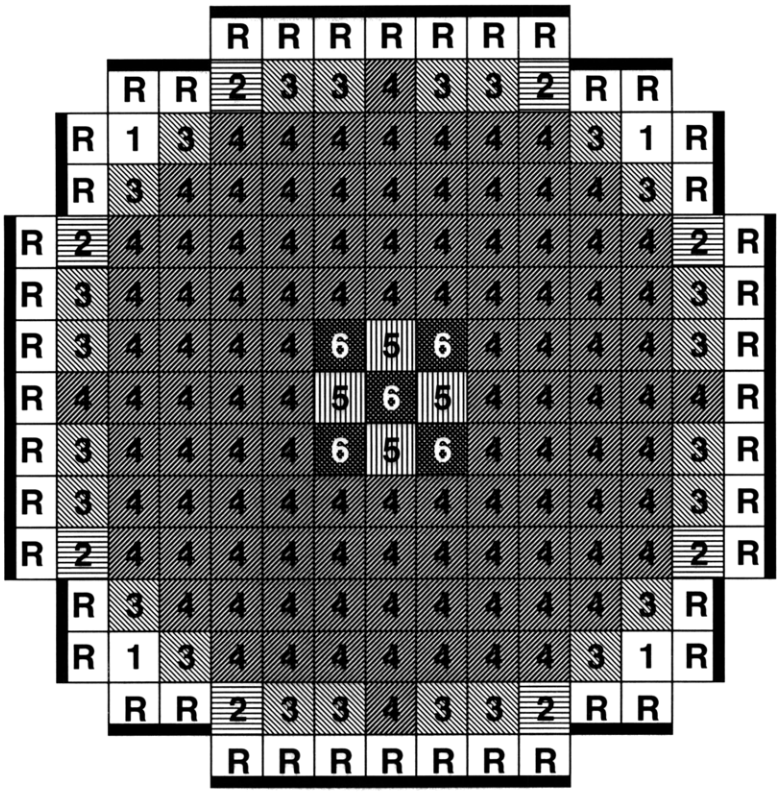

Figure 24: Extended Cycle Design PWR Core Loading Pattern

Table 7: PWR Extended Cycle Design Fuel Assembly Characteristics

Assembly Type	Number of Assemblies in Core	Fuel Enrichment ($^{w}/_{o}$ U^{235})	Number of Burnable Absorber Pins	Axial Blanket Enrichment ($^{w}/_{o}$ U^{235})
1	4	7.0	24	5.25
2	8	7.0	32	5.25
3	24	7.0	36	5.25
4	104	7.0	40	5.25
5	4	7.0	44	5.25
6	5	6.0	44	5.25
RBA	44	7.0/0.711	0	5.25

Chapter 6 which follows analyzes the performance of the PWR extended cycle neutronic design using a full core three-dimensional SIMULATE-3 model and measures this performance relative to design goals outlined in Chapter 3.

CHAPTER 6

PWR Neutronic Design Performance

SIMULATE-3 calculations of the neutronic performance of the extended cycle PWR core design are summarized in Table 8. Also shown is the cycle length in terms of core-average cycle burnup (GWD/MTU), EFPM, and calendar months at the target capacity factor, L = 87. Note that at the target 87% capacity factor, only a 44.6 calendar month operating cycle is possible. The table measures these performance parameters against the design goal limits set in Chapter 3 and also compares them to the parameters calculated for the same Westinghouse 4-Loop PWR operating with a conventional, multi-batch, nominal 18 month fuel cycle. The SIMULATE-3 model of the conventional core was provided by the Yankee Atomic Electric Company. Although the conventional core was designed to operate at an overall capacity factor of ~81% in an 18 month fuel cycle, the table shows that at the target 87% capacity factor of the extended cycle design, only 17 calendar months of operation can be achieved. The fuel characteristics of the conventional core and the extended cycle core are compared in Table 9. Each of the basic design goals outlined in Chapter 3 are discussed in greater detail in the sub-sections which follow.

6.1 PWR Basic Design Goals

6.1.1 Maximum Enthalpy Rise Hot Channel Factor ($F_{\Delta H}$)

Figure 25 contains a 1/8 core model of the extended cycle PWR design showing the type of assembly, maximum $F_{\Delta H}$ at any time in core life, and assembly discharge burnup at EOC. The assembly numbering scheme used in the figure corresponds to the numbering system of the full

core map shown in Figure A.1 in Appendix A. Figure 26 shows $F_{\Delta H}$ against core-average cycle

Table 8: Summary of Extended Cycle PWR Core Design Performance

	Maximum $F_{\Delta H}$	Maximum F_Q	Peak CBC	Cycle Length (at 87% Target *L*)
Design Goal	1.56	2.36	1780 ppm	41.8 EFPM (48 Cal. Months)
Extended Cycle Core Performance	1.55 (30 GWD/MTU)	2.35 (36 GWD/MTU)	1730 ppm (24 GWD/MTU)	38.8 EFPM (44.6 Cal. Months) 47.217 GWD/MTU
Conventional "18-month" Core	1.40 (5 GWD/MTU)	1.89 (2 GWD/MTU)	1306 ppm (0 GWD/MTU)	14.8 EFPM (17.0 Cal. Months) 17.125 GWD/MTU

Table 9: Comparison of PWR Core Fuel Characteristics

Fuel Characteristic	Conventional Core	Extended Cycle Core
Feed Assemblies	72	193
Core Total Loading (MTU)	89.4	85.4
Feed Enrichment ($^w/_o$ U^{235})	3.6 (36)/4.0 (36)	6.0(5)/7.0(188)
Avg. Discharge Burnup (GWD/MTU)	~40	47.2
Burnable Absorbers	IFBA (1.5 mg B^{10}/in.)	$12^w/_o$ Gd_2O_3 and IFBA (1.545 mg B^{10}/in.)

exposure for both the extended cycle and the conventional core design. Figure 26 also marks the assembly location of extended cycle $F_{\Delta H}$ at 5 GWD/MTU intervals. If $F_{\Delta H}$ location remains unchanged for more than 5 GWD/MTU then a band of values is indicated.

As seen in the figures, the peak $F_{\Delta H}$ for the cycle occurs near the core center in the heavily poisoned (G-8) Type 5 assembly. Peaking takes place nearly 2/3 of the way through the cycle, at a core-average cycle burnup of 30 GWD/MTU. The maximum value of 1.55 meets the design goal of 1.56 and provides a 6% margin for meeting the limit of 1.65 without uncertainties. Compared to the behavior of the conventional PWR core, $F_{\Delta H}$ in the extended life design experiences large oscillations in magnitude throughout the operating cycle. These sinusoidal oscillations stem from the initial core loading pattern and from the depletion behavior of the higher enrichment, heavily poisoned fuel required to achieve ultra-long cycle lengths.

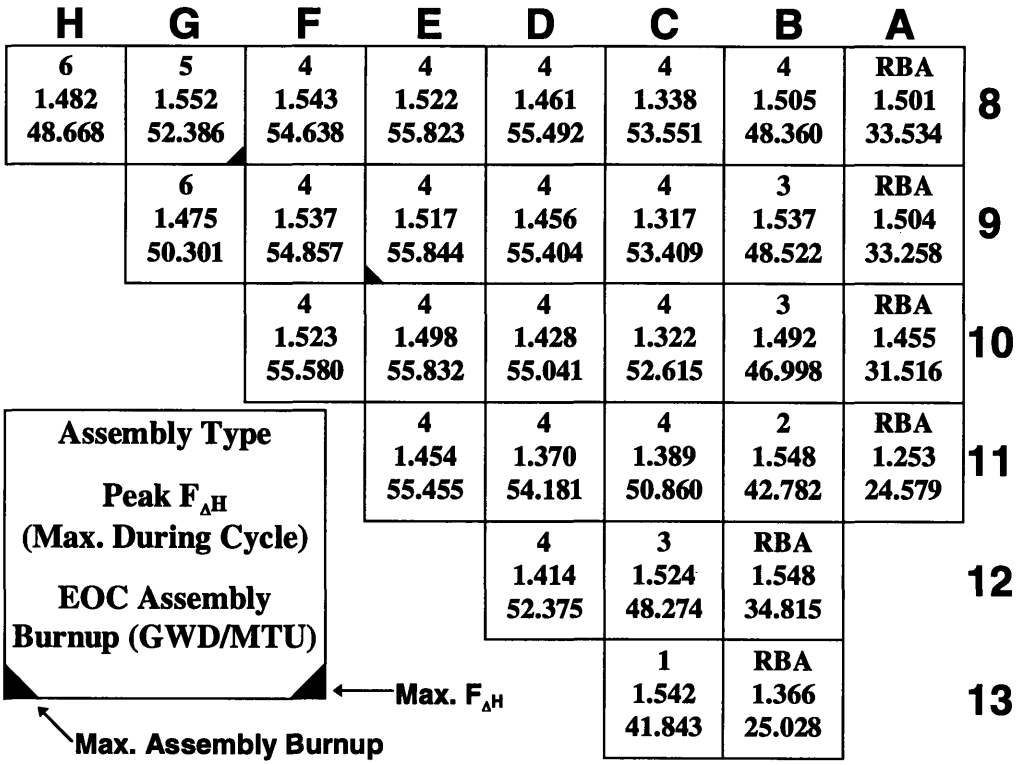

Figure 25: 1/8 Core Map of PWR Extended Cycle Design

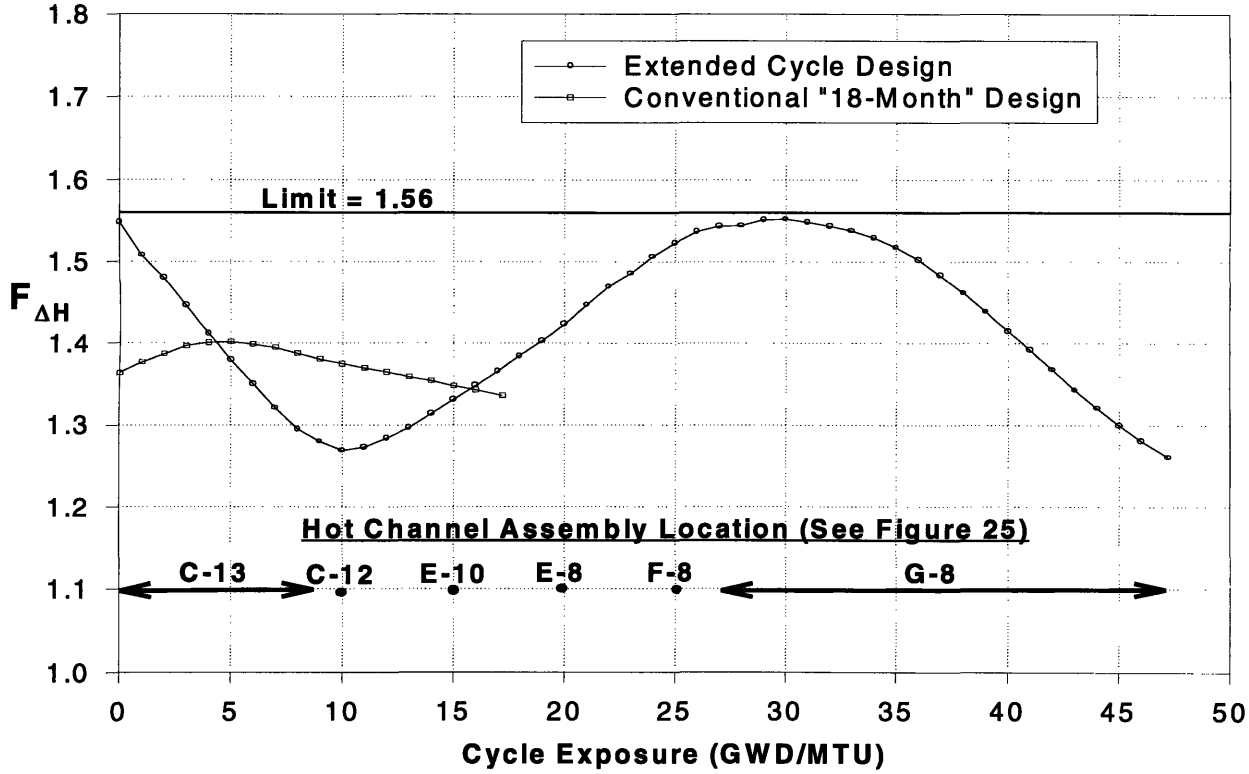

Figure 26: PWR Maximum Enthalpy Rise ($F_{\Delta H}$) vs. Core-Average Exposure

The core power maps contained in Figure 27 and Figure 28 illustrate the behavior of reactor radial power distribution as a function of core-average exposure. These power maps show mesh plots of the average power in each assembly in the PWR core at different times in core life. Note that the figures show *assembly-average* power instead of the peak $F_{\Delta H}$ of individual coolant sub-channels. However, the dynamic behavior of both parameters is similar, as the "hot channel" of the reactor tends to be located in the hottest region of the core.

As shown in Figure 27, heavily poisoned assemblies in the center and lightly poisoned and unpoisoned fuel on the periphery give the extended cycle PWR core a radial power shape that is peaked near the exterior and depressed in the middle at the beginning of cycle. However, as the cycle progresses, power immediately begins to move to the center of the core. The reactivity depletion behavior of the extended cycle PWR core's fuel assemblies causes this initial migration of power toward the interior. As illustrated in Figure 10 and Figure 17 in Chapter 5, heavily poisoned center assemblies initially *gain* reactivity with burnup, while lightly poisoned assemblies and unpoisoned RBAs on the periphery lose it. These relative changes in regional reactivity transfer power from hot running exterior assemblies to low power interior ones, thus causing $F_{\Delta H}$ to decrease in magnitude and move toward the center. At 10 GWD/MTU of core-average exposure, these burnup induced reactivity shifts force $F_{\Delta H}$ to a minimum. At this time in core life, Figure 27 also shows that the core radial power distribution is fairly flat and is devoid of its BOC peaks, although it remains slightly depressed near the exact center.

From this point forward, $F_{\Delta H}$ begins to grow in magnitude as the cycle length progresses because the positive reactivity feedback of the heavily poisoned center assemblies increases the severity of power peaking. In this regime, central hotter running assemblies gain reactivity faster than their cooler running neighbors. This relative increase in the reactivity of higher power fuel bundles concentrates even more power into these assemblies and causes the rapid growth in $F_{\Delta H}$. $F_{\Delta H}$ continues to rise until it reaches its maximum value at 30 GWD/MTU of core-average exposure. Figure 28 contains the corresponding core radial power distribution at the same point in the operating cycle. Note that the severity of radial power peaking at 30 GWD/MTU is mitigated by the presence of the five reduced enrichment assemblies placed in the center of the core.

Following its peak at 30 GWD/MTU, $F_{\Delta H}$ decreases in magnitude as the interior assemblies accrue enough exposure to enter the negative reactivity feedback regime shown on the right side

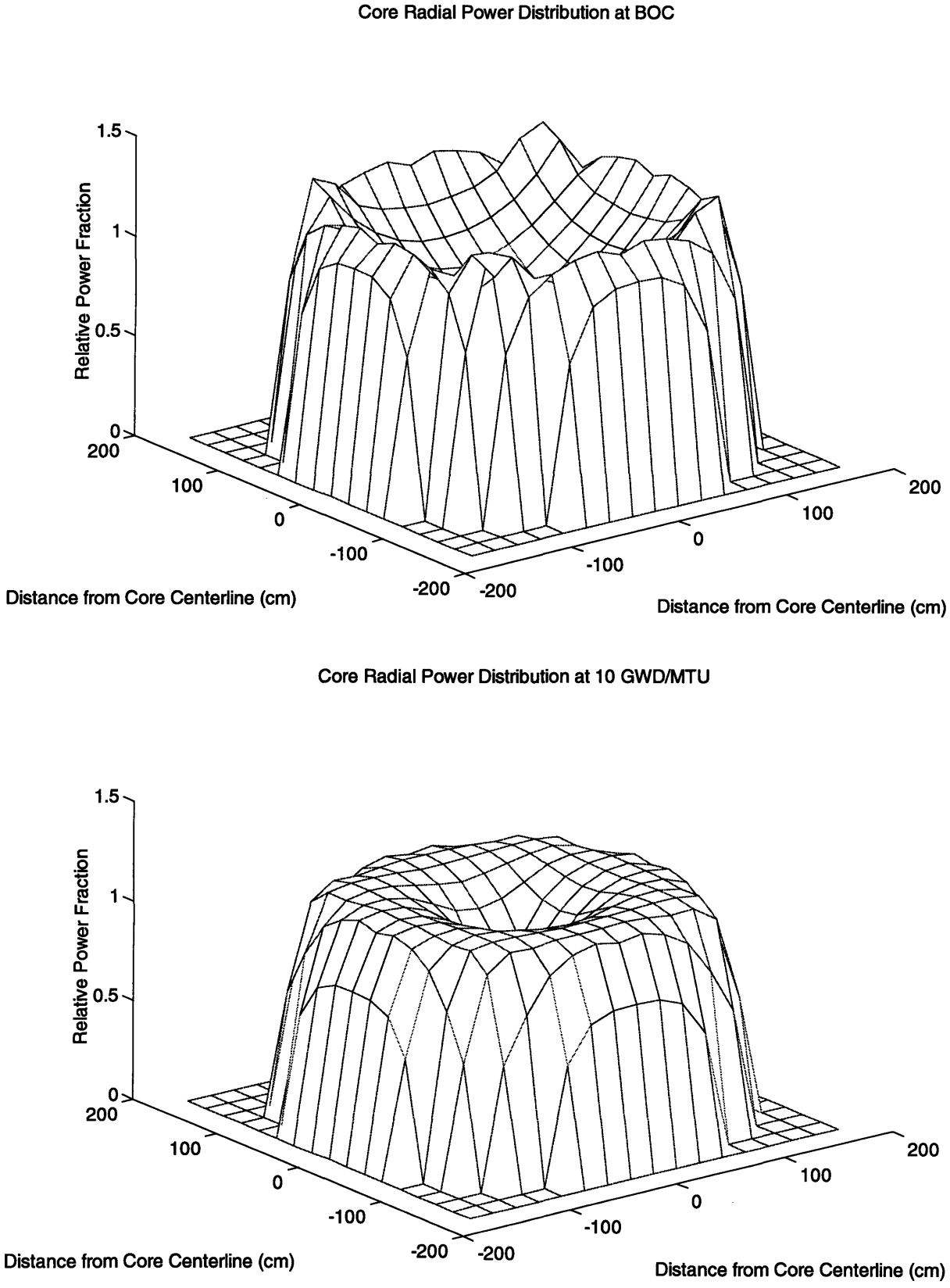

Figure 27: PWR Core Radial Power Distribution at BOC and 10 GWD/MTU

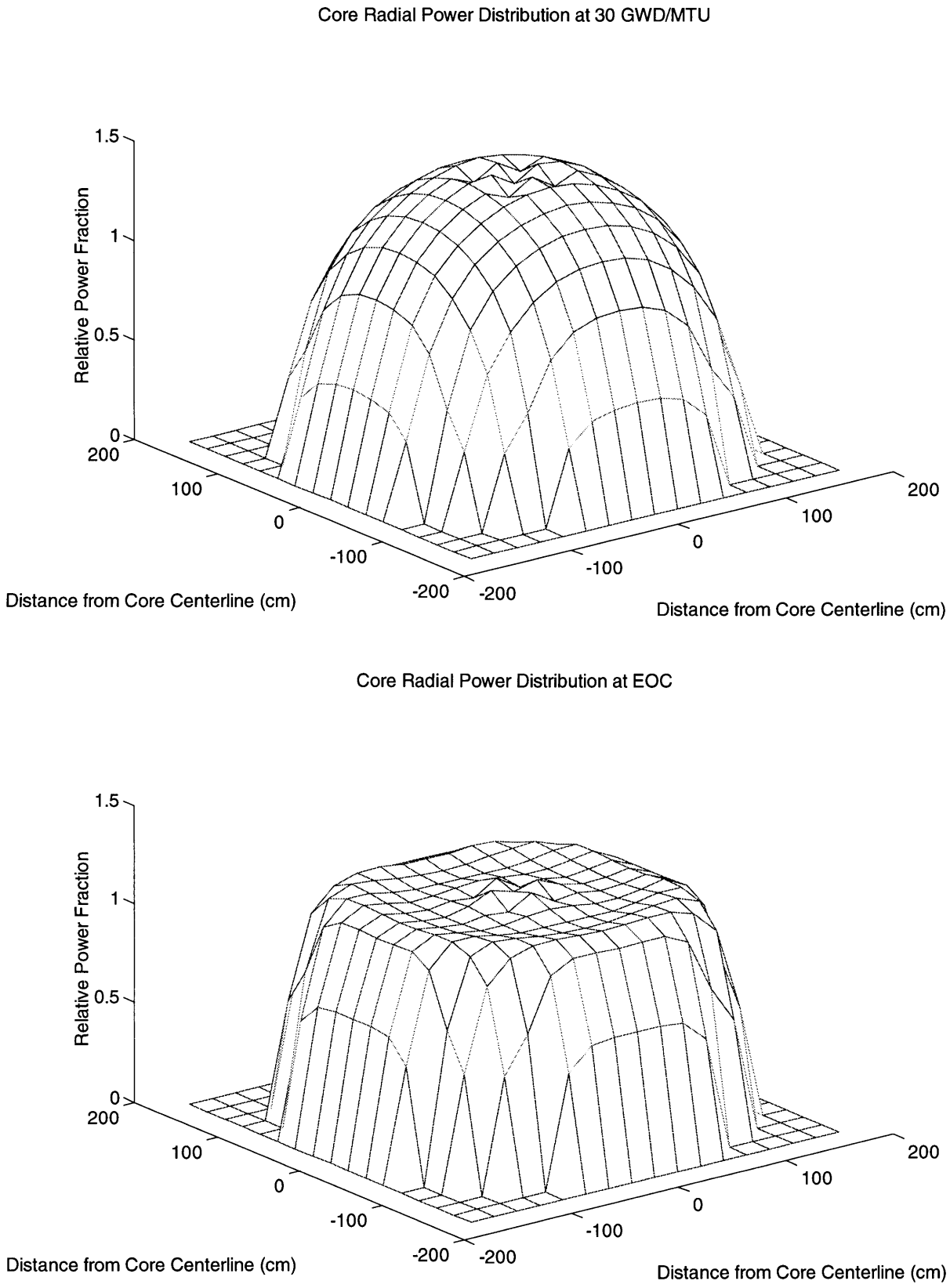

Figure 28: PWR Core Radial Power Distribution at 30 GWD/MTU and EOC

of Figure 10. With burnable poisons largely depleted, the loss of fissile atoms now controls the changes in reactivity in these higher burnup assemblies. High power assemblies now begin to lose reactivity more rapidly than their slower burning neighbors, and the core radial power distributions "flattens out" as the cycle progress. Note, however, that the location of the hot channel remains unchanged for the remainder of the cycle. As shown in Figure 28, the four heavily poisoned Type 5 assemblies in the center have the highest radial power in the core (and contain the hot channel) from 28 GWD/MTU until EOC.

Because these assemblies contain the highest initial poison loading, the power generated in them is suppressed for the majority of the operating cycle (until the burnable absorbers are largely depleted). Thus at the time of $F_{\Delta H}$ peaking, these assemblies have accumulated only ~90% of the exposure of their similarly enriched neighbors. With the interior assemblies operating on the "down-slope" of the reactivity-burnup curves of Figure 10, lower accumulated burnup now translates into a higher assembly reactivity. Because the Type 5 assemblies are operating at higher power, the gap in accumulated exposure and reactivity gradually narrows as the cycle progresses, resulting in the decrease in $F_{\Delta H}$ observed in Figure 26. However, this gap goes not close rapidly enough to shift peak power to a different region of the core by EOC.

The burnable poison distribution must be carefully optimized to meet the design limits set for the extended cycle PWR core. Attempts to reduce peaking in the center assemblies by adding more poison can actually cause an *increase* in the maximum $F_{\Delta H}$ both at BOC and later in the cycle. At BOC, a heavier burnable poison loading drives power to the periphery, increasing the peaking in the lightly poisoned assemblies near the exterior. As the cycle progresses, the increased poison loading maintains a lower power in the center. This enhanced hold down of power causes a larger accumulated exposure deficit between these assemblies and their similarly enriched neighbors when the neutron absorbers finally deplete late in life. This larger differential in assembly exposure (and therefore, reactivity) increases the severity of late-in-life power peaking in the extended cycle PWR core. Additionally, because higher burnable poison concentrations require more time to burn out fully, the peak value of $F_{\Delta H}$ will occur at a later time in core life. Conversely, reducing the poison loading in the center assemblies runs the risk of increasing $F_{\Delta H}$ by not sufficiently suppressing power in these low leakage, high reactivity locations. The effect of burnable absorber loading on the behavior of late-in-life core power distribution increases the complexity of extended cycle PWR core design.

While the peak value of $F_{\Delta H}$ in the extended cycle PWR core remains below the established limit of 1.56, it occurs it late in the cycle and is located in fuel assemblies which have accumulated a significant amount of total burnup. In conventional multi-batch designs, highly burned fuel is much less reactive than the fresh fuel that is inserted into the reactor every 18-24 months, and it therefore does not experience significant power peaking. However, in the single batch extended cycle PWR core, heavily burned assemblies must still operate at relatively high powers since power must be evenly distributed throughout the core. With heavily depleted fuel in the extended cycle design running at power levels greater than those experienced by the high exposure fuel in conventional cores, concerns are raised over the effects of extended cycle lengths on fuel thermal and mechanical performance. The analyses of fuel pin internal pressure detailed in Chapter 8 were performed to determine if the operation of heavily burned assemblies at high power for long periods of time results in fuel performance problems.

6.1.2 Total peaking factor (F_Q)

In the same manner as Figure 26, Figure 29 plots F_Q against core-average cycle exposure for both the extended cycle and the conventional core design. In addition to listing the assembly location of extended cycle F_Q at 5 GWD/MTU intervals, the figure also indicates where total peaking occurs axially in the core. The axial height of the area of highest total power peaking is given in inches, with 144" marking the top of the core. As before, if F_Q location remains unchanged for more than 5 GWD/MTU then a band of values is shown.

From the figure, the maximum total peaking value of 2.35 meets the limit of 2.36 set for the extended cycle PWR core. Similarly to $F_{\Delta H}$, the value of F_Q provides a 6% margin for meeting the limit of 2.50 without uncertainties. Highest total peaking occurs relatively late in life at core-average burnup of 36 GWD/MTU. A comparison of Figure 26 and Figure 29 reveals that F_Q exhibits the same large sinusoidal oscillations as $F_{\Delta H}$, and that the two metrics also follow a similar "migration path" from core exterior to interior as the cycle progresses. The distinctive double peaking behavior of F_Q shown in the figure originates from the effect of positive reactivity feedback on the extended cycle PWR core's axial power distribution.

In the early part of the operating cycle, the flattening of the core's radial power distribution due to the inward migration of power dominates the behavior of F_Q. Because of this, total power

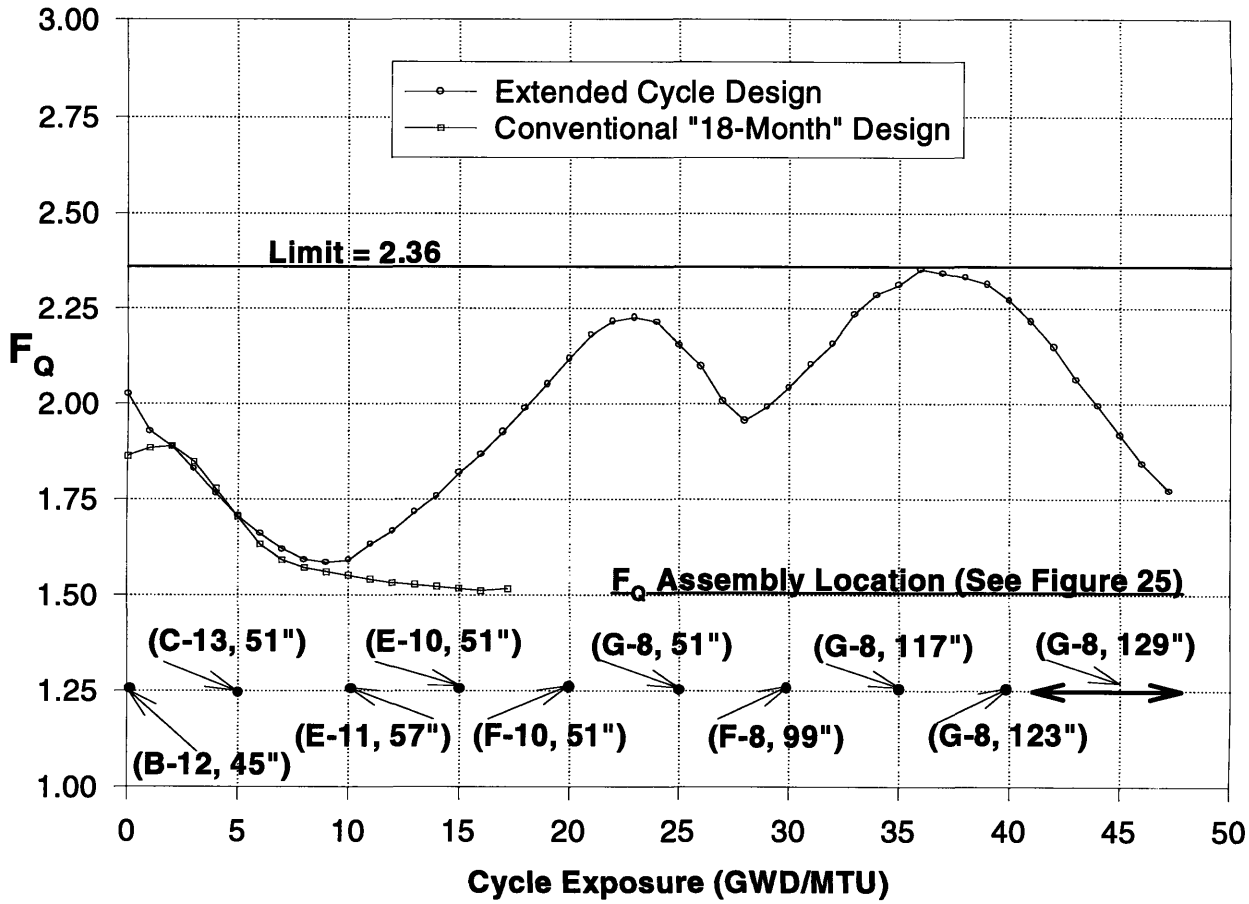

Figure 29: PWR Total Peaking Factor (F_Q) vs. Core-Average Exposure

peaking initially decreases in the same way that $F_{\Delta H}$ drops at the beginning of the cycle. Axial power peaking also initially begins to lessen in severity at BOC. From 0 GWD/MTU to approximately 6 GWD/MTU of core-average burnup, the axial power distribution "flattens out," because a large fraction of power is being generated on the core's lightly poisoned exterior. As described in Section 5.4.2.2, axial power will become more evenly distributed as burnup increases in the more lightly poisoned assemblies which exhibit negative reactivity feedback. Conversely, positive reactivity feedback in the heavily poisoned interior assemblies of the core increases the severity of axial power peaking as the operating cycle progresses. With 50% of reactor power being generated in Type 1, 2, and 3 assemblies and RBAs at BOC, the behavior of the lightly poisoned exterior dominates very early in core life. However, the radial shift in power away from the periphery increases the influence of the heavily poisoned interior fuel bundles, and after 6 GWD/MTU, axial peaking begins to rise. By 9 GWD/MTU, the growing axial power peak begins

to affect total peaking behavior, causing F_Q to reach a nadir slightly ahead of the minimum value of $F_{\Delta H}$ achieved at 10 GWD/MTU. For the remainder of the cycle, the behavior of the core's axial power distribution controls the value of total power peaking.

The extended cycle PWR core axial power distribution at BOC, EOC, and the times of F_Q peaking are shown in Figure 30. For comparative purposes, Figure 31 also contains a plot of the axial power distribution of the conventional PWR core at BOC, mid-cycle, and EOC. As shown in Figure 30, at the start of the cycle, the temperature gradient across the core and the negative MTC of the extended cycle design give rise to an axial power peak in the lower half of the core. In contrast with the behavior of the conventional core, positive reactivity vs. burnup feedback in the long cycle design causes this peak to grow in magnitude as burnup increases. The strong increase in core axial power peaking drives F_Q to its first peak value at 23 GWD/MTU. At 23 GWD/MTU of core-average burnup, much of the fuel running at the highest peak power has accumulated enough exposure to begin operating on the down-slope of the burnup-reactivity curves of Figure 10. As the cycle progresses, power begins to shift to the less depleted, higher reactivity fuel in the upper regions of the core. Comparing Figure 26 and Figure 29 illustrates that this upward shift in the axial power distribution has a greater impact on total power peaking than the burnup induced changes in the radial power shape. From 23 to 28 GWD/MTU, flattening of the axial power distribution causes F_Q to drop while $F_{\Delta H}$ continues to increase. More importantly, severe axially peaking high in the core creates a second, higher peak value of F_Q at 36 GWD/MTU even as radial peaking in the core is decreasing, having reached its own maximum value at 30 GWD/MTU.

Because total power peaking reaches a maximum late in the cycle, concerns are again raised over the thermal and mechanical performance of the fuel in the uni-batch extended cycle PWR core. The increased linear heat generation rate of fuel running at the highest peak power produces higher fuel and cladding temperatures. Higher temperatures increase the rate of fission gas release from the fuel, raise fuel pin internal pressure, and accelerate cladding waterside corrosion. The analyses in Chapter 8 focus on the effects of elevated linear heat generation rates in the high burnup assemblies of the extended cycle PWR core.

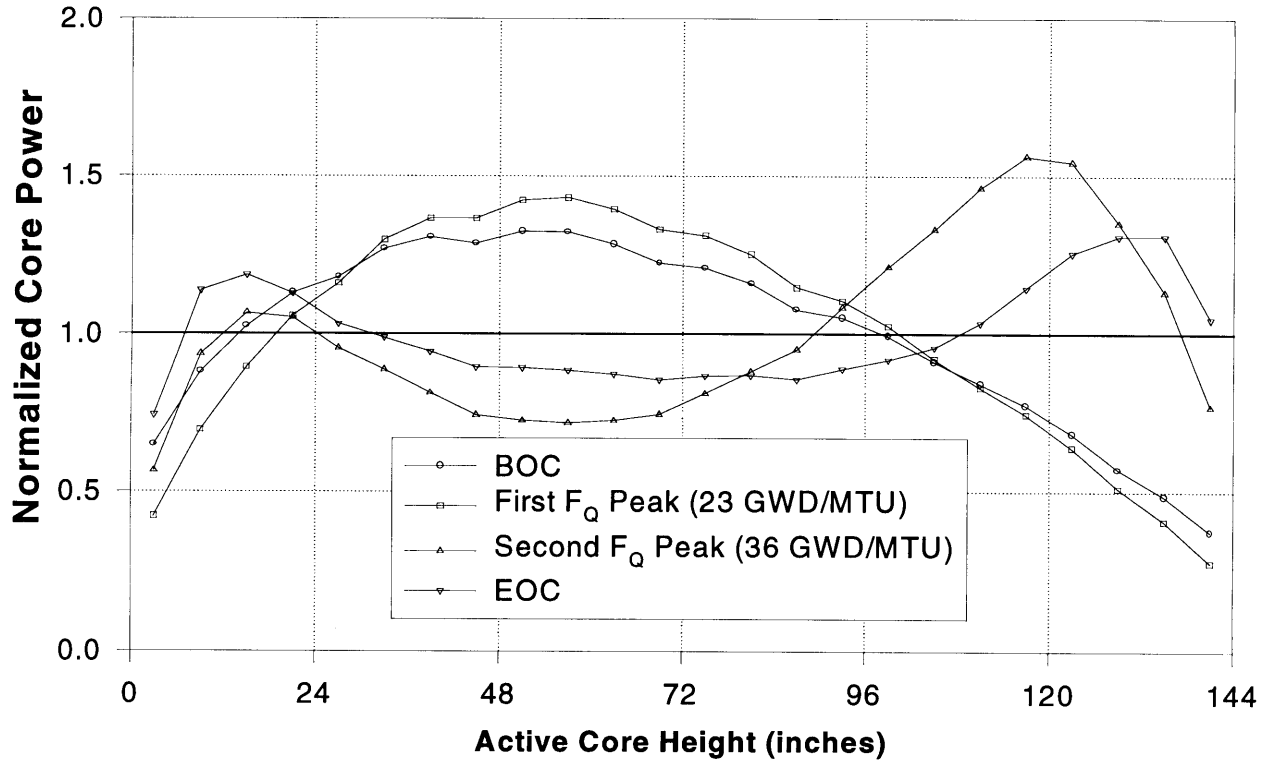

Figure 30: Extended Cycle PWR Core Axial Power Distribution

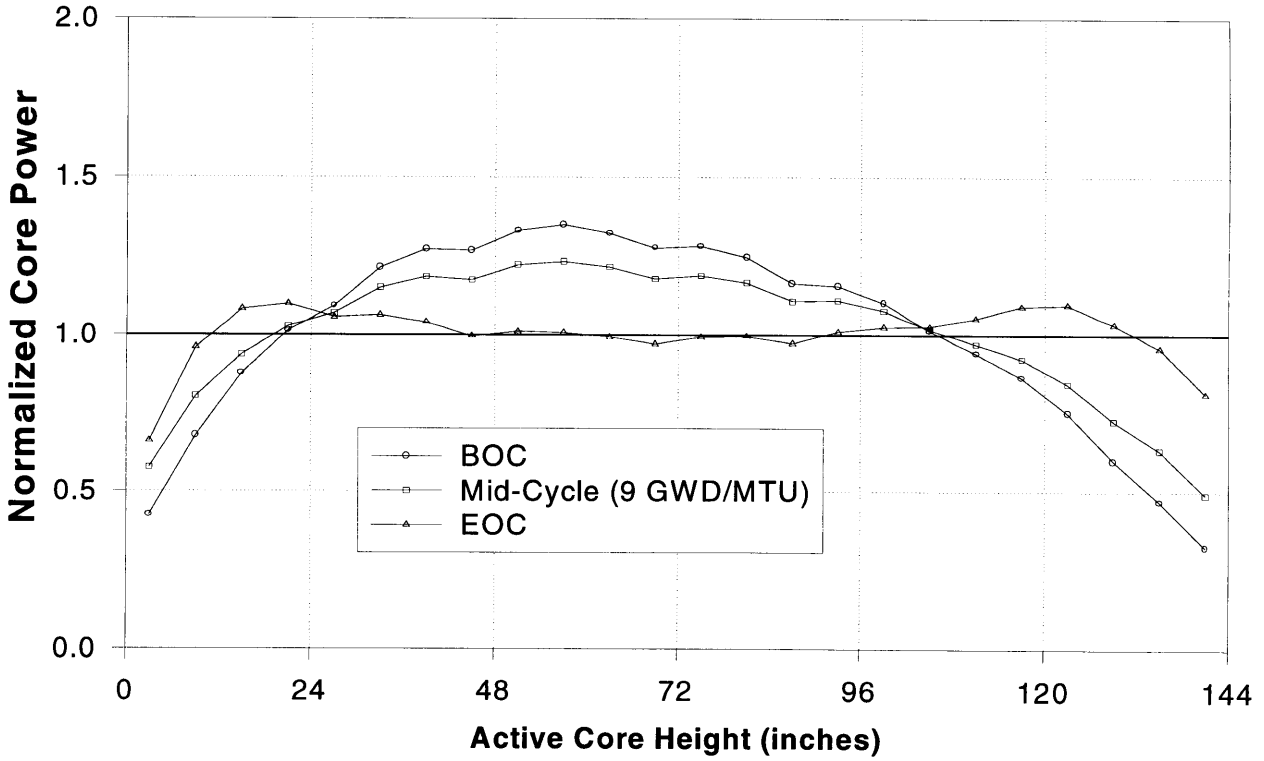

Figure 31: Conventional PWR Core Axial Power Distribution

6.1.3 Critical Boron Concentration (CBC)

Figure 32 reveals the behavior of reactor Hot Full Power (HFP) coolant critical boron concentration as a function of core average exposure for both the extended cycle and the conventional PWR core designs. At BOC, the sharp drop in CBC observed in both cores results from the rapid buildup of xenon and samarium fission product poisons to HFP equilibrium levels. As the figure shows, extended cycle core equilibrium xenon CBC stays below the 1780 ppm design goal limit.

Because CBC indicates the magnitude of core hot excess reactivity, its behavior during the cycle shows the net effects of the burnup induced changes in fuel reactivity that have been highlighted in previous sections. Once saturating fission product poisons reach an equilibrium value, fuel reactivity behavior with respect to burnup governs the changes in CBC. In the early part of the cycle, the rapid shifts in regional reactivity which produce large oscillations in core power distribution appear to have little effect on the critical boron concentration. The gentle slope of the CBC curve in Figure 32 shows that these dynamic variations within the core cause only slight net changes in core-wide reactivity.

Additionally, the PWR extended cycle design's neutron poison burnout characteristics cause it to experience a peak CBC near mid-cycle, rather than at BOC as in the conventional core. After a slight initial decrease, CBC gently increases until it reaches a maximum value of 1730 ppm at a core-average cycle exposure of 24 GWD/MTU. Following this peak, enough burnable poison has been removed from the fuel so that fissile atom depletion and the accumulation of non-saturating fission products controls the behavior of hot excess reactivity, and CBC decreases linearly to EOC. Compared to the conventional PWR core, the extended cycle design requires a higher concentration of soluble boron in the coolant for a much longer period of time. However, with the maximum value of dissolved boron kept below 1780 ppm, the EPRI-recommended limiting values for coolant pH (>6.9) and dissolved lithium concentration (<2.2 ppm) described in Section 3.3 are never exceeded.

Note that when HFP CBC reaches 0 ppm, the End of Full Power Life (EOFPL) for the extended cycle core is reached. Although the cycle length can be extended by reducing reactor power to lower overall temperatures, thereby lowering fuel Doppler and moderator negative reactivity, critical operation at 100% power is no longer possible. The cycle length achieved by the extended cycle core design is discussed in greater detail below.

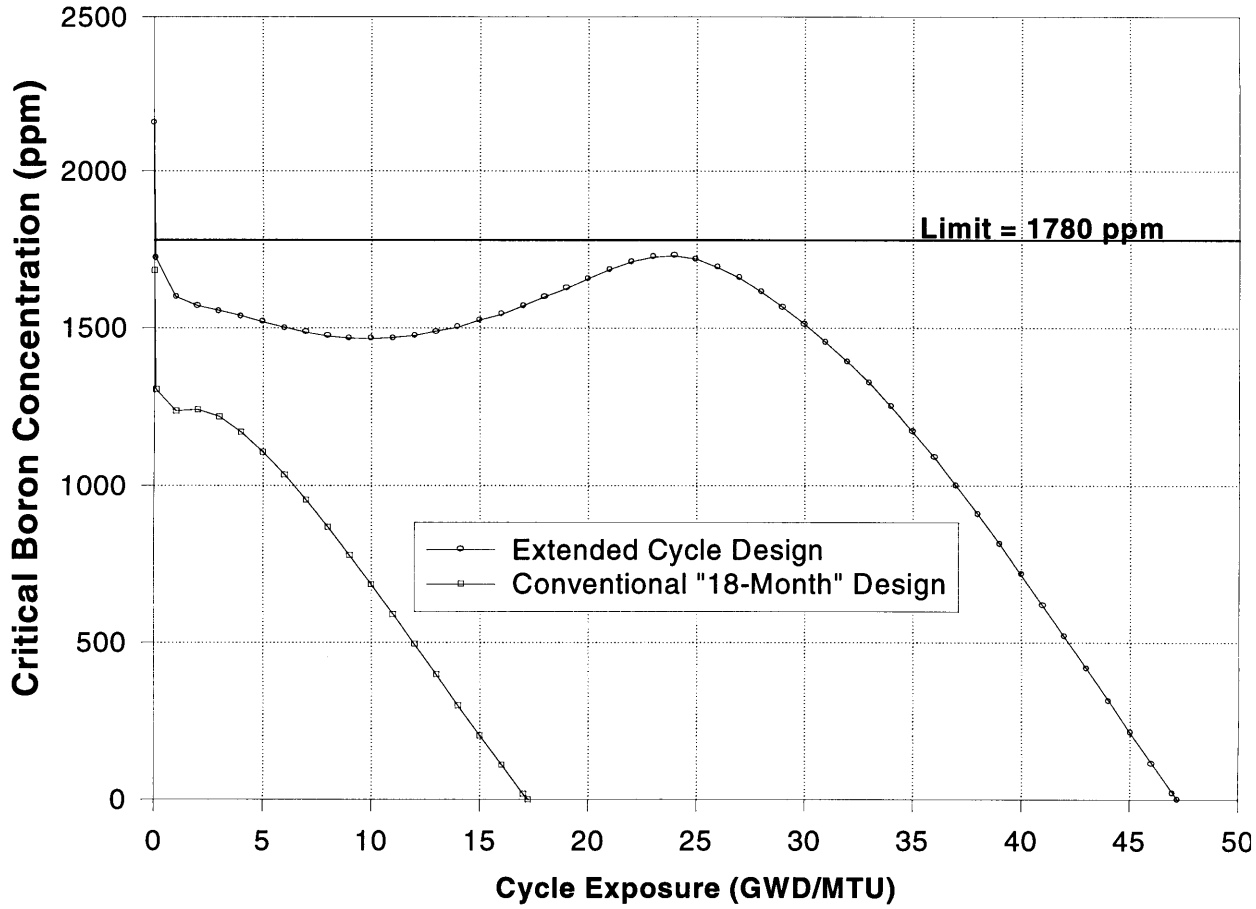

Figure 32: PWR Critical Boron Concentration vs. Core-Average Exposure

6.1.4 Cycle Length

As mentioned in Section 1.1, this project targets an achievable cycle length of 41.76 EFPM for the PWR, which corresponds to 48 calendar months of operation at an overall capacity factor of 87%. However, the heavy poison loading required to reduce the peak CBC and the need to control fuel costs (and therefore enrichment) combine to constrain the cycle length to 38.8 EFPM. The actual calendar length of the operating cycle depends upon the capacity factor achieved by the plant. To convert from EFPM into units of operating cycle calendar months, the cycle length is divided by an assumed capacity factor. The cycle length achieved by this design produces:

- 47,217 MWD/MTU core-average discharge burnup
- 55,844 MWD/MTU discharge burnup for the most highly burned *assembly*
- 59,959 MWD/MTU discharge burnup for the most highly burned *fuel pin*
- 1182 Effective Full Power Days (EFPD)

- 48 calendar months of operation at a capacity factor of 80.9%
- 44.6 calendar months of operation at a capacity factor of 87%
- 42 calendar months of operation at a capacity factor of 92.5%

Although the present PWR core design is actually reactivity limited (i.e., EOFPL is reached when HFP CBC = 0 ppm), cycle length cannot be increased much further without exceeding the lead pin exposure limit of 60,000 MWD/MTU. The high discharge exposure of the lead pin in the PWR core limits any possible cycle length extension from coastdown to ~1 EFPD. As described earlier, coastdown involves extending achievable cycle length by operating at reduced power and temperature to increase core reactivity. The cycle length achieved here demonstrates the technical feasibility of achieving an ultra-long cycle length in a currently operating PWR design.

6.2 Core Reactivity Coefficients

As discussed in Section 3.3, enriching the fuel to 7 $^{w}/_{o}$ U^{235} in the extended cycle PWR core increases its macroscopic cross-sections for absorption and fission in the thermal energy range. The increase in these cross-sections "hardens" or shifts the neutron energy spectrum to higher energies by causing a relative reduction in the thermal neutron flux. The hardened neutron energy spectrum of the extended cycle PWR core drives changes in core reactivity coefficients, boron worth, and control rod worth. Reactivity coefficients (i.e., the change in reactivity (ρ) per degree of temperature or percent power) determine whether the core can protect itself against autocatalytic power and temperature excursions. Using SIMULATE-3, the following parameters were calculated for the extended cycle core design:

- Moderator Temperature Coefficient (MTC): Defined as the reactivity change associated with a uniform change in moderator inlet temperature divided by the change in the average moderator temperature (pcm/°F). Calculated using a 5°F perturbation in moderator inlet temperature.
- Fuel Temperature (Doppler) Coefficient (FTC): Defined as the reactivity change associated with a uniform change in fuel temperature divided by the change in average fuel temperature (pcm/°F). Calculated using a 5°F change in fuel temperature.
- Boron Coefficient (BC): Defined as the reactivity change associated with the uniform perturbation of the boron concentration divided by the boron change (pcm/ppm). Calculated using a 10 ppm perturbation in boron concentration.

- Total Power Coefficient (PC): Defined as the reactivity change associated with the uniform change in the power level divided by the percent change in power (pcm/percent power). Calculated using a 1% perturbation in power level.

The values of these coefficients at various times in life for the PWR extended cycle design and for the conventional PWR core are shown in Table 10 through Table 13 Analysis of the values in Table 10 shows that while the extended cycle core MTC is generally more negative than that of the conventional core, the magnitude of its most negative value (at EOC) does not exceed the magnitude of the safety analysis limit for currently operating Westinghouse 4-loop PWRs, which is -42 pcm/°F at EOC HFP, equilibrium xenon conditions [W-2]. Thus the extended cycle design maintains a desirable negative MTC value for operation at power and does not increase the severity of any accidents affected by a highly negative MTC (steam line rupture and cold water injection).

Table 10: Comparison of PWR Moderator Temperature Coefficients

Extended Cycle PWR Core		Conventional PWR Core	
Core Condition	**MTC (pcm/°F)**	**Core Condition**	**MTC (pcm/°F)**
HFP, 0 GWD/MTU (BOC) No Xe, CBC = 2156 ppm	-10.19	HFP, 0 GWD/MTU (BOC) No Xe, CBC = 1684 ppm	-5.67
HFP, 0 GWD/MTU (BOC) Eq. Xe, CBC = 1725 ppm	-11.69	HFP, 0 GWD/MTU (BOC) Eq. Xe, CBC = 1306 ppm	-9.03
HZP, 0 GWD/MTU (BOC) No Xe, CBC = 2487 ppm	-2.96	HZP, 0 GWD/MTU (BOC) No Xe, CBC = 1853 ppm	+0.89
HFP, 24 GWD/MTU, (Peak CBC) Eq. Xe, CBC = 1730 ppm	-11.86		
HZP, 24 GWD/MTU, (Peak CBC) No Xe, CBC = 2744 ppm	+0.50		
HFP, 47.2 MWD/MTU (EOC), Eq. Xe, CBC = 0 ppm	-39.56	HFP, 17.2 MWD/MTU (EOC) Eq. Xe,CBC=0 ppm	-34.32

At BOC, the FTC values calculated for the extended cycle length PWR core are slightly less negative than those for the conventional core. This variation can be primarily attributed to the higher concentration of U^{238} (a strong resonance region absorber) in the fuel of the conventional core. A comparison of the values in Table 12 shows that the boron coefficient of the extended cycle PWR core has a lower magnitude than that of the conventional core. This difference is due to the neutron energy spectral shift discussed earlier. Finally, the extended cycle PWR core exhibits negative power feedback that is roughly comparable to that of the conventional design throughout the life of the core.

Table 11: Comparison of PWR Fuel Temperature Coefficients

Extended Cycle PWR Core		Conventional PWR Core	
Core Condition	**FTC (pcm/°F)**	**Core Condition**	**FTC (pcm/°F)**
HFP, 0 GWD/MTU (BOC) No Xe, CBC = 2156 ppm	-1.36	HFP, 0 GWD/MTU (BOC) No Xe, CBC = 1684 ppm	-1.37
HFP, 0 GWD/MTU (BOC) Eq. Xe, CBC = 1725 ppm	-1.35	HFP, 0 GWD/MTU (BOC) Eq. Xe, CBC = 1306 ppm	-1.38
HZP, 0 GWD/MTU (BOC) No Xe, CBC = 2487 ppm	-1.52	HZP, 0 GWD/MTU (BOC) No Xe, CBC = 1853 ppm	-1.66
HFP, 24 GWD/MTU, (Peak CBC) Eq. Xe, CBC = 1730 ppm	-1.45		
HZP, 24 GWD/MTU, (Peak CBC) No Xe, CBC = 2744 ppm	-1.71		
HFP, 47.2 MWD/MTU (EOC), Eq. Xe, CBC = 0 ppm	-1.57	HFP, 17.2 MWD/MTU (EOC) Eq. Xe,CBC=0 ppm	-1.53

Table 12: Comparison of PWR Boron Coefficients

Extended Cycle PWR Core		Conventional PWR Core	
Core Condition	**BC (pcm/ppm)**	**Core Condition**	**BC (pcm/ppm)**
HFP, 0 GWD/MTU (BOC) No Xe, CBC = 2156 ppm	-4.19	HFP, 0 GWD/MTU (BOC) No Xe, CBC = 1684 ppm	-6.85
HFP, 0 GWD/MTU (BOC) Eq. Xe, CBC = 1725 ppm	-4.18	HFP, 0 GWD/MTU (BOC) Eq. Xe, CBC = 1306 ppm	-6.83
HZP, 0 GWD/MTU (BOC) No Xe, CBC = 2487 ppm	-4.36	HZP, 0 GWD/MTU (BOC) No Xe, CBC = 1853 ppm	-7.11
HFP, 24 GWD/MTU, (Peak CBC) Eq. Xe, CBC = 1730 ppm	-4.24		
HZP, 24 GWD/MTU, (Peak CBC) No Xe, CBC = 2744 ppm	-4.47		
HFP, 47.2 MWD/MTU (EOC), Eq. Xe, CBC = 0 ppm	-6.29	HFP, 17.2 MWD/MTU (EOC) Eq. Xe,CBC=0 ppm	-8.52

Table 13: Comparison of PWR Total Power Coefficients

Extended Cycle PWR Core		Conventional PWR Core	
Core Condition	PC (pcm/%)	Core Condition	PC (pcm/%)
HFP, 0 GWD/MTU (BOC) No Xe, CBC = 2156 ppm	-14.04	HFP, 0 GWD/MTU (BOC) No Xe, CBC = 1684 ppm	-11.59
HFP, 0 GWD/MTU (BOC) Eq. Xe, CBC = 1725 ppm	-13.76	HFP, 0 GWD/MTU (BOC) Eq. Xe, CBC = 1306 ppm	-12.35
HZP, 0 GWD/MTU (BOC) No Xe, CBC = 2487 ppm	-14.04	HZP, 0 GWD/MTU (BOC) No Xe, CBC = 1853 ppm	-13.12
HFP, 24 GWD/MTU, (Peak CBC) Eq. Xe, CBC = 1730 ppm	-13.29		
HZP, 24 GWD/MTU, (Peak CBC) No Xe, CBC = 2744 ppm	-14.79		
HFP, 47.2 MWD/MTU (EOC), Eq. Xe, CBC = 0 ppm	-20.59	HFP, 17.2 MWD/MTU (EOC) Eq. Xe,CBC=0 ppm	-19.12

6.3 Control Rod Worth

6.3.1 Comparison of Control Rod Worth

In addition to affecting the core's reactivity coefficients, the hardened neutron energy spectrum of the extended cycle PWR core also alters the worth of the reactor's control rods. To quantify these effects, CASMO-3 runs were made to compare the change in assembly reactivity due to rod insertion in a "conventional" assembly for an 18 month PWR core and in a typical assembly for the extended cycle PWR core. The 18 month assembly used standard Westinghouse 24 finger silver/indium/cadmium ($80^{w}/_{o}$ Ag/$15^{w}/_{o}$ In /$5^{w}/_{o}$ Cd) Rod Control Cluster Assemblies (RCCA). It contained fuel enriched to 4.4 $^{w}/_{o}$ U^{235} and 20 pins loaded with 6 $^{w}/_{o}$ Gd_2O_3 as burnable poisons. The extended cycle fuel bundle is a Type 4 assembly with 7 $^{w}/_{o}$ U^{235} and 40 burnable poison pins containing a combination of 12 $^{w}/_{o}$ Gd_2O_3 and 1.545 mg B^{10}/in. IFBA. From Table 7 on page 85, the Type 4 assembly is the most common type of fuel bundle in the extended cycle core, and thus the most likely to be located beneath an RCCA. Three different types of neutron absorber material were analyzed for use in the RCCAs of the extended cycle assembly. The four cases modeled are listed below:

- Standard Case: 4.4$^{w}/_{o}$ U^{235} w/ 6$^{w}/_{o}$ Gd_2O_3 in 20 BA pins. Uses standard Westinghouse 24 finger Ag-In-Cd RCCAs
- Extended Cycle Case w/ Standard RCCAs: 7.0$^{w}/_{o}$ U^{235} w/ 12$^{w}/_{o}$ Gd_2O_3 & IFBA in 40 BA pins. Uses standard Ag-In-Cd RCCAs
- Extended Cycle Case w/ B_4C RCCAs: 7.0$^{w}/_{o}$ U^{235} w/ 10$^{w}/_{o}$ Gd_2O_3 & IFBA in 40 BA pins. Uses B_4C RCCAs, which have a higher worth than Ag-In-Cd RCCAs.
- Extended Cycle Case w/ hybrid RCCAs: 7.0$^{w}/_{o}$ U^{235} w/ 10$^{w}/_{o}$ Gd_2O_3 & IFBA in 44 BA pins. Uses hybrid RCCAs which have 40" of Ag-In-Cd absorber and 102" of B_4C. Ag-In-Cd is added to make the RCCAs heavy enough to avoid decreasing rod drop times unacceptably during a scram.

The environmental conditions for each case were identical and were selected to represent typical HFP operating conditions. These conditions were as follows:

- Fuel Temperature = 627°C (1160°F)
- Moderator Temperature = 310°C (590°F)
- Boron Concentration = 450 ppm

For each case, rod worth was calculated as:

$$\Delta\rho = \ln\left(\frac{k_1}{k_2}\right) \tag{6.1}$$

where k_1 and k_2 represent the k_∞ values for the unrodded and rodded assemblies, respectively.

Control rod worth as a function of assembly average burnup is shown in Figure 33. CASMO-3 results show that Ag-In-Cd RCCAs are inadequate for the extended cycle design since their worth in the extended cycle assembly is 20%-30% lower than for the conventional assembly. However, using the higher worth B_4C or hybrid RCCAs, rod worths comparable to the standard case can be achieved. The figure also shows that the control rod worth in the extended cycle assemblies experiences a greater change in magnitude than that of the 18 month assembly. Since these changes in rod worth are driven primarily by shifts in assembly neutron energy spectrum, an analysis of their behavior reveals much about the energy spectrum performance of the extended cycle core design.

Figure 33 illustrates that a key characteristic of the extended cycle core is not the hardened energy spectrum (which can be compensated for) but rather the magnitude of the shift in the energy

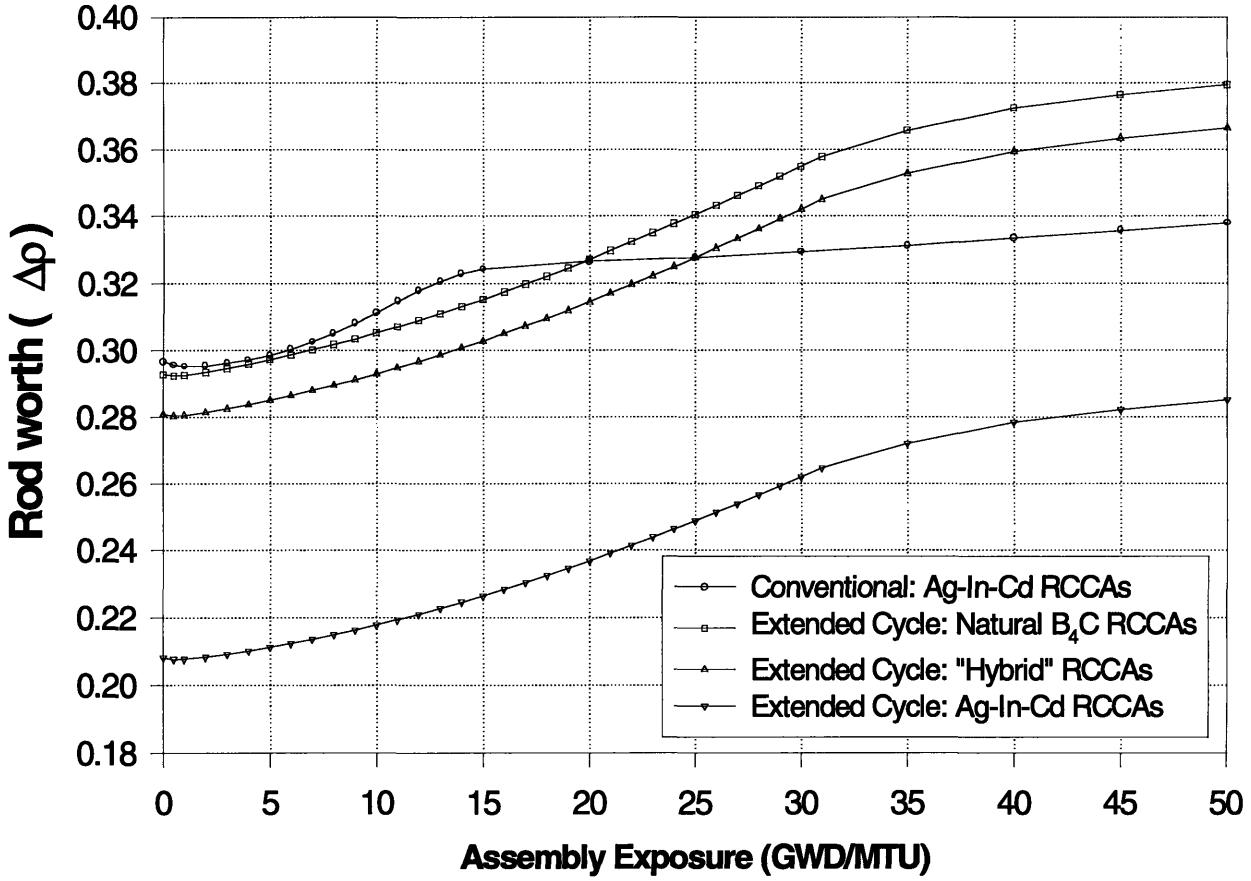

Figure 33: CASMO-3 Comparison of Control Rod Worth

spectrum over core life. As burnup progresses, the core becomes less "black" to thermal neutrons as strong thermal absorbers (U^{235} and Gd) are depleted. With fewer thermal absorbers present, thermal flux in the core increases, and the neutron energy spectrum "softens" or shifts toward lower energies. In the extended cycle core, the presence of a strong thermal absorber such as gadolinium increases the rate of spectral shift since for the same amount of exposure, more thermal absorbers (i.e., fuel and poison) are removed. Therefore the magnitude of the spectral shift during one cycle for the extended life design will be much greater than that of a conventional core because it occurs at a faster rate and because the cycle exposure is much longer. This spectral shift may result in an excessive control rod worth at EOC for a rod ejection accident. Additionally, this problem will only be exacerbated if (as discussed in Section 6.1.4) longer cycle lengths are achieved by increasing fuel enrichment.

6.3.2 Demonstration of Adequate Shutdown Margin

In order to demonstrate that an adequate shutdown margin can be achieved, CASMO-3 runs were made to compare rod worth at the most reactive time in core life for each case. To demonstrate adequate shutdown margin, rod worth calculated for the PWR extended cycle design should equal or exceed the value calculated for the conventional PWR core. In this study the most reactive time in core life for the PWR is defined as the time of peak HFP CBC. The reactor is considered to be cold (68°F) and xenon free, with soluble boron at the HFP critical concentration. The scenario modeled for the comparison assumes that the reactor must be shut down and cooled down from HFP conditions at the most reactive time in core life. Xenon is assumed to decay away, and no credit is taken for any increase in soluble boron concentration.

In the conventional core, HFP CBC occurs at BOC. Because standard fuel management practice precludes the placement of fresh fuel under an RCCA, the typical exposure for assemblies in these locations is ~20 GWD/MTU [Y-1]. Therefore, for the conventional core, CASMO-3 calculations to evaluate shutdown margin determine rod worth at an assembly exposure of 20 GWD/MTU. With the PWR extended cycle design, peak CBC takes place near the mid-life point at 24 GWD/MTU. Because the single batch design of the extended cycle core reduces the variation in exposure between assemblies, the CASMO-3 calculations in this case were made at an assembly exposure of 24 GWD/MTU. The environmental conditions and the results of these rod worth calculations are summarized in Table 14. The CASMO-3 results in the table show that by using B_4C or hybrid B_4C/Ag-In-Cd RCCAs in an extended cycle core assembly, it is possible to achieve the equivalent rod worth of a conventional assembly using Ag-In-Cd RCCAs. These comparisons demonstrate the technical feasibility of achieving adequate control rod worth and shutdown margin in the extended cycle PWR core design.

Table 14: Comparison of Shutdown Rod Worth

Assembly Type	Fuel Temp.	Mod. Temp.	Boron (ppm)	RCCA Type	Assembly Exposure	Rod Worth (pcm)
Conventional	20°C	20°C	1306	Ag-In-Cd	20 GWD/MTU	22,090
Extended Cycle	20°C	20°C	1730	Ag-In-Cd	24 GWD/MTU	18,807
Extended Cycle	20°C	20°C	1730	B_4C	24 GWD/MTU	26,040
Extended Cycle	20°C	20°C	1730	"Hybrid"	24 GWD/MTU	25,031

6.4 Conclusions

The analyses performed in this section show that the neutronic design of the extended cycle core is technically feasible for reload into currently operating PWRs. To ensure an adequate shutdown margin in the extended cycle core, the Ag-In-Cd RCCAs currently in use will have to be replaced with higher worth B_4C or combination B_4C/Ag-In-Cd control rods.

Chapter 7 which follows addresses the thermal and mechanical performance of nuclear fuel in the extended cycle PWR core design.

CHAPTER 7

PWR Fuel Performance Evaluation

While neutronic design performance criteria have already been considered in the PWR extended cycle core, fuel thermal and mechanical performance also present potential design barriers and limitations to long cycle operation. The operating envelope of batch loaded cores in extended cycles can be fuel performance limited because the fuel operates at high temperatures for long periods of time. This gives rise to problems such as waterside corrosion and rod internal pressure. A preliminary investigation of extended cycle fuel has been launched in coordination with the PWR core neutronic design to assess any potential barriers to technical feasibility.

7.1 Waterside Corrosion

Waterside corrosion in a PWR depends both on temperature and water chemistry control. The zirconium in Zircaloy PWR cladding combines with water at the operating temperatures (250°C-350°C) and pressures (1000 psia-2250 psia) found in PWRs to produce zirconium oxide (ZrO_2) and hydrogen in the following reaction:

$$Zr + 2H_2O \rightarrow ZrO_2 + 4xH + 2(1-x)H_2\uparrow \tag{7.1}$$

where the reactants are zirconium (Zr) and water; and the products include the zirconium oxide layer formed on the outside of the fuel (ZrO_2), the molecular hydrogen picked up by the cladding

(H), and the diatomic hydrogen gas released into the reactor coolant system (H_2). The symbol x in this case represents the fraction of hydrogen picked up by the cladding.

This reaction has two negative consequences with respect to cladding performance. The first, formation of an oxide layer, not only serves to weaken the structural integrity of the cladding by taking away zirconium metal, but also creates an insulated region around the cladding which drives up the average temperature of the fuel. As this temperature increases, so does the rate of the corrosion process, creating an autocatalytic effect. The second negative effect seen from the Zircaloy-water reaction is that of hydrogen pick-up, which decreases cladding ductility and strength. Both of these effects may be increased in the extended cycle PWR core. Fuel in the extended cycle uni-batch PWR core cannot be shuffled into locations having reduced power late in life. Because of this, many of the assemblies will run at high power for longer periods of time than their conventional multi-batch counterparts. Tools exist to quantitatively evaluate the effects of oxide layer formation and hydrogen pickup by the clad with respect to longer operating cycles. The results of this and all other fuel performance investigations will be reported in January, 1998, by Handwerk [H-4].

7.2 Rod Internal Pressure

7.2.1 Description

Another fuel performance issue that will be a concern for longer operating cycles is rod internal pressure. As uranium fissions, it creates fission products, some of which are gaseous and which become trapped in the UO_2 ceramic lattice. As the operating temperature of the fuel rod increases, the amount of this gas that is released from the fuel pellets also increases. Assemblies having power greater than core average will be in a high temperature gas release regime for extended periods of time. Excessive internal pin pressure can produce thermal and irradiation-induced outward creep in the cladding. If internal pin pressure becomes much greater than primary pressure it can cause the fuel-clad gap to widen. This will reduce gap thermal conductivity and raise fuel temperatures, releasing more fission gas and leading to possible fuel damage through autocatalytic clad ballooning. Additionally, the gases released, primarily xenon (Xe) and krypton (Kr), have thermal conductivities which are appreciably less than that of the initial fill gas helium (He)

[M-1]. These gases lower gap thermal conductivity even further as exposure increases, thereby exacerbating conditions in the later stages of fuel lifetime [M-2].

The high burnable poison loading used in the extended cycle PWR core further complicates the fuel performance situation. As mentioned in the neutronic design section, the high Gd_2O_3 loading in the burnable absorber pins necessitates the use of annular pellets to control fuel temperatures, since high concentrations of Gd_2O_3 degrade the thermal conductivity of UO_2, producing higher fuel temperatures and higher gas release fractions [I-1]. Finally, the neutron absorbing B^{10} isotope in the IFBA coating releases helium into the fuel-clad gap as it undergoes the following (n,α) reaction in core:

$$B_5^{10} + n_0^1 \rightarrow He_2^4 \uparrow + \ Li_3^7 \tag{7.2}$$

The release of helium into the fuel-clad gap from this reaction will also contribute to an increase in fuel pin internal pressure. Although He helps to improve the thermal conductivity of the gap gas, any beneficial effect is far outweighed by the sheer magnitude of the rise in fuel pin internal pressure produced by this reaction.

7.2.2 Analytical Method

To evaluate fuel performance with respect to fission gas release, pin internal pressures for the extended cycle PWR core operating under steady-state conditions have been evaluated using the fuel performance code FROSSTEY-2. The FROSSTEY (**F**uel **RO**d **S**teady-**S**tate **T**hermal **E**ffects) package, developed by the Yankee Atomic Electric Company, calculates fuel rod temperature distributions, fuel-to-cladding gap conductance, fuel rod dimensional changes, fission gas release, internal gas pressure, and stored energy predictions as a function of fuel rod operating history [S-9]. To prevent fuel damage, the rod internal pressure must stay below the level at which the diametrical fuel-clad gap begins to increase due to outward cladding creep during normal operation. For Westinghouse 17×17 fuel this design requirement pressure is 2800 psia at a system pressure of 2250 psia [R-4]. At or below this pressure, the outward clad creep rate is less than or equal to the outward radial fuel displacement rate from swelling, and the gap does not open.

Because the analyses in this study only consider steady-state operations, some allowance must be made for the effects of transients on fuel performance. A sharp, temporary jump in local power

produces a fuel temperature "spike" which can cause a burst of gaseous fission products to be released from the ceramic matrix of UO_2 fuel. This sudden release of fission gases causes pin internal pressure to rise and to remain elevated even after temperatures return to normal. Because of this, the limit selected for fuel pin internal pressure for the extended cycle core design is **2600 psia**. This more conservative limit provides a 200 psi "buffer zone" to account for pressure increases due to transients encountered during normal operation.

To generate the fuel rod power histories required by FROSSTEY-2, this study uses the concept of an "envelope" fuel pin. Using the envelope pin concept, the operating history is developed from SIMULATE-3 calculations of the axially averaged exposure and power of the hottest burning fuel pin in the core at each time step of the analysis. Because the identity of the peak power pin changes as the cycle progresses (see Figure 26 on page 89), the operating history developed in this manner is actually a conglomerate of the behavior of the hottest burning pins in the core. By attributing all of these "worst case" power histories to a single "envelope pin," this method ensures conservative analysis results.

Envelope pin power histories used in the extended cycle PWR fuel pin internal pressure analysis are shown in Figure 34. An envelope pin power history for the conventional PWR core is also included for comparison. The power histories show that, as has been described earlier, assemblies in the uni-batch, extended cycle PWR core will operate at significantly higher powers at high exposures than their conventional PWR core counterparts. Close scrutiny of the figure also reveals discontinuities in the power histories of both the extended cycle and the conventional PWR core design. The discontinuities result from the need to generate envelope pin data for the highest exposure fuel in the core. In the extended cycle core, the envelope pin at EOC has an exposure of approximately 55 GWD/MTU. Therefore the envelope pin data for the high burnup "tail" from 55 to 59.9 GWD/MTU comes from the highest exposure (and not the peak power) fuel rods in the core. In the *n*-batch conventional core, the discontinuities result from tracking the hottest burning fuel rod in each (shuffled) batch in order to generate high burnup envelope pin data.

Note that for the extended cycle core separate traces are shown for the poisoned and unpoisoned fuel. Because of their heavy burnable absorber loading, the poisoned pins in the extended cycle design are never the peak burning fuel pin in the core for a given time step. However, even though these fuel rods run at lower powers, the combined detrimental effects of Gd_2O_3 and IFBA

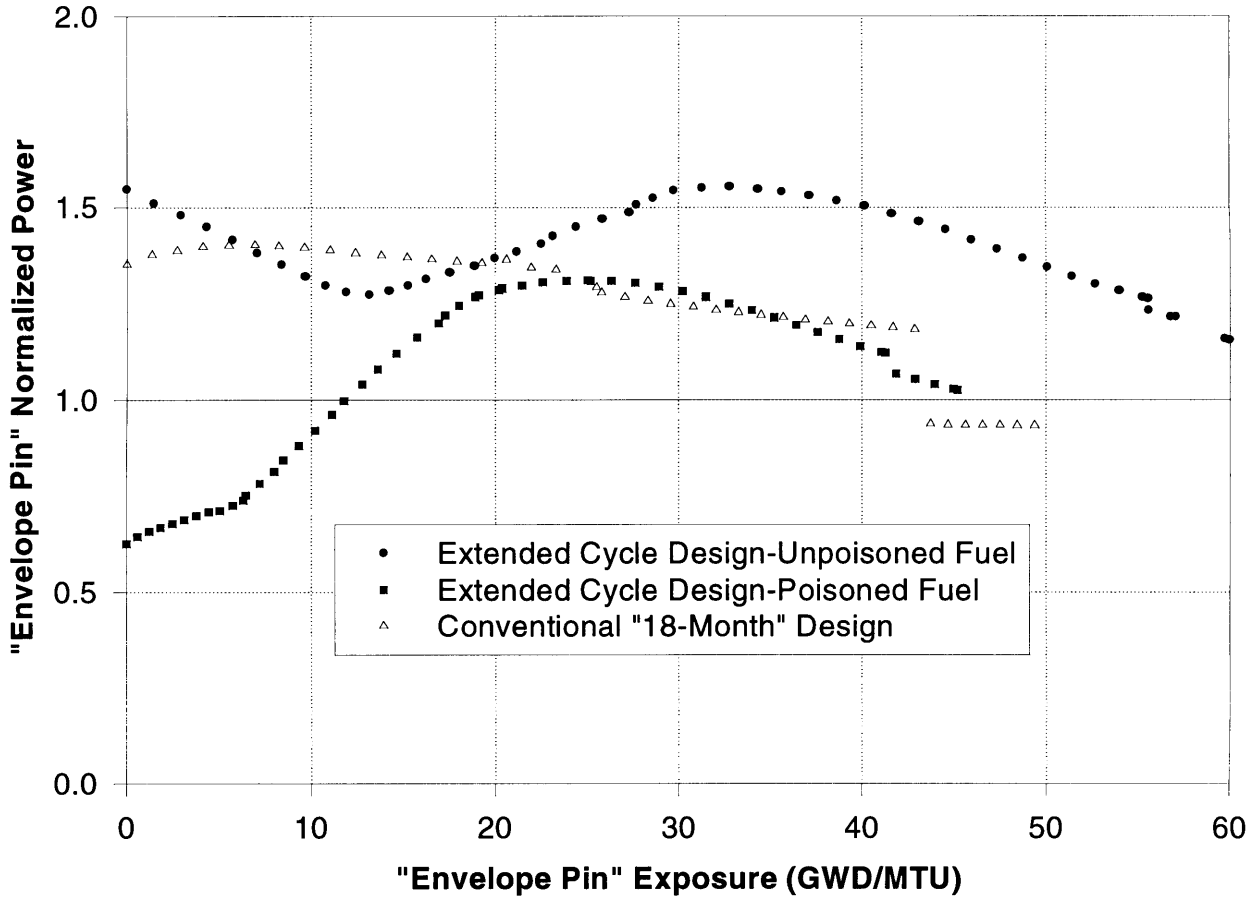

Figure 34: Comparison of Envelope Pin Power Histories

make a separate FROSSTEY-2 evaluation of the poisoned pins necessary to ensure that the limit on internal pressure is met.

In order to quantify the effects of the heavy neutron absorber loading required by the PWR extended cycle design, FROSSTEY-2 calculations of fuel pin internal pressure were performed as an initial scoping study for the following burnable poison schemes:

- Case 1: $10^{w}/_{o}$ Gd_2O_3 and a 3.09 mg B^{10}/inch IFBA surface coating
- Case 2: 3.09 mg B^{10}/inch IFBA surface coating only
- Case 3: $10^{w}/_{o}$ Gd_2O_3 and a 3.09 mg B^{10}/inch IFBA surface coating in 10% central void annular fuel
- Case 4: $10^{w}/_{o}$ Gd_2O_3 only
- Case 5: Unpoisoned fuel

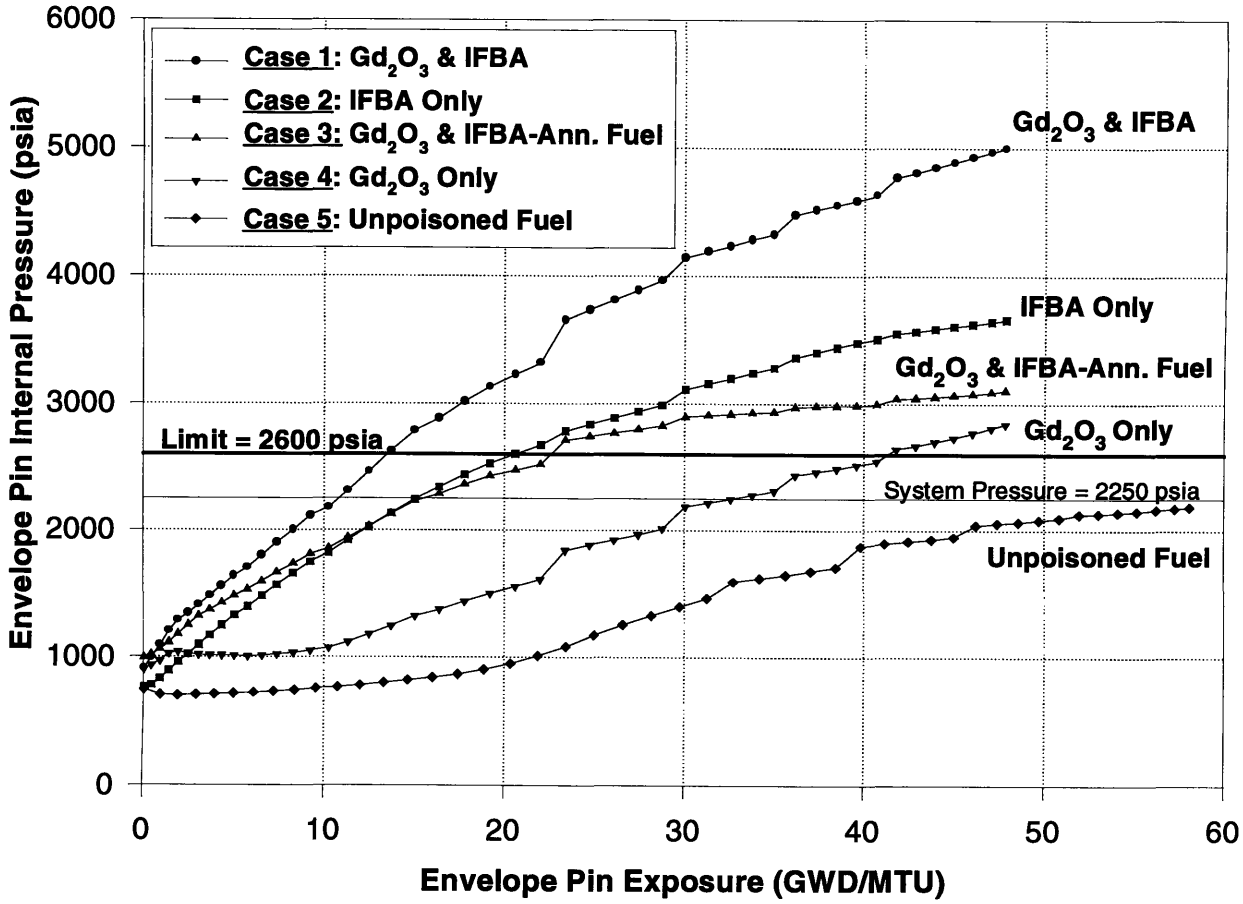

Figure 35: Effect of Burnable Absorbers on Pin Internal Pressure

To make these comparisons, envelope pin power histories for Case 1 & Case 5 were generated from a SIMULATE-3 model of an extended cycle PWR core design. To isolate the effects of changes in burnable absorber loading on pin internal pressure, the FROSSTEY-2 calculations for Cases 2 through 4 were made using the same envelope pin power history generated for Case 1. Each of the pins being modeled contains central zone fuel enriched to $7^{w}/_{o}$ U^{235} and uses $5^{w}/_{o}$ U^{235} unpoisoned annular axial blankets (15.24 cm) at the top and bottom. For Case 3, the entire pin consists of 10% central void annular fuel, although the top and bottom 15.24 cm remain unpoisoned and have an enrichment of $5^{w}/_{o}$ U^{235}. The FROSSTEY-2 calculations of pin internal pressure vs. envelope pin exposure for the five cases listed above are shown in Figure 35.

As shown in the figure, the removal of IFBA from the fuel pins produces the largest change in internal pressure, with a difference of nearly 2200 psi between the EOC values of Case 1 and Case 4. With lower fuel temperatures and a larger volume for fission gas expansion, the annular

fuel used in Case 3 also reduces pin pressure significantly, causing a 1900 psi drop compared to Case 1. Note also that the complete removal of Gd_2O_3 in Case 2 only lowers peak pressure by approximately 1300 psi.

The results of the above analysis show that the most promising strategies for lowering rod internal pressure below the design goal limit are the reduction of IFBA loading and the use of annular fuel in the poisoned fuel pins. However, because the PWR extended cycle design relies so heavily on burnable poisons for reactivity and power distribution control, any changes in the burnable poison scheme will have a significant impact on the neutronic behavior of the core. The development of a burnable poison scheme that satisfies both the fuel mechanical and neutronic design goals of the extended cycle PWR core design is detailed in the following sub-section.

7.2.3 Burnable Absorber Fuel Pin Design

Although removing IFBA from the fuel decreases pin pressure significantly, the resulting reduction in burnable absorber excess reactivity hold-down necessitates a corresponding increase in soluble boron concentration in order to maintain reactivity control. As discussed in Section 3.3, unacceptably high levels of soluble boron lead to water chemistry and cladding corrosion problems. In order to keep pin internal pressure *and* soluble boron concentration within acceptable limits, burnable absorber excess reactivity hold-down lost due to the removal of IFBA must be made up with an increase in the concentration of Gd_2O_3. As described in Section 5.2, the final design for the extended cycle core uses $12^{w}/_{o}$ Gd_2O_3 and a 1.545 mg B^{10}/inch IFBA surface coating. Because IFBA has a larger impact on the amount of gas released to the fuel-clad gap than Gd_2O_3, "swapping out" half of the IFBA loading for a 20% increase in Gd_2O_3 loading lowers pin internal pressure while maintaining acceptable reactivity control within the core. However, because gadolinium has a larger EOC negative residual reactivity penalty than IFBA, this swap *decreases* the achievable cycle length of the extended cycle core.

Even with a reduced IFBA loading, annular fuel must be used in the burnable absorber pins of the extended cycle design in order to keep pin internal pressure below 2600 psia. To compare the effect of changes in void size on fuel mechanical and neutronic performance, CASMO-3 and FROSSTEY-2 calculations were performed for the following two annular fuel poison schemes:

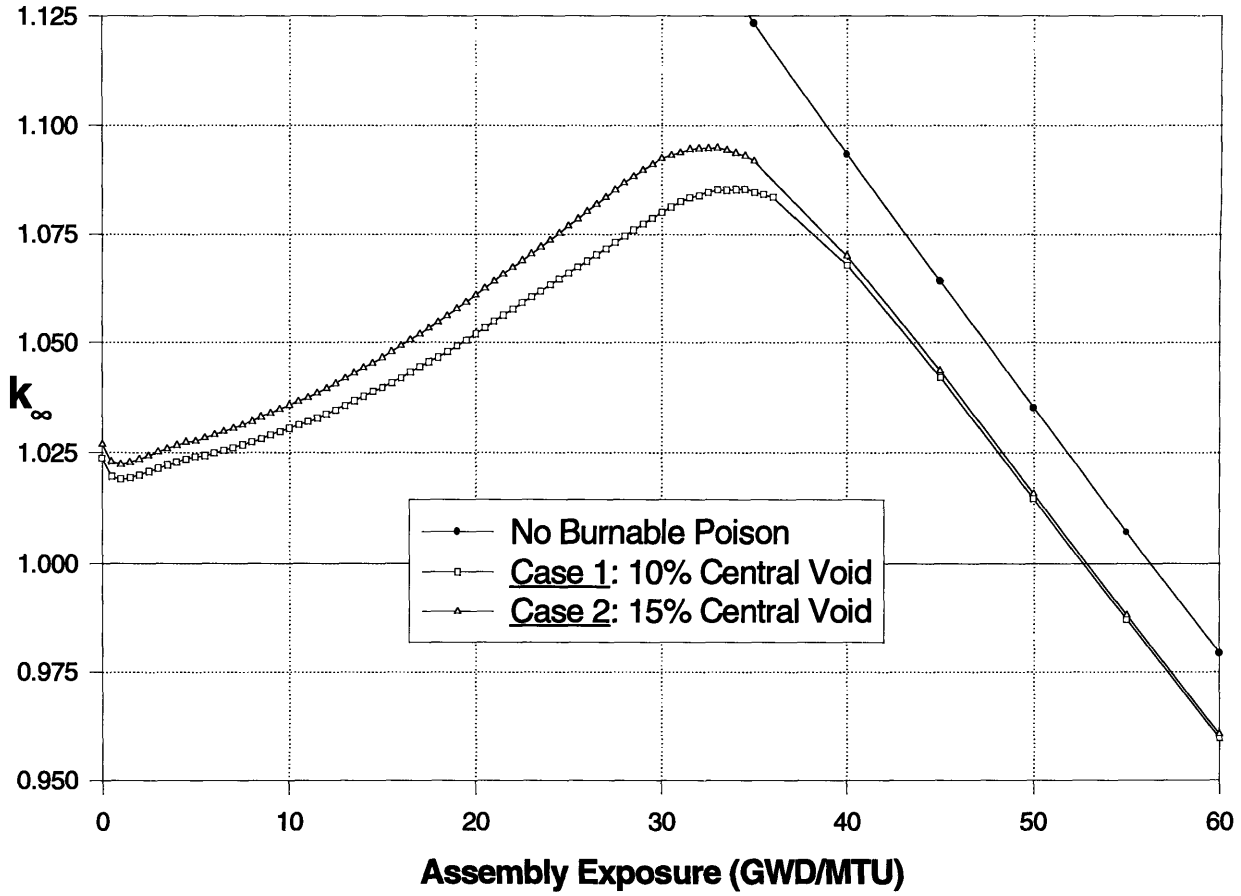

Figure 36: Effect of Annular Fuel Central Void Size on Assembly Reactivity

- Case 1: $12^{w}/_{o}$ Gd_2O_3 & 1.545 mg B^{10}/in. IFBA, 10% volume central void (void radius, r_v = 1.295 mm)
- Case 2: $12^{w}/_{o}$ Gd_2O_3 & 1.545 mg B^{10}/in. IFBA, 15% volume central void (r_v = 1.59 mm)

CASMO-3 calculations of assembly k_∞ vs. exposure for Table 3 Base Case conditions are shown in Figure 36. The assemblies modeled are of the Type 5 design, with a central zone enrichment of $7^{w}/_{o}$ U^{235} and 44 burnable absorber pins. The figure shows that expanding the volume of the annular fuel central void leads to a rise in peak assembly reactivity. This higher peak results from the removal of Gd_2O_3 atoms from the assembly as the void radius (r_v) of the annular pellets is increased. FROSSTEY-2 calculations show the use of the larger 15% volume void in Case 2 decreases pin internal pressure by 500 psi compared to Case 1. However, the negative impact on neutronic performance that the rise in assembly reactivity produces makes the use of a larger central void an undesirable strategy for improving fuel mechanical performance. A larger

void/higher burnable absorber loading design was not pursued because the concentration of Gd_2O_3 must be maintained at $12^{w}/_{o}$ to remain near the current burnable poison experience base. Therefore, 10% volume central void annular fuel was selected for use in the extended cycle PWR core design.

7.2.4 PWR Extended Cycle Design Performance

FROSSTEY-2 calculations of the pin internal pressure for the poisoned and unpoisoned fuel of the extended cycle design PWR core are shown in Figure 37. The peak pin pressure for the conventional PWR core design is also included for comparative purposes. In addition, Figure 38 shows the peak centerline temperature for the envelope pin in both core designs. This figure also plots the values of UO_2 melting temperature as a function of pin exposure calculated from the following empirical correlation [S-10]:

$$T_{melt}(B) = 2805°C - 32°C\left(\frac{B}{10\frac{GWD}{MTU}}\right) \tag{7.3}$$

where: B = Fuel pin exposure in GWD/MTU

The figures show that the peak pin internal pressure in the extended cycle core design occurs at EOC in the envelope pin of the *unpoisoned* fuel. The peak value of 2530 psia stays below the design goal limit of 2600 psia set for the extended cycle core. Although the burnable absorbers produce a higher pin internal pressure in the poisoned pins early in the cycle, the greater exposure accumulated by the more reactive unpoisoned fuel results in a higher EOC pressure.

The plots of centerline temperature in Figure 38 and power history in Figure 34 reveal that despite the fact that it has an annular design and operates at a lower power, the poisoned fuel of the extended cycle core generally operates at the highest peak centerline temperature. These high temperatures stem from the degradation of UO_2 thermal conductivity caused by the heavy Gd_2O_3 loading in these pins. The higher temperatures in the unpoisoned fuel at EOC result from operation at high linear heat generation rates and from the degradation of UO_2 thermal conductivity due to the build up of fission products in high burnup fuel.

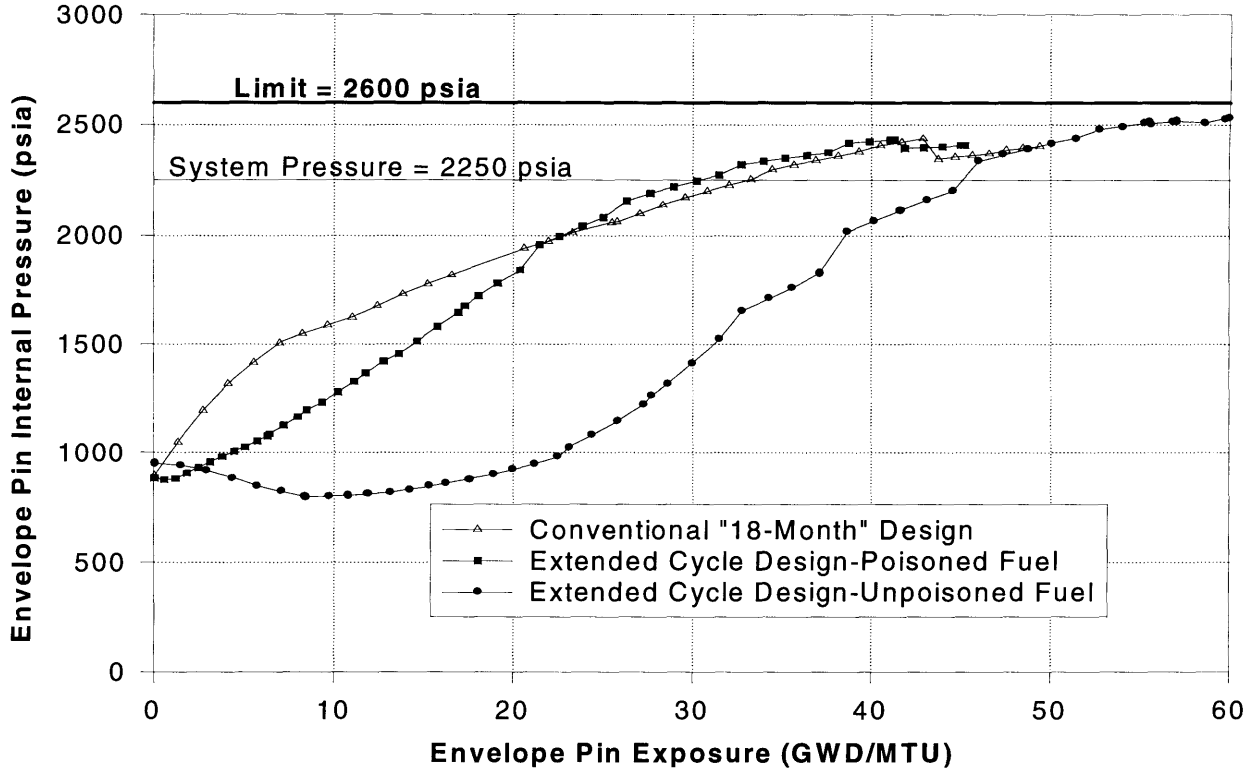

Figure 37: Fuel Pin Internal Pressure vs. Exposure

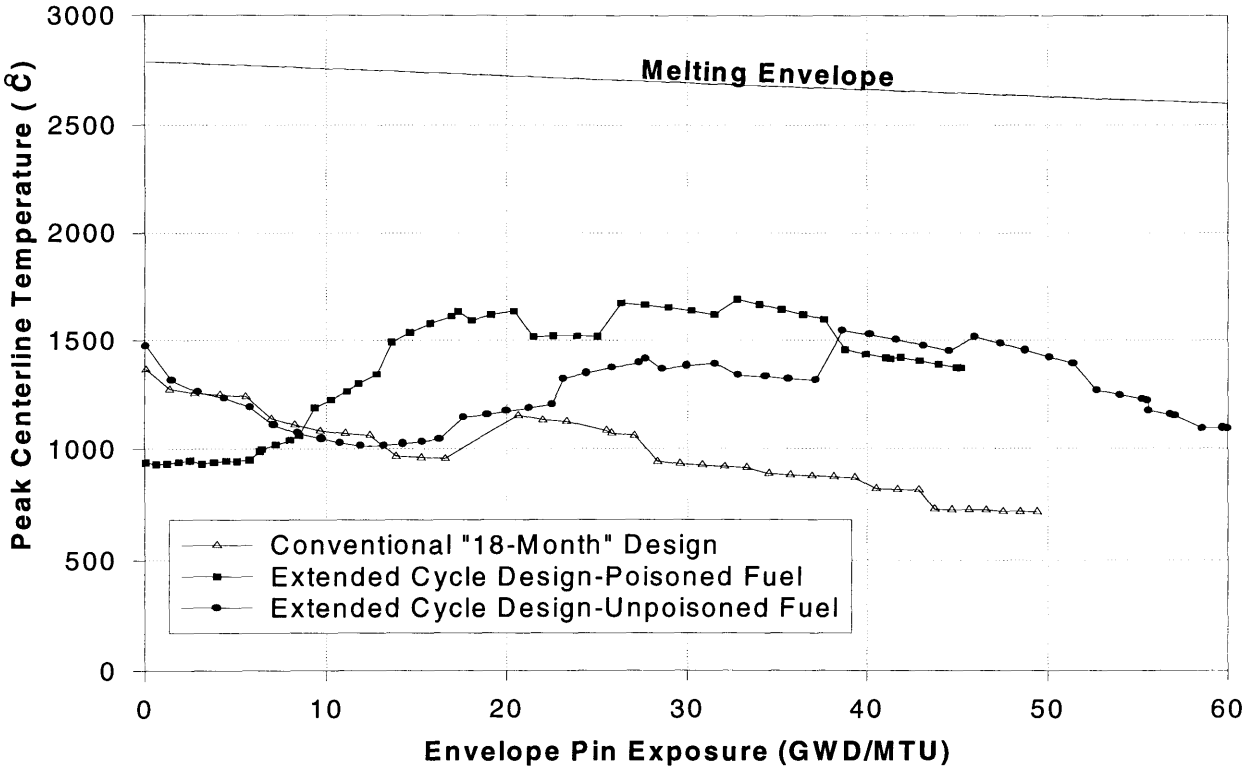

Figure 38: Fuel Peak Centerline Temperature vs. Exposure

7.3 Other Quantifiable Effects

Other fuel performance concerns associated with running nuclear power plants on longer operating cycles include irradiation induced fuel pellet swelling and Zircaloy cladding growth, and Axial Offset Anomaly (AOA). In an extended cycle core, fuel pins may swell more because the assemblies are operating at higher power levels than their conventional counterparts for longer periods of time. This swelling can cause problems in the rod radially as the fuel pellets may increase in diameter rapidly enough to close the fuel-clad gap and physically interact with the cladding. Excessive radiation induced growth of Zircaloy cladding may cause buckling in the fuel rods as they interact with fixed supports. The fuel performance investigations being performed by Handwerk will quantify the core parameters contributing to these effects in order to assess their impact on the performance of the PWR extended cycle core design [H-4].

In addition, fuel bundles which experience a large flux gradient (e.g., peripheral assemblies) are susceptible to bowing and twisting due to uneven Zircaloy growth. Bowed fuel rods are a concern because they can hinder control rod insertion and can therefore cause increased rod drop times or rod insertion failures during a reactor scram. Note from Figure A.1 in Appendix A that in the Westinghouse 4-Loop PWR the eight RCCAs in Shutdown Bank A are located on the core periphery.

AOA is defined as the difference between the predicted and actual measure of axial offset and is predicted to increase with cycle length. Although not yet verified, heavy crud deposition with boron hideout is suspected to suppress power in parts of the core, creating this effect. AOA is a concern because it challenges the thermal and mechanical limits of the fuel in a concentrated area much more than predicted.

7.4 Qualifiable Effects

Some of the effects of running at longer operating cycles which are not as easily quantified as those in the previous section are grid-to-rod fretting, debris fretting, and structural design issues. Grid-to-rod fretting has many initiating mechanisms, all of which would be enhanced by longer

cycle operation: damage occurring to grid cell features from crud in the coolant resulting in inadequate rod support, fluid forces on the fuel, excessive clad creep-down, and excessive relaxation of the grid support spring resulting in inadequate rod support. Fluid forces on the fuel may initiate grid-to-rod fretting by exciting the fuel assembly at a critical frequency and causing it to vibrate. Longer operating cycles will have a more negative effect in this area because the fuel remains in the same position and orientation for a longer period of time. Fuel assemblies will therefore be subjected to these same damaging fluid forces for longer periods of time without the benefit of periodic inspections during refueling to detect and prevent problems and without the opportunity to shuffle and/or rotate. One can neither "coddle" highly burned fuel nor average-out the effects of asymmetric forces. All other initiators are typically functions of operating time and will be amplified with longer cycle length operation.

Debris fretting is similar to grid-to-rod fretting in that it is a failure mechanism which is caused by a mechanical interaction between the fuel rod and another object. While the longer in-core residence time without shuffling associated with longer cycle length operation would allow more time for these mechanical interactions and would therefore increase the chance of fuel failure, the smaller number of refuelings inherent with such a strategy would decrease the opportunity for debris to be introduced into the reactor coolant system. While there is certainly a trade-off between less debris introduced and longer time to fret with longer cycle operation, the exact balance is not easily quantified.

Longer cycles may also affect fuel performance because rod bowing, buckling and twisting result from fluid forces on the fuel assemblies as well as from irradiation induced growth. Longer in-core residence times without shuffling or bundle rotation would amplify these effects and would have the potential to compromise structural integrity and inhibit control rod insertion [R-5].

Finally it should be noted that regardless of the fuel failure mechanism, the consequences of experiencing a failed fuel rod at 15 months of operation and allowing the plant to run until the next refueling outage at 18 months are significantly smaller than in a similar scenario in which the plant is allowed to run until the next refueling outage at 45 months.

7.5 Conclusions

The analyses performed in this section demonstrate that the extended cycle core design meets the established limits for fuel pin internal pressure under steady-state conditions. Detailed analyses of other fuel performance parameters in the extended cycle design are ongoing and will be detailed in a separate report.

The section which follows examines some of the economic considerations of ultra-long operating cycles and outlines the framework for a more detailed comparative analysis.

CHAPTER 8

Economic Aspects of Ultra-Long Operating Cycles

8.1 Introduction to Uranium and Separative Work Utilization

The relationships governing the economics of fuel costs in extended cycle cores can best be explained by introducing the concepts of uranium utilization, U_U, and separative work utilization, U_{SWU}. In this study, "uranium utilization" is defined as the thermal megawatt days of energy generated per kilogram of natural uranium purchased, and has units of MWD/kg U_{NAT} [D-2]. Similarly, "separative work utilization" is defined as the thermal megawatt days of energy generated per kilogram SWU (i.e., Separative Work Units expressed in mass units of kilograms) purchased, and is given in units of MWD/kg SWU. These quantities can be written as:

$$U_U\left(\frac{MWD}{kgU_{NAT}}\right) = \frac{B_d\left(\frac{MWD}{MTU}\right)}{\left[\frac{F(kgU_{NAT})}{P(kgU)}\right]} \tag{8.1}$$

$$U_{SWU}\left(\frac{MWD}{kgSWU}\right) = \frac{B_d\left(\frac{MWD}{MTU}\right)}{\left[\frac{S(kgSWU)}{P(kgU)}\right]} \tag{8.2}$$

where P = fuel batch heavy metal mass (kg U [enriched])

S = fuel batch required separative work (kg SWU)
F = natural uranium feed required to produce P or S (kg U_{NAT})

Thus the ratio F/P can be defined as the mass of natural uranium needed to produce one unit mass of enriched product for reactor fueling. Similarly, S/P represents the amount of separative work required to produce one unit mass of enriched product for reactor fueling. By performing mass and separative work balances around the enrichment process, and ignoring processing losses, the following linear relationships can be developed (for uranium tails of $0.25^{w}/_{o}$ U^{235}) [M-3]:

$$\frac{F}{P} = 2.17X_p - 0.54 \tag{8.3}$$

which is exact, and the following good approximation for the enrichment ranges of interest:

$$\frac{S}{P} = 2.13X_p - 2.70 \tag{8.4}$$

where X_p is the weight percent enrichment of nuclear fuel.

Thus in order to calculate U_U and U_{SWU} from the above relationships, it is necessary to correlate reload fuel enrichment, X_p, with achievable discharge burnup, B_d. For the Westinghouse 4-Loop PWR used in this study, the following quadratic relationship provides an excellent fit of plant data [P-4]:

$$\bar{X}_p = 1.820 + 2.98 \times 10^{-5}\bar{B}_{CEOC} + 1.464 \times 10^{-9}(\bar{B}_{CEOC})^2 \tag{8.5}$$

where: $\bar{X}_p$ = Reload fuel weighted average initial enrichment ($^{w}/_{o}$ U^{235})
B_{CEOC} = Core-average End-Of-Cycle (i.e., EOFPL) fuel burnup (MWD/MTU)

Using a linear model of reactivity, B_d can be calculated from $\bar{B}_{CEOC}$ and the batch number, n, as follows [D-2]:

$$B_d = \left(\frac{2n}{n+1}\right)\bar{B}_{CEOC} \tag{8.6}$$

By combining equations (8.1) through (8.6), U_U and U_{SWU} can be expressed as functions of average initial reload enrichment, $\bar{X}_p$, for the Westinghouse 4-Loop PWR analyzed in this study. Figure 39 illustrates the relationship between U_U, and U_{SWU}, and reload enrichment for a single batch ($n = 1$) fuel management scheme. The plots show a weak optimum for uranium utilization

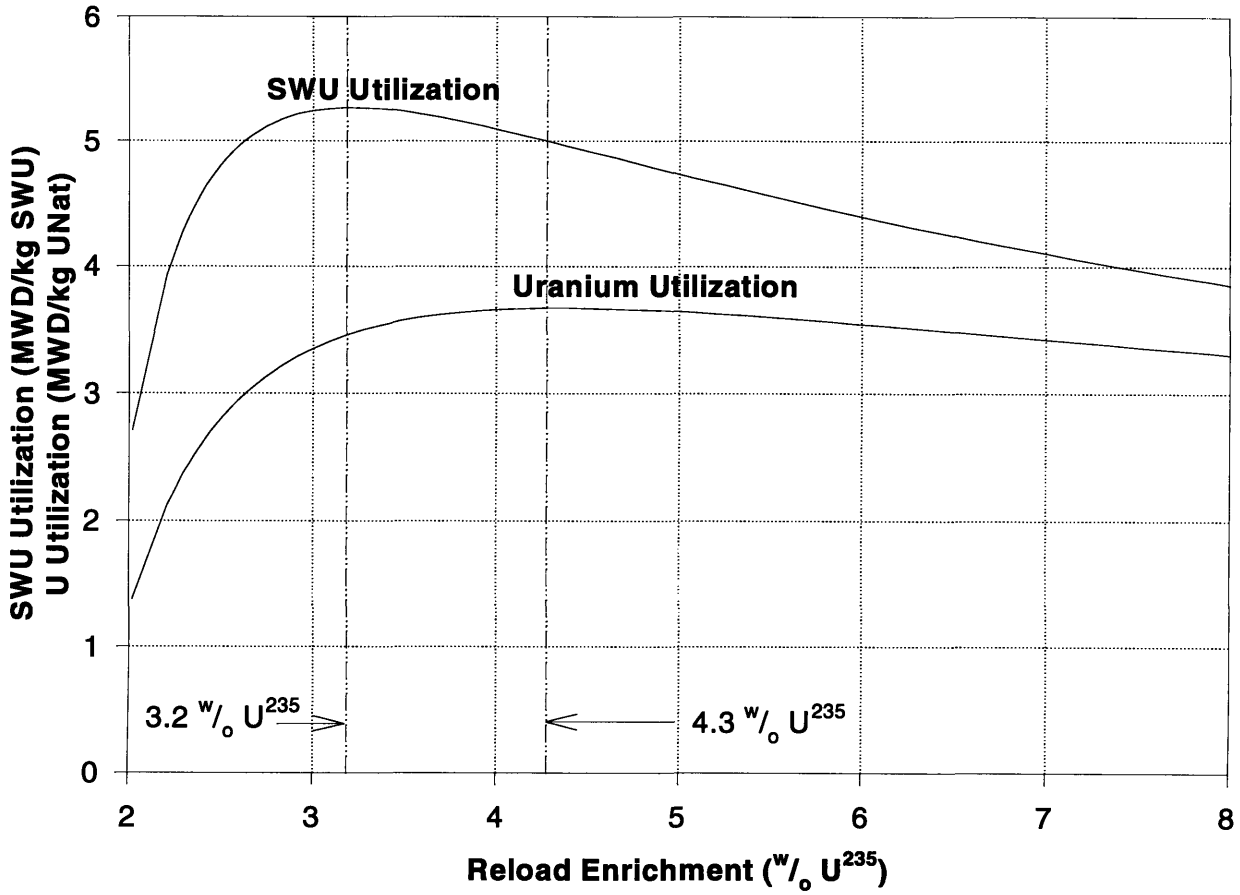

Figure 39: Uranium and SWU Utilization for a Single Batch PWR Core (n = 1)

at an enrichment of $4.3^{w}/_{o}$ U^{235} and a stronger maximum for separative work utilization at an enrichment of $3.2^{w}/_{o}$ U^{235}. Note that for multi-batch schemes ($n > 1$), utilization can be calculated by multiplying the single batch values in the figure by the factor $2n/(n + 1)$ from equation (8.6). Thus, with multi-batch fuel management, utilization increases but the optima remain at the same enrichments calculated for the single batch case. The figure clearly shows that the higher enrichments required for ultra-long cycle lengths are well beyond the optimum values for both U_U and U_{SWU}. Consequently, when fuel at these higher enrichments is used, the amount of energy (and therefore, revenue) generated for the amount of natural uranium feed and SWU purchased is less than the amount of energy that would have been generated if the same amount of SWU and natural uranium had been used to manufacture a (larger) batch of lower enrichment fuel. In the following section the relationships shown in Figure 39 are used to quantify the increases in direct fuel costs resulting from ultra-long fuel cycles.

8.2 Calculation of Direct Fuel Costs

The following simple analysis quantifies the differences in fuel cost between the extended cycle and the conventional PWR core design which stem directly from variations in uranium and separative work utilization. The amount of energy, E, generated in a given time period by the 3411 MW_{th} PWR in this study can be calculated by multiplying the thermal power of the reactor by the effective capacity factor and the number of calendar days of operation. Thus at the target capacity factor of 87%, the amount of energy (in MWD) generated in a single year of operation is given by:

$$E(MWD) = Q(MW) \cdot T_c(days) \cdot L(\%)/100 \tag{8.7}$$

$$E(MWD) = 3411MW \cdot 365.25days \cdot 0.87 = 1.084 \times 10^6 MWD \tag{8.8}$$

The annual amount of natural uranium and separative work required to generate this amount of energy is calculated by simply dividing through by U_U and U_{SWU} as follows:

$$M_U(kgU_{NAT}) = \frac{E(MWD)}{U_U\left(\frac{MWD}{kgU_{NAT}}\right)} \tag{8.9}$$

$$M_{SWU}(kgSWU) = \frac{E(MWD)}{U_{SWU}\left(\frac{MWD}{kgSWU}\right)} \tag{8.10}$$

where: M_U = Mass of natural uranium required to generate E
M_{SWU} = Amount of separative work required to generate E

The direct fuel cost comparison of the extended cycle and the conventional PWR core is summarized in Table 15. Note that with natural uranium in the RBAs and reduced enrichment axial blankets, the average enrichment of the extended cycle core is $6.5^{w}/_{o}$ U^{235}. The prices used to calculate the dollar values of M_U and M_{SWU} are OECD study values of \$50/kg U_{NAT} and \$110/ kg SWU [O-1]. The table shows that for the same amount of energy produced, the extended cycle core increases direct nuclear fuel costs by \$17.1M per year due to its lower uranium and SWU utilization. While this quantification of costs is far from complete (for example, carrying charges are not assessed), it clearly illustrates that lengthening the operating cycle produces a significant

increase in fuel costs. The reduction in uranium and separative work utilization which results from both the use of higher than optimum enrichments (i.e., the $n = 1$ value of $U_U = 3.49$ for $\bar{X}_p = 6.5$ vs. a peak value of 3.67) *and* the single batch fuel management scheme (i.e., even at the same value of $\bar{X}_p$, U_U and U_{SWU} for an n-batch core will always be larger by a factor of $2n/[n + 1]$) dramatically raises the cost of producing energy. In order for extended fuel cycles to become economically attractive, these increased fuel costs must be compensated for by increased capacity factors and the elimination of costly refueling outages.

Table 15: Comparison of PWR Direct Nuclear Fuel Costs

Core Design	$\bar{X}_p$ (w/o)	U_U (MWD/kgU_{NAT})	U_{SWU} (MWD/kgSWU)	M_U (kgU_{NAT}) [$M/year]	M_{SWU} (kgSWU) [$M/year]	Total Fuel Cost
Extended Cycle ($n = 1$)	6.5	3.49	4.24	3.11×10^5 [15.5]	2.56×10^5 [28.1]	$43.6M per year
Conventional Cycle ($n = 2.68$)	4.3	5.34	7.28	2.03×10^5 [10.1]	1.49×10^5 [16.4]	$26.5M per year

8.3 Conclusions

The extended cycle PWR core design will have increased fuel costs compared to a conventional multi-batch core. The benefits of a higher capacity factor and fewer refueling outages which will come from an extended operating cycle must outweigh these increased fuel costs in order for longer operating cycles to be economically attractive to utilities. A detailed economic analysis of the extended cycle core design is currently in progress and will be detailed in a separate report.

The design framework established for the extended cycle PWR will next be applied to the development and evaluation of an ultra-long operating cycle reload core for a large modern BWR. Chapter 9 which follows introduces the BWR extended cycle design.

CHAPTER 9

BWR Extended Cycle Core Design

As already described, a single-batch reload PWR core has been designed which demonstrates the technical feasibility of operating at cycle lengths greater than 40 months while staying within current discharge fuel burnup limits. In this and succeeding chapters, the development of an extended cycle core design for a large modern BWR is described using the framework of single-batch loaded, higher enrichment, and heavily poisoned fuel that was established for the PWR. With its increased neutronic and thermal hydraulic complexity, the BWR requires a correspondingly more intricate core design in order achieve extended operating cycle lengths.

9.1 Introduction

One of the most important differences between the reference plants for the PWR and BWR extended cycle core designs is their specific power rating. The General Electric BWR/5 plant selected for this study has a nominal specific power of 24.4 kW/kgU compared to 38.7 kW/kgU for the extended cycle PWR. In a four year operating cycle, this lower specific power will allow the BWR to operate at a higher overall capacity factor than the PWR while still staying within current fuel discharge exposure limits. Accordingly, the BWR extended cycle core is based on a design capacity factor of 95% compared to 87% for the PWR. The 95% goal was selected as the highest reasonably achievable overall capacity factor for a well run plant operating on a four year refueling cycle.

Recalling the development of the relationship between discharge burnup and cycle length detailed in Section 1.2.2, and substituting the values of $L = 95\%$ and $Q_{sp} = 24.4\ kW_{th}/kgU$ into equation (1.4a), the discharge burnup of the extended cycle BWR can be expressed in terms of operating cycle length as follows:

$$B_d\left(\frac{MWD}{MTU}\right) = n \cdot 706\left(\frac{MWD/MTU}{month}\right) \cdot T_c(months) \tag{9.1}$$

By combining equation (9.1) with the same burnup/enrichment correlation that was presented for the PWR in equation (1.5), BWR discharge burnup can also be written in terms of core average fresh reload enrichment, as shown in the equation below.

$$B_d\left(\frac{MWD}{MTU}\right) \approx [14{,}784 \cdot (X_p(\%) + 0.1072)]\left(\frac{MWD}{MTU}\right) - 706\left(\frac{MWD/MTU}{month}\right) \cdot T_c(months) \tag{9.2}$$

Analysis of data on spent nuclear fuel discharged from U.S. reactors indicates that within a tolerance band to account for varying operational strategies, the burnup/enrichment correlation of equation (1.5) is equally applicable to both PWRs and BWRs [E-3].

Using equations (9.1) and (9.2) a burnup-enrichment map for the representative BWR plant is plotted in Figure 40 for n = 1, 2, 3, 4, and for $X_p = 4^w/_o$ and $5^w/_o\ U^{235}$. Comparing Figure 40 to the PWR burnup-enrichment map in Figure 1 reveals that in addition to being able to operate at a higher overall capacity factor than the PWR, the BWR will also require a lower core-average fresh reload enrichment to achieve an extended cycle length. The GE BWR/5 target plant selected for the extended cycle core design is described in detail in the section which follows.

9.2 BWR Plant Description

The target plant selected for this study is a General Electric 1100 MW_e BWR/5 with 764 fuel assemblies. As with the PWR, this plant type was selected because of its relatively widespread use and high (for BWRs) specific power rating. Of the 37 commercial BWRs currently operating in the United States, 14 are 764 assembly BWR/4 or BWR/5 units [F-2]. Additionally, only four currently operating U.S. BWRs (all BWR/6 units) have a higher specific power rating than the

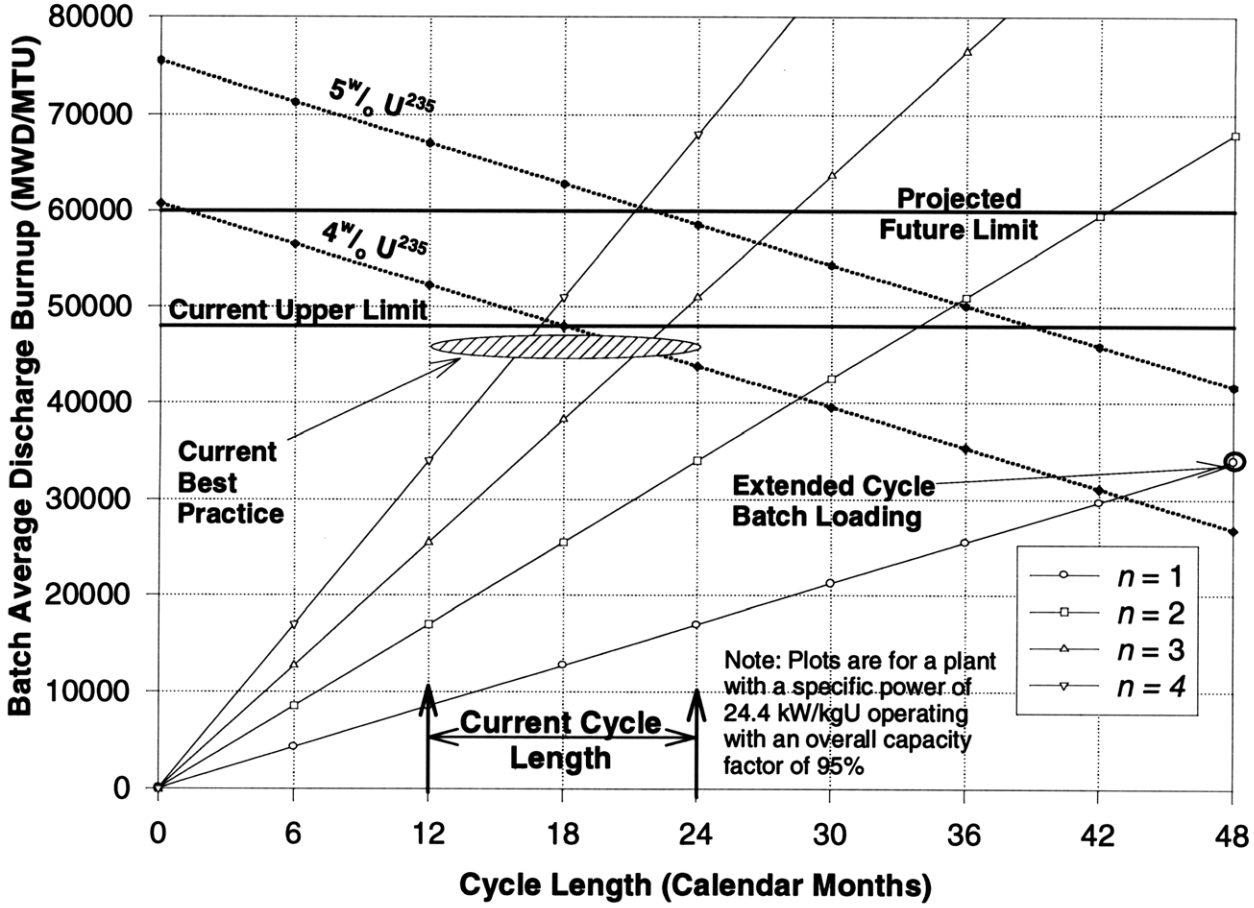

Figure 40: Burnup-Cycle Length Map for a Representative BWR

BWR/5 selected for this study. The target plant core is loaded with high performance ATRIUM-10 fuel bundles manufactured by Siemens Power Corporation. The 10×10 lattice and other advanced features of this bundle design provide an increased margin to core design limits throughout the extended fuel cycle. Much of the information on the operating parameters for the BWR/5 and the ATRIUM-10 fuel assemblies was provided by STUDSVIK of America and by Siemens Power Corporation. These parameters are summarized in the table below [S-11], [S-12]. All dimensions given in the table are cold dimensions.

One of the key neutronic differences between the PWR and the BWR is the presence of substantial steam voids within the reactor core. The axial void gradient of a BWR caused by the increase in coolant quality as it flows upward through the heated core causes significant bottom power peaking at the beginning of the operating cycle. To counteract this phenomenon, the control rods in a BWR (which enter from the bottom of the reactor) are positioned to flatten this bottom

Table 16: Operating Parameters for a General Electric BWR/5

	Operating Parameter	Value
1.	Plant	
	Number of recirculation loops	2
	Total heat output of the core (MW_{th})	3380
	Total plant thermal efficiency (%)	32.5
	Electrical output of plant (MW_e)	1100
2.	Core	
	Mass of fuel as UO_2 (MT)	157.4
	Mass of fuel as U (MTU)	138.7
	Rated power density (kW/L)	50
	Specific power (kW/kgU)	24.4
	Average linear heat generation rate (kW/ft), 10×10 ATRIUM fuel	4.0
	Core volume (m^3)	67.6
3.	Primary Coolant	
	System pressure (MPa) [100% power, 100% flow]	7.2
	Total core flow rate (Mg/sec)	13.13
	Rated coolant mass flux (kg/m^2-sec)	739.7
	Core inlet temperature (^oC) [100% power, 100% flow]	278.9
4.	Fuel Rods	
	Total number	69,524
	Fuel density (% of theoretical)	95
	Pellet diameter (mm)	8.67
	Pellet height (mm)	10.5
	Fuel-clad radial gap width (μm)	85
	Cladding material	Zircaloy-2
	Cladding thickness (mm)	0.605
	Clad outer diameter (mm)	10.05

Table 16: Operating Parameters for a General Electric BWR/5

	Operating Parameter	Value
	Full-length fuel rod height (m)	3.81
	Part-length fuel rod height (m)	2.59
5.	Fuel Assemblies	
	Number of assemblies	764
	Assembly array	10×10
	Array geometry	square
	Water gap symmetry	C-lattice (symmetric)
	Assembly pitch (cm)	15.24
	Number of full-length fuel rods per assembly	83
	Number of part-length fuel rods per assembly	8
	Rod pitch (mm)	13.0
	Overall dimensions (mm×mm)	133.6×133.6
6.	Control Rods	
	Neutron absorbing material	B_4C
	Active Control rod length (m)	3.66
	Cladding material	Type 304 SS
	Number of control rods	185
	Control rod geometry	cruciform blades

peaking and to bring the core power distribution to within design limits. In addition to shaping reactor power distribution, the control rods in a BWR also control core reactivity during operation. Because boiling in the core precludes the use of a soluble neutron poison such as boron, control rods are used to respond to reactivity changes within the core due to the depletion of fuel and burnable poisons as the cycle progresses. Finally, as in the PWR, the control rods must be able to effect a prompt shutdown (i.e., a "scram") at any time in core life and must be able to maintain the reactor in a continuously subcritical condition with the maximum worth rod in the core fully

withdrawn [G-1]. In order to accomplish this triple mission of power shaping, operational reactivity control and shutdown safety, the control rods in a BWR are inserted into the core in carefully planned pattern sequences. The physics characteristics which govern the selection and implementation of these control rod patterns are described in the following section.

9.2.1 BWR Control Rod Patterns

9.2.1.1 BWR Control Rod Description

The control rods in a GE BWR/5 are formed into cruciform blades which are inserted into the core through the water gap between clusters of four enclosed fuel assemblies. The neutron absorbing material for these rods is boron carbide (B_4C) powder, which is compacted into stainless steel tubes that are then placed vertically in a stainless steel sheath within the blade section of each rod. Each blade contains 18 tubes for a total of 72 in each rod. The boron used in the B_4C powder is natural boron with an $18^{w}/_{o}$ minimum concentration of the neutron absorbing B^{10} isotope. Control rods remain in service until boron depletion results in a 10% loss of relative rod worth in any axial section of the blade. Although actual reactivity loss will vary from rod to rod, the average expected service life for a control rod is 15 years [C-3].

Figure 41 shows a BWR control rod, with some of the major dimensions. Note that the active length of the neutron absorbing material in the rod is only 144 in. (3.66 m) compared to 150 in. (3.81 m) of active fuel height in the assemblies. The upper 6 in. (15.24 cm) of each rod consists of a stainless steel handle section. BWR control rods are hydraulically inserted into the core in 3" (7.62 cm) "steps" at an operational speed of 3 in. per second. In this study, control rod positions are reported by the number of steps that a rod is withdrawn from full insertion, with a position of '0' indicating full insertion and a position of '48' indicating full withdrawal.

Neutronically, while the worth of any given control rod worth will vary with position, fuel and poison loading, and core average exposure, an average control rod in the BWR extended cycle core is worth approximately 0.0013 Δk_{eff} at mid-cycle. Approximately 20% of control rod total worth is inserted by moving 58% of rod's total insertion length into the core (from position 48 to position 20), with another 20% inserted for each additional four steps of insertion until 92% of the full insertion length (position 4) is reached. There is very little effect on the core eigenvalue from

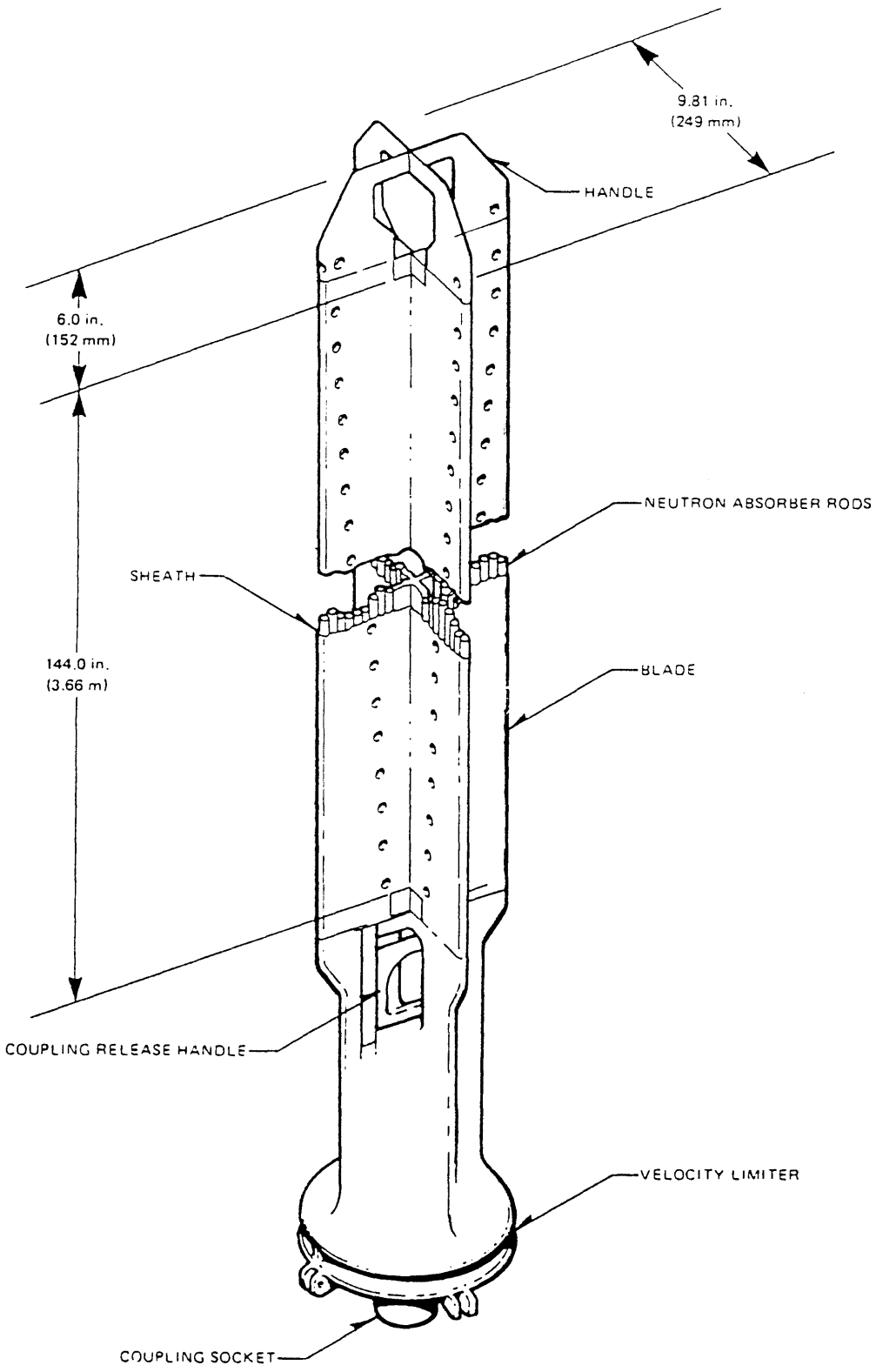

Figure 41: BWR Control Rod Schematic [G-1]

moving rods from a position of 4 to full insertion, although this move will have some impact on core power distribution.

9.2.1.2 BWR Control Rod Pattern Description

A control rod inserted into a BWR produces a strong localized distortion of the neutron flux in surrounding fuel assemblies. The presence of a strong thermal neutron absorber depresses the thermal neutron flux in adjacent fuel bundles and shifts the local neutron energy spectrum upward. The depressed thermal flux and hardened neutron energy spectrum reduce the burnup rate in nearby fuel rods and also increase the rate of U to Pu conversion resulting from U^{238} neutron capture. As a result, when the control rod is withdrawn, these low burnup, high Pu containing fuel pins operate at a higher power than they would if they had not been previously controlled. The magnitude of this power increase depends upon the amount of exposure accumulated with the control rods inserted and upon the amount of exposure accumulated in the uncontrolled state. This control blade history (CBH) effect on local power distribution can reduce margins to core thermal limits by producing strong local power peaks in axial sections of fuel assemblies adjacent to recently withdrawn control rods [G-1]. The presence of high concentrations of gadolinium in fuel adjacent to control rods further complicates the issue as the depressed neutron flux produced by an inserted rod slows the burnable poison depletion rate and can therefore produce further distortions in the local power distribution.

In order to lessen the impact of accumulated control blade history on fuel assembly performance, the control rods in the extended cycle BWR core are divided into four separate groupings, or patterns. Figure 42 shows the configuration of the BWR/5 core and indicates the position of its 185 control rods. Because of the high neutron flux gradient in the outlying regions of the reactor, the 40 control rods on the core periphery are generally not inserted into the core during normal operation at power. The remaining 145 control blades are separated into the four patterns (designated A_1, A_2, B_1, B_2) shown in Figure 43. During operation, each pattern is further subdivided into groups of 'deep' and 'shallow' rods in order to dissipate CBH effects as much as possible. Deep rods are inserted from 0 to 20 steps into the core and are generally used to control reactivity and the core radial power distribution. Shallow rods are positioned from 30 to 48 steps into the core and are used to shape the core axial power distribution. The use of 'mid-range' rods from 20

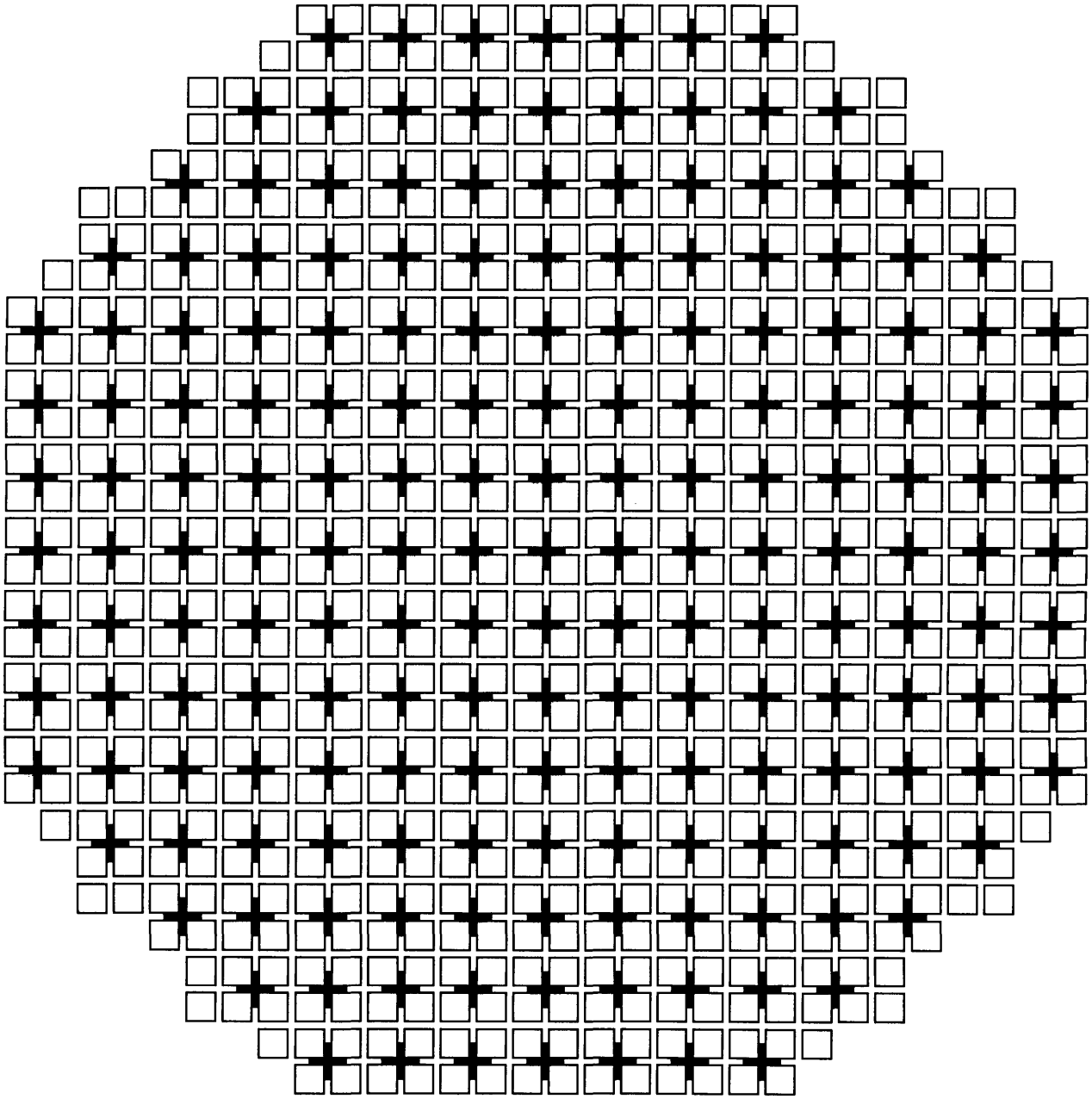

Figure 42: BWR/5 Control Rod Positions

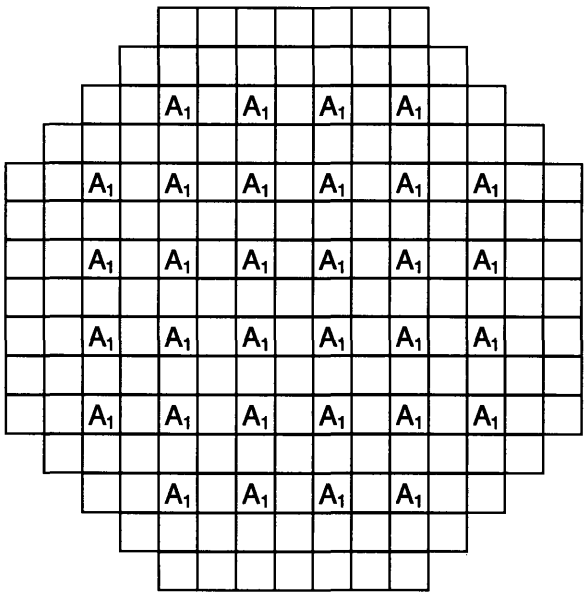

Control Rod Pattern A_1

(32 Available Control Rod Locations)

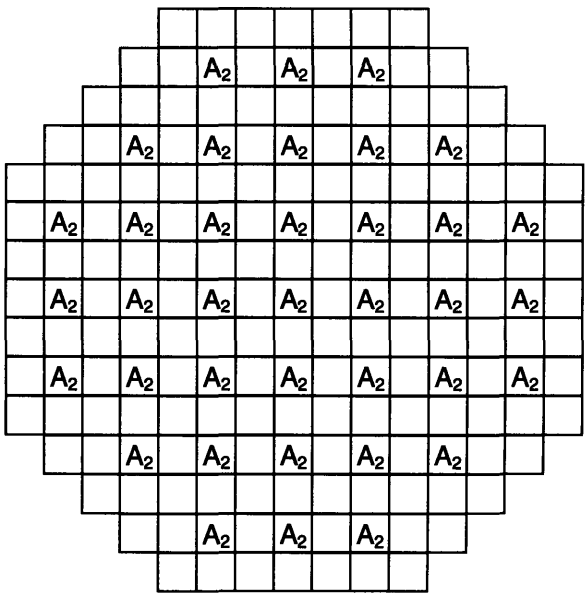

Control Rod Pattern A_2

(37 Available Control Rod Locations)

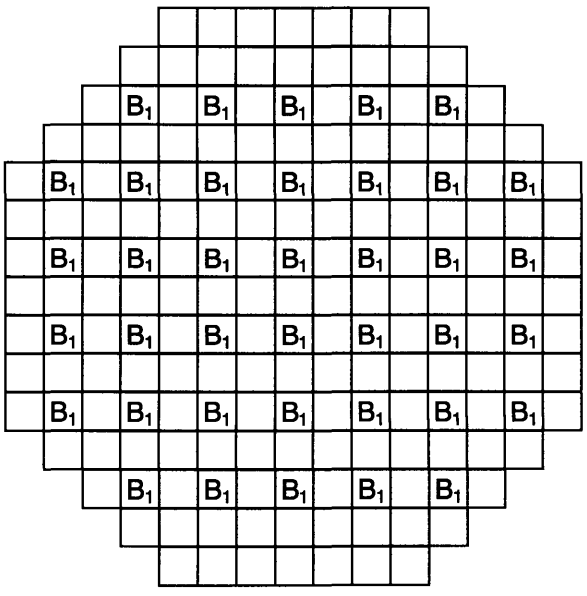

Control Rod Pattern B_1

(38 Available Control Rod Locations)

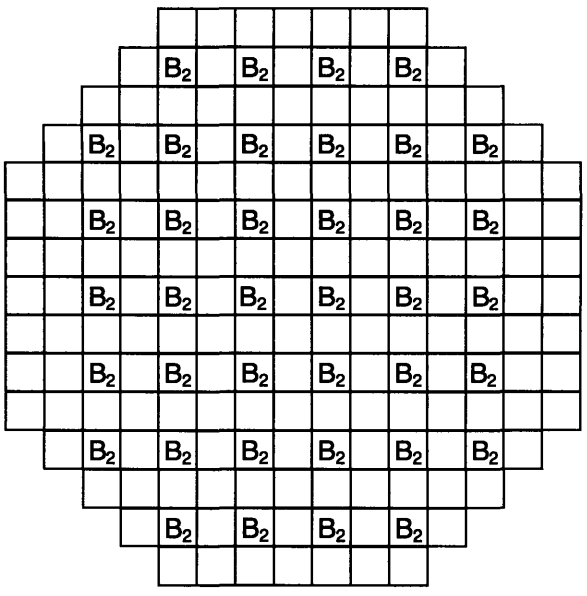

Control Rod Pattern B_2

(38 Available Control Rod Locations)

Figure 43: BWR Extended Cycle Design Control Rod Patterns

to 30 steps is allowable, although this obviously tends to blur the distinction between deep and shallow rods.

In the extended cycle BWR core design, the control rod patterns are implemented in a repeating sequence of A_2, B_2, A_1, B_1. The control rod patterns in the extended cycle core design are changed every 1.5 GWD/MTU of core average exposure, or approximately every two calendar months of operation at the target capacity factor. Additionally, the deep and shallow rods in each pattern are alternated every 0.75 GWD/MTU of core average exposure.

An alternative to the conventional control rod patterns used in the BWR extended cycle design is the Control Cell Core (CCC) concept developed by General Electric. In a Control Cell Core, control rod motion is limited to a fixed number of control rods (which, with their four surrounding fuel assemblies are designated 'control cells'). All other control rods in the core a kept fully withdrawn during normal reactor operation. Additionally, all assemblies in the control cell contain low reactivity fuel in order to eliminate control rod motion adjacent to high power fuel bundles. In a multi-batch equilibrium cycle core, this is accomplished by loading the control cells with high burnup fuel, while in a start-up core or in the single-batch extended cycle design, the control cells would contain low enrichment fuel. By limiting rod motion to a fixed number of rods, the CCC concept can improve plant capacity factor by eliminating the need to reduce power in order to effect rod pattern changes. Additionally, with only low reactivity fuel subject to CBH effects, local power peaking in the core is reduced and margins to thermal limits can be increased [G-1].

However, the requirement to use low enrichment fuel in the control cell assemblies would severely impair the mission of the extended cycle design. The 764 assembly BWR/5 selected for this study would typically use 37 control cells containing 148 fuel assemblies. These control cell assemblies represent 22% of the core's inventory of 672 non-peripheral assemblies. The significant reduction in core fissile atom inventory that would result from reducing the enrichment in over one-fifth the interior assemblies would unacceptably reduce the achievable cycle length of the core. For this reason, the CCC concept was not deemed to be a viable option for the BWR extended cycle design. Instead, the rod-swapping method used much earlier in BWR operating history is revived and updated for long-cycle use.

9.2.2 BWR Recirculation Flow Control

The control rods in the BWR are used to compensate for the long term changes in core reactivity resulting from fuel and poison depletion. Rapid changes in core reactivity, such as those produced by fluctuations in reactor electrical load, are controlled by varying core recirculation flow. Flow through the reactor core is driven by two large external recirculation pumps in two external loops and by an array of internal jet pumps. An increase in reactor recirculation flow sweeps steam voids out of the core and inserts positive reactivity by reducing the overall void fraction of the moderator. In addition to altering reactivity, the increased flow also reduces axial power peaking in the bottom of the core by lowering the core axial void gradient. At the same reactor power level, the more rapidly flowing coolant experiences a smaller enthalpy rise as it travels upward through the core. At saturated conditions, this lower magnitude enthalpy gain translates into a diminished rise in the core void fraction and a correspondingly smaller difference in moderator effectiveness (and therefore reactivity) between the top and bottom of the core.

In order to increase its operational flexibility, the BWR extended cycle core design takes advantage of the Maximum Extended Operating Domain of BWR power to flow relationships. Use of the Maximum Extended Operating Domain permits plant operation at 100% rated power with significantly less than core rated flow [I-2]. In this study the extended domain allows a reduction in core flow (to a minimum value of 80% of rated capacity, which is consistent with current practice) to control peak hot excess reactivity produced by the high fissile atom loading required to achieve ultra-long cycle lengths. Increased flow flexibility also permits the adjustment of the core axial power distribution without requiring excessive control rod movement.

The section which follows details the CASMO-3 and SIMULATE-3 models used to design the extended cycle BWR.

9.3 BWR Model Description

In this study, SIMULATE-3 is used to create a three-dimensional model of the BWR with 1/4 core mirror symmetry. Each fuel assembly consists of a single radial node and 25 axial nodes. The core is depleted at 100% power, although as described above, core flow is varied from 100% to 80% of rated capacity in order to stay within design goal limits. At each depletion point, control

rod positions and core flow are adjusted to produce a core eigenvalue of k_{eff} = 1.000 ± 0.001 at 100% reactor power. The BWR begins the cycle free of samarium and with equilibrium levels of iodine, xenon and promethium.

Table 17: Varied Parameters in CASMO-3 BWR Runs

	Parameter	Base Value	Branches
1.	Control Rod History Case		
	Coolant Void Fraction (%)	40.0	-
	Moderator Temperature (°C)	286.9	-
	Fuel Temperature (°C)	523.9	-
	Control Rod Position	Fully Inserted	Fully Withdrawn
2.	0% Void Fraction Case		
	Coolant Void Fraction (%)	0.0	40.0, 70.0
	Moderator Temperature (°C)	286.9	19.9, 79.9
	Fuel Temperature (°C)	532.9	19.9, 79.9, 286.9
	Control Rod Position	Fully Withdrawn	Fully Inserted
3.	40% Void Fraction Case		
	Coolant Void Fraction (%)	40.0	0.0, 70.0
	Moderator Temperature (°C)	286.9	19.9, 79.9
	Fuel Temperature (°C)	532.9	19.9, 79.9, 286.9
	Control Rod Position	Fully Withdrawn	Fully Inserted
4.	70% Void Fraction Case		
	Coolant Void Fraction (%)	70.0	0.0, 40.0
	Moderator Temperature (°C)	286.9	19.9, 79.9
	Fuel Temperature (°C)	532.9	19.9, 79.9, 286.9
	Control Rod Position	Fully Withdrawn	Fully Inserted

Table 17 summarizes the CASMO-3 cases run for each different fuel type in the BWR core. These CASMO-3 cases develop a cross-section library capable of accurately reflecting the changes

in neutronic characteristics resulting from variations in moderator temperature, fuel temperature, moderator void fraction, and the presence of control rods.

9.4 BWR Core Design Goals

9.4.1 Design Power Distribution

The limits on the power shape for the extended cycle BWR design are based on the concept of a design power distribution. The design power distribution represents the most limiting thermal operating state at rated conditions and includes design allowances for the combined effects of the gross and steady state local power density distributions, control rod adjustments, and the reactor power level on fuel rod and fuel assembly heat flux and temperature. For the single-batch reload BWR core developed in this study, maintaining core neutronic power within the design power distribution envelop for a BWR/5 should ensure that thermal hydraulic design limits are also observed.

The design power distribution used in this study was developed for a BWR/5 loaded with 8×8 fuel assemblies [C-3]. However, the BWR core designed for this study uses advanced ATRIUM-10 10×10 fuel bundles. These assemblies incorporate several design improvements which increase margins to core thermal limits. The 10×10 lattice used in these bundles greatly increases the assembly total active rod fuel length, thus permitting a higher bundle power peaking limit for the same limiting Linear Heat Generation Rate (LHGR). The design also features swirl vanes on the assembly grid spacers which allow the bundles to operate at higher critical power levels than previous fuel designs [W-3]. Because no credit is taken for the improved thermal performance margins of the ATRIUM-10 fuel assemblies, the use of a design power distribution established for a BWR/5 loaded with less advanced 8×8 bundles introduces an additional layer of conservatism into the BWR extended cycle design.

The power peaking components of the design power distribution are discussed individually in the following sections.

9.4.1.1 Local Power Peaking Factor

The local power peaking factor is defined as the maximum fuel rod heat flux in a fuel assembly divided by the assembly average fuel rod heat flux at the same elevation. Essentially, the local power peaking factor quantifies the pin-to-pin power peaking within a given fuel assembly. In a BWR, multiple fuel enrichment levels are used to reduce pin-to-pin power peaking by compensating for variations in bundle thermal flux distribution resulting from the uneven distribution of steam voids (and therefore moderator) within an assembly. The local peaking factor limit of the design power distribution is 1.24.

9.4.1.2 Relative Fuel Assembly Power

Relative fuel assembly power is defined as the total power produced in a fuel assembly divided by the core average fuel assembly power. Relative assembly power is controlled through variations in bundle enrichment and neutron absorber loading and by the use of control rods to alter the core's radial power distribution. The relative assembly power limit in the design power distribution is 1.40.

9.4.1.3 Axial Power Peaking Factor

The axial peaking factor for the BWR extended cycle design is defined as the maximum planar average heat flux at a given elevation divided by core average heat flux. The axial peaking factor quantifies the peaking of the core axial power distribution. Because the void gradient in a BWR produces large axial variations in moderator effectiveness, axial enrichment zoning and carefully selected control rod insertion sequences must be used to stay within this design limit. The maximum allowable axial peaking factor for the extended cycle core design is 1.50.

9.4.1.4 Gross Peaking Factor

Gross peaking factor is given as the maximum fuel assembly average fuel rod heat flux at any elevation in the core divided by core average heat flux. The limit of 2.10 set for the gross peaking is simply a multiplicative combination of the limits for relative assembly power and the axial power peaking factor (1.40×1.50).

9.4.1.5 Total Peaking Factor (F_Q)

As with the PWR, F_Q places a limit on combined axial, assembly, and pin-to-pin power peaking and is defined as the maximum fuel rod heat flux in the core divided by core average heat flux. The F_Q limit of 2.60 combines the limits on the gross peaking factor and the local peaking factor (2.10×1.24).

9.4.2 Thermal Hydraulic Limits

The thermal hydraulic limits established by GE Nuclear Energy to preclude fuel damage in the BWR/5 are defined in the sub-sections below [G-2].

9.4.2.1 Average Planar Linear Heat Generation Rate (APLHGR)

APLHGR is a measure of the average linear heat generation rate of all fuel rods in a fuel assembly at a given axial location. Limits on APLHGR are specified to assure that the fuel design limits will not be exceeded during anticipated operational occurrences and that the peak centerline temperature (PCT) will not exceed the limits specified in 10CFR50.46. In this study the limits on APLHGR are internally generated by SIMULATE-3 and vary with core conditions and exposure. The APLHGR limiting values for the BWR extended cycle core design vary from 12.0 kW/ft at BOC to 9.8 kW/ft at EOC. The margin to this limit is generally expressed as MAPRAT (or RAPLHGR) which is defined as the ratio of the Maximum value of APLHGR in the core (MAPLHGR) divided by the APLHGR limit. This ratio must always remain below 1.0 throughout the cycle or the APLHGR limit will be exceeded.

9.4.2.2 Linear Heat Generation Rate (LHGR)

LHGR measures the heat generation rate of a fuel rod in a fuel assembly at an axial location. Limits on LHGR are specified to assure that the fuel design limits will not be exceeded anywhere in the core during normal operation including anticipated operational occurrences. The margin to the LHGR limit is commonly expressed in terms of the Maximum Fraction of Limiting Power Density (MFLPD) which is defined as the ratio of the Maximum value of LHGR in the core (MLHGR) divided by the LHGR limit of 13.4 kW/ft calculated by Siemens for ATRIUM-10 fuel.[S-12]. This ratio must always remain below 1.0 throughout the cycle or the LHGR limit will be exceeded.

9.4.2.3 Minimum Critical Power Ratio (MCPR)

In addition to examining the above limits, thermal hydraulic analysis of a BWR includes a quantification of the core's Minimum Critical Power Ratio (MCPR). MCPR is measure of the operating fuel assembly power relative to the fuel assembly power that would result in the onset of boiling transition. Safety Limit MCPR (SLMCPR) is set such that 99.9% of the fuel rods will avoid boiling transition if the limit is not violated. Operating Limit MCPR (OLMCPR) is established to assure that no fuel damage results during anticipated operation occurrences.

The margin to MCPR is expressed as CPR Ratio (CPRAT), or the Maximum Fraction of the Limiting CPR (MFLCPR), which is the ratio of OLMCPR divided by the smallest CPR calculated for the entire core. This ratio must always remain below 1.0 for the entire cycle or the OLMCPR will be violated. In this study, limitations in the capabilities of the University Version of SIMULATE-3 preclude the meaningful quantification of MFLCPR. Unlike production versions of SIMULATE-3, the University Version does not explicitly model assembly core support plate and shroud leakage, assembly leakage flow to the bypass interstitial region, or the flow characteristics of internal water rods [C-4]. Additionally, detailed flow characteristic modeling information is generally proprietary to individual vendors in the highly competitive nuclear fuel market. Without more detailed flow information and the ability to incorporate it into the BWR core design model, a meaningful measurement of the margin to MCPR could not be developed. Instead, the limits on APLHGR, LHGR, and the design power distribution will be observed in order to demonstrate the operational technical feasibility of the extended cycle BWR.

9.4.3 Minimum Cold Shutdown Margin

Technical Specifications require that a BWR core must be able to be brought to a cold shutdown condition at any point in the cycle even with the strongest control rod withdrawn [G-2]. In order to cover known prediction uncertainties, an additional requirement is typically added to ensure shutdown safety. Accordingly, for the BWR extended cycle design a minimum design margin of 1% Δk is established, which corresponds to a maximum shutdown core eigenvalue of 0.99.

9.4.4 Maximum Discharge Exposure

For ATRIUM-10 fuel, the maximum assembly discharge exposure limit is 53 GWD/MTU [F-3]. A further limit of 60 GWD/MTU is placed on maximum pellet discharge burnup to prevent cladding failure from excessive pellet-clad mechanical interaction (PCMI) [W-5].

9.4.5 Summary

The core design goal limits for the extended cycle BWR are summarized in the table below.

Table 18: Design Goal Limits for the BWR Core

Parameter	Limit
Local Power Peaking Factor	1.24
Relative Fuel Assembly Power	1.40
Axial Power Peaking Factor	1.50
Gross Peaking Factor	2.10
Total Peaking Factor (F_Q)	2.60
APLHGR (limit depends upon core conditions)	12.0 kW/ft - 9.8 kW/ft
LHGR	13.4 kW/ft
Minimum Cold Shutdown Margin	1% Δk
Maximum Fuel Assembly Exposure	53 GWD/MTU
Maximum Fuel Pellet Exposure	60 GWD/MTU

9.5 BWR Core Design Description

9.5.1 Assembly Design

In addition to providing increased margins to fuel thermal limits, the ATRIUM-10 fuel bundles selected for this study also contain advanced features which result in improved neutronic performance compared to previous fuel designs. Many of these features directly address the challenges presented by the extended cycle core design. As with the PWR, the higher levels of fuel enrichment required to achieve very long cycle lengths produce a harder neutron energy spectrum in the BWR extended cycle core design. As described in Section 3.3, in extended cycle cores this hardened neutron energy spectrum results in a larger positive reactivity addition for a given

increase in moderator concentration than for conventional cores. In a BWR, this results in a more negative void reactivity coefficient for the extended cycle core design. Analyses performed on BWRs show that an excessively negative void coefficient worsens reactor behavior during transients and reduces overall flow stability [U-2].

In order to reduce void reactivity feedback, the ATRIUM-10 bundles contain a large central water channel which occupies the space of nine fuel rods in an off-center 3×3 array within the assembly. The diagram in Figure 44 shows the location of the water channel along with the configuration used in the extended cycle design for positioning the asymmetric fuel assemblies around a central control rod. Flow within the central water channel is adjusted such that the moderator within it remains free of steam voids for the entire length of the fuel assembly. By increasing the amount of non-boiling water within the assembly, the water channel softens the neutron energy spectrum and thus reduces void reactivity feedback with respect to previous fuel designs using smaller interior channels [W-3].

Flow stability in the ATRIUM-10 fuel is also improved by the use of part-length fuel rods (PLFR) in the assemblies. Figure 44 shows the position of the eight PLFRs in each ATRIUM-10 fuel bundle. In the BWR extended cycle design, the PLFRs extend 102 in. (259.08 cm) up the fuel assembly, so that the upper 48 in. (121.92 cm) of the core contains only 83 fuel rods. In a heated two-phase flow system (such as a BWR core) so-called pressure drop-flow rate instabilities can arise whenever the pressure drop vs. flow rate curve for the system has a flat or negative sloping region [G-3]. When operating in this regime, a small decrease in the mass flow rate results in a condition in which more pressure is required to maintain flow than is available from external pumping sources. If the slope of the system response curve is more negative than the slope of the external pump curve, a large flow excursion can result as flow decreases further until a new stable operating point is reached. Thus a small perturbation in flow can produce a potentially large flow oscillation which will undermine core flow stability. In a heated, saturated, two-phase flow system such as a BWR assembly, a negative slope in the system response curve stems from the increase in frictional pressure losses which result from the rise in coolant quality caused by a decrease in mass flow [T-2]. The magnitude of this negatively sloping region therefore depends upon the two-phase to single-phase pressure drop ratio of the system. By reducing the wetted perimeter and increasing the flow area in the upper highly voided region of the core, the PLFRs lower the two-phase to

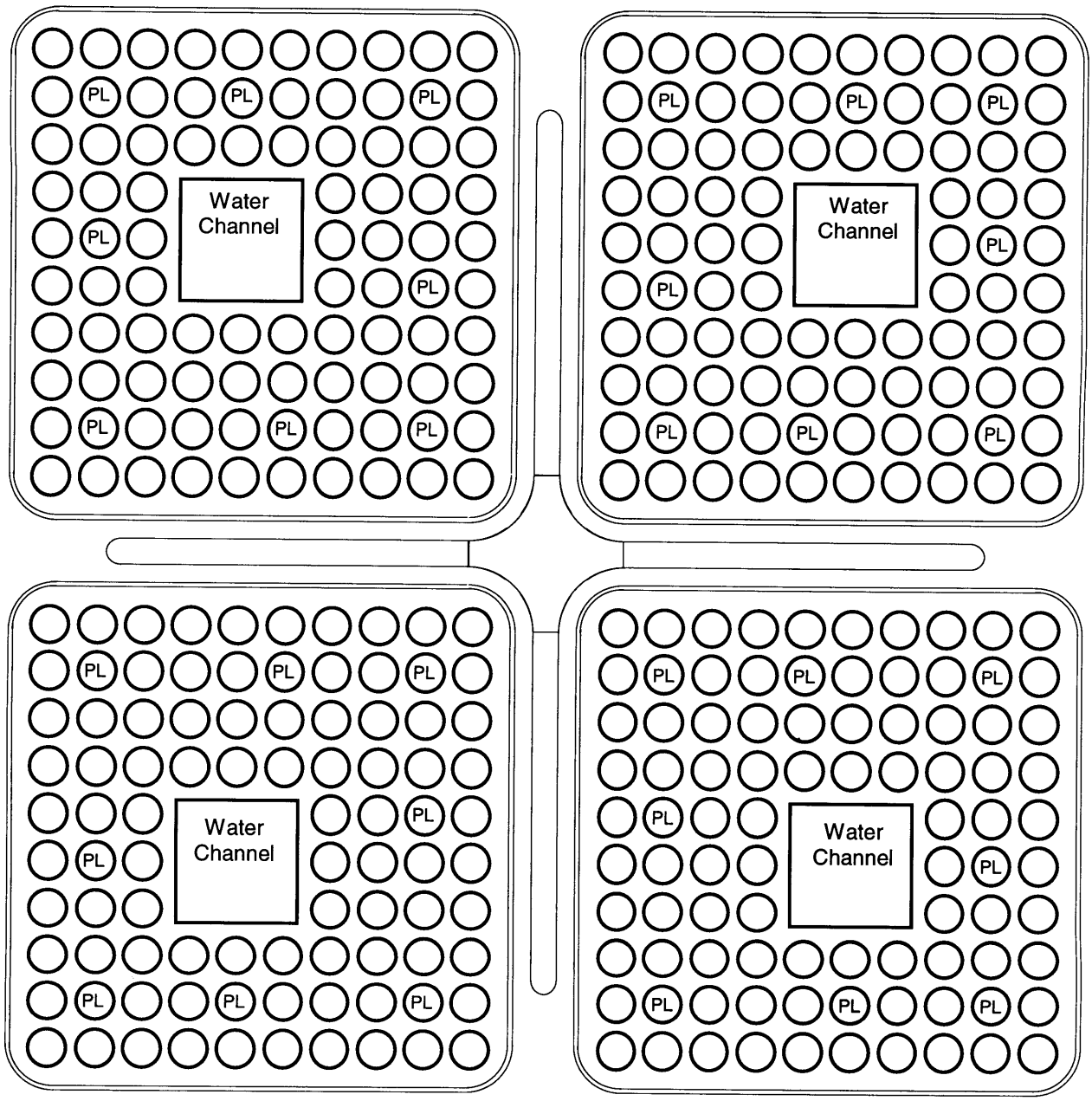

Figure 44: Extended Cycle BWR Fuel Bundle Configuration

single-phase pressure drop ratio of the assembly and improve its overall flow stability performance [W-3].

Another design challenge caused by the higher fuel enrichment used in the extended cycle core design is the reduction in cold shutdown margin. Shutdown margin is diminished both because the core must have a higher hot excess reactivity in order to reach the target cycle length goal, and because, as discussed in Section 6.3, the core's harder neutron energy spectrum significantly lowers control rod worth. The large water channel in the ATRIUM-10 improves cold shutdown margin by increasing the magnitude of assembly hot-to-cold reactivity swing. Under hot operating conditions, the water channel acts as an excellent source of thermal neutrons for the surrounding fuel. However, at cold temperatures the reduction in the average neutron thermal diffusion length by a factor of approximately 1.5 turns the water channel into a thermal neutron 'trap' which lowers overall assembly reactivity [U-2]. This effect is not observed in fuel designs with smaller internal water channels.

The PLFRs in the bundles also help to improve the shutdown margin. The axial variation in the core void fraction results in a shift in the neutron energy spectrum toward higher energies in the upper regions of the core. As a result these upper regions experience a lower burnup and higher conversion rate of U to Pu from U^{238} neutron capture. When the core is taken to a cold shutdown condition and the voids are collapsed, the low burnup, high Pu upper regions of the core can experience high flux peaking very similar to the CBH effect observed in previously controlled assemblies following the withdrawal of a rod. This peaking increases as the operating cycle progresses, and it can result in a reduced cold shutdown margin later in core life. The PLFRs increase the water-to-fuel ratio in the upper regions of the core, increasing fuel exposure and reducing the rate of Pu breeding. The axial optimization of the water-to-fuel ratio lowers shutdown flux peaking and improves cold shutdown margin later in core life [W-4].

The BWR extended cycle core design employs six different types of interior assemblies in addition to a low enrichment peripheral assembly. To reduce axial leakage and improve fuel utilization, each assembly makes use of 6 in. axial blankets of natural uranium in 10% central void volume annular pellets. In addition to these axial blankets, each assembly is also divided into three central axial enrichment zones in order to improve the core axial power distribution. The assemblies contain Gd_2O_3 at a concentration of $12^{w}/_{o}$ mixed in with the UO_2 of selected pins and formed

into 10% central void annular fuel pellets. As with the long-cycle PWR, annular fuel pellets are employed in the poison bearing pins to mitigate the negative effects of the degraded thermal conductivity of Gd-loaded UO_2 on fuel pin performance. In order to obtain a flat radial power shape the number of burnable pins in the six interior assemblies varies from 16 in the center of the core to 10 near the periphery. Core axial zoning information with respect to fuel height, axial nodalization, and control rod position for all fuel assemblies is summarized in Table 19.

The three central axial zones of each fuel assembly are given the following designations:

- Low Enrichment Zone (LEZ): Extends from 6 in. (15.24 cm) to 60 in. (152.4 cm)
- Mid-Enrichment Zone (MEZ): Extends from 60 in. (152.4 cm) to 102 in. (259.08 cm)
- "Vanished" Fuel Rod Zone (VRZ): Extends from 102 in. (259.08 cm) to 144 in. (365.76 cm). This zone begins at the top of the PLFRs, and therefore contains only 83 fuel pins.

Reducing fuel enrichment in the LEZ lessens the severity of axial power peaking at BOC, as does increasing the enrichment in the VRZ. The higher VRZ enrichment also compensates somewhat for the fuel lost from the 'vanished' tops of the PLFRs. Note that the burnable poison concentration in each interior assembly remains axially uniform. Using Gd_2O_3 at loadings below the extended cycle core design limit of $12^{w}/_{o}$ results in an unacceptably high hot excess reactivity peak due the more rapid burnout at these less self-shielded lower concentrations. Axial variations of burnable poison in a given fuel assembly were not explored in this study, but this option may offer improved performance in future iterations of the BWR extended cycle core design. Note that unlike the PWR, the BWR design does not use IFBA as a burnable neutron absorber. The motivation to exclude IFBA from the BWR design stems from the differences between the methods of hot excess reactivity control used in each reactor type. This decision is discussed in detail in Chapter 10.

In order to meet the design goal limit on the local power peaking factor, the assemblies in the extended cycle length core utilize up to nine different fuel enrichment levels within a given axial zone. The pin enrichment layout maps for all assembly axial enrichment zones (with the exception of the axial blankets, which consist only of natural uranium) are shown in Appendix B. The highest allowable level of fuel enrichment in the extended cycle BWR core is $7.4^{w}/_{o}$ U^{235}. Monte Carlo calculations show that for typical conditions in fabrication and enrichment plants, UO_2

Table 19: BWR Core Design Axial Enrichment Zoning

Height to Node Top		Axial Node No.	Control Rod Steps to Node Top	Axial Zone Average Enrichment by Assembly Type ($^{w}/_{o}$ U^{235})						
In.	Cm			1	2	3	4	5	6	P
150	381.00	25	-	0.711	0.711	0.711	0.711	0.711	0.711	0.711
144	365.76	24	00	6.50	6.50	6.35	6.40	5.65	6.15	1.34
138	350.52	23	02							
132	335.08	22	04							
126	320.04	21	06							
120	304.80	20	08							
114	289.56	19	10							
108	274.23	18	12							
102	259.08	17	14	6.40	6.40	6.10	6.40	5.40	5.90	1.34
96	243.84	16	16							
90	228.60	15	18							
84	213.56	14	20							
78	198.12	13	22							
72	182.88	12	24							
66	167.64	11	26							
60	152.4	10	28	6.20	6.20	5.80	6.20	5.20	5.70	1.34
54	137.16	9	30							
48	121.92	8	32							
42	106.68	7	34							
36	91.44	6	36							
30	76.20	5	38							
24	60.96	4	40							
18	45.72	3	42							
12	30.48	2	44							
6	15.24	1	46	0.711	0.711	0.711	0.711	0.711	0.711	0.711
Assembly Average Enr. ($^{w}/_{o}$ U^{235})				5.90	5.90	5.63	5.87	5.02	5.48	1.29
No. of Burnable Absorber Pins				10	12	12	16	12	16	0
Burnable Poison Conc. ($^{w}/_{o}$ Gd_2O_3)				12.0	12.0	12.0	12.0	12.0	12.0	-
Number of Assemblies In Core				40	40	48	68	240	236	92

achieves an infinite medium eigenvalue of $k_{\infty} = 1$ at U^{235} enrichments greater than $7.4^{w}/_{o}$ [S-13]. The use of fuel at higher levels of enrichment would therefore greatly increase the difficulty of ensuring that criticality safety is maintained during the fuel enrichment and fabrication process.

In an unrodded fuel assembly, the presence of unvoided moderator on the exterior of the enclosed fuel bundle produces thermal flux concentrations which are the highest in fuel

pins adjacent to the channel wall. Because of the higher concentration of moderator near the corners of the assembly, flux reaches a peak in the exterior corner pins and decreases toward the assembly centerline. In order to minimize local power peaking within the assembly, fuel enrichments are lower in pins on the fuel bundle exterior, and they are the lowest in the assembly corner positions. Additionally, because the interior water channel of the ATRIUM-10 fuel provides a good source of neutron moderation within the assembly, the fuel pins adjacent to its exterior faces (excluding the corners) have a slightly reduced enrichment.

The large flux gradients within the fuel bundles also influence the positioning of the burnable absorber pins. In the extended cycle BWR core design, Gd_2O_3 pins are never placed on the bundle exterior or adjacent to the interior channel. If the poison pins are placed in the high thermal flux concentrations located in these positions, the burnable absorber depletes too rapidly and produces and unacceptably high hot excess reactivity peak as the cycle progresses. Further, the depletion behavior of gadolinium in a strong flux gradient location (such as the exterior of a BWR assembly) is quite complex and cannot be accurately modeled with the burnup models used in CASMO-3 [C-4]. Maintaining at least one row of separation between the burnable absorber pins and the unvoided moderator in and around the fuel assembly ensures the even and predictable depletion of gadolinium throughout the cycle.

As with the long-cycle PWR, the peripheral assemblies (designated as assembly Type 'P' in Table 19) in the BWR core contain no poison and have a significantly reduced fuel enrichment compared to the interior assemblies. Note the significant differences between the RBA of the PWR extended cycle design and the Type P assembly of the BWR. First, in the BWR, the fuel enrichment in the peripheral assemblies is lowered primarily to reduce radial leakage, thereby improving overall neutron economy. An analysis of the effect of power shape on neutron leakage shows that leakage is dominated by the source shape in the last ~15 cm (a distance equal to twice the fast neutron migration length, M) of core adjacent to the periphery [D-2]. Thus, in the BWR design there is no need for an asymmetric RBA-type assembly, because unlike the (21.5 cm wide) PWR assemblies, the smaller (13.3 cm wide) BWR are ideally sized to effect radial leakage.

Second, because of the annulus of recirculating water and downward flowing feedwater between the core and the pressure vessel, RPV neutron embrittlement is much less of a concern in a BWR than it is in a PWR [G-1]. Accordingly, the BWR core design can tolerate a higher relative

power (and therefore, a higher enrichment) on the extreme periphery of the core than can the PWR design. As can be inferred from the analyses in Section 5.4.2.2, using a more optimally enriched fuel at $1.29^{w}/_{o}$ U^{235} instead of natural uranium on the outer edge of the core gives the BWR design a longer cycle length and a lower total power peaking factor.

For simplicity, the peripheral assemblies contain only two axial enrichment zones and three different enrichment levels. Because the peripheral assemblies contain no burnable poisons (which increase assembly pin-to-pin peaking by suppressing power in the pins into which they are loaded) they require a less extensive variation in enrichment to achieve an acceptable local power peaking factor.

9.5.2 Assembly Reactivity Behavior

Figure 45 plots k_{∞} against exposure for the MEZ of the six interior and one peripheral assembly types used in the BWR extended cycle core design. The CASMO-3 calculations shown in the figure were made using the Base Value parameters of the 40% Void Fraction Case listed in Table 17 on page 141 (i.e., an unrodded assembly with coolant void fraction = 40%, moderator temperature = 286.9°C, and fuel temperature = 532.9°C). These parameters represent typical mid-core operating conditions at HFP.

As with the PWR assembly behavior described in Section 5.3.3, the burnup response of these assemblies stems directly from the higher levels of fuel enrichment and the heavy burnable loading required to achieve extended operating cycle lengths. In assembly types 1, 2, and 4, the MEZs have the same fuel enrichment but contain different numbers of burnable absorber pins. As was noted for the PWR design, the positive reactivity burnup coefficient in similarly enriched assemblies increases with the number of burnable poison pins. In assemblies with the same number of poison pins but different levels of enrichment, such as types 4 and 6, the increased self shielding in the higher enrichment assembly (type 4 in this case) decreases the magnitude of the positive reactivity burnup coefficient and shifts the time of assembly peak reactivity to a later point in life.

The motivation for creating the individual enrichment zone reactivity responses shown in Figure 45 is best explained in the context of the BWR extended cycle design core loading pattern, which is described in the following section.

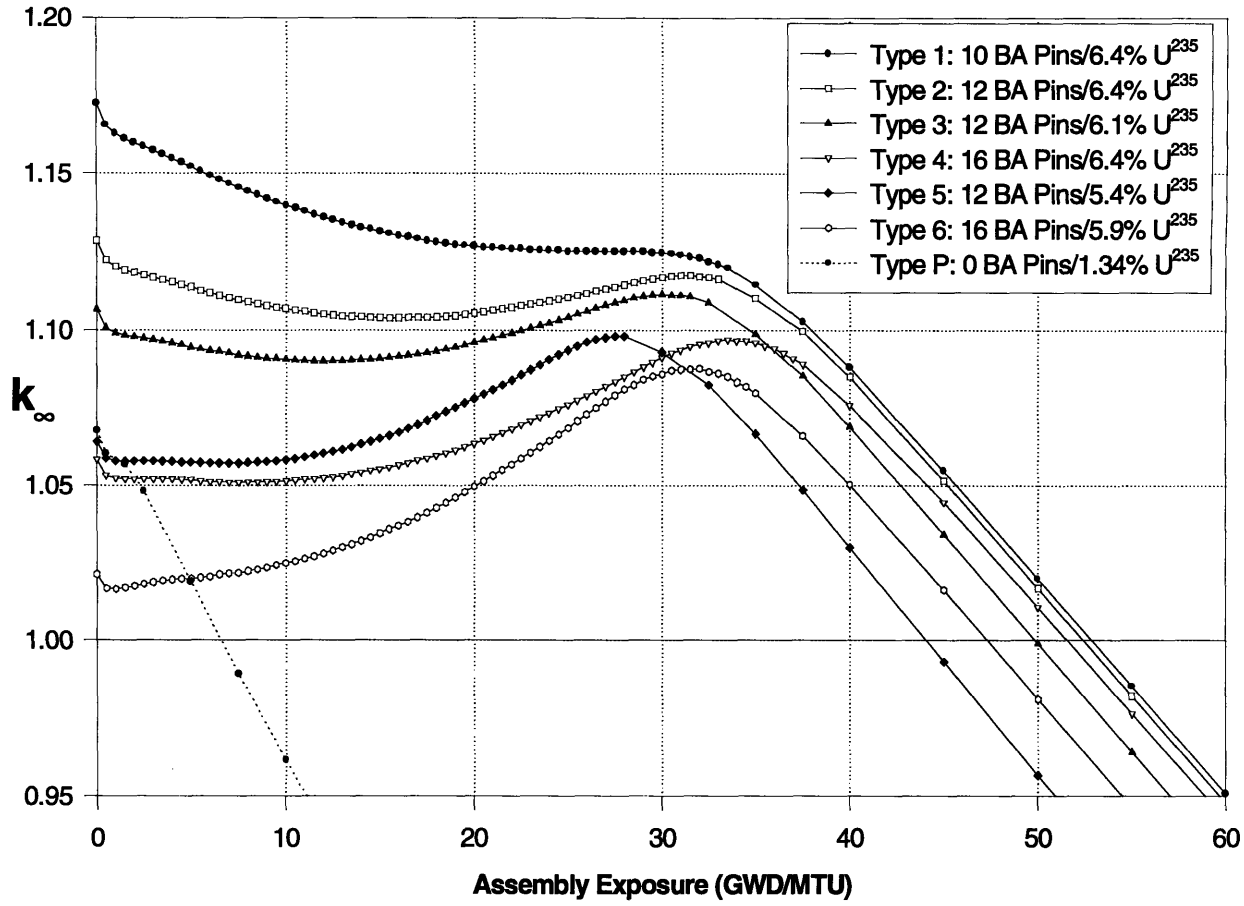

Figure 45: Reactivity Behavior of BWR Fuel Assembly MEZs

9.5.3 Core Loading Pattern

Figure 46 contains a quarter core map of the loading pattern for the BWR extended cycle design. Comparing Figure 46 to the PWR core loading pattern shown in Figure 24 on page 85 illustrates the similar framework of the two extended cycle, single-batch core designs. Both designs utilize low reactivity fuel on the core periphery in order to minimize radial leakage and improve neutron economy. In the interior, both designs place lower reactivity fuel in the center and higher reactivity assemblies toward the exterior in order to suppress power peaking and flatten the core radial power distribution. However, in the BWR, the rudimentary radial enrichment 'checkerboarding' seen only in the center nine assemblies of the PWR design has expanded to encompass nearly all of the interior fuel assemblies in the core.

In the long-cycle BWR core, lower enrichment fuel assemblies with fewer burnable absorber pins (e.g., assembly types 3 and 5) are paired with higher enrichment fuel bundles having more

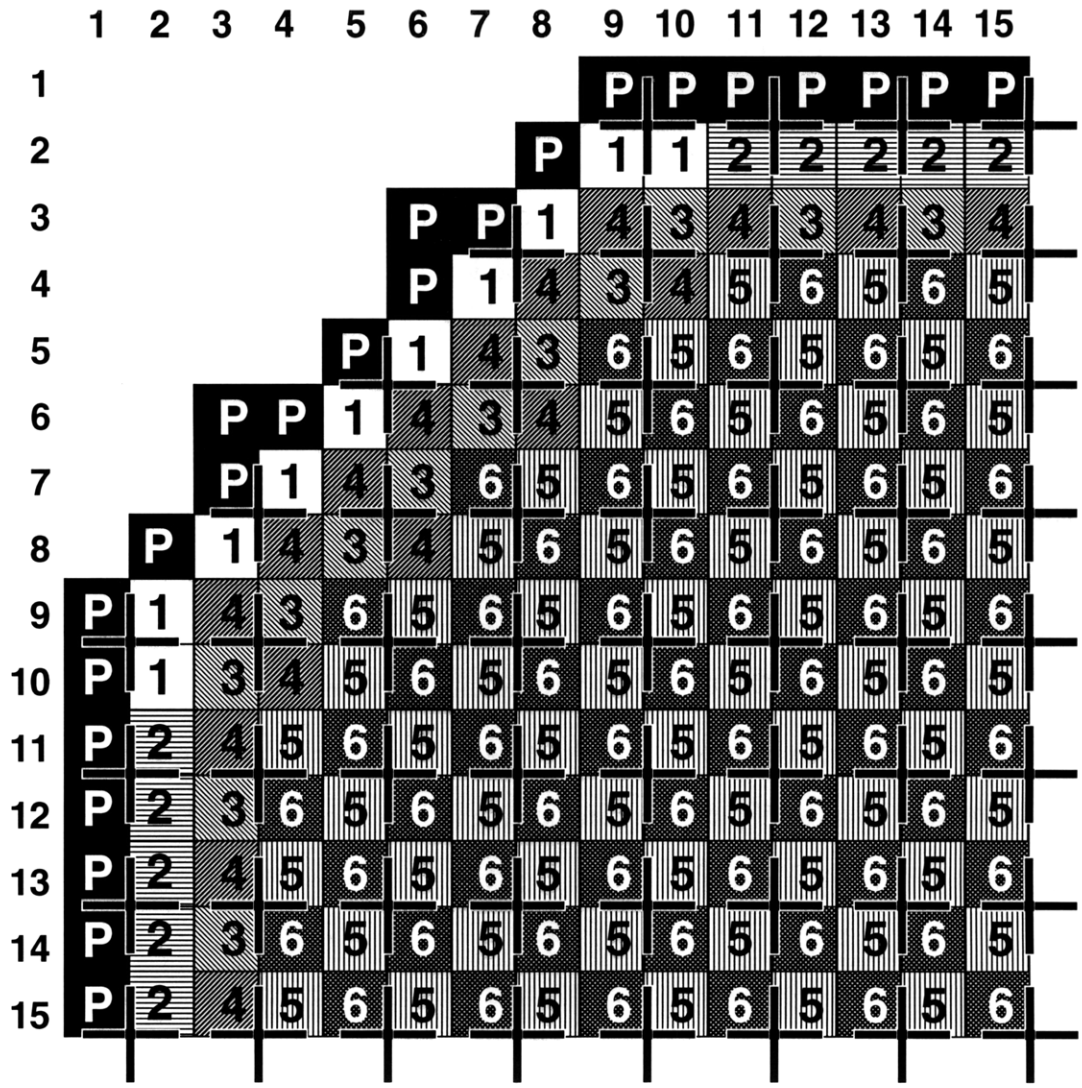

1 — 5.90% U^{235} with 12% Gd_2O_3 (10 rods)

2 — 5.90% U^{235} with 12% Gd_2O_3 (12 rods)

3 — 5.63% U^{235} with 12% Gd_2O_3 (12 rods)

4 — 5.87% U^{235} with 12% Gd_2O_3 (16 rods)

5 — 5.02% U^{235} with 12% Gd_2O_3 (12 rods)

6 — 5.48% U^{235} with 12% Gd_2O_3 (16 rods)

P — Low enrichment Peripheral Assembly (1.29% U^{235})

Cruciform Control Blade Location

Figure 46: Extended Cycle Design BWR Core Loading Pattern

burnable absorber pins (types 4 and 6) in order to effect a more even core radial exposure distribution throughout the cycle. Generally, the lower enrichment type 5/6 pairings are loaded in the center and the more reactive type 3/4 pairs are placed toward the periphery. Some mixed pairing does occur on the core flats near the periphery in order to lower power peaking. The reactivity response behavior calculated in Figure 45 shows how these fuel assembly pairs work together to optimize the distribution of exposure throughout the core.

Using a 5/6 pairing as an example, the values in Figure 45 indicate that for assemblies clustered around the same control location, the type 5 assemblies will have a higher power at BOC due to the smaller number of burnable absorber pins that they contain. However, as the cycle progress, the peak power eventually shifts to the more highly enriched type 6 assemblies in the pairing. The shift in reactivity between the pairs ensures a more even accumulation of exposure and prevents individual assemblies from acquiring excessive amounts of exposure.

Chapter 10 which follows analyzes the performance of the BWR extended cycle core and evaluates the relative success of the design in meeting the goals outlined in Section 9.4.

CHAPTER 10

BWR Core Design Performance

The BWR extended cycle core design developed in this study achieves a core average discharge burnup of 34.2 GWD/MTU. This burnup level corresponds to a cycle length of 45 EFPM, or 47.4 calendar months of operation at the target capacity factor of 95%. All of the core design goal limits established in Section 9.4 are met with the exception of minimum cold shutdown margin, but this limit can be met by using higher worth control rods. The performance of the BWR extended cycle core design with respect to individual design goal limits is detailed in the sections below. This chapter also compares the performance the long-cycle BWR design to that of a conventional, multi-batch BWR/5 core operating on an annual fuel cycle.

10.1 Design Power Distribution

With the combination of carefully positioned control rods and variations in recirculation flow, the power shape in the BWR extended cycle core design can be controlled to meet the limits of the design power distribution established in Section 9.4.1. Core flow and core aggregate control rod position for the extended cycle design as a function of cycle exposure are shown in Figure 47 and Figure 48, respectively. Core flow is listed as a percentage of rated flow, and control rod position is given by the total number of control rod steps inserted into the core at a given depletion point. The slight fluctuations in core flow from 8 GWD/MTU to 12 GWD/MTU and again after 30 GWD/MTU are implemented in order to aid in the control of axial power distribution. The more

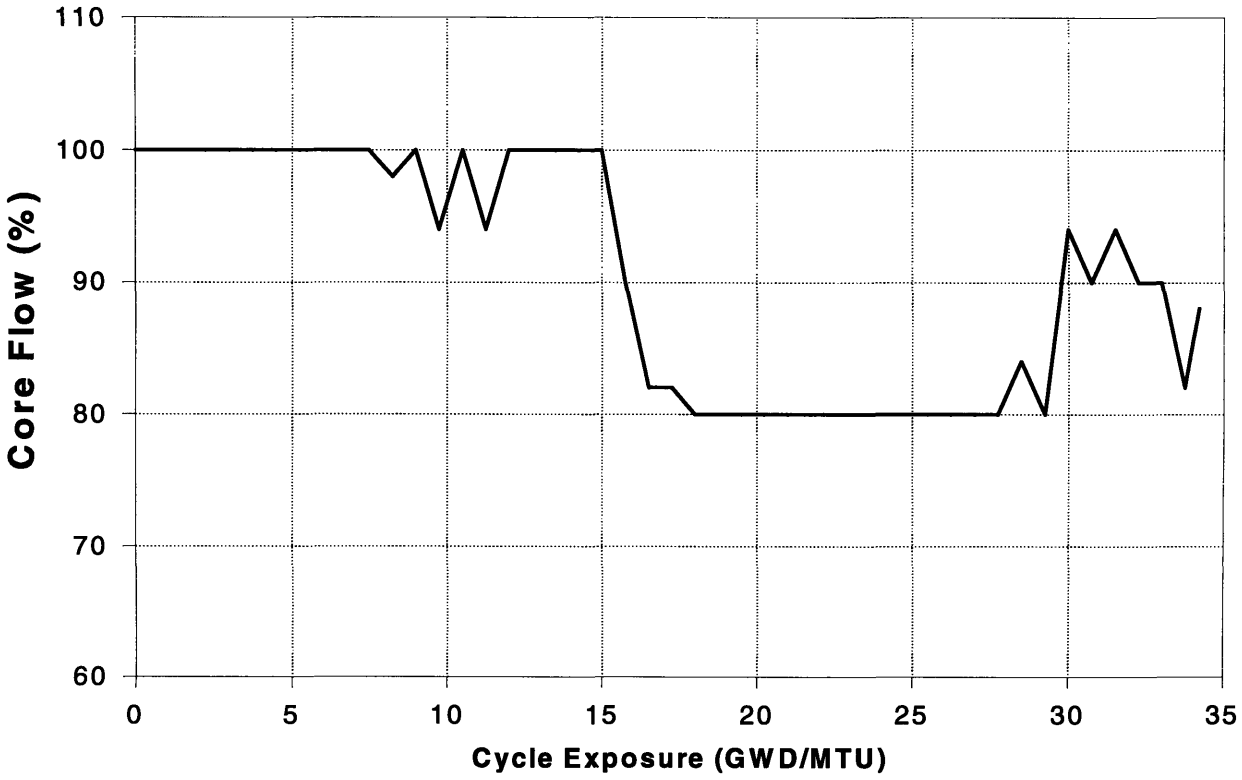

Figure 47: BWR Core Flow vs. Core-Average Exposure

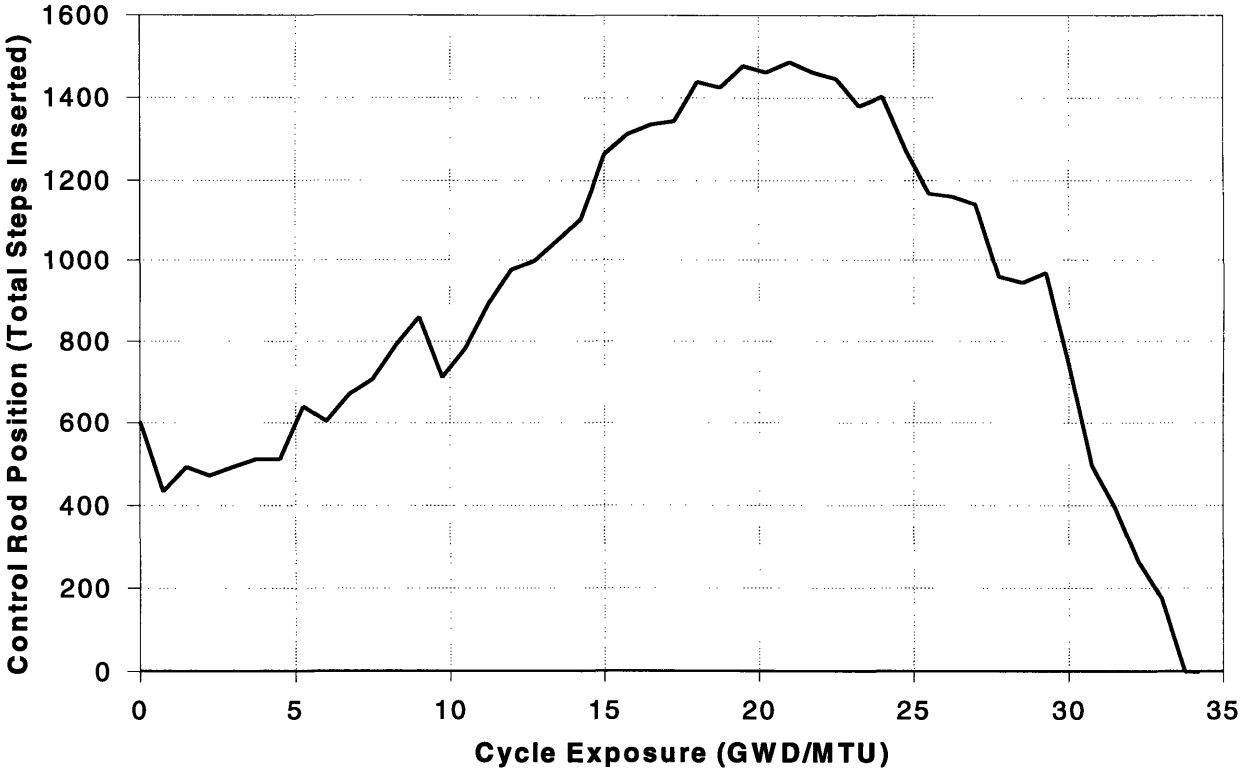

Figure 48: BWR Control Rod Position vs. Core-Average Exposure

significant drop in flow that begins at 15 GWD/MTU reduces the core eigenvalue at the time of peak hot excess reactivity.

Table 20 summarizes the performance of the long-cycle core against the limits of the design power distribution and also lists the peak values achieved by an annual fuel cycle, conventional core loaded with 8×8 fuel assemblies. Recall from Section 9.4.1 that limit values for the

Table 20: Summary of BWR Core Design Power Distribution Performance

Parameter	Limit	Extended Cycle Core Performance	Conventional Core Performance
Local Power Peaking Factor	1.24	1.24 (0 GWD/MTU)	1.15 (0 GWD/MTU)
Relative Fuel Assembly Power	1.40	1.39 (21 GWD/MTU)	1.38 (4 GWD/MTU)
Axial Power Peaking Factor	1.50	1.50 34.2 (GWD/MTU)	-
Gross Peaking Factor	2.10	2.10 (18 GWD/MTU)	2.09 (4 GWD/MTU)
Total Peaking Factor (F_Q)	2.60	2.59 29.25 (GWD/MTU)	2.32 (0 GWD/MTU)

Table 21: Comparison of BWR Core Characteristics

Core Characteristic	Extended Cycle Core	Conventional Core
Feed Assemblies	764	252
Batch Number, *n*	1	3
Core Total Loading (MTU)	135.5	138.7
Fresh Core-Average Reload Enrichment ($^{w}/_{o}$ U^{235})	4.92	2.45
Burnable Absorbers	$12^{w}/_{o}$ Gd_2O_3	$4^{w}/_{o}$ Gd_2O_3
Cycle Length	45 EFPM (47.4 Cal. Months 34.2 GWD/MTU)	10.9 EFPM (11.5 Cal. Months) 8.1 GWD/MTU

design power distribution shown in Table 20 include allowances for uncertainties in measurement and analysis. Also shown in the table is the cycle exposure at the time that the peak value of a given parameter is reached. Note that not all performance information is available for the

1.237	1.236	1.240	1.238	1.239	1.233	1.220	1.232	1.238	1.239
1.236		0.404 Gd	1.016		0.399 Gd	0.968	0.409 Gd		1.239
1.240	0.404 Gd	0.775	0.378 Gd	0.957	0.941	0.952	0.902	0.410 Gd	1.237
1.238	1.016	0.378 Gd	0.901	1.143	1.237	1.176	1.008	0.994	1.228
1.239		0.957	1.143				1.154	0.404 Gd	1.240
1.233	0.399 Gd	0.941	1.237				1.240		1.224
1.220	0.968	0.952	1.176				1.139	0.398 Gd	1.208
1.232	0.409 Gd	0.902	1.008	1.154	1.240	1.139	0.956	0.401 Gd	1.216
1.238		0.410 Gd	0.994	0.404 Gd		0.398 Gd	0.401 Gd		1.220
1.239	1.239	1.237	1.228	1.240	1.224	1.208	1.216	1.220	1.219

Figure 49: Type 4 BWR Assembly VRZ Relative Pin Power at BOC, Hot, 40% Voids

conventional core model. Table 21 compares the key core characteristics of the extended cycle and the conventional BWR core design, including the achievable cycle length in terms of core average cycle burnup, EFPM, and calendar months of operation at the target capacity factor, L = 95%. Modeling information on the conventional cycle BWR/5 was supplied by STUDSVIK of America.

In the extended cycle BWR design the maximum local power peaking factor is determined from CASMO-3 calculations of pin-to-pin power peaking for each different fuel segment type in the core. The calculations are performed using the Base Value parameters of the 40% Void Fraction Case listed in Table 17. As discussed in Section 9.5.2, these values correspond to core average conditions at HFP. The maximum calculated local power peaking factor in the extended cycle BWR occurs in the Type 4 assembly VRZ at the beginning of the cycle. Figure 49 shows the CASMO-3 calculation of the relative power of each fuel pin in this segment at BOC. The high

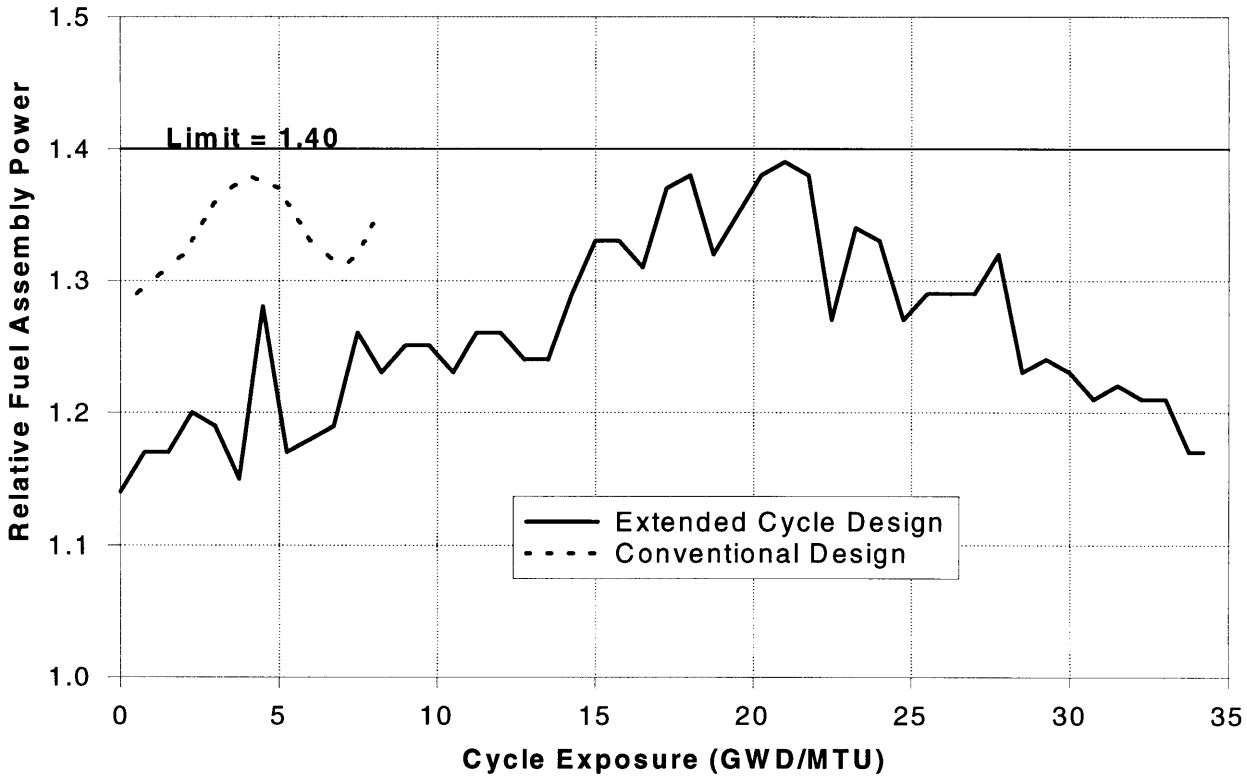

Figure 50: BWR Relative Fuel Assembly Power vs. Core-Average Exposure

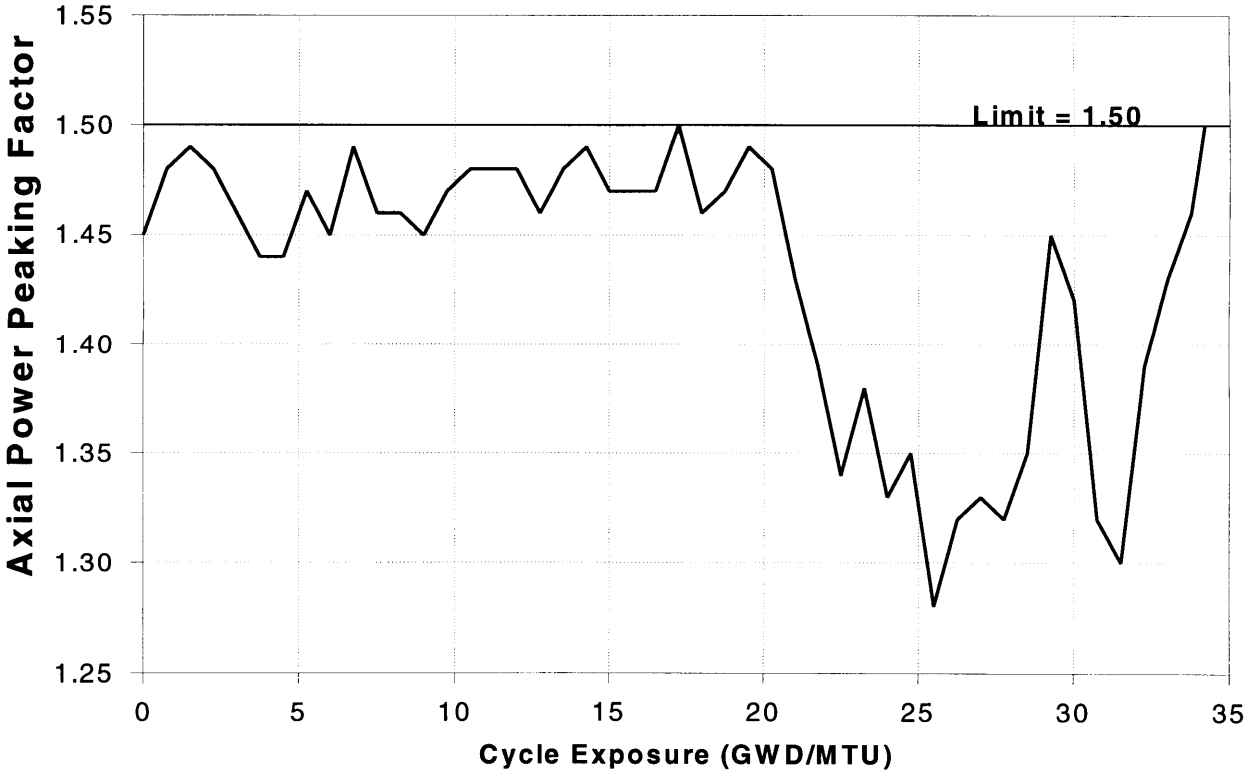

Figure 51: BWR Axial Power Peaking Factor vs. Core-Average Exposure

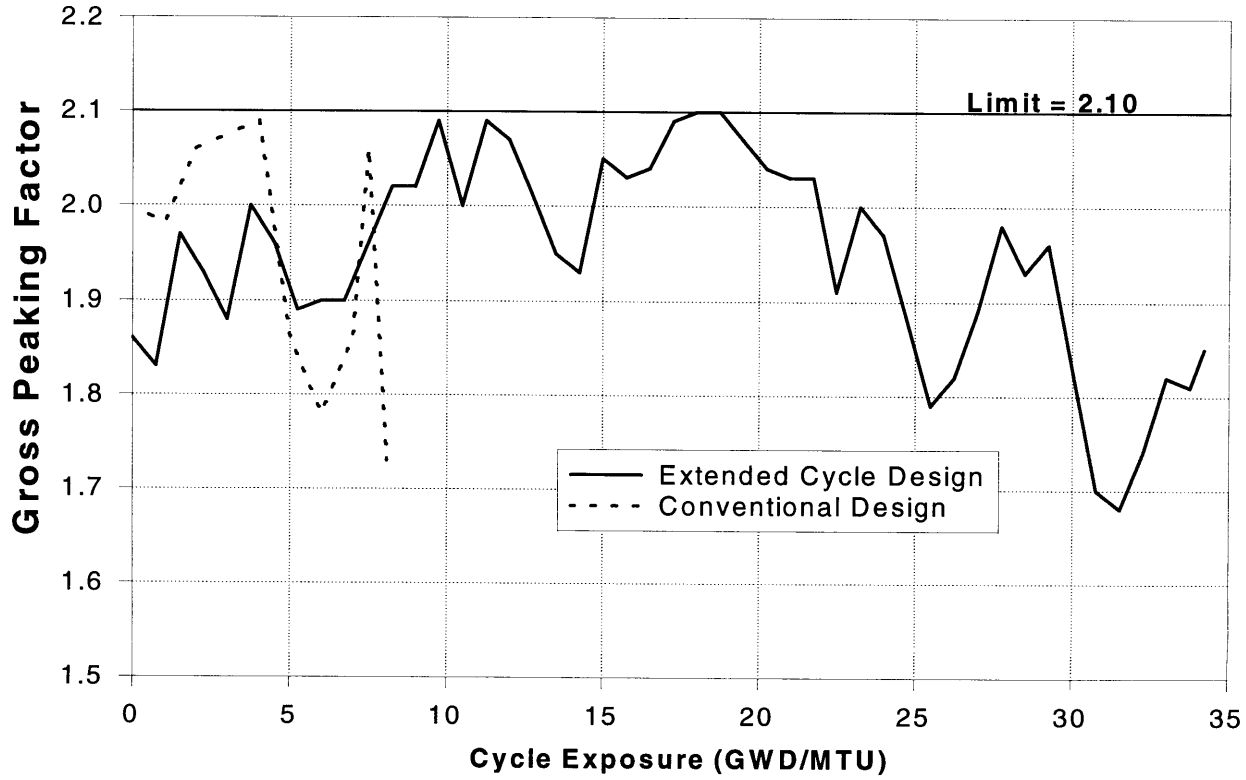

Figure 52: BWR Gross Peaking Factor vs. Core-Average Exposure

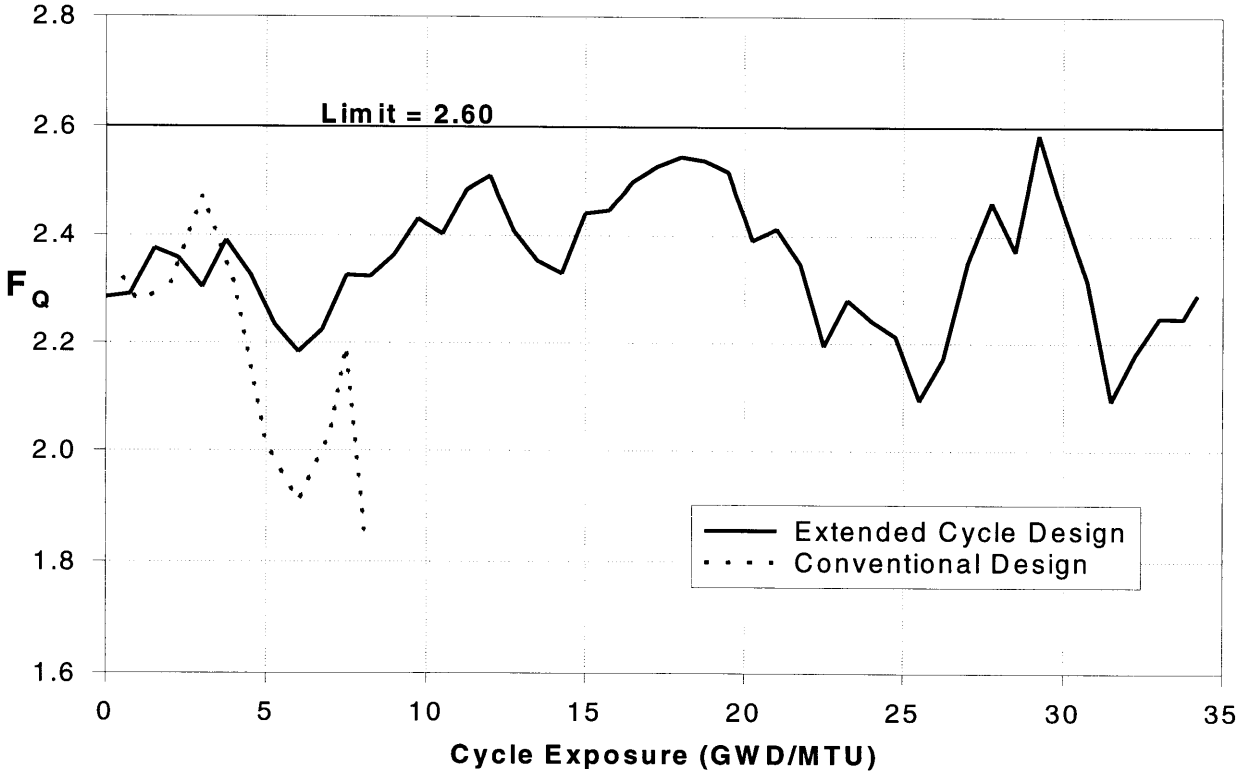

Figure 53: BWR Total Peaking Factor (F_Q) vs. Core-Average Exposure

number of poison pins in this region increases peaking in the unpoisoned fuel rods. Additionally, the high average enrichment requirement in this zone ($6.40^{w}/_{o}$ U^{235}) and the maximum fuel enrichment limit of $7.4^{w}/_{o}$ U^{235} reduce the extent to which variations in pin enrichment zoning can be used to control power peaking. The fuel enrichment of the pins in the high-flux locations on the bundle exterior cannot be lowered further without reducing the zone average enrichment unacceptably.

SIMULATE-3 calculations of relative fuel assembly power, axial power peaking factor, gross peaking factor, and F_Q for the BWR extended cycle core design are shown in Figure 50 through Figure 53. The performance of the conventional core is also plotted for all performance parameters with the exception of the axial peaking factor. The jagged nature of the plots results from the change in control rod position caused by changing control rod patterns or by exchanging the deep and shallow control rods within a given pattern.

The figures show that the extended cycle BWR meets design power distribution limits at all times during the operating cycle. However, because these maximum peaking values are extremely sensitive to changes in control rod position, the plots do not provide much information on the long term dynamic reactivity behavior of the BWR extended cycle core. The following section analyzes global reactivity behavior in the reactor and examines the complex relationship between burnable poisons, core flow, and control rods in the long-cycle design.

10.2 Core Dynamic Reactivity Behavior

Figure 54 through Figure 61 show the control rod pattern, amount of core flow, and the axial and radial distributions at selected depletion points throughout the extended operating cycle. Figure 54 shows the condition of the unrodded core at BOC. As expected, without any control rods inserted, the core axial void gradient would produce a strong power peak at the bottom of the reactor. The core loading pattern effectively flattens out the radial power distribution, with the uneven appearance of the mesh plot resulting from the load-distributing assembly reactivity pairings discussed in Section 9.5.3.

The BWR extended cycle design begins the cycle with the A_1 rod pattern. Figure 55 shows the slight perturbation in the radial power shape as control rods are inserted to bring axial power

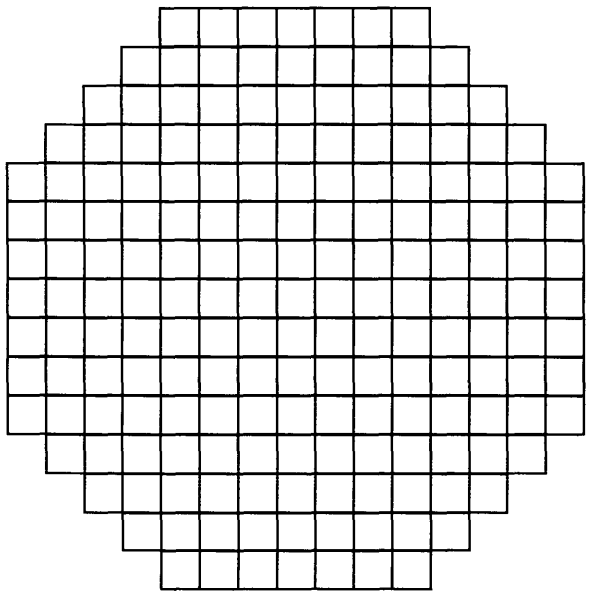

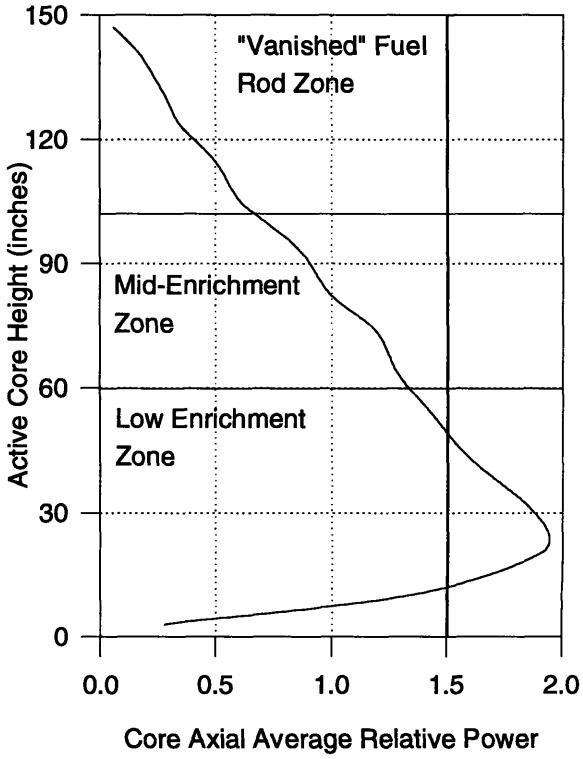

BWR Core Unrodded Radial Power Distribution at BOC

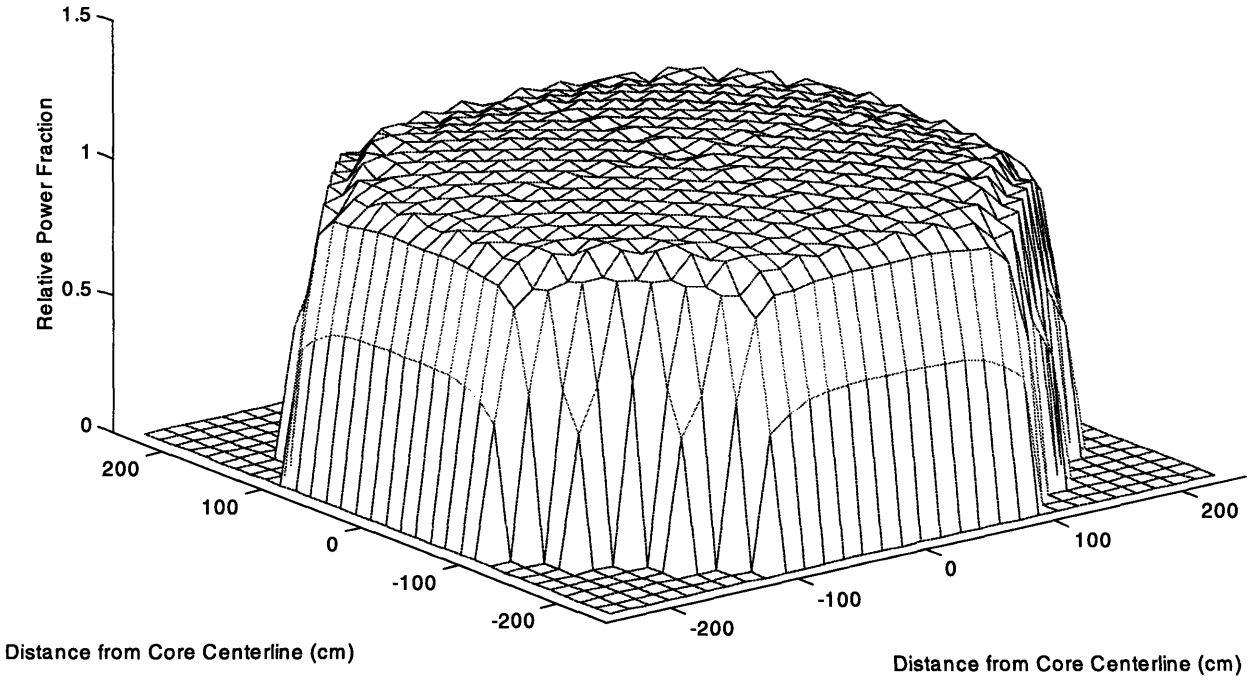

Figure 54: BWR Unrodded Power Distribution at BOC

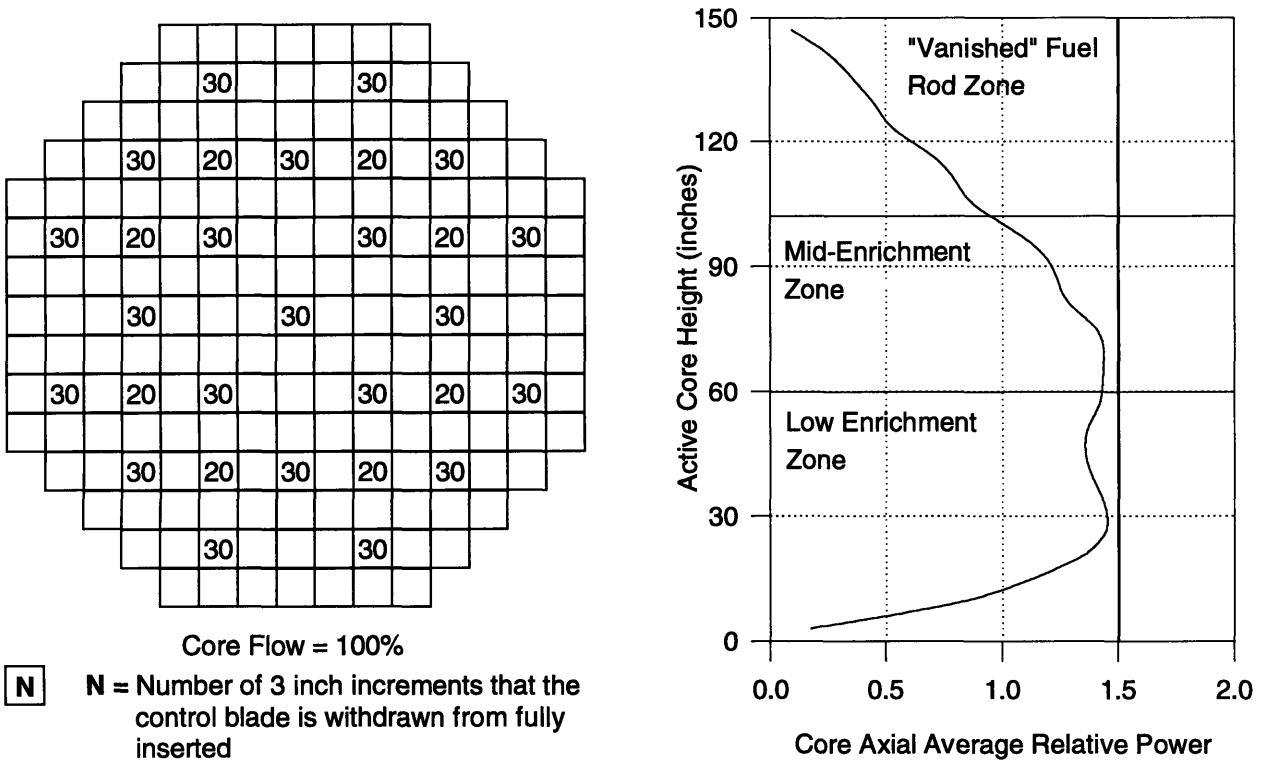

BWR Core Rodded Radial Power Distribution at BOC

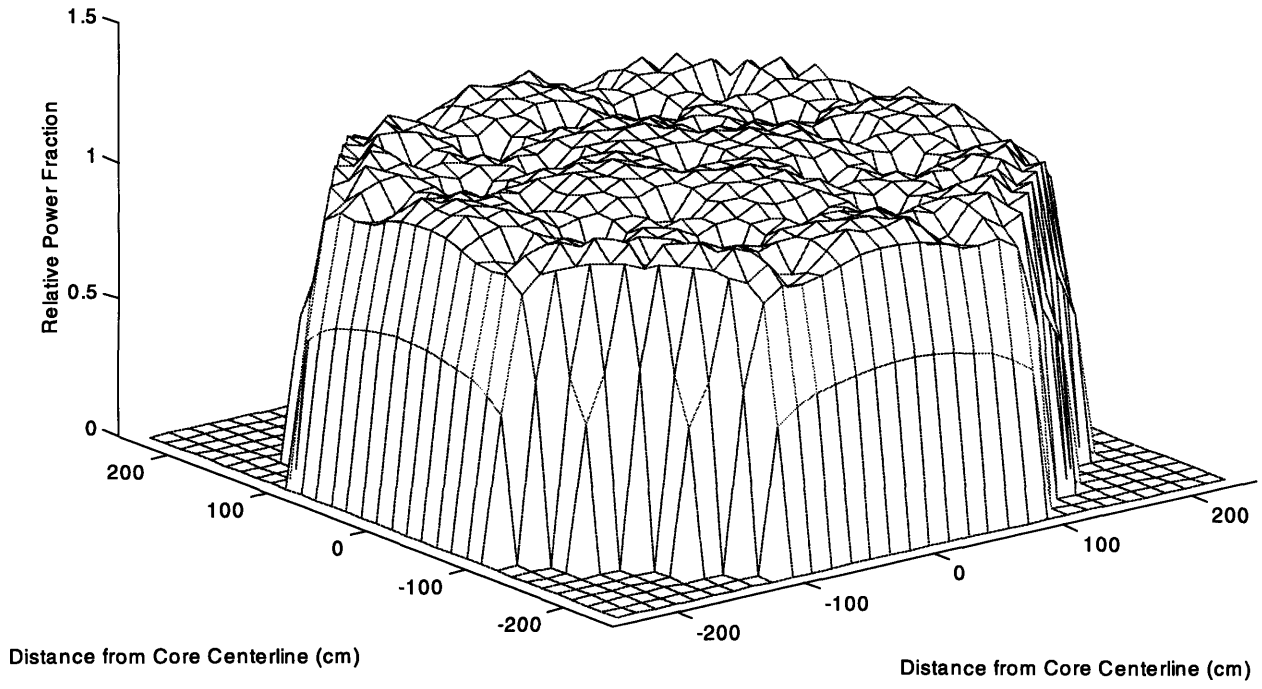

Figure 55: BWR Control Rod Pattern and Power Distribution at BOC

peaking to within design goal limits. Note that due to the core's heavy burnable poison loading, only eight of sixteen available 'deep' control rods in the A_1 pattern are required to control criticality once all of the available shallow rods have been inserted. Note therefore that unlike PWRs, BWRs must start the cycle with enough hot excess reactivity to allow for the insertion of control rods to control axial power distribution. Unrodded core eigenvalues are generally designed to be approximately 1.010 in order to permit adequate control of the axial power distribution.

Therefore, in a BWR more care must be taken to ensure that strategies to reduce peak cycle reactivity do not inadvertently erode the required hot excess reactivity margin at BOC. This concern over BOC reactivity precludes the use of an IFBA/Gd_2O_3 poison combination in the extended cycle BWR. The CASMO-3 results shown in Figure 6 on page 53 demonstrate that the co-location of Gd_2O_3 and IFBA results in a lower peak cycle excess reactivity without an increase in the EOC residual reactivity penalty. However the figure also shows this drop in peak excess reactivity is accompanied by an equal magnitude decrease in BOC reactivity. Because of this, IFBA/Gd_2O_3 co-location does not offer a clear performance advantage to BWRs, and this feature was therefore not included in the BWR extended cycle core design.

Returning to the discussion of BWR dynamic reactivity behavior, Figure 56 shows the status of the core at a cycle exposure of 17.25 GWD/MTU. During the first half of the cycle, the characteristic positive burnup reactivity coefficient of the heavily poisoned extended cycle fuel dominates every aspect of core behavior. As core hot excess reactivity increases due to the burnout of burnable poisons, more control rods are required at each depletion point in order maintain critically control. Note that control rod positions at each depletion point are indicated in Appendix C. Additionally, by 17.25 GWD/MTU, core flow has been lowered to 82% of rated capacity in order to control excess reactivity. The peaking observed in the radial power shape also results from positive burnup reactivity feedback as the Type 1, 2, and P assemblies near the periphery lose reactivity relative to the more heavily poisoned interior fuel bundles. Figure 50 reflects a rise and fall in relative fuel assembly power which mimics the oscillations in $F_{\Delta H}$ observed in the PWR extended cycle core design. Perhaps most significantly, the positive burnup reactivity coefficient of the fuel increases the severity of axial power peaking in the extended cycle BWR design.

Because hotter burning sections are gaining reactivity at a relatively faster rate, aggressive control rod intervention is needed to keep the axial power peak at the bottom of the core within the

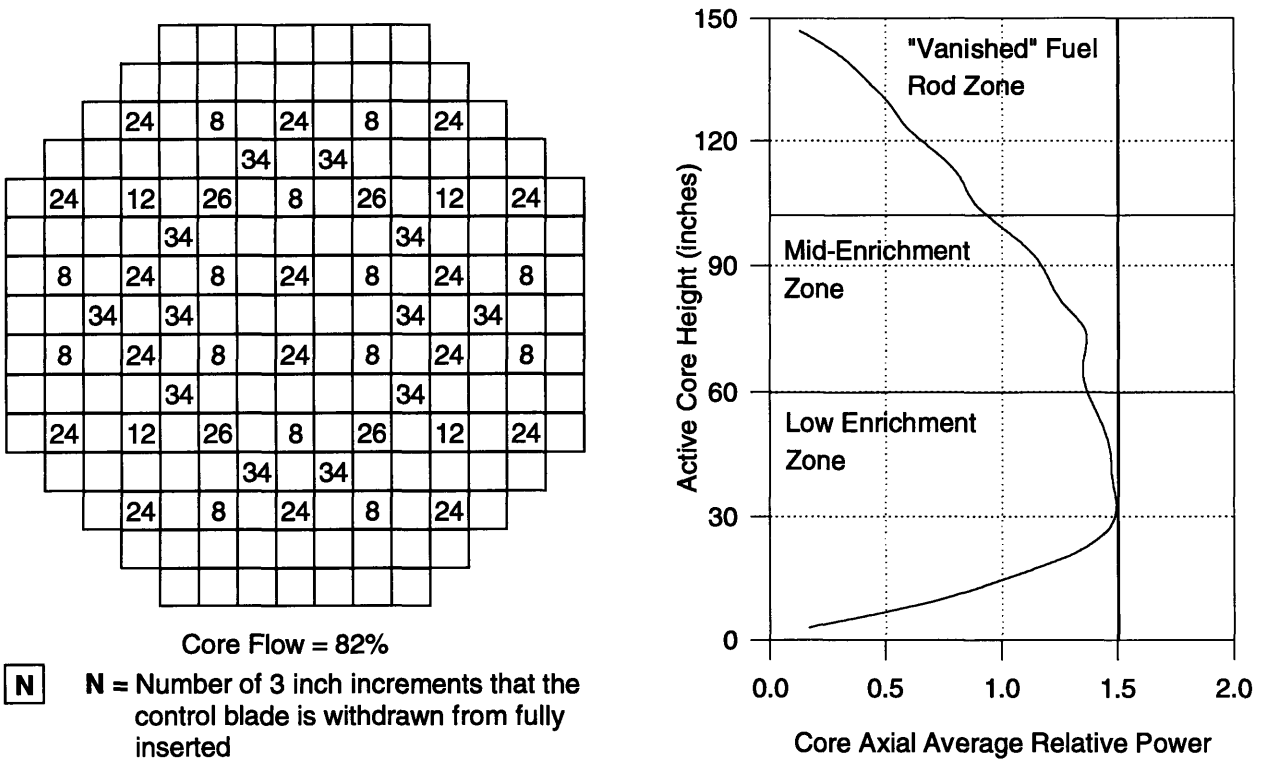

BWR Core Rodded Radial Power Distribution at 17.25 GWD/MTU

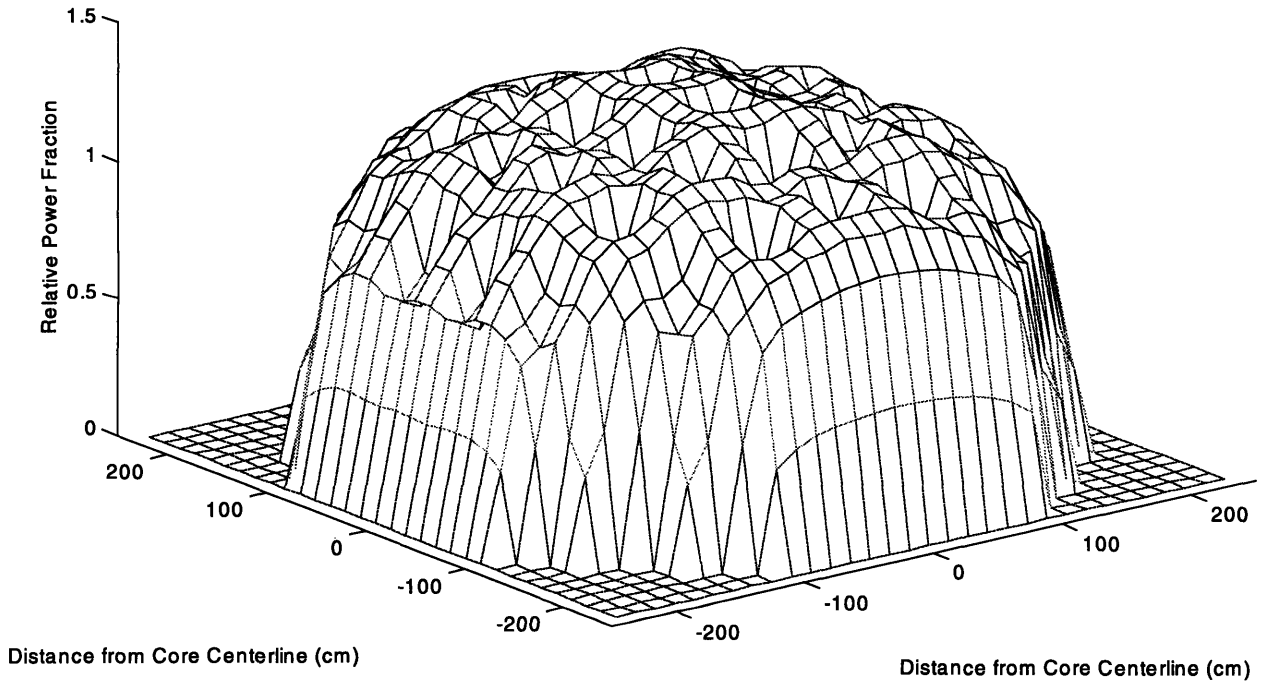

Figure 56: BWR Control Rod Pattern and Power Distribution at 17.25 GWD/MTU

design power distribution limit. By 15.75 GWD/MTU additional shallow rods from inactive patterns must be inserted to keep the axial power distribution within specification. With the core using a nominal B_1 rod sequence, Figure 56 shows that even with twelve additional shallow rods from the B_2 pattern, core axial power peaking is barely within limits at 17.25 GWD/MTU.

Figure 57 shows the core at a cycle exposure of 21 GWD/MTU, when relative fuel assembly power and the total number of control rod steps inserted into the core are at a maximum. Note that the axial power peaking factor has begun to drop off as fuel in the hot burning bottom of the core passes through a point of peak reactivity and power begins to drift toward the less heavily depleted upper regions of the core. By 25.5 GWD/MTU, axial power peaking is at a minimum and Figure 58 indicates that additional shallow control rods from non-active patterns are no longer required. At 29.25 GWD/MTU, the top-peaked axial power distribution portrayed in Figure 59 demonstrates that enough reactivity has been gained in the upper part of the core to allow the complete withdrawal of all shallow control rods.

At 31.5 GWD/MTU of core average exposure, Figure 60 shows that the removal of all shallow control rods has produced a sharp drop in axial power peaking. Core flow has been increased, raising reactivity enough to allow the deep insertion of control rods in the interior of the core. At this point in the cycle, control rods which are not deeply inserted can produce excessive axial power peaks in the upper part of the core. Finally, Figure 61 shows the condition of the core at EOC. Note that cycle length is limited not by a lack of hot excess reactivity, but rather by the axial power shape that can be achieved with flow control with all control rods fully withdrawn. Enough hot excess reactivity remains in the core so that the core could continue critical operation at HFP by increasing recirculation to boost core reactivity. However, raising core flow higher than 88% produces excessive power peaking in the upper regions of the core due to a decreased axial void gradient across the core. Thus the length of the achievable operating cycle is limited by the inability to remain within the design power distribution at cycle exposures greater than 34.2 GWD/MTU.

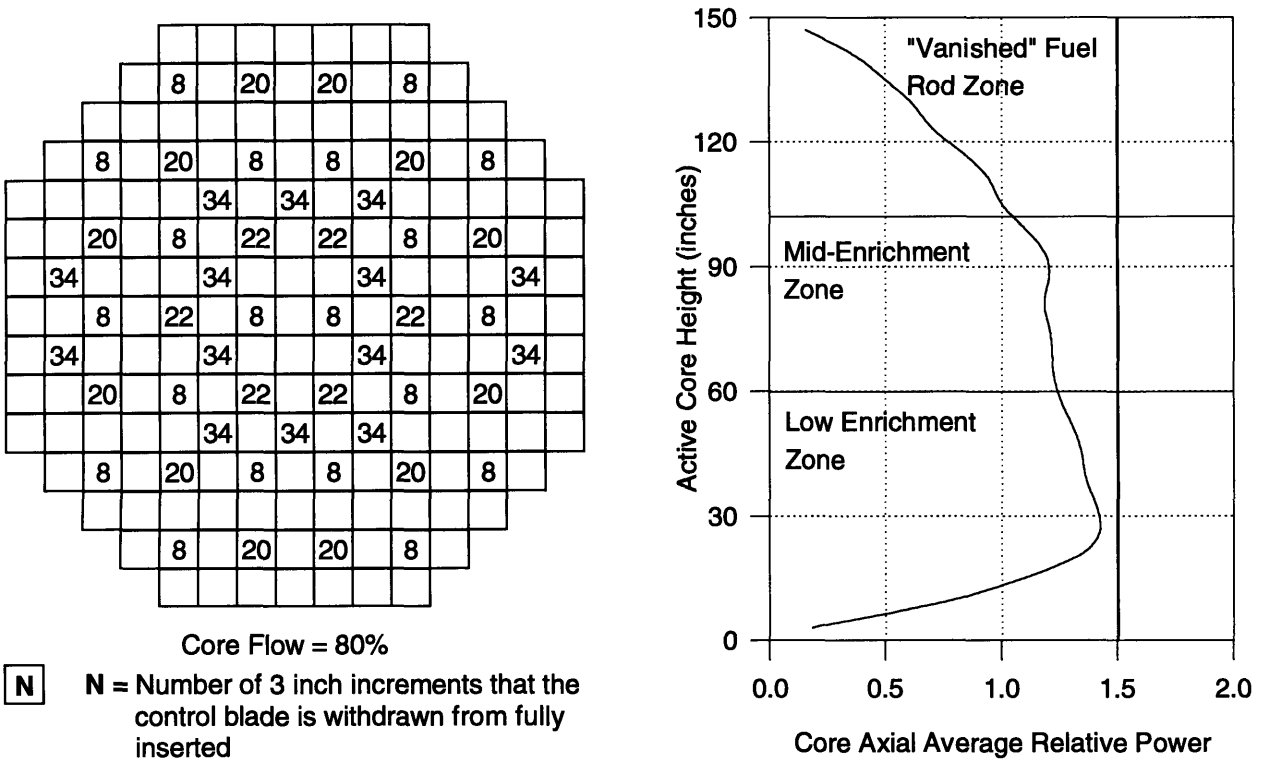

BWR Core Rodded Radial Power Distribution at 21 GWD/MTU

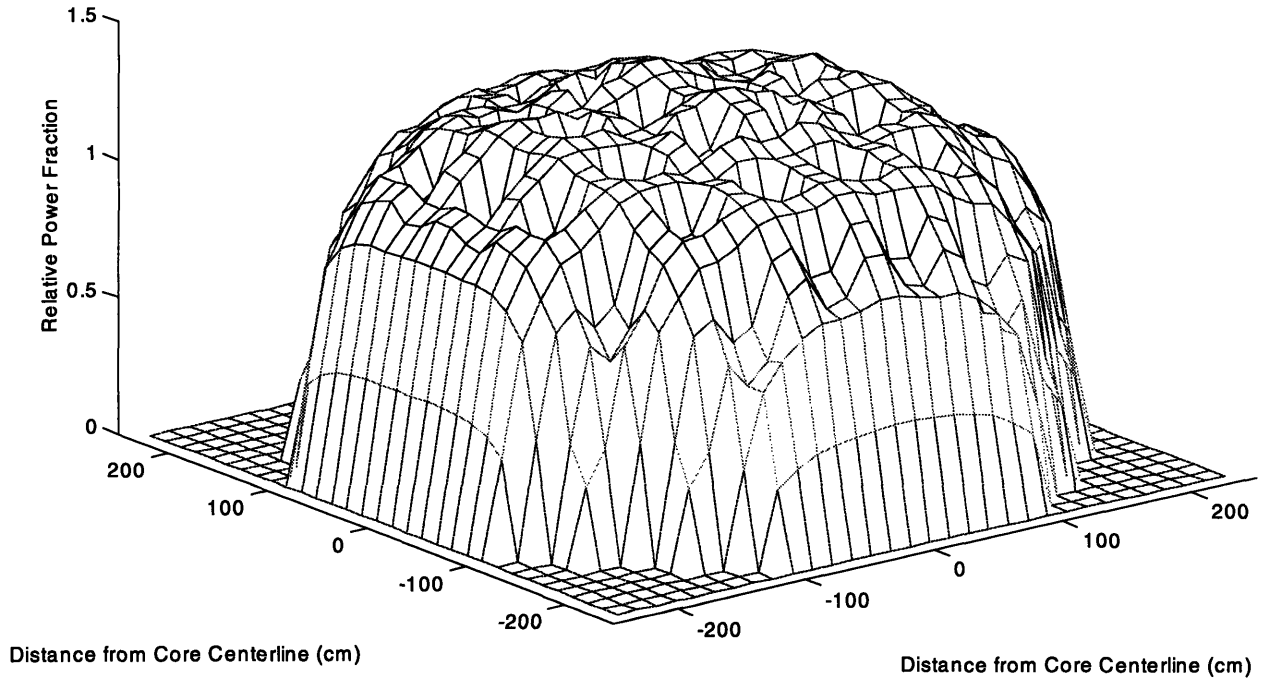

Figure 57: BWR Control Rod Pattern and Power Distribution at 21 GWD/MTU

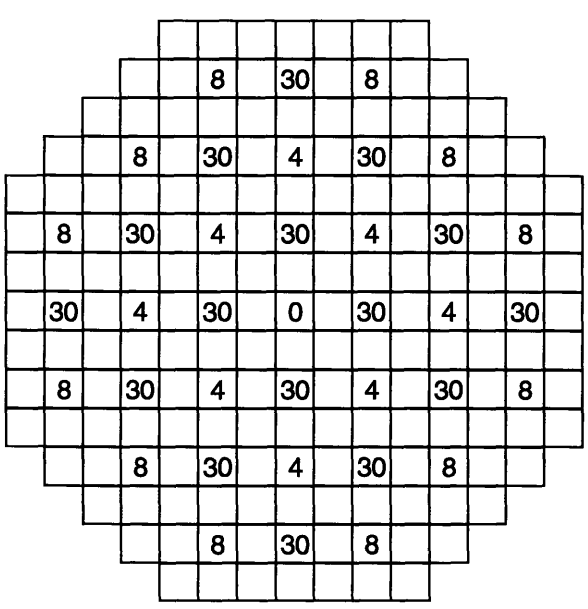

Core Flow = 80%

N = Number of 3 inch increments that the control blade is withdrawn from fully inserted

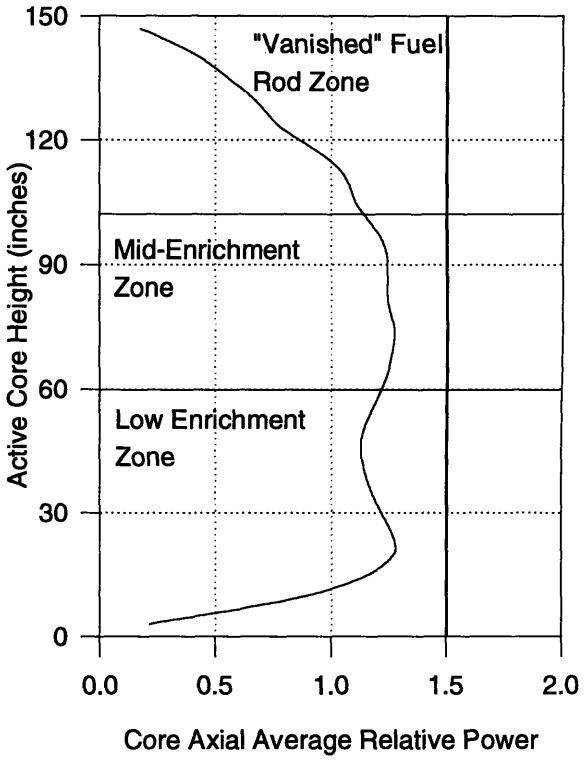

BWR Core Rodded Radial Power Distribution at 25.5 GWD/MTU

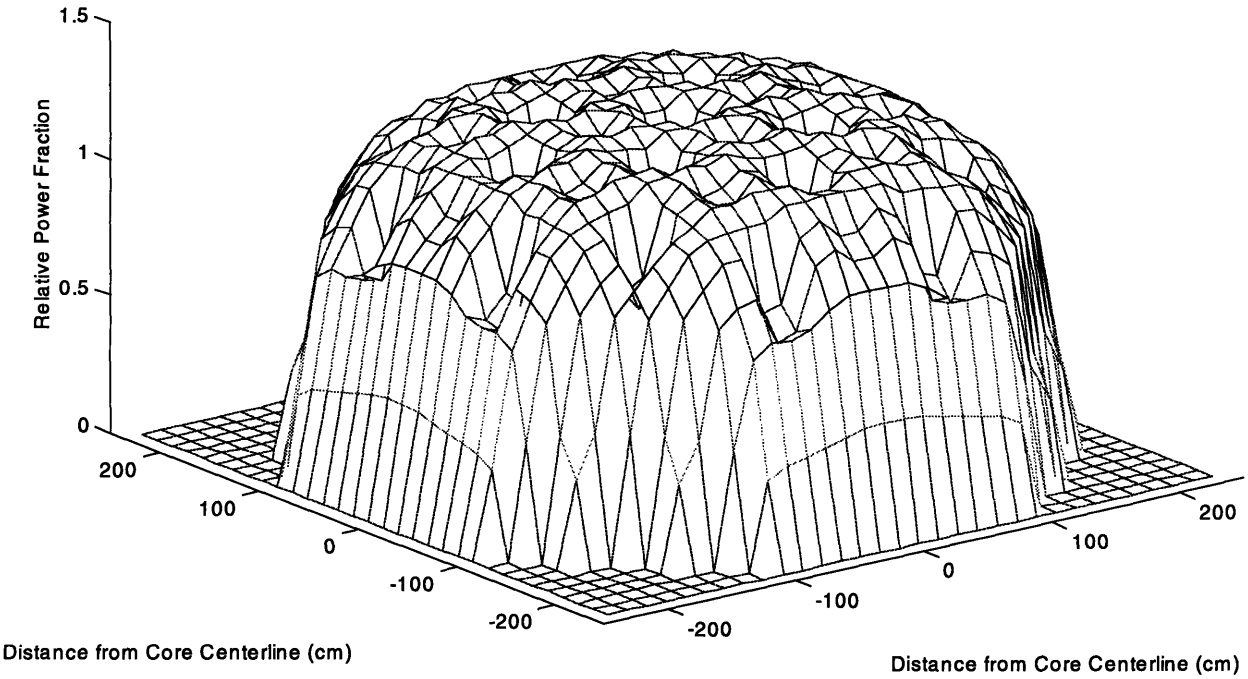

Figure 58: BWR Control Rod Pattern and Power Distribution at 25.5 GWD/MTU

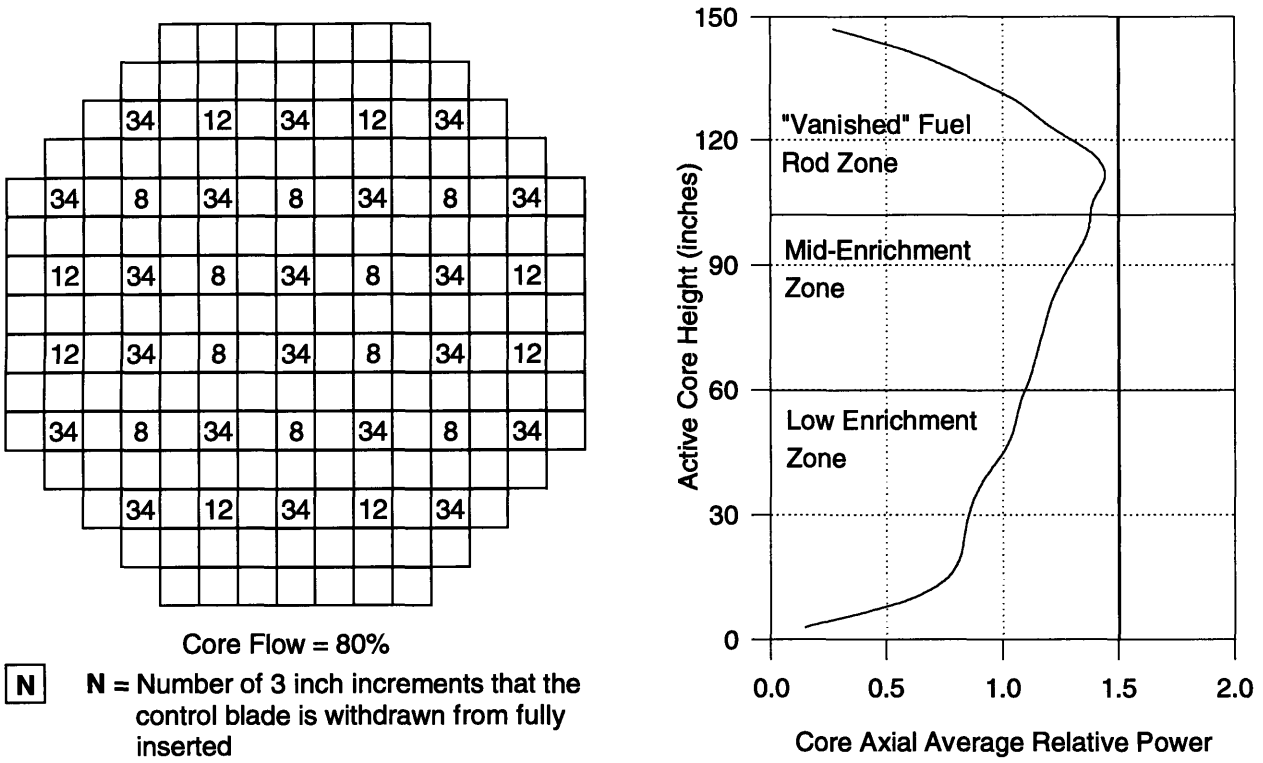

BWR Core Rodded Radial Power Distribution at 29.25 GWD/MTU

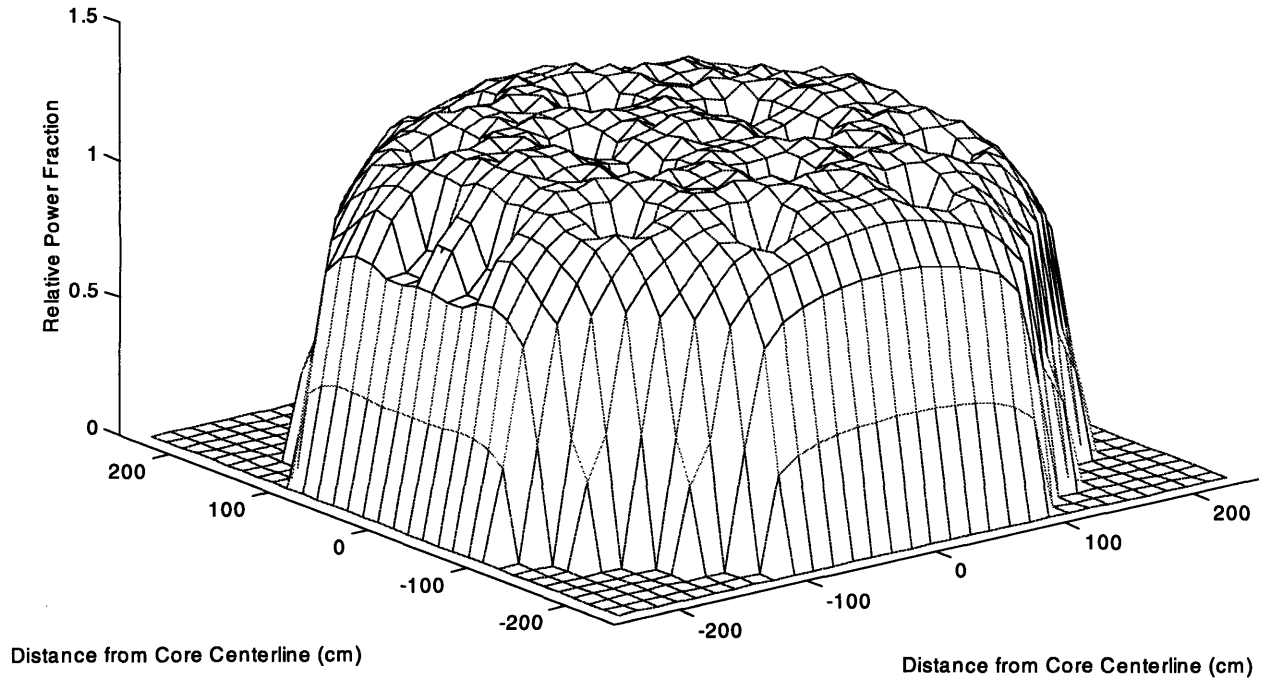

Figure 59: BWR Control Rod Pattern and Power Distribution at 29.25 GWD/MTU

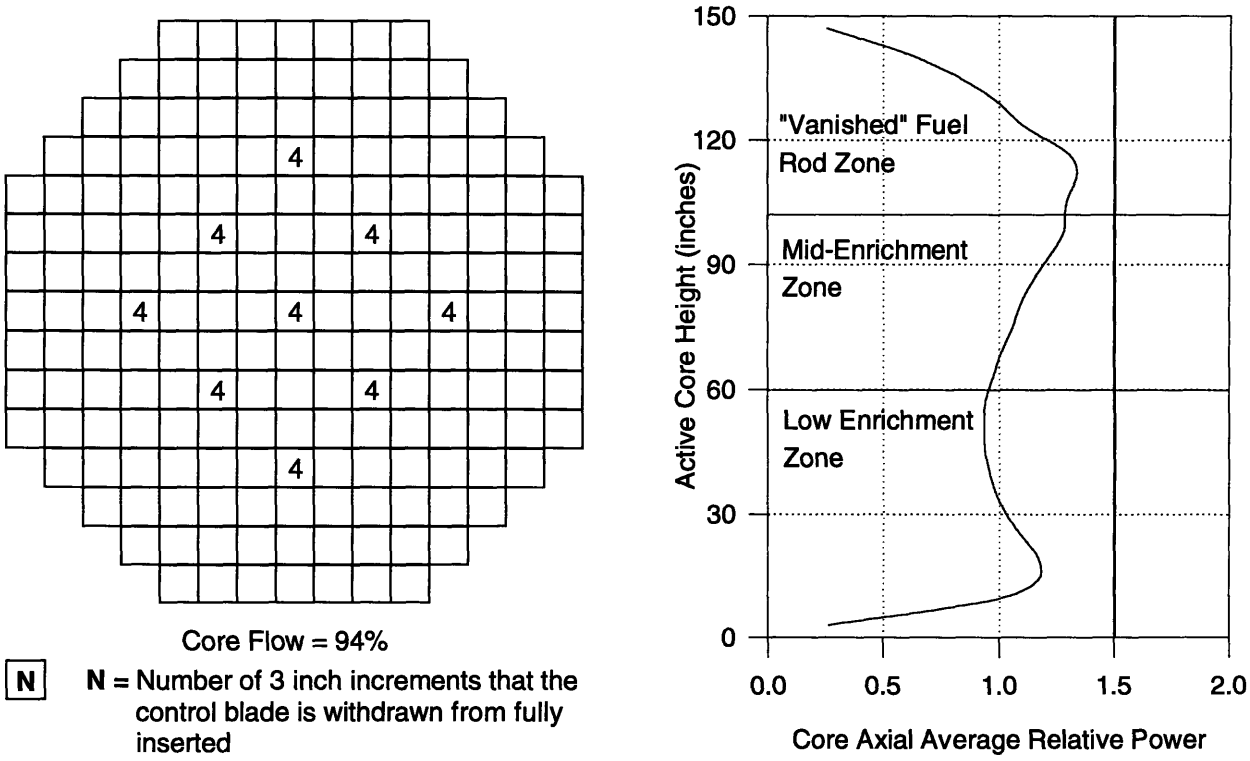

Figure 60: BWR Control Rod Pattern and Power Distribution at 31.5 GWD/MTU

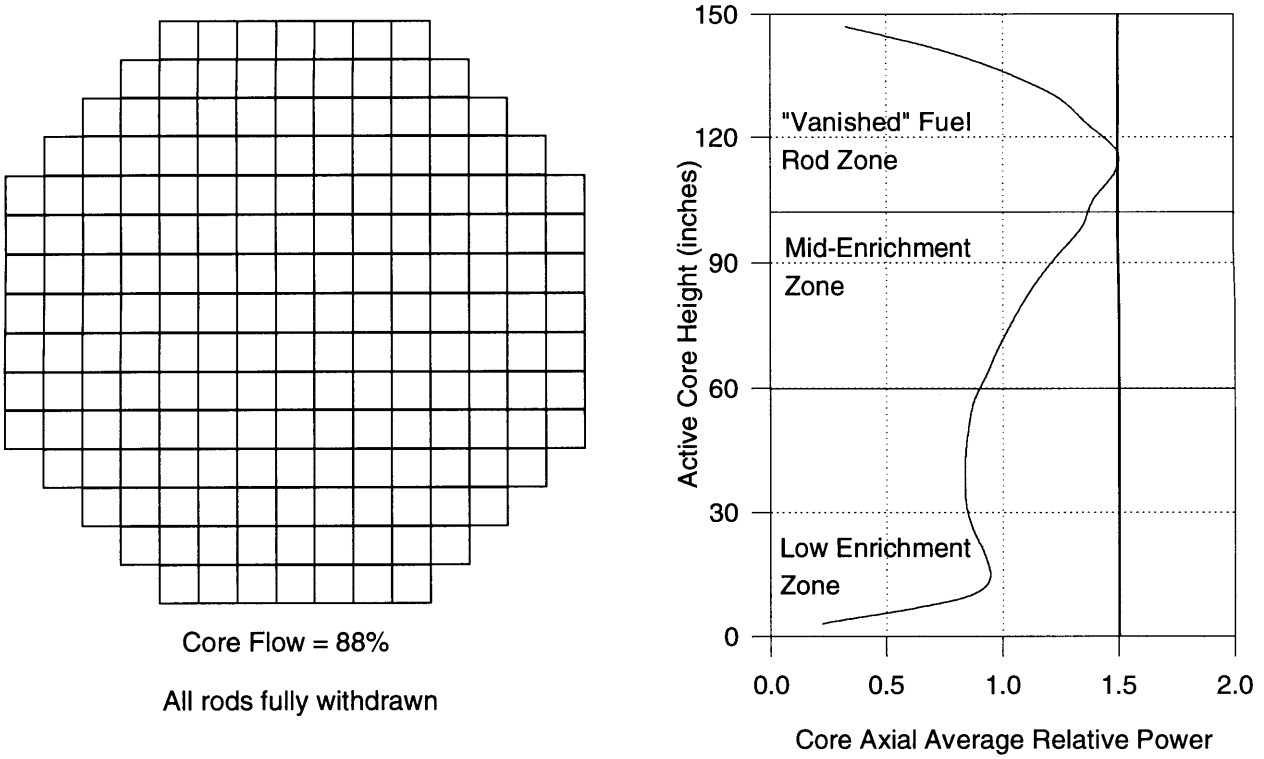

BWR Core Rodded Radial Power Distribution at EOC

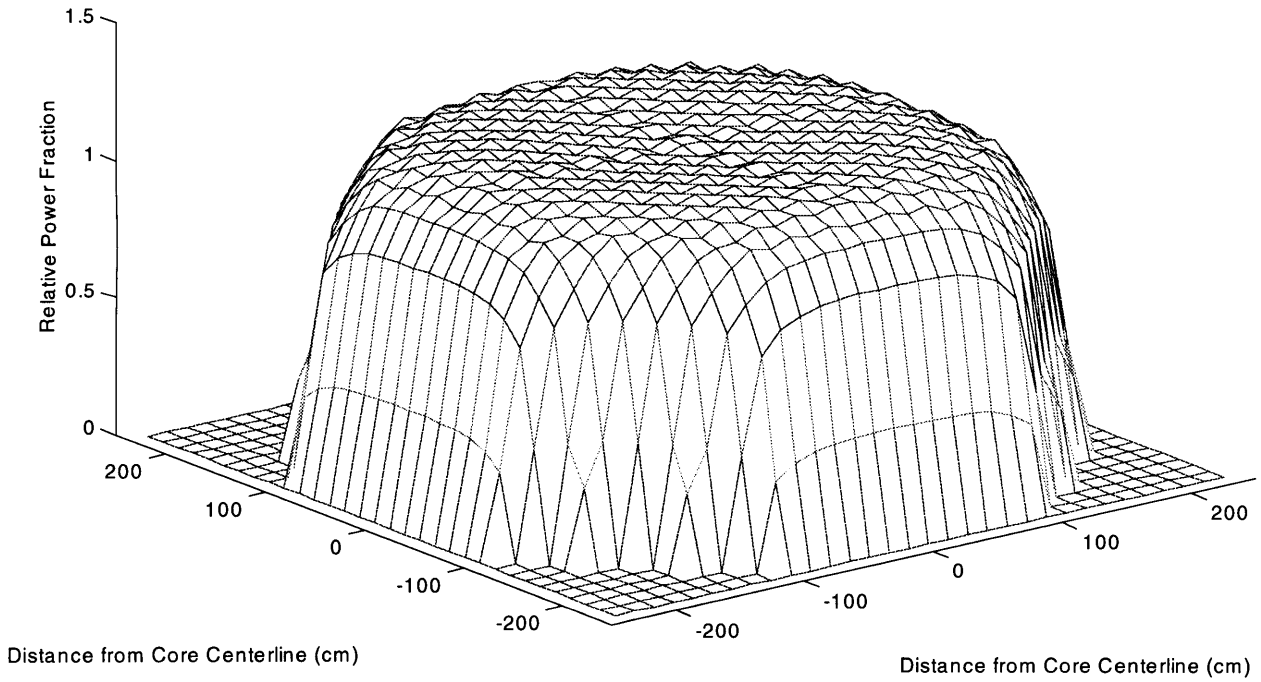

Figure 61: BWR Control Rod Pattern and Power Distribution at EOC

10.3 Thermal Hydraulic Limits

SIMULATE-3 calculated values of MAPRAT and MFLPD for the extended cycle and conventional BWR core designs are shown in Figure 62 and Figure 63. The figures show the ATRIUM-10 fuel in the extended cycle BWR core design provides an excellent margin to calculated thermal hydraulic limits. With its lower LHGR for a given bundle power, the 10×10 fuel in the extended cycle core substantially outperforms the 8×8 fuel used in the conventional core design.

Recall that MFLCPR was not calculated for the BWR extended cycle core design due to a lack of detailed flow path data and the limitations on the ability of the University Version of SIMULATE-3 to incorporate this information into the core model. However, the large margins to MAPRAT and MFLPD calculated here and the proven improved critical power performance of ATRIUM-10 fuel point to well behaved MCPR performance in the BWR extended cycle design.

10.4 Minimum Cold Shutdown Margin

SIMULATE-3 calculated values of the minimum cold shutdown margin for the extended cycle and the conventional BWR core designs are shown in Figure 64. As was the case for the long-cycle PWR core, the BWR extended cycle design does not meet the established design limit for the minimum cold shutdown margin at all times in core life using standard worth control rods. The higher hot excess reactivity and the reduced control rod worth characteristic of the extended design combine to reduce the shutdown margin to below the 1% Δk minimum. Figure 65 compares the hot excess reactivity of the BWR extended cycle design to that of the conventional core. With Gd_2O_3 concentration limited to $12^{w}/_{o}$, the higher enrichments required to achieve longer cycle lengths produce a much higher hot excess reactivity in the long-cycle core than in the conventional design. Additionally, the higher enrichments and heavy burnable poison loadings in an extended cycle core result in fuel assemblies which are much blacker to thermal neutrons than their conventional counterparts. When placed adjacent to control blades these black assemblies compete with them for thermal neutrons and thereby reduce control rod worth.

As with the long-cycle PWR core, shutdown margin in the BWR extended cycle design can be improved by using higher worth control rods. To quantify this effect, CASMO-3 runs were made

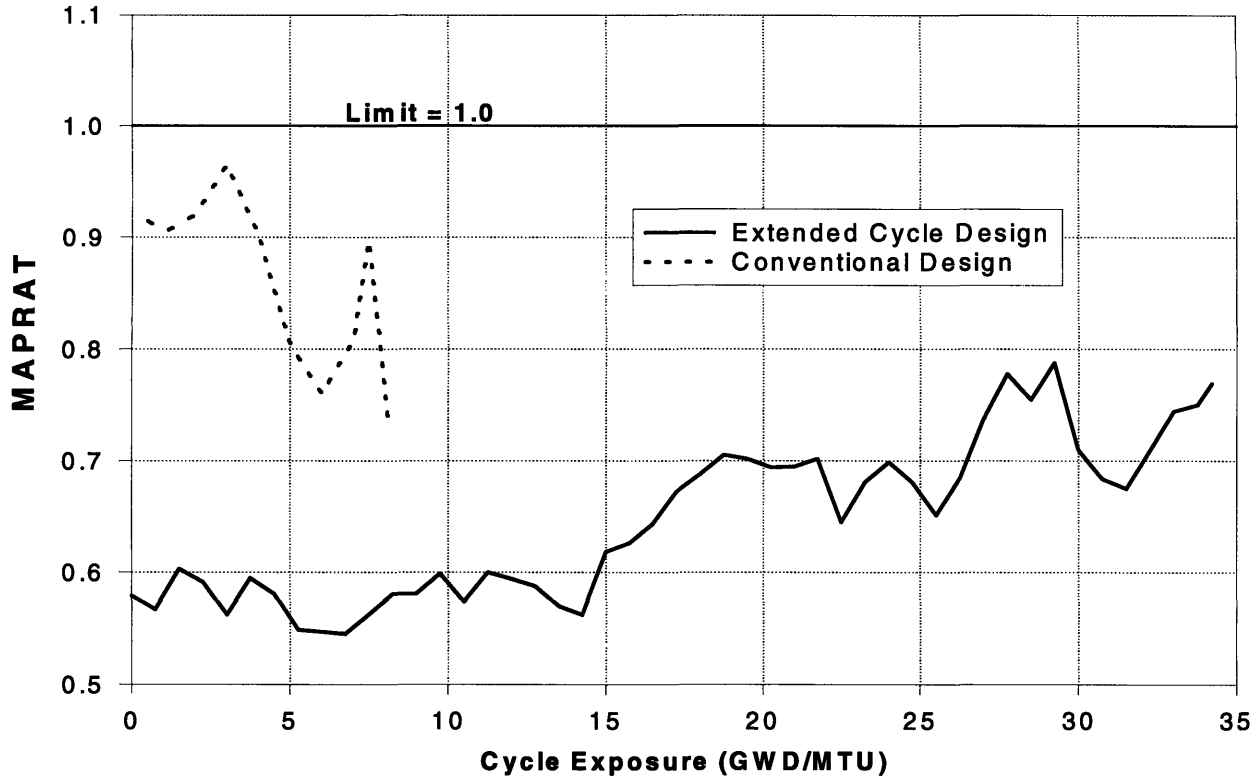

Figure 62: BWR MAPRAT vs. Core-Average Exposure

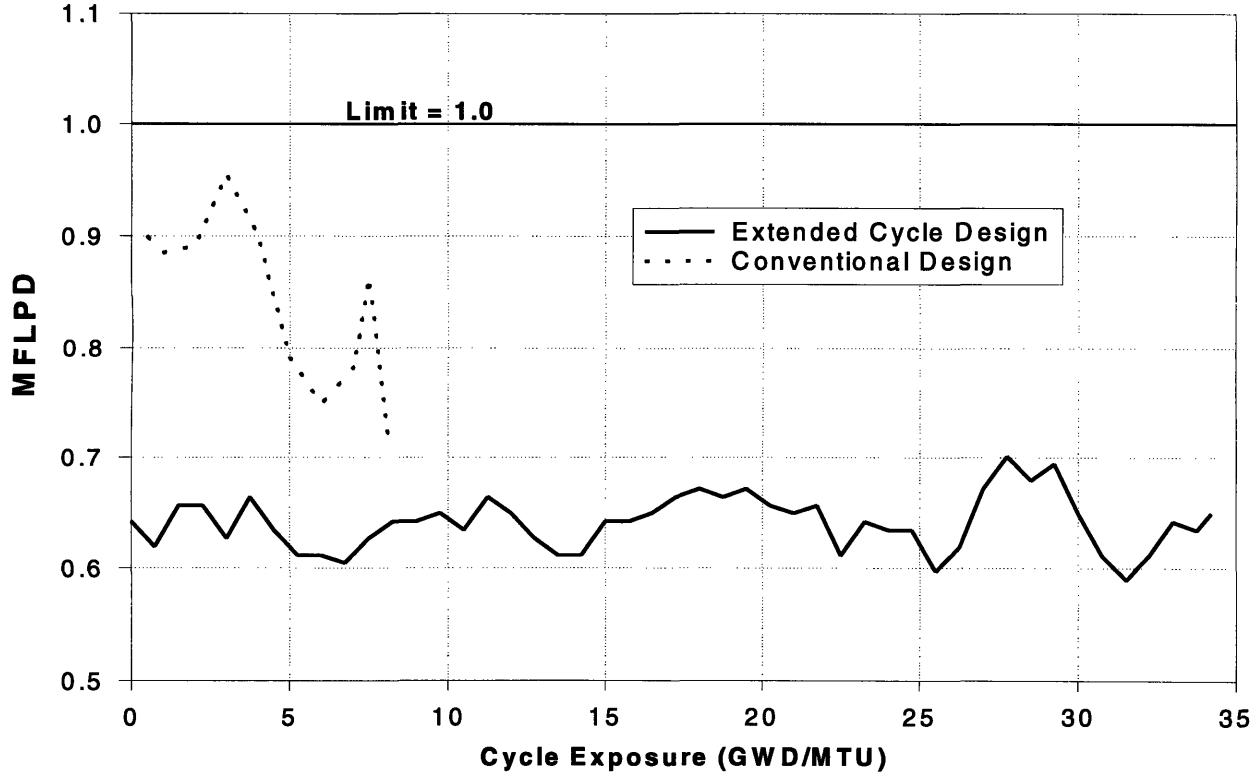

Figure 63: BWR MFLPD vs. Core-Average Exposure

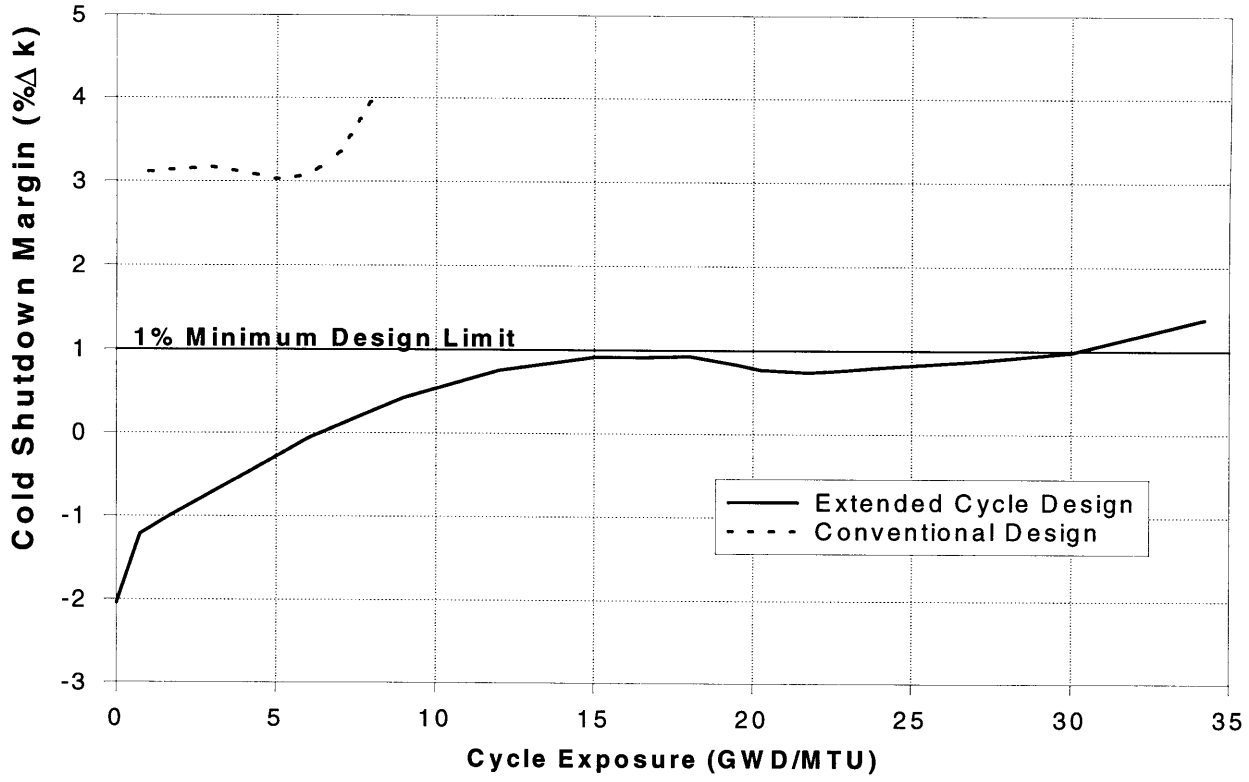

Figure 64: BWR Cold Shutdown Margin vs. Core-Average Exposure

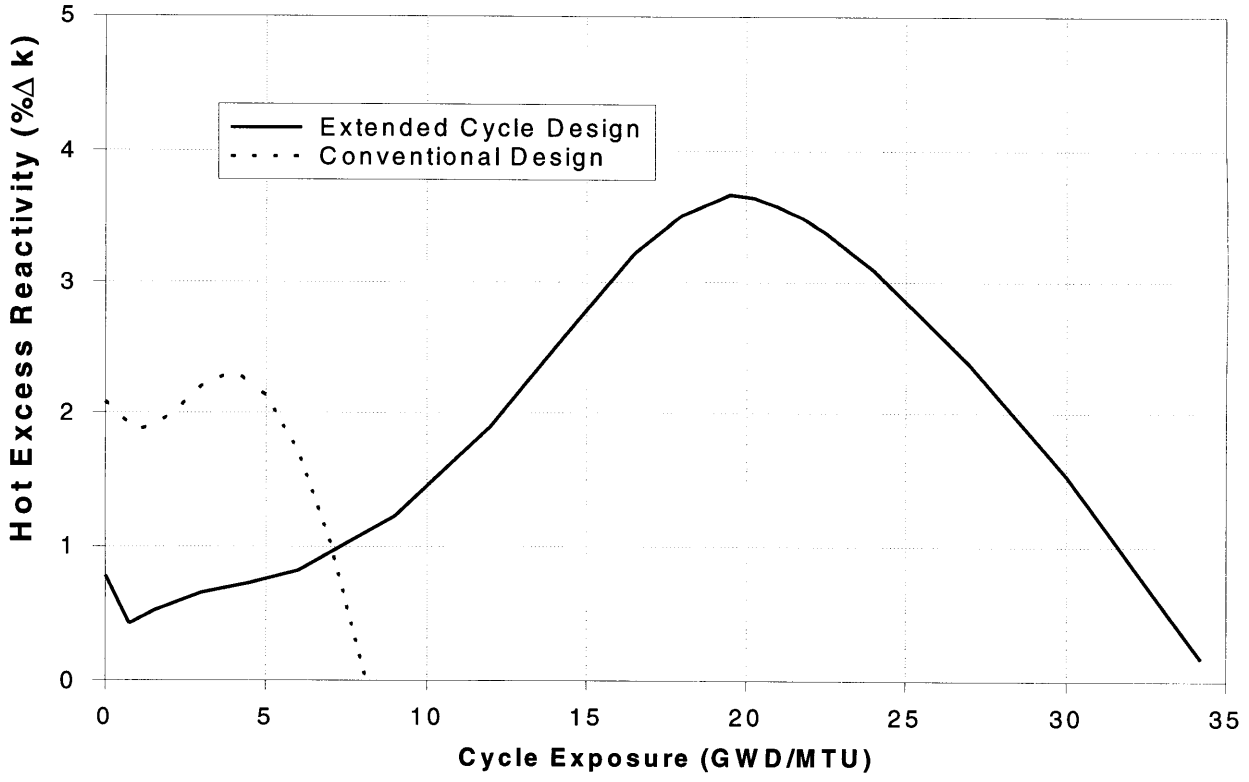

Figure 65: BWR Hot Excess Reactivity vs. Core-Average Exposure

to compare the change in assembly reactivity due to rod insertion in a "conventional" assembly for a 12 month BWR core and in a typical assembly for the extended cycle BWR core. The conventional assembly uses standard B_4C control blades. It has an average fuel enrichment of $2.6^{w}/_{o}$ U^{235} and 4 pins loaded with $4^{w}/_{o}$ Gd_2O_3 as burnable poisons. The extended cycle fuel bundle is a Type 5 assembly MEZ segment with a zone average enrichment of $5.4^{w}/_{o}$ U^{235} and 12 burnable poison pins containing 12 $^{w}/_{o}$ Gd_2O_3. From Table 19 on page 151, the Type 5 assembly is the most common type of fuel bundle in the extended cycle BWR core. Two different types of neutron absorber material were analyzed for use in the RCCAs of the extended cycle assembly. The three cases modeled are listed below:

- Standard Case: $2.6^{w}/_{o}$ U^{235} w/ $4^{w}/_{o}$ Gd_2O_3 in 4 BA pins. Uses standard B_4C control blades
- Extended Cycle Case w/ Standard Control Blades: $5.4^{w}/_{o}$ U^{235} w/ $12^{w}/_{o}$ Gd_2O_3 in 12 BA pins. Uses standard B_4C control blades
- Extended Cycle Case w/ 100% B^{10} Control Blades: $5.4^{w}/_{o}$ U^{235} w/ $12^{w}/_{o}$ Gd_2O_3 in 12 BA pins. Uses B_4C control blades with boron consisting of 100% B^{10}.

The environmental conditions for each case represent typical HFP operating conditions with a void fraction of 40%. For each case, rod worth was calculated as:

$$\Delta\rho = \ln\left(\frac{k_1}{k_2}\right) \tag{10.1}$$

where k_1 and k_2 represent the k_∞ values for the unrodded and rodded assemblies, respectively.

The CASMO-3 calculations of rod worth for the three cases described above are shown in Figure 66. As expected, the rod worth in the extended cycle assembly with standard control blades is much lower than that of the conventional assembly. However, using the 100% B^{10} control blades with the extended cycle assembly, rod worths comparable to those in the conventional assembly can be achieved. Although 100% B^{10} control blades are not available commercially, GE Nuclear energy manufactures commercially available currently licensed high worth rods which could be used to improve the shutdown margin in the BWR extended cycle design. These rods are being considered for use in longer operating cycles with the mission of excess plutonium disposition [G-2]. Finally, new control rods materials incorporating stronger resonant absorbers (such as

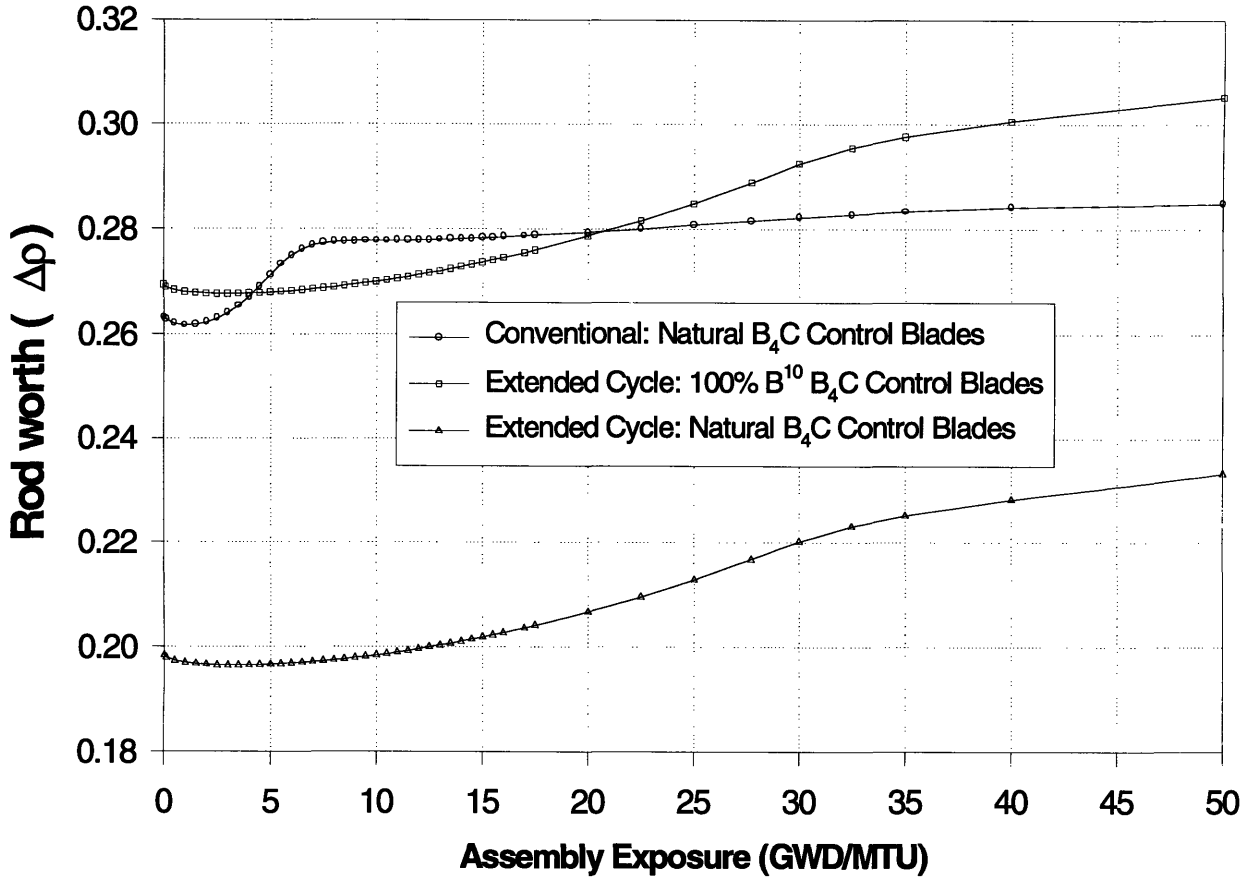

Figure 66: CASMO-3 Comparison of BWR Control Rod Worth

HfB_2) could prove to be extremely effective in improving the cold shutdown margin in the BWR extended cycle design.

10.5 Cycle Length and Maximum Discharge Exposure

The BWR core design achieves a cycle length of 45 EFPM or 47.4 calendar months at the target capacity factor of 95%. Although a hot excess reactivity of 0.17% Δk remains in the core at EOC, the cycle is terminated because the level of recirculation flow required to maintain criticality in the unrodded core produces an unacceptably high axial power peaking factor in the upper region of the core. This cycle length produces:

- 34,200 MWD/MTU core-average discharge burnup
- 40,171 MWD/MTU discharge burnup in the most highly burned *assembly*

- 46,833 MWD/MTU discharge burnup in the most highly burned *fuel pin*
- 59,260 MWD/MTU discharge burnup in the most highly burned *fuel pellet*
- 1371 Effective Full Power Days (EFPD)
- 48 calendar months of operation at a capacity factor of 93.8%
- 47.4 calendar months of operation at a capacity factor of 95%

Figure 67 contains a quarter core map which shows assembly average discharge exposure in the extended cycle BWR core at EOC. The BWR extended cycle design satisfies both the maximum assembly burnup limit (53 GWD/MTU) and the maximum fuel pellet burnup limit (60 GWD/MTU) established for ATRIUM-10 fuel.

10.6 Core Reactivity Coefficients

Although all analyses performed on the BWR extended cycle design take place under steady state conditions, some estimation of transient response behavior can be made by quantifying the core's dynamic reactivity coefficients. In a BWR, some of the more important reactivity coefficients which affect core dynamic behavior include the void coefficient (VC), power coefficient (PC), and the fuel temperature (Doppler) coefficient (FTC). PC and FTC have been defined previously in Section 6.2. In this study, VC is defined as reactivity change associated with a uniform change in core void fraction divided by the change in the average void fraction. VC is given in units of pcm/%. Generally, core reactivity coefficients should have negative values in order to ensure that power will be suppressed by negative reactivity feedback during rapid up-power transients. However, excessively negative reactivity coefficients can lead to large instabilities. Research performed by General Electric shows that VC is the most significant primary driving parameter for flow instabilities in BWRs [G-2].

Table 22 shows the values of the reactivity coefficients calculated for the BWR extended cycle core design. Also included in the table are VC and FTC calculated for the conventional BWR core described in Section 10.1, and VC, PC, and FTC determined by General Electric for BWR cores designed to burn plutonium in mixed oxide fuel [C-5]. The assemblies for the GE Pu disposition study are GE11 9×9 bundles, and they are loaded into a BWR/6 reactor. The 'UO_2-alike' (their terminology) assembly in the GE Pu disposition study represents a lightly Pu loaded fuel assembly

Assembly Type EOC Exposure (GWD/MTU)														
							P 12.29	P 14.03	P 15.04	P 15.48	P 15.70	P 15.81	P 15.85
						P 15.35	1 26.26	1 28.75	2 29.65	2 30.24	2 30.54	2 30.76	2 30.75
				P 11.68	P 16.21	1 28.92	4 30.29	3 32.41	4 32.95	3 33.55	4 33.87	3 34.18	4 34.07
				P 16.72	1 29.99	4 32.27	3 34.15	4 35.31	5 34.64	6 35.25	5 35.33	6 35.77	5 35.59
			P 17.02	1 30.26	4 32.27	3 35.02	6 35.57	5 36.06	6 36.80	5 36.70	6 36.96	5 36.75	6 37.26
		P 11.65	P 16.68	1 30.21	4 32.82	3 35.25	4 36.86	5 36.65	6 37.54	5 37.54	6 38.08	5 37.62	6 38.06	5 37.92
		P 16.18	1 29.90	4 32.16	3 35.08	6 35.88	5 36.66	6 37.75	5 37.84	6 38.42	5 38.24	6 38.80	5 38.49	6 38.74
	P 15.33	1 28.88	4 32.19	3 34.81	4 36.66	5 36.63	6 37.74	5 37.99	6 38.72	5 38.51	6 39.06	5 38.89	6 39.35	5 38.87
P 12.29	1 26.24	4 30.28	3 34.12	6 35.49	5 36.59	6 37.79	5 38.05	6 38.82	5 38.72	6 39.17	5 38.93	6 39.52	5 39.52	6 39.58
P 14.02	1 28.74	3 32.41	4 35.29	5 35.99	6 37.48	5 37.87	6 38.78	5 38.72	6 39.35	5 38.99	6 39.52	5 39.51	6 39.81	5 39.44
P 15.04	2 29.64	4 32.93	5 34.59	6 36.68	5 37.42	6 38.36	5 38.48	6 39.14	5 38.96	6 39.44	5 39.19	6 39.85	5 39.52	6 39.86
P 15.48	2 30.24	3 33.53	6 35.19	5 36.57	6 37.93	5 38.13	6 38.97	5 38.85	6 39.46	5 39.16	6 39.71	5 39.55	6 40.04	5 39.59
P 15.71	2 30.56	4 33.90	5 35.33	6 36.86	5 37.49	6 38.59	5 38.70	6 39.40	5 39.23	6 39.80	5 39.53	6 40.08	5 39.73	6 40.09
P 15.83	2 30.79	3 34.23	6 35.79	5 36.65	6 37.89	5 38.26	6 39.12	5 39.04	6 39.67	5 39.44	6 39.99	5 39.71	6 40.17	5 39.75
P 15.87	2 30.79	4 34.17	5 35.63	6 37.03	5 37.63	6 38.52	5 38.67	6 39.29	5 39.20	6 39.71	5 39.53	6 40.07	5 39.74	6 39.84

Figure 67: BWR Core EOC Assembly Exposure Map

which mimics the reactivity behavior of a conventional UO_2 assembly. The 'MO_2-alike' assembly designates an assembly that is still licensable but that contains a higher concentration of Pu.

For the extended cycle BWR (and for the conventional cycle calculation of FTC), PC and FTC are calculated by using the perturbation functions of SIMULATE-3 to evaluate conditions at EOC. Generally, the most negative (and therefore the most limiting) values of core reactivity coefficients are found at EOC. In order to evaluate VC, CASMO-3 was used to calculate the effect of a change

in the void concentrations on assembly reactivity. The assemblies used in the CASMO calculation of VC are the same assembly types used to calculate control rod worth in Section 10.4. All CASMO-3 calculations were made at hot operating conditions with an initial void concentration of 40%. In order to simulate EOC conditions, coefficients were determined at an assembly average exposure of 40 GWD/MTU. Note that this exposure corresponds to the highest assembly discharge burnup achieved by the BWR extended cycle design.

Table 22: BWR Core Reactivity Coefficients at EOC

Reactor Type	VC (pcm/%)	PC (pcm/%)	FTC (pcm/°F)
BWR/5-Extended Cycle Design	-88.8	-50.7	-1.53
BWR/5-Conventional Design	-105.7	-	-1.52
BWR/6-GE Pu Study UO_2-alike	-110	-49	-1.167
BWR/6-GE Pu Study MO_2-alike	-123	-53	-1.178

The values in Table 22 show that the reactivity coefficients of the BWR extended cycle design lie within the general range of values seen in designs that have already been licensed. Thus the reactivity coefficients determined for the extended cycle BWR suggest a well behaved response to operational (or accident category) transients. The use of advanced ATRIUM-10 fuel in the core also results in a less negative VC than for the other designs and implies improved flow stability in the BWR extended cycle core.

10.7 Fuel Performance

A detailed fuel performance analysis for the BWR extended cycle core design has not yet been performed. This analysis and the additional PWR fuel performance studies described in Chapter 7 will be completed by Handwerk [H-4]. Note that because of the lower discharge exposures, the fuel in the BWR should encounter fewer severe performance challenges than the fuel in the PWR long-cycle core design

10.8 Economic Performance

Using the methodology described in Chapter 8, the direct nuclear fuel costs of the extended cycle BWR core design can be compared to those of the of the conventional design. As described earlier, the same enrichment-burnup correlation (see equation (8.5) on page 124) developed for the PWR can also be applied to the BWR.

Table 23 tabulates the direct nuclear fuel cost of producing the same amount of energy in a single calendar year that was used in the comparison of PWR fuel costs in Section 8.2 (i.e., the 1.082×10^6 MWD calculated in equation (8.8)). The PWR fuel cost values from Table 15, "Comparison of PWR Direct Nuclear Fuel Costs," on page 127 are also included in Table 23 for comparison. The calculations show that the use of an extended cycle design in a BWR increases direct nuclear fuel costs by \$9.7M per year compared to the BWR conventional core for the same amount of energy produced. Although this difference is much smaller than the \$17.1M increase calculated for the PWR, much of this difference stems from the selection of the conventional cycle for each reactor type. The PWR conventional core employs a more aggressive fuel management strategy which uses fuel at enrichment levels which produce nearly optimum values of U_U and U_{SWU}. In contrast, the enrichment level of the fuel in the BWR conventional design falls on the steeply sloped lower regions of the curves in Figure 39. In LWRs, these low levels of enrichment can result in poor neutron economy due to increased parasitic absorptions in the coolant and in structural materials. Lower enrichment fuel tends toward overmoderation and therefore yields lower values of U_U and U_{SWU}.

The values in Table 23 also show that with its lower fuel enrichment requirements, the extended cycle BWR core design reduces annual direct nuclear fuel costs by \$3.7M compared to the PWR extended cycle core. Note that these costs are computed on the basis of thermal energy produced, (while actual revenues are generated on the basis of electrical energy product) and hence the slight difference in plant thermal efficiency (34% for the PWR vs. 32.5% for the BWR) is neglected. The comparison shows that the BWR extended cycle design yields a direct nuclear fuel cost increase of \$13.4M per year compared to the PWR conventional core design. Note however that preliminary economic studies show that the optimum cycle length at which to operate a BWR using a single batch core design is approximately 48 months: i.e., close to that analyzed in the present

Table 23: Comparison of PWR and BWR Direct Nuclear Fuel Costs

Core Design	$\bar{X}_p$ ($^w/_o$)	U_U (MWD/kgU_{NAT})	U_{SWU} (MWD/kgSWU)	M_U (kgU_{NAT}) [$M/year]	M_{SWU} (kgSWU) [$M/year]	Total Fuel Cost
PWR Extended Cycle (n = 1)	6.5	3.49	4.24	3.11×10^5 [15.5]	2.56×10^5 [28.1]	$43.6M per year
PWR Conventional Cycle (n = 2.68)	4.3	5.34	7.28	2.03×10^5 [10.1]	1.49×10^5 [16.4]	$26.5M per year
BWR Extended Cycle (n = 1)	4.92	3.65	4.77	2.97×10^5 [14.9]	2.27×10^5 [25.0]	$39.9M per year
BWR Conventional Cycle (n = 3.03)	2.45	4.07	7.08	2.66×10^5 [13.3]	1.53×10^5 [16.9]	$30.2M per year

study. However, with its higher power density, the economically optimum cycle length for a single batch PWR core design apparently lies in the vicinity of 36 calendar months [H-6]. Hence an optimized long cycle PWR is likely to have very nearly the same fuel cycle cost as a comparably treated BWR.

10.9 Conclusions

The analyses performed in this chapter demonstrate the technical feasibility of implementing the BWR extended cycle design as a reload core in currently operating BWR plants. Like the PWR long-cycle design, the BWR core requires the use of higher worth control rods to ensure that minimum cold shutdown safety margins are met. Additionally, *for the same long cycle length* the BWR design offers improved economic performance over the PWR extended cycle core because of its lower fuel enrichment requirements.

The following chapter provides a summary of this work and recommends areas of future investigation for the PWR and BWR extended cycle core designs.

CHAPTER 11

Conclusions and Future Work

In order to improve nuclear power plant capacity factors, reload cores for a 38.3 EFPM PWR and a 45 EFPM BWR operating cycle have been developed. The cores employ a single-batch loading design and require nuclear fuel with a higher fissile enrichment than the current licensing limit of $5^{w}/_{o}$ U^{235} ($6^{w}/_{o}$ to $7^{w}/_{o}$ for the PWR and $2.5^{w}/_{o}$ to $7.4^{w}/_{o}$ U^{235} for the BWR). To reduce excess reactivity and control power peaking, $12^{w}/_{o}$ Gd_2O_3 and 1.545 mg B^{10}/in. IFBA (Integral Fuel Burnable Absorbers - a thin fuel pellet surface coating of ZrB_2) are loaded as burnable neutron absorbers into the PWR core. Because of the need to maintain enough hot excess reactivity at BOC to permit insertion of rods to control axial power distribution, the BWR design employs $12^{w}/_{o}$ Gd_2O_3 without IFBA. These designs demonstrate the technical feasibility of operating at cycle lengths greater than 40 months while staying within current discharge fuel burnup limits. The only plant hardware modification required is the replacement of current control rods with higher worth rods in order to meet minimum cold shutdown margin safety requirements. A preliminary economic analysis indicates that the use of extended cycle core designs raises direct nuclear fuel costs by $13M to $17M per year compared to current best-practice multi-batch fuel management. In order for extended cycle lengths to become an economically attractive option, this deficit would have to be outweighed by the inherent benefits of longer operating cycles. These benefits include lower replacement energy costs due to a higher capacity factor and a reduction in the number of expensive refueling outages required over the lifetime of the plant.

The following sections suggest topics for future investigation in the areas of neutronic design, fuel performance modeling, regulatory issues, and economic analysis.

11.1 Neutronic Design

A signature feature of the extended cycle design is the existence of slow, large-magnitude oscillations in radial and axial power distribution throughout core life. These roughly sinusoidal variations are a consequence of the positive burnup reactivity coefficient produced by the higher enrichments and heavy burnable poison concentrations required to achieve longer cycle lengths. These perturbations challenge power peaking licensing limits and decrease achievable cycle length. Cycle length is limited by excessive lead pin discharge burnup resulting from the uneven distribution of exposure within the core. Decreasing the magnitude of these oscillations will improve core performance by increasing margins to thermal limits and allowing a longer operating cycle by lowering lead pin discharge exposure through a more homogeneous distribution of accumulated burnup.

11.1.1 Future Work - Current Extended Cycle Lengths

Future work in the neutronic area should focus on reducing the severity of the power shifts in the present designs, assuming that future economic analyses indicate that cycles this long are worth continued investigation. In the BWR, these efforts should concentrate initially on the core axial power distribution, since it is the violation of the axial power peaking limit which directly restricts the achievable cycle length of the current design. The key to success in this endeavor is to diminish the magnitude of the positive burnup reactivity coefficient of the most heavily poisoned assemblies in the cores. More sophisticated fuel enrichment and burnable absorber zoning schemes (both axially and radially) should be able to produce a "flatter" assembly reactivity response with respect to burnup. Recent French work with "duplex" poisoning schemes (which use more than one concentration of Gd_2O_3) has been successful in producing extremely flat reactivity vs. burnup behavior in PWR assemblies designed for 18-month fuel cycles [A-2]. Also, because of its uni-batch design, the extended cycle core could easily take advantage of radially asymmetric interior assemblies, which have been shown to decrease both peak pin power and the peak to average burnup ratio in PWRs [B-3].

Additionally, while the extended cycle designs developed in this study have met all *steady-state* design goal limits, no analysis of transient behavior has yet been performed. Instead, it was

confirmed that all parameters which govern transient behavior fell within the tolerable band of values established for conventional core loadings. In order to ensure licensabilty of the extended cycle core designs, the impact of such unique features as positive burnup reactivity coefficients and increased EOC control rod worth must be explicitly quantified using state-of-the-art plant transient codes.

11.1.2 Future Work - Further Increases in Cycle Length

If the operating cycle lengths of these LWR core designs are to be increased even further, the issues of excessive lead pin and lead pellet discharge burnup *and* insufficient EOC reactivity must both be addressed. Using currently available technology, EOC reactivity can be raised by either increasing fuel enrichment or by reducing the burnable poison loading to decrease the EOC negative residual reactivity penalty. However, both of these methods will increase peak cycle excess reactivity. In the PWR, a higher peak excess translates into a higher CBC. If these methods can be combined with the use of enriched soluble boron (i.e., boron with an increased concentration of the neutron absorbing B^{10} isotope), then EOC reactivity in the PWR design might be improved without unacceptably degrading primary water chemistry. To increase cycle length further in the BWR, these methods could be used in combination with the higher worth control rods required to improve the cold shutdown safety margin.

Using more exotic technologies, EOC reactivity could be reduced by using Atomic Vapor Laser Isotope Separation [AVLIS] to create "boutique" burnable neutron poisons. Using AVLIS technology, the even numbered "fertile" isotopes of naturally occurring gadolinium (Gd^{154}, Gd^{156}, Gd^{158}) can be removed, leaving a mixture which should exhibit much less residual reactivity at EOC [H-5]. Unfortunately, AVLIS has not been deployed commercially on a large scale, so these isotopes are not yet widely available.

11.2 Fuel Thermal and Mechanical Performance

Steady-state analysis of fuel rod internal pressure shows that the fuel in the extended cycle PWR core meets design goal limits. An assessment of the steady-state corrosion behavior of the PWR core is currently in progress. An analysis should also be performed on the fuel in the BWR core design, although fewer fuel performances problems are anticipated in the BWR design

because of its lower average exposures. As with core neutronic performance, the fuel performance of the extended cycle design must also be analyzed under transient conditions. Additionally, the less quantifiable fuel performance issues outlined in Section 7.4 must be carefully assessed in order to ensure that unacceptable degradation in fuel performance does not result from the shift to longer operating cycles.

11.3 Fuel Cycle Regulatory Issues

In order to complete the design and evaluation of extended cycle reload cores, the regulatory issues surrounding the use of nuclear fuel enriched to as high as $7.4^{w}/_{o}$ U^{235} must be addressed. At the front end of the fuel cycle, these issues center around the costs and methods of ensuring criticality safety at enrichment and fabrication plants and at in-plant facilities such as the nuclear storage vault. The primary concern at the back end of the fuel cycle stems from the shipment and storage of spent nuclear fuel from the extended cycle core.

The extended cycle core produces more spent fuel assemblies on an annualized basis than a conventional core. Additionally, this spent fuel will have a higher reactivity than fuel discharged from a conventional, multi-batch core. CASMO-3 models show that fuel discharged from the both the PWR and BWR extended cycle core designs at EOC has an enrichment of $\sim 2^{w}/_{o}$ U^{235} and contains $\sim 1^{w}/_{o}$ of fissile plutonium. This compares to an enrichment of $0.8^{w}/_{o}$ U^{235} and a fissile plutonium loading of $0.8^{w}/_{o}$ for the fuel from a conventional core. The resulting increase in EOC reactivity presents a challenge for spent fuel safe shipping and storage. The spent fuel pools of plants must be analyzed in order to assess the impact of this increased reactivity on criticality safety. The increased fuel reactivity may necessitate the insertion of poison shims into the pool and/or assemblies in order to control criticality.

Shipping spent fuel from extended cores presents a further challenge, since current spent fuel casks take no credit for burnup or for burnable poisons. Presently casks are licensed up to $5^{w}/_{o}$ U^{235}. A cask design must maintain sub-criticality when loaded with fresh, unpoisoned, $5^{w}/_{o}$ U^{235} fuel. Efforts are presently underway at TRW, Inc. to develop and license a methodology for taking credit for fuel burnup [U-1]. This methodology (expected to be licensed in 1998) will be used by vendors to design the next generation of spent fuel casks. Using this methodology, current spent

fuel casks could be licensed to accept spent fuel from extended cycle cores [L-1]. Without this methodology, the spent fuel from the cores designed in this study cannot be shipped. Even with the burnup credit methodology in place, there will probably be a cost increase associated with shipping fuel from an extended cycle core. For example, estimates show that only 24 of the "under-burned" extended cycle PWR assemblies can be loaded per shipping canister instead of 32 for standard spent fuel. However, fresh fuel shipment should not be a problem since fresh fuel requires little shielding and can be moved in smaller quantities.

Finally, increased fuel reactivity may also affect the capacity of the proposed geologic repository at Yucca Mountain, Nevada. The impact of extended cycle fuel on the long term criticality concerns at the repository must be assessed. Current research into the use of depleted uranium oxides and silicates as a waste package fill material may hold promise for reducing these concerns [L-1].

11.4 Economic Performance

11.4.1 Quantification of Economic Performance

Because the impetus for increasing operating cycle length is improved economic performance, a detailed economic study must be done to properly judge the viability of the extended cycle design. This study is currently underway and will seek to quantify all costs associated with increased operating cycles. In addition to the direct nuclear fuel costs calculated in Section 8.2, some additional economic penalties stemming from the extended cycle design are summarized in Table 24.

11.4.2 Improving Economic Performance

Preliminary economic studies show that the optimum cycle length at which to operate a BWR using a single batch core design is approximately 48 months: i.e., close to that analyzed in the present study. However, with its higher power density, the economically optimum cycle length for a single batch PWR core design apparently lies in the vicinity of 36 calendar months [H-6]. Therefore, future efforts should be focused on producing a PWR core to operate at this shorter, more economically competitive length. Note that the lower fuel enrichment and burnable poison

requirements of this shorter cycle length should also improve neutronic performance by reducing the magnitude of the positive burnup reactivity coefficient of the assemblies in the core. The shorter cycle may also permit re-use of assemblies for a second cycle on the periphery, which would yield a significant savings since reload fuel batch size would be reduced by approximately 25%.

Table 24: Sources of Economic Penalties in Extended Cycle Core Designs

	Design Aspect	Economic Penalty
1.	Increased fuel enrichment (up to $7.4^{w}/_{o}\ U^{235}$)	• Fuel costs increase with no increase in discharge burnup over current best-practices. • A premium will be paid to amortize the cost of relicensing fabrication facilities to handle $>5^{w}/_{o}\ U^{235}$ fuel. • Underburned spent fuel has a higher reactivity than standard spent fuel. Additional measures are required to ensure criticality safety in the spent fuel pool.
2.	Reduction in Ag-In-Cd control rod worth	• Existing control rods must be replaced with a stronger absorbing material.
3.	Increased time at higher clad temperatures and (for the PWR) lower pH values	• Increased waterside cladding corrosion is possible which will necessitate the use of a more expensive, advanced cladding material such as Zirlo® (PWR).
4.	Full core reloads	• On-site fuel handling and storage facilities must accommodate an entire core of fresh fuel. • Refueling the whole core may extend the length of the refueling outage.
5.	Transition cycle	• Premature discharge of fuel that is not fully burned from the conventional 3-batch core
6.	Operational Considerations	• In the BWR, the power reductions during required control rod pattern shifts will lower plant capacity factor slightly relative to a plant using the CCC concept for reactivity control.

11.5 Conclusion

In conclusion, the results of the present study confirm the technical feasibility of devising highly-rated LWR core designs which can achieve ultra-long operating cycles (42-48 months depending on capacity factor). Foreseeable problems can be overcome, but some solutions imply progressively higher economic penalties. Assessing and minimizing such penalties is a major focus of the near term future effort.

References

[A-1] A.F.A Ayoub and M.J. Driscoll, "A Strategy for Extending Cycle Length to Improve Pressurized Water Reactor Capacity Factor," Massachusetts Institute of Technology, Program for Advanced Nuclear Power Studies, Cambridge, MA, MIT-ANP-TR-032 (June 1995).

[A-2] M. Asou and J. Porta, "Prospects for Poisoning Reactor Cores of the Future," *Nuclear Engineering and Design*, **168**, pp. 261-270 (May 1997).

[B-1] C.W. Bagnal, et al, "Reduction in Reactor Vessel Irradiation Through Fuel Management," *Trans. Am. Nucl. Soc.*, **45**, pp. 98-99 (1983).

[B-2] J.F. Briesmeister, ed., "MCNP - A General Monte-Carlo N-Particle Transport Code Version 4A," Los Alamos National Laboratory, LA-12625-M (1993).

[B-3] B.R. Beebe and C.R. Savage, "Fine Tuned Power Distribution Control," *Trans. Am. Nucl. Soc.*, **76**, pp. 352-353 (1997).

[C-1] "Consumers Power gears up for annealing by 2000," *Nuclear News*, **38**-2, pp. 24-26 (February 1995).

[C-2] P. Chodak, M.J. Driscoll, M.M. Miller, and N.E. Todreas, "Destruction of Plutonium using Non-Uranium Fuels in Pressurized Water Reactor Peripheral Assemblies," Massachusetts Institute of Technology, Nuclear Fuel Cycle Economics and Environmental Management Program, Cambridge, MA, MIT-NFC-TR-001 (January 1997).

[C-3] Commonwealth Edison Company, "La Salle County Station Preliminary Safety Analysis Report," (1970).

[C-4] L. Covington, STUDSVIK of America, Newton, MA, personal communication, August, 1997.

[C-5] R-T. Chiang and E.H. Ehrlich, "BWR Core Designs for Plutonium Disposition," ANS Proc.of the Topical Meeting - Advances in Nuclear Fuel Management II, EPRI TR-107728-V2, Vol. 2, pp. 18-53 - 18-60 (March 1997).

[D-1] G. Dalporto and N.E. Todreas, Achieving Higher Capacity Factors through Longer Cycle Lengths," *Trans. Am. Nucl. Soc.*, **72**, p. 327 (1995).

[D-2] M.J. Driscoll, T.J. Downar, and E.E. Pilat, The Linear Reactivity Model for Nuclear Fuel Management, American Nuclear Society, La Grange Park, IL (1990).

[D-3] H. Druenne, "Experience of Extensive Use of Gadolinium as Burnable Absorber in Belgian NPPs," ANS Proc.of the Topical Meeting - Advances in Nuclear Fuel Management II, EPRI TR-107728-V2, Vol. 2, pp. 16-9 - 16-16 (March 1997).

[E-1] Electric Power Research Institute, "PWR Primary Water Chemistry Guidelines: Revision 3," EPRI TR-105714 (November 1995).

[E-2] M. Edenius and B.-H. Forssén, "CASMO-3 A FUEL ASSEMBLY BURNUP PROGRAM--User's Manual," STUDSVIK/NFA-89/3 Rev. 3, STUDSVIK AB (June 1993).

[E-3] Energy Information Administration, "Spent Nuclear Fuel Discharges from U.S. Reactors," SR/CNEAF/95-01 (February 1995).

[F-1] C.W. Forsberg, "Depleted Uranium Oxides and Silicates as Spent Nuclear Fuel Waste Package Fill Materials," Materials Research Society 1996 Fall Meeting: Symposium II Scientific Basis for Nuclear Waste Management XX, paper II26.6, Boston, MA, December 2-6, 1996.

[F-2] H. Fujii, ed., "Directory of Nuclear Power Plants in the World 1994," Japan Nuclear-Energy Information Center Co., Ltd., Tokyo, Japan (1994).

[F-3] "Fuel Review 1996: Fuel Designs-BWR," *Nuclear Engineering International*, **41**-506, p. 22 (September 1996).

[G-1] General Electric Company, "BWR/6 General Description of a Boiling Water Reactor," San Jose, CA (September 1980).

[G-2] GE Nuclear Energy, "Study of Pu Disposition Using Existing GE Boiling Water Reactors," NEDO-32361, San Jose, CA (June 1, 1994).

[G-3] P. Griffith, "Pressure Drop - Flow Rate Instabilities in Two Phase Systems," Lecture Notes, Course 22.313 (Thermal Hydraulics in Nuclear Power Technology), Department of Nuclear Engineering, Massachusetts Institute of Technology, Cambridge, MA, Spring 1995.

[H-1] L. Hochreiter, "PWR Accident Analysis," Lecture Notes--Reactor Technology Course for Utility Executives, Massachusetts Institute of Technology, June 17-July 19, 1996.

[H-2] J.A. Haglund and O. Hunter, Jr., "Elastic Properties of Polycrystalline Monoclinic Gd_2O_3," *Journal of the American Ceramic Society*, **56**-6, pp. 327-330 (June 1973).

[H-3] L.C. Hill and K.D. Hartley, "Siemens Power Corporation - Nuclear Division: Gadolinia Fuel Experience," ANS Proc. of the 1994 Int. Topical Meeting on Light Water Reactor Fuel Performance, pp. 133-139, West Palm Beach, FL, April 17-21, 1994.

[H-4] C.S. Handwerk, "Economic and Fuel Performance Issues Associated with Extended Operating Cycles," S.M. Thesis in progress, Department of Nuclear Engineering, Massachusetts Institute of Technology, Cambridge, MA, *to be completed January, 1998.*

[H-5] C.M. Hove and S.W. Spetz, "Improved PWR Gadolinia Fuel Assembly Design Using Isotopic Enrichment of Gd-157," ANS Proc.of the Topical Meeting - Advances in Nuclear Fuel Management, Pinehurst, NC, 2-5 March 1986.

[H-6] C.S. Handwerk et al., "Economic Analysis of Implementing a Four Year Extended Operating Cycle in Existing PWRs," Massachusetts Institute of Technology, Program for Advanced Nuclear Power Studies, Cambridge, MA, MIT-ANP-TR-049 (January 1997).

[I-1] S. Ishimoto, M. Hirai, K. Ito, and Y. Korei, "Effects of Soluble Fission Products on Thermal Conductivities of Nuclear Fuel Pellets," Journal of Nuclear Science and Technology, **31**(8), p. 796-802 (August 1994).

[I-2] Institute of Nuclear Power Operations, "Delayed Manual Scram Following a Core Flow Reduction Event and Entry Into a Region of Core Instability," INPO Significant Event Report (SER) 22-93, October 25, 1993.

[J-1] A. Jonsson, J. R. Parrette, and N. L. Shapiro, "Application of Erbium in Modern Fuel Cycles", The 6th KAIF/KNS Annual Conference, Seoul, Korea, Combustion Engineering, Inc. (1991).

[J-2] A. Jonsson and J.E. Gunn, "The Erbium Burnable Absorber in the Design and Operation of 18- and 24-Month Fuel Cycles," *Trans. Am. Nucl. Soc.*, **73**, pp. 376-377 (1995).

[K-1] G. Kohse, "LWR Water Chemistry and Dose Reduction," Lecture Notes--Reactor Technology Course for Utility Executives, Massachusetts Institute of Technology, June 17-July 19, 1996.

[L-1] D. Lancaster and E. Fuentes, "Appropriate Burnup Measurements for Transportation Burnup Credit," *Trans. Am. Nucl. Soc.*, **76**, pp. 60-61 (1997).

[M-1] P.E. MacDonald and L.B. Thompson, "MATPRO: Version 09, A Handbook of Materials and Properties for Use in the Analysis of Light Water Reactor Fuel Behavior," TREE-NUREG-1005 (December 1976).

[M-2] M.V. McMahon, "Fuel Burnup Effects on the Performance of a Reactor Power Controller," S.M. Thesis, Department of Nuclear Engineering, Massachusetts Institute of Technology, Cambridge, MA (February 1990).

[M-3] M.V. McMahon, M.J. Driscoll and E.E. Pilat, "Natural Uranium and Separative Work Utilization in LWRs," *Trans. Am. Nucl. Soc.*, **76**, pp. 348-349 (1997).

[O-1] Organization for Economic Co-operation and Development, The Economics of the Nuclear Fuel Cycle, NEA/OECD (1994).

[P-1] Public Service Company of New Hampshire, "Seabrook Station Final Safety Analysis Report," (November 1985).

[P-2] V.I. Pavlov, "Analysis of the Neutron-Physical Characteristics of the Fuel Lattice of the VVÉR-1000 Reactor," Russian Scientific Center "Kurchatov Institute." Translated from *Atomnaya Énergiya*, Vol. **74**, No. 1, pp 10-21 (January 1993).

[P-3] R.H. Pitulski, et al, "Analysis of Radial Blanket Design Options for PWR Reload Application," *Trans. Am. Nucl. Soc.*, **45**, pp. 100-101 (1983).

[P-4] E. Pilat, Yankee Atomic Electric Company, Bolton, MA, personal communication, August, 1996.

[R-1] P.C. Rohr, G.A. Davis, and R.A. Matzie, "Safety Aspects of the System 80+™ Plant with Mixed Oxide Cores," ANS Proc. Int. Topical Mtg on Safety of Operating Reactors, Seattle, WA, Sept. 17-20, 1995.

[R-2] P.F. Rose, ed., "ENDF/B Summary Documentation," BNL-NCS-17541 (ENDF-201), 4th ed. (ENDF/B-VI), Brookhaven National Laboratory (October 1991; Release-2, 1993; Release-3, 1995).

[R-3] E.L. Redmond, "Monte Carlo Methods, Models, and Applications for the Advanced Neutron Source," S.M. Thesis, Department of Nuclear Engineering, Massachusetts Institute of Technology, Cambridge, MA (June 1990).

[R-4] J. Rivera, Yankee Atomic Electric Company, Bolton, MA, personal communication, May, 1997.

[R-5] J. Rivera, Yankee Atomic Electric Company, "Fuel Reliability and Performance: Zeno's Paradox," Presentation at the Massachusetts Institute of Technology Department of Nuclear Engineering Monday Afternoon Seminar Series, November 4, 1996.

[S-1] STUDSVIK of America, "TABLES-3 User's Manual," STUDSVIK/SOA-92-03-Rev. 0 (April, 1992).

[S-2] STUDSVIK of America, "SIMULATE-3 User's Manual," STUDSVIK/SOA-92/01-Rev. 0 (April, 1992).

[S-3] L.C. Stephenson and A. Neufert, "Gadolinia in Economically Competitive PWR Fuel Cycles," ANS Proc.of the Topical Meeting - Advances in Nuclear Fuel Management II, EPRI TR-107728-V1, Vol. 1, pp. 7-17 - 7-24 (March 1997).

[S-4] J.R. Secker, J.E. Pritchett, D.Y. Chung, and H.W. Keller, "Design and Operational Experience with Westinghouse ZrB_2 Integral Fuel Burnable Absorbers in

Advanced PWR Fuel," ANS Proc. of the 1988 Int. Reactor Physics Conference, Jackson Hole, WY, Sept. 18-22, 1988.

[S-5] D.L. Stucker, W.L. Carlson, and R. D. Erwin, "High-Burnup Optimization of Axial Blanket Design Parameters," *Trans. Am. Nucl. Soc.*, **69**, pp. 481-482 (1993).

[S-6] N.L. Shapiro, "An Evaluation of the Use of Annular Fuel in PWRs," *Trans. Am. Nucl. Soc.*, **38**, pp. 150-151 (1981).

[S-7] J.R. Secker and F.J. Frank, "Optimum Blanket Design for PWRs," *Trans. Am. Nucl. Soc.*, **45**, pp. 101-102 (1983).

[S-8] D.L. Stucker, W.A. Boyd, J.M. Huckabee, "Flux Reduction Fuel Management Techniques," *Trans. Am. Nucl. Soc.*, **45**, pp. 99-100 (1983).

[S-9] K.E. St. John, S.P. Schultz, and R.P. Smith, "Methods for the Analysis of Oxide Fuel Rod Steady-State Thermal Effects (FROSSTEY-2)," Yankee Atomic Electric Company, Bolton, MA, YAEC-1912P (January 1995).

[S-10] Siemens Power Corporation, "Qualification of Exxon Nuclear Fuel for Extended Burnup," XN-NF-82-06 (NP) (A) Rev. 1 (May 1987).

[S-11] STUDSVIK of America, input data for CASMO-3 and SIMULATE-3 for modeling a generic BWR/5, 1995.

[S-12] Siemens AG, "ATRIUM™ Fuel Assemblies for Boiling Water Reactors," Erlangen, Germany (1993).

[S-13] R. Sanchez, Los Alamos National Laboratory, personal communication, April, 1997.

[T-1] O.J. Thomsen. R.Y. Chang, and C.W. Gabel, "Comparative Study of Burnable Poisons for San Onofre Units 2 and 3," *Trans. Am. Nucl. Soc.*, **68 (Part A)**, pp. 417-418 (1993).

[T-2] N.E. Todreas and M.S. Kazimi, Nuclear Systems I: Thermal Hydraulic Fundamentals, Taylor & Francis, New York, NY (1990).

[U-1] U.S. Department of Energy, "Topical Report on Actinide-Only Burnup Credit for PWR Spent Nuclear Fuel Packages," DOE/RW-0472 Rev. 0 (May 1995), Rev. 1 (May 1997).

[U-2] P. Urban, J. Schulze, and D. Bender, "Core and Fuel Design for Flexible Boiling Water Reactor Operation," *Kerntechnik*, **52**-4, pp. 238-240 (August 1988).

[W-1] Westinghouse Electric Corporation, "Westinghouse Reference Safety Analysis Report," RESAR-3 (June 1972), as amended (October 1972).

[W-2] R. Weader, Yankee Atomic Electric Company, Bolton, MA, personal communication, October, 1996.

[W-3] K. Walters, "ATRIUM™-10 Lattice and Fuel Assembly Design," ANS Proc.of the Topical Meeting - Advances in Nuclear Fuel Management II, EPRI TR-107728-V1, Vol. 1, pp. 3-1 - 3-8 (March 1997).

[W-4] G. Watford, "GE 10x10 Advanced BWR Fuel Design," ANS Proc.of the Topical Meeting - Advances in Nuclear Fuel Management II, EPRI TR-107728-V1, Vol. 1, pp. 3-17 - 3-24 (March 1997).

[W-5] K. Walters, Siemens Power Corporation, Richland, WA, personal communication, September, 1997.

[Y-1] Yankee Atomic Electric Company, input data for CASMO-3 and SIMULATE-3 for modeling Seabrook Nuclear Station Unit 1, July 1995.

[Z-1] S.G. Zimmerman and J.A. Umbarger, "Design of Aggressive Loading Patterns with X-IMAGE/SIMAN for Palo Verde Nuclear Generating Station," ANS Proc.of the Topical Meeting - Advances in Nuclear Fuel Management II, EPRI TR-107728-V2, Vol. 2, pp. 16-17 - 16-28 (March 1997).

APPENDIX A

PWR Structural Details

The figures shown here are taken from the Seabrook Station Final Safety Analysis Report [P-1]. All dimensions shown are cold dimensions and are given in units of inches.

Figure A.1: PWR Rod Cluster Control Assembly Pattern

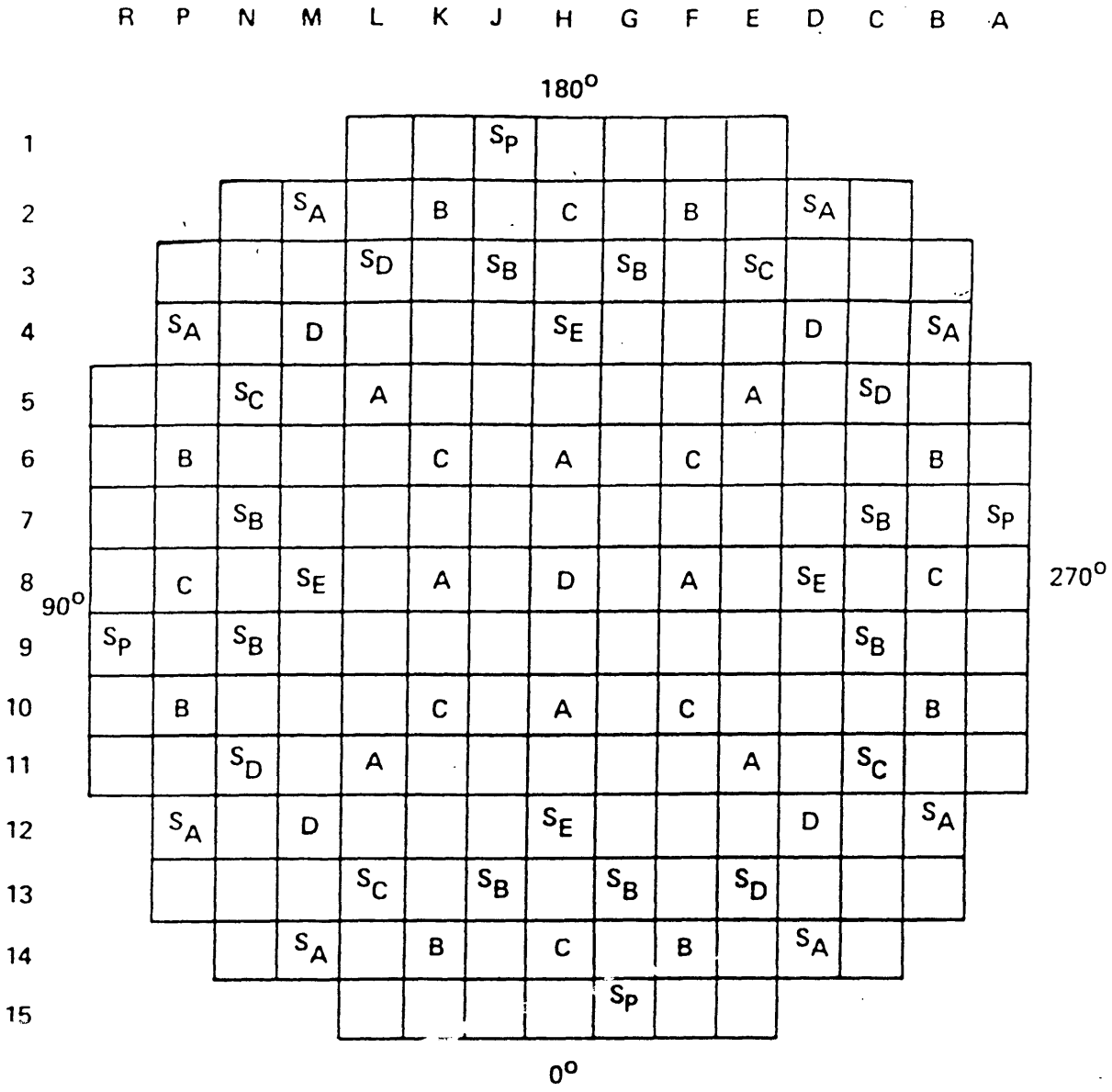

CONTROL BANK	NUMBER OF RODS
A	8
B	8
C	8
D	5
TOTAL	29

S_P – SPARE LOCATIONS

SHUTDOWN BANK	NUMBER OF RODS
SA	8
SB	8
SC	4
SD	4
SE	4
TOTAL	28

Figure A.2: PWR Fuel Assembly Cross Section - 17×17 Array

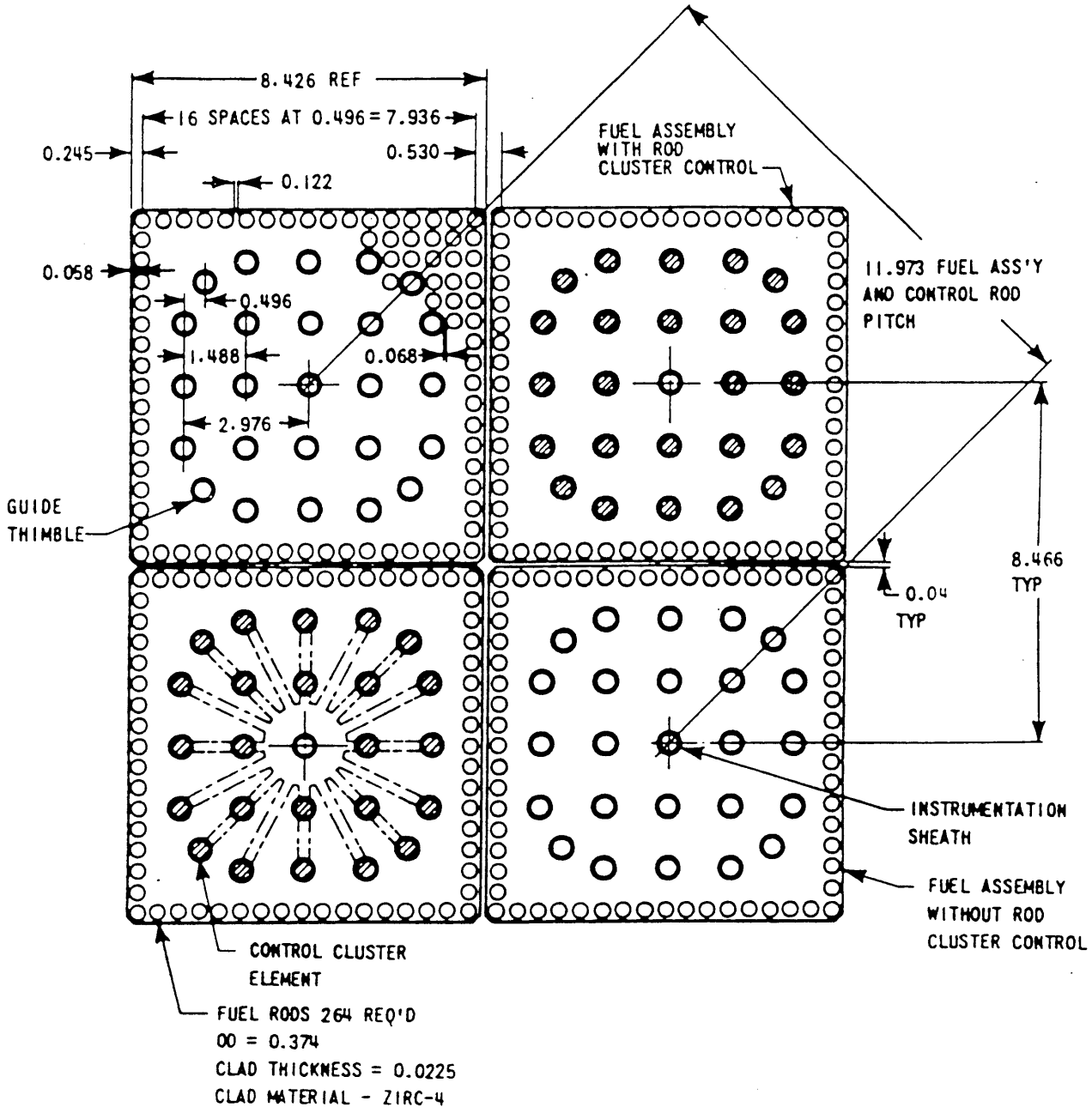

APPENDIX B

BWR Assembly Enrichment Maps

The figures contained in this appendix show the individual fuel pin enrichments in the axial enrichment zones of the BWR extended cycle core design. The three zones shown for each fuel assembly are located as follows:

- Low Enrichment Zone (LEZ): Extends from 6 in. (15.24 cm) to 60 in. (152.4 cm)
- Mid-Enrichment Zone (MEZ): Extends from 60 in. (152.4 cm) to 102 in. (259.08 cm)
- "Vanished" Fuel Rod Zone (VRZ): Extends from 102 in. (259.08 cm) to 144 in. (365.76 cm). This zone begins at the top of the PLFRs, and therefore contains only 83 fuel pins.

All distances are measured from the bottom of the core active fuel height (see Table 19).

Figure B.1: Enrichment Map for a Type 1 BWR Assembly - LEZ

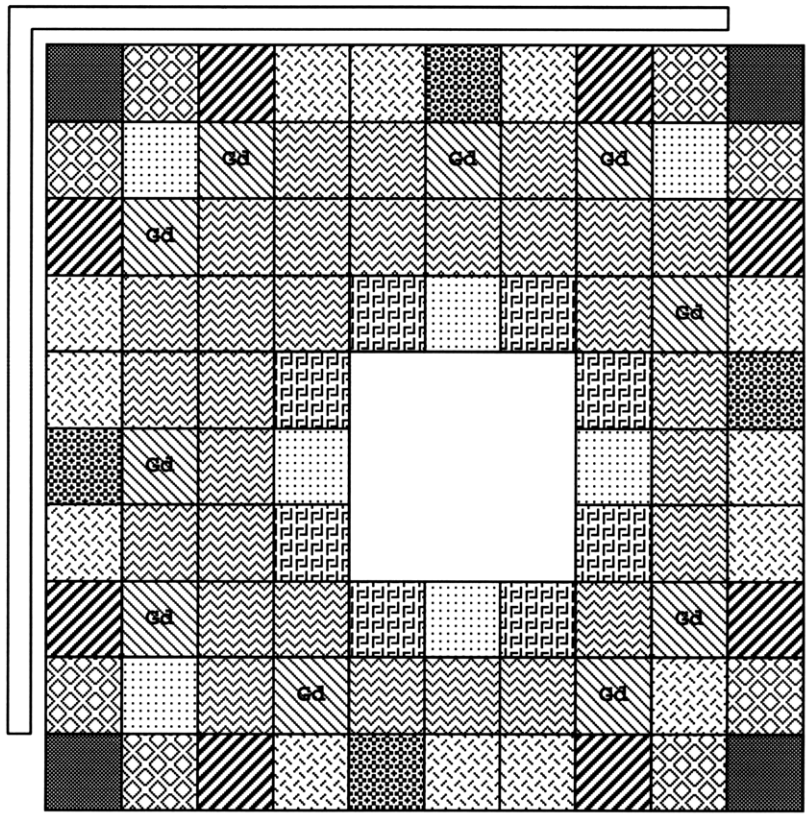

Zone Average Enrichment = $6.20^{w}/_{o}$ U^{235}

$10x12^{w}/_{o}$ Gd_2O_3 Burnable Absorber Pins

Figure B.2: Enrichment Map for a Type 1 BWR Assembly - MEZ

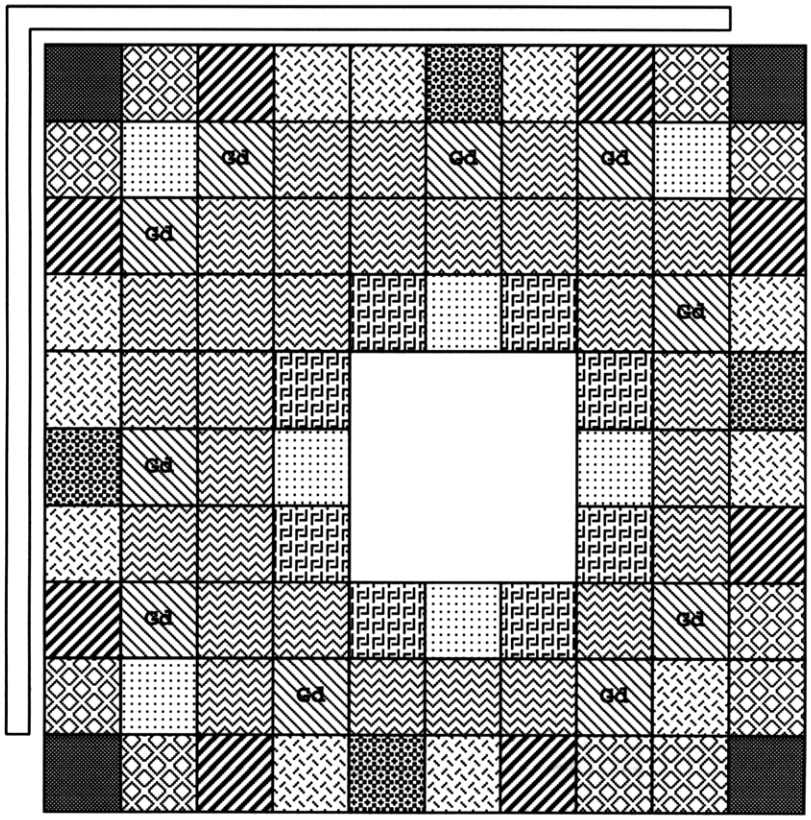

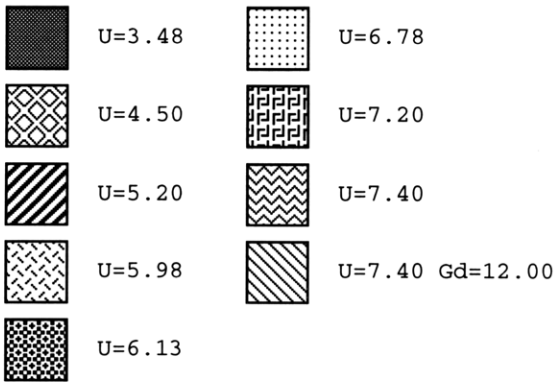

Zone Average Enrichment = 6.40 $^{w}/_{o}$ U^{235}

10x12 $^{w}/_{o}$ Gd_2O_3 Burnable Absorber Pins

Figure B.3: Enrichment Map for a Type 1 BWR Assembly - VRZ

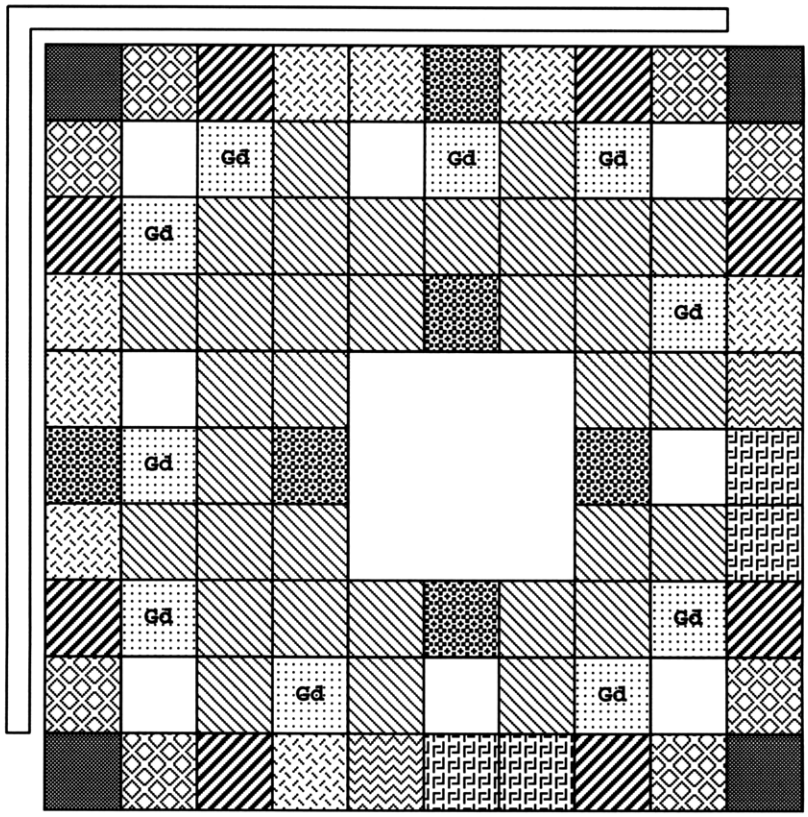

Zone Average Enrichment = $6.50^{w}/_{o}$ U^{235}

$10x12^{w}/_{o}$ Gd_2O_3 Burnable Absorber Pins

Figure B.4: Enrichment Map for a Type 2 BWR Assembly - LEZ

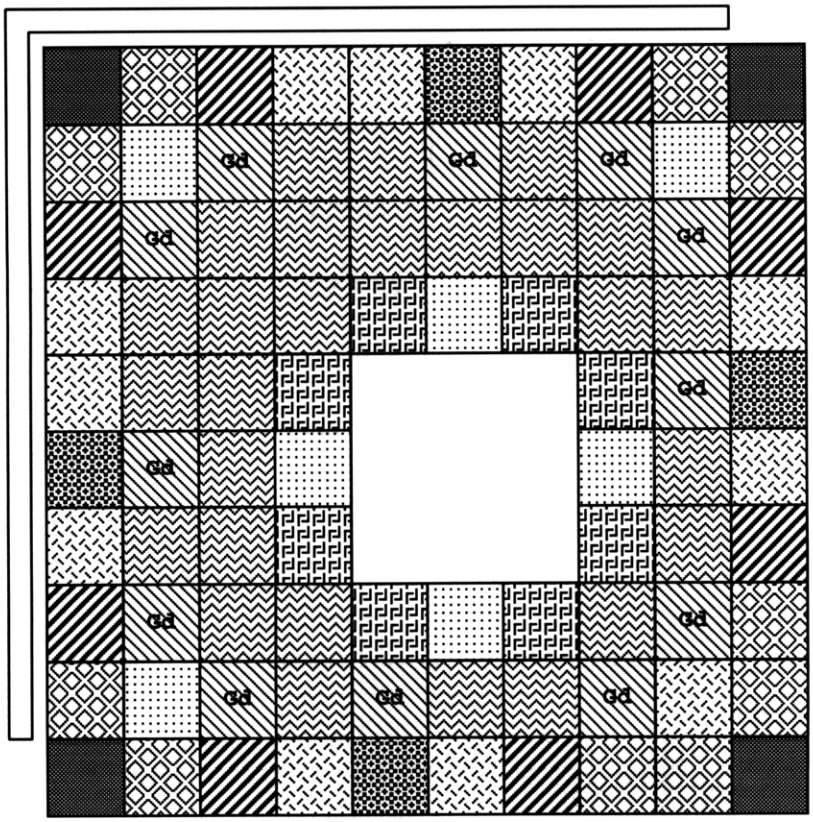

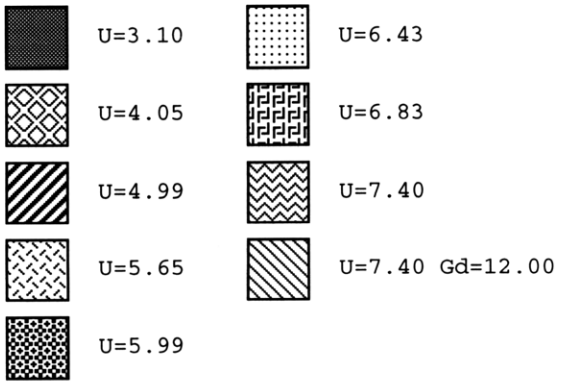

Zone Average Enrichment = $6.20^{w}/_{o}$ U^{235}

$12x12^{w}/_{o}$ Gd_2O_3 Burnable Absorber Pins

Figure B.5: Enrichment Map for a Type 2 BWR Assembly - MEZ

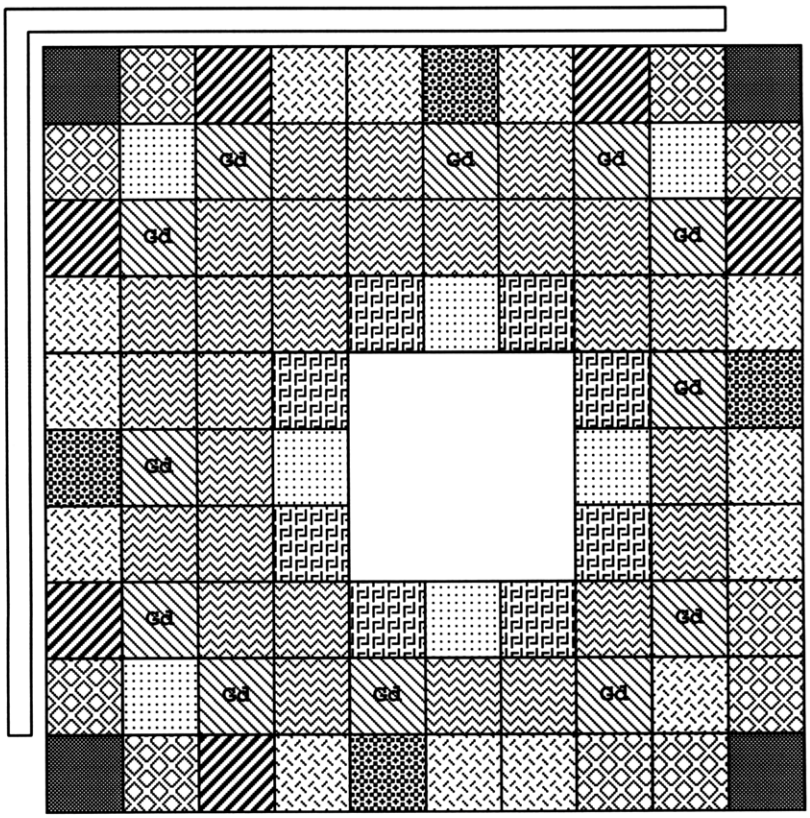

Zone Average Enrichment = $6.40^{w}/_{o}$ U^{235}

$12x12^{w}/_{o}$ Gd_2O_3 Burnable Absorber Pins

Figure B.6: Enrichment Map for a Type 2 BWR Assembly - VRZ

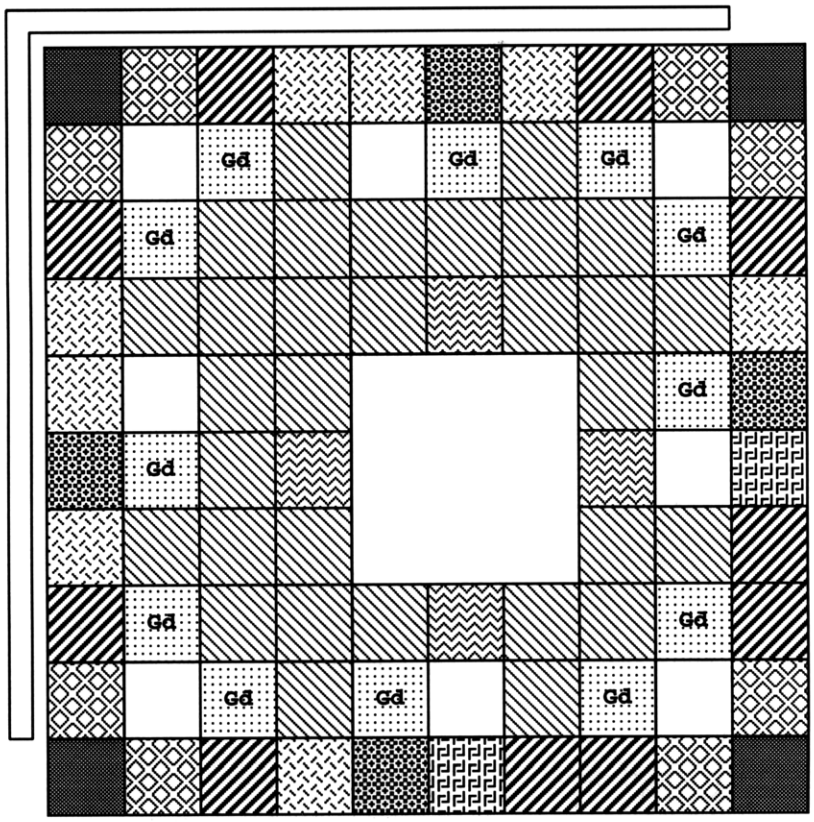

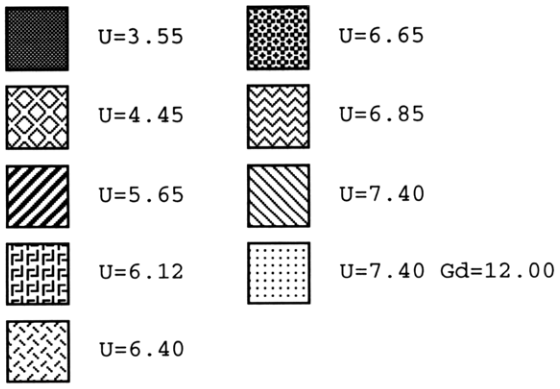

Zone Average Enrichment = $6.50^{w}/_{o}$ U^{235}

$12x12^{w}/_{o}$ Gd_2O_3 Burnable Absorber Pins

Figure B.7: Enrichment Map for a Type 3 BWR Assembly - LEZ

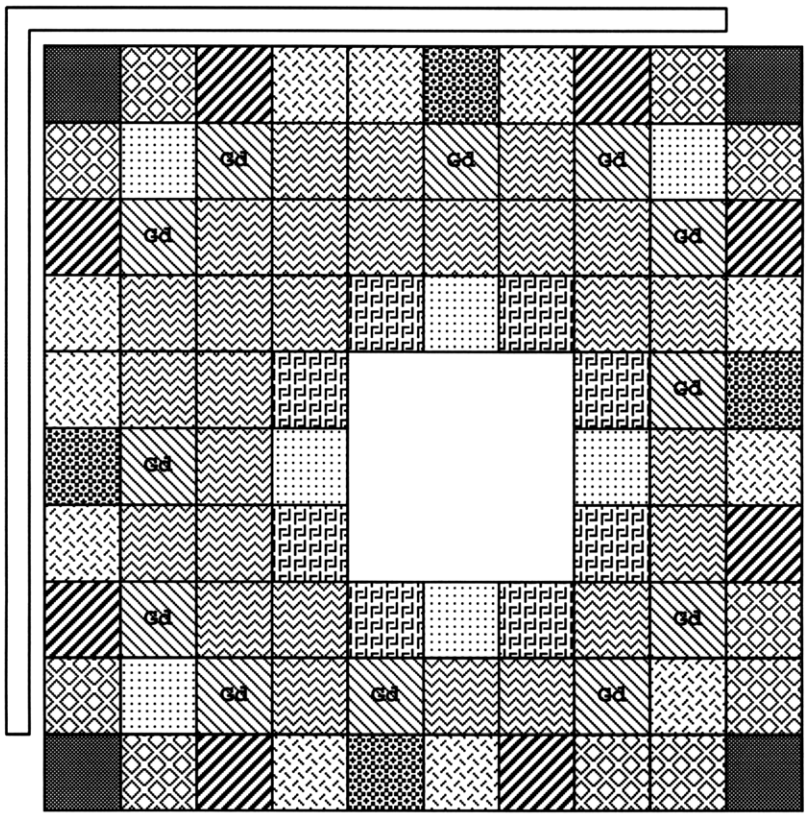

Zone Average Enrichment = $5.80^{w}/_{o}$ U^{235}

$12x12^{w}/_{o}$ Gd_2O_3 Burnable Absorber Pins

Figure B.8: Enrichment Map for a Type 3 BWR Assembly - MEZ

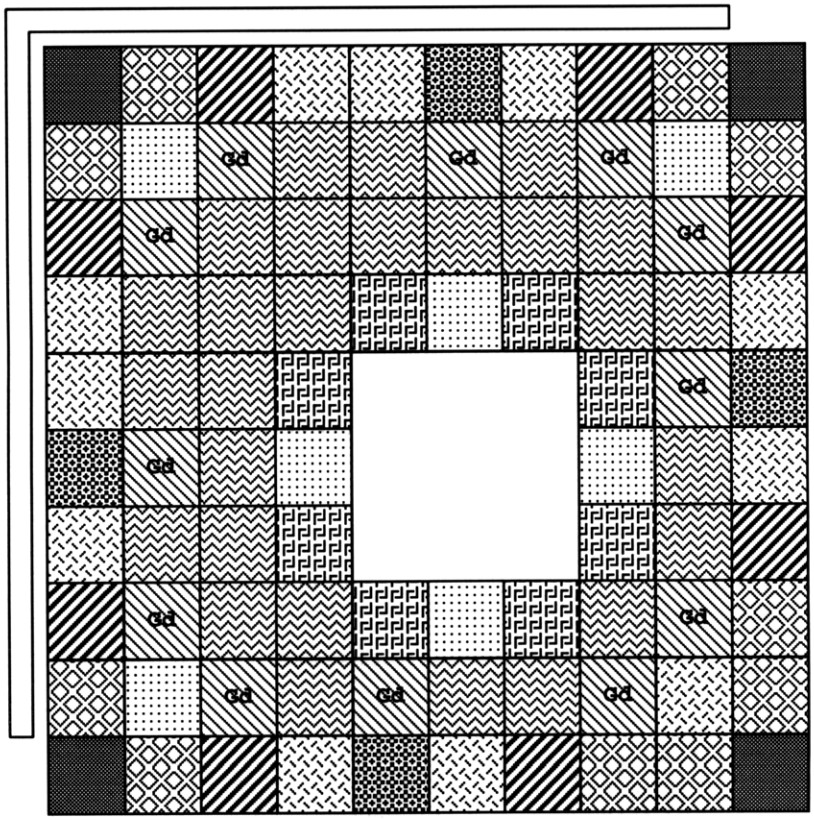

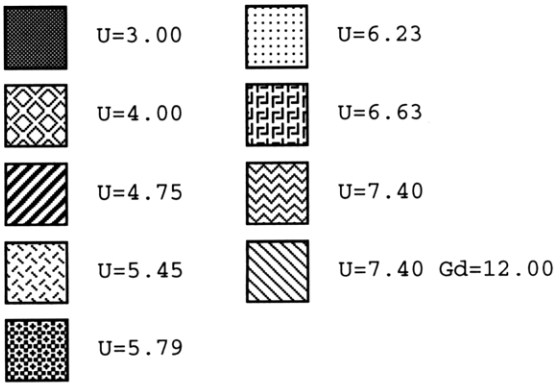

Zone Average Enrichment = $6.10^{w}/_{o}$ U^{235}

$12x12^{w}/_{o}$ Gd_2O_3 Burnable Absorber Pins

Figure B.9: Enrichment Map for a Type 3 BWR Assembly - VRZ

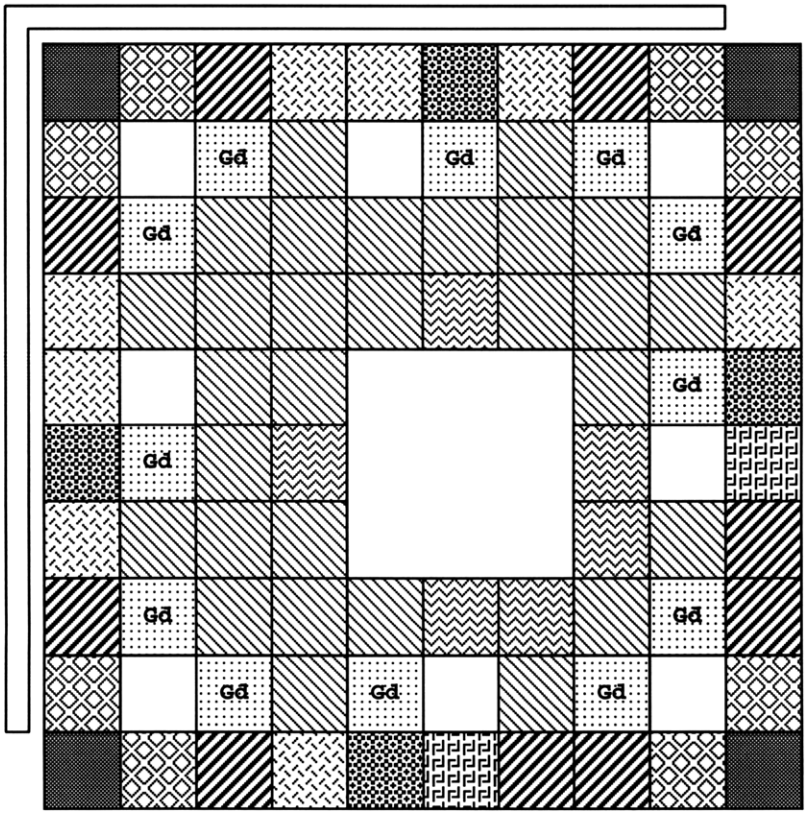

Zone Average Enrichment = $6.35^{w}/_{o}$ U^{235}

$12x12^{w}/_{o}$ Gd_2O_3 Burnable Absorber Pins

Figure B.10: Enrichment Map for a Type 4 BWR Assembly - LEZ

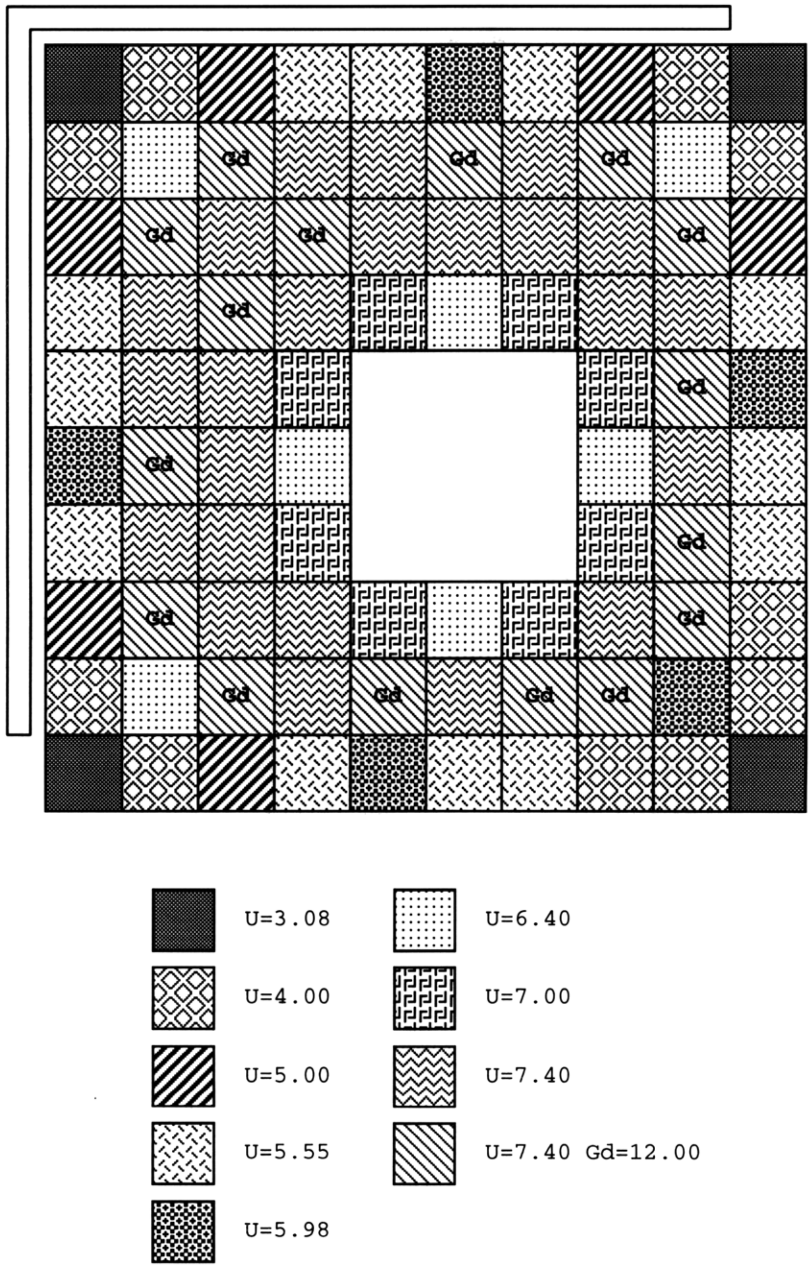

Zone Average Enrichment = 6.20 $^{w}/_{o}$ U^{235}

16x12 $^{w}/_{o}$ Gd_2O_3 Burnable Absorber Pins

Figure B.11: Enrichment Map for a Type 4 BWR Assembly - MEZ

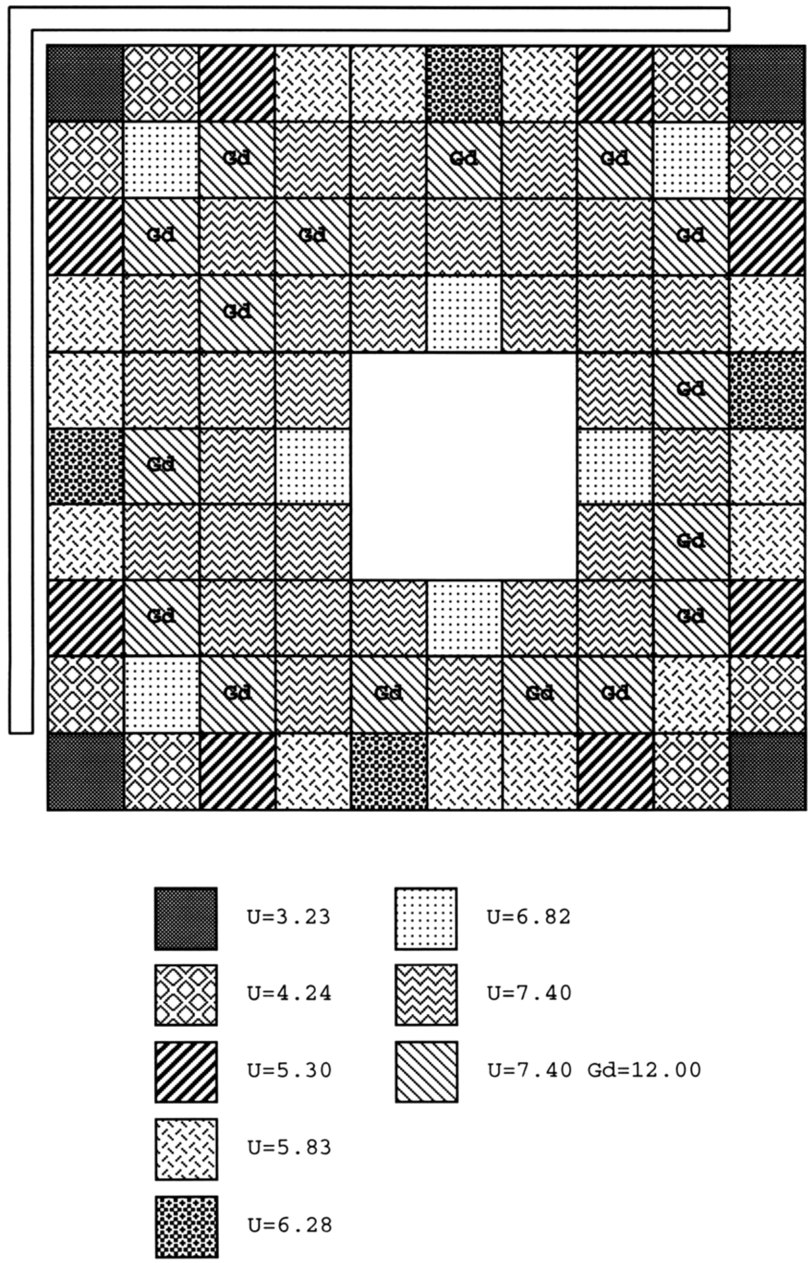

Zone Average Enrichment = 6.40$^{w}/_{o}$ U^{235}

16x12$^{w}/_{o}$ Gd_2O_3 Burnable Absorber Pins

Figure B.12: Enrichment Map for a Type 4 BWR Assembly - VRZ

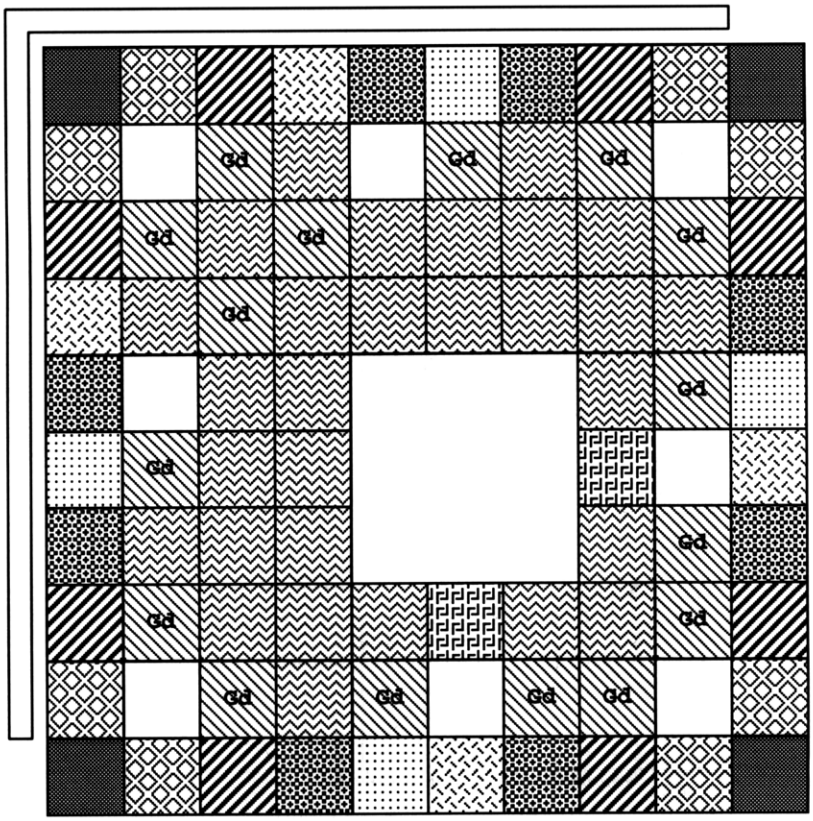

Zone Average Enrichment = 6.40 $^{w}/_{o}$ U^{235}

16x12 $^{w}/_{o}$ Gd_2O_3 Burnable Absorber Pins

Figure B.13: Enrichment Map for a Type 5 BWR Assembly - LEZ

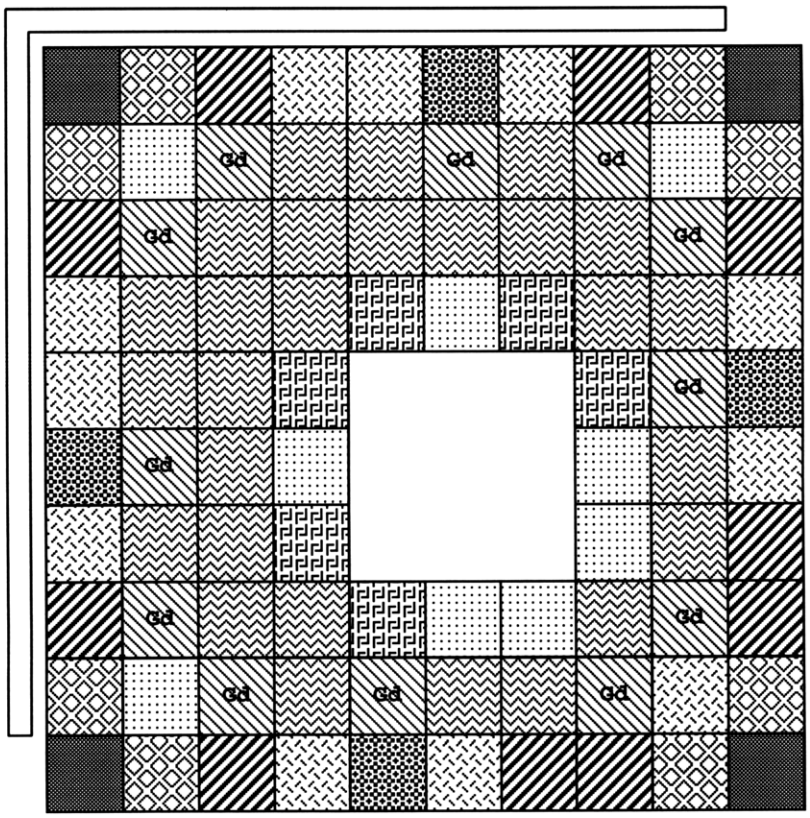

Zone Average Enrichment = 5.20$^{w}/_{o}$ U^{235}

12x12$^{w}/_{o}$ Gd_2O_3 Burnable Absorber Pins

Figure B.14: Enrichment Map for a Type 5 BWR Assembly - MEZ

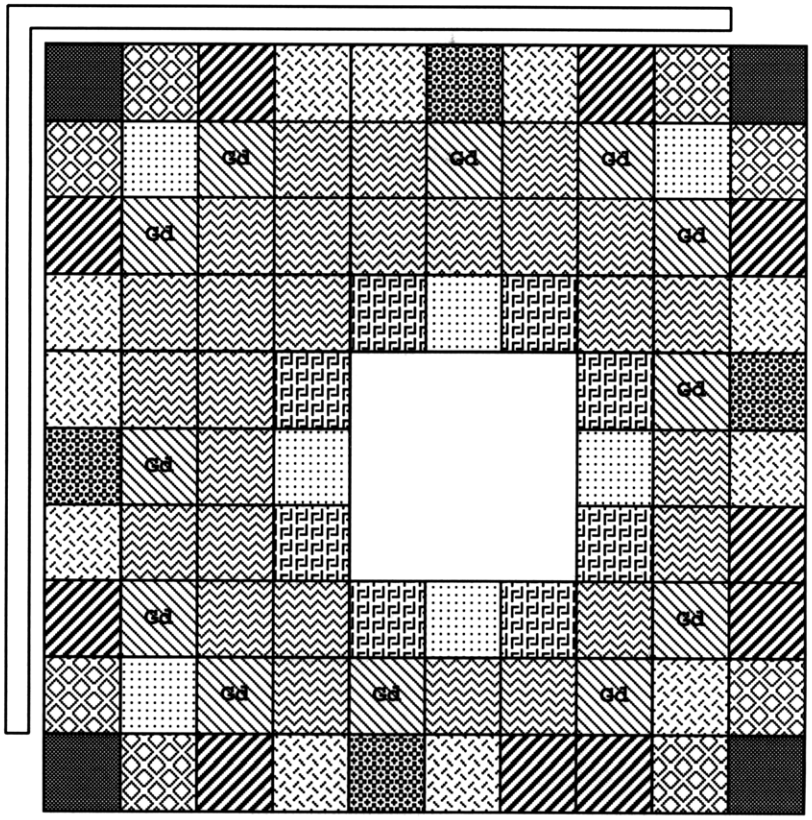

Zone Average Enrichment = $5.40^{w}/_{o}$ U^{235}

$12x12^{w}/_{o}$ Gd_2O_3 Burnable Absorber Pins

Figure B.15: Enrichment Map for a Type 5 BWR Assembly - VRZ

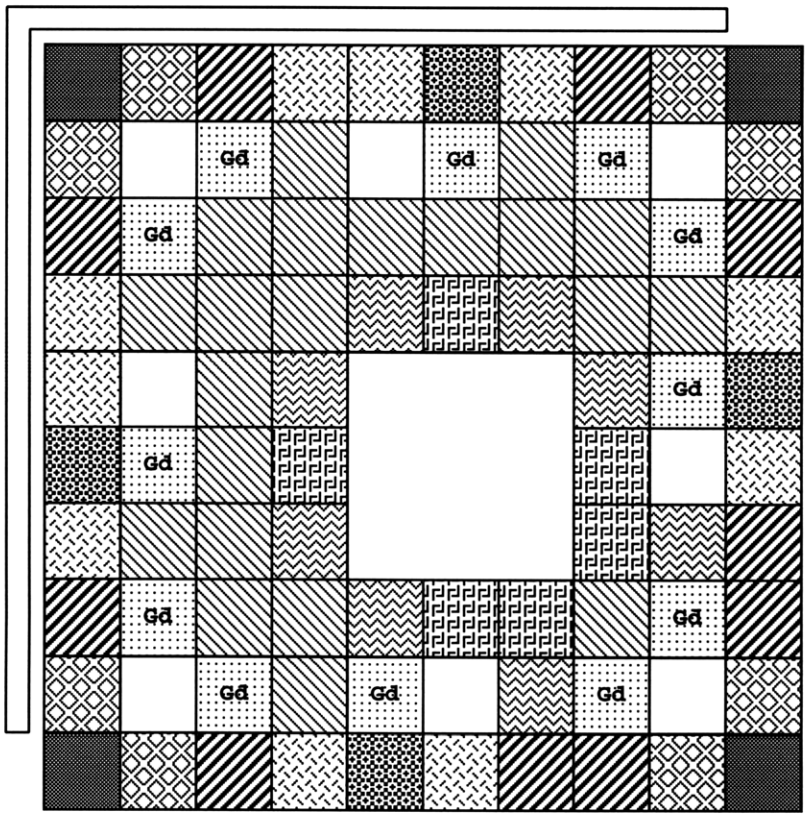

Zone Average Enrichment = 5.65 $^{w}/_{o}$ U^{235}

12x12 $^{w}/_{o}$ Gd_2O_3 Burnable Absorber Pins

Figure B.16: Enrichment Map for a Type 6 BWR Assembly - LEZ

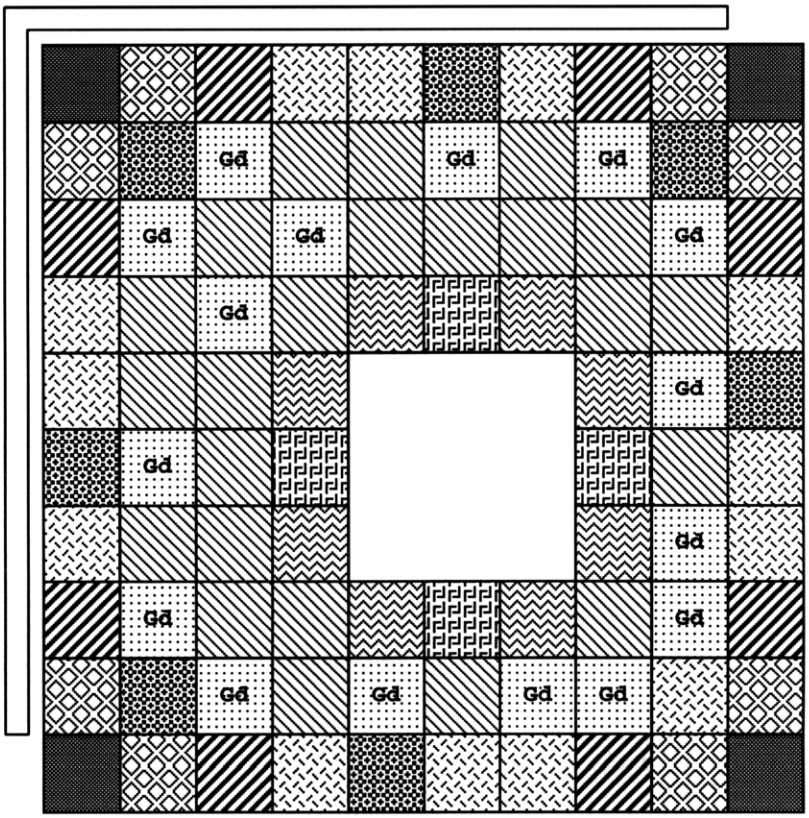

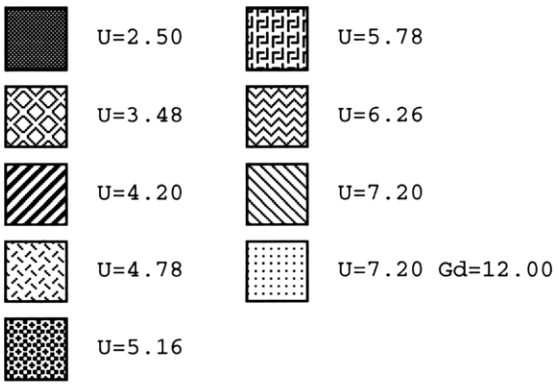

Zone Average Enrichment = $5.70^{w}/_{o}$ U^{235}

$16x12^{w}/_{o}$ Gd_2O_3 Burnable Absorber Pins

Figure B.17: Enrichment Map for a Type 6 BWR Assembly - MEZ

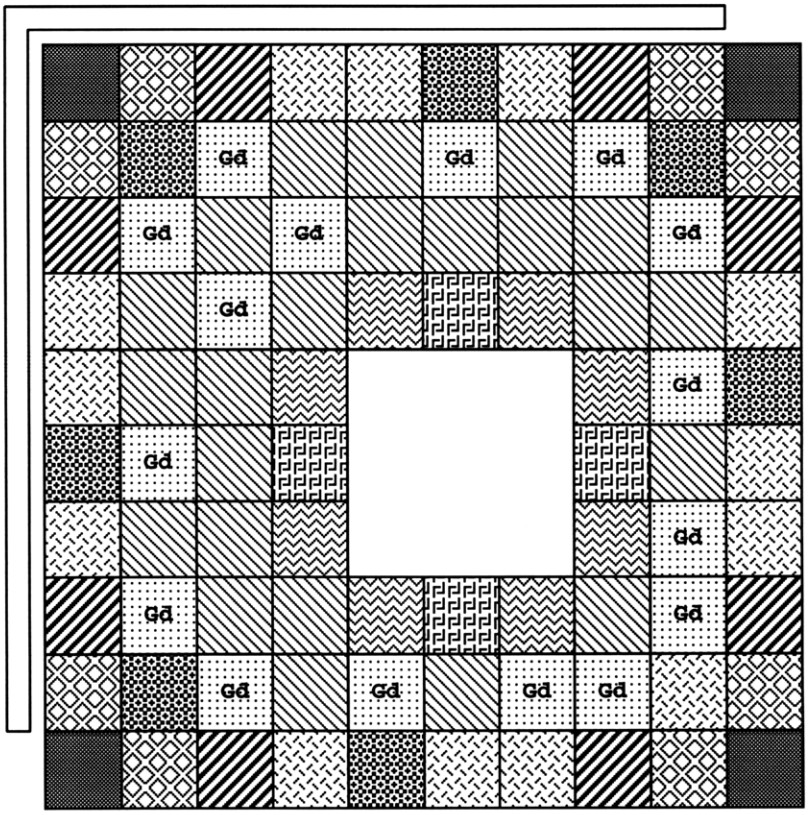

Zone Average Enrichment = 5.90 $^{w}/_{o}$ U^{235}

16x12 $^{w}/_{o}$ Gd_2O_3 Burnable Absorber Pins

Figure B.18: Enrichment Map for a Type 6 BWR Assembly - VRZ

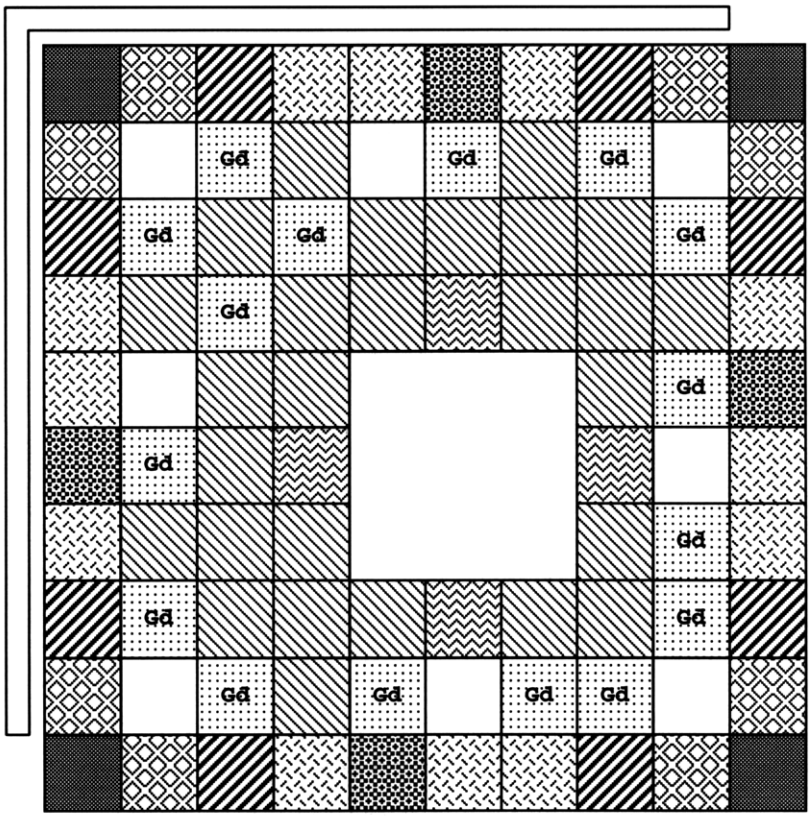

Zone Average Enrichment = $6.15^{w}/_{o}$ U^{235}

$16x12^{w}/_{o}$ Gd_2O_3 Burnable Absorber Pins

Figure B.19: Enrichment Map for a Peripheral BWR Assembly - LRZ and MEZ

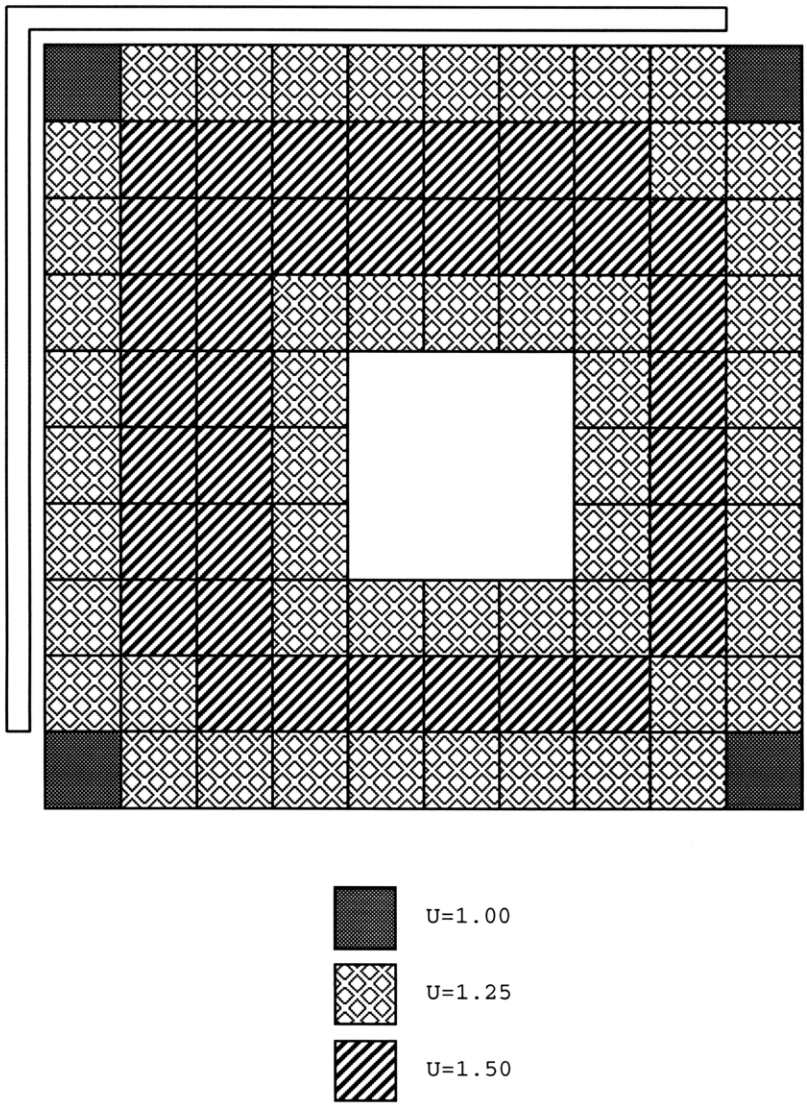

Zone Average Enrichment = $1.34^{w}/_{o}\ U^{235}$

Figure B.20: Enrichment Map for a Peripheral BWR Assembly - VRZ

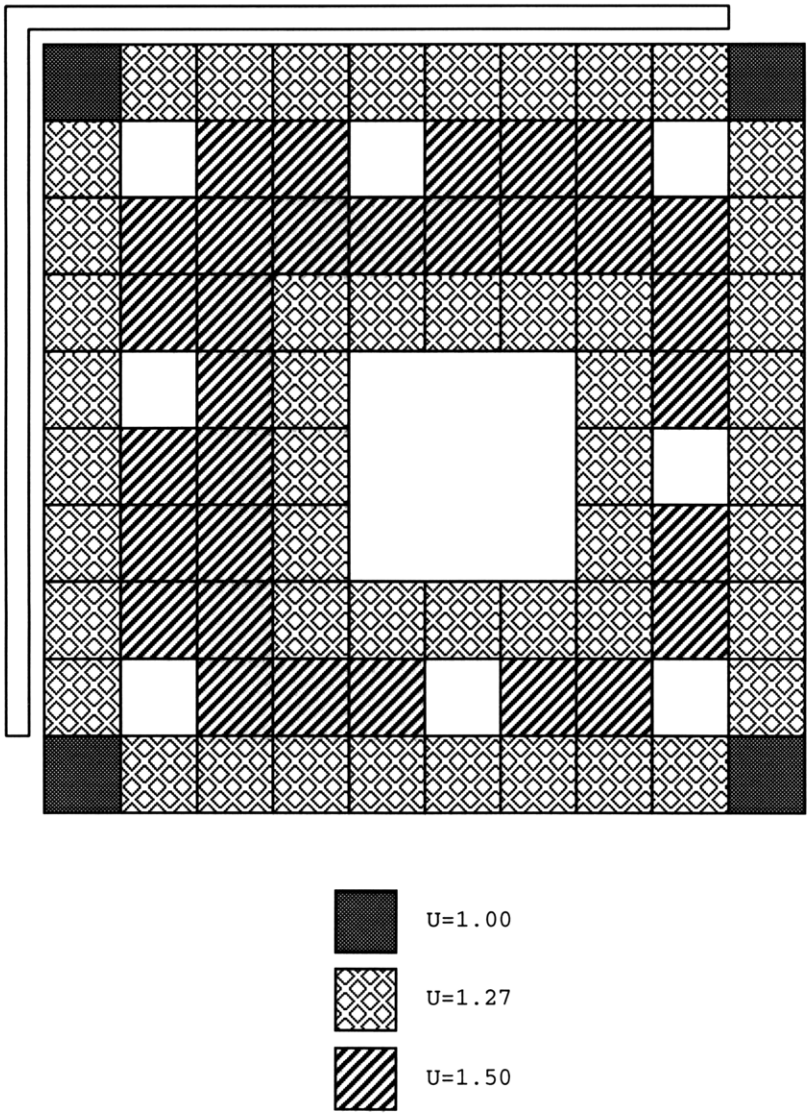

Zone Average Enrichment = $1.34^{w}/_{o}\ U^{235}$

APPENDIX C

BWR Control Rod Pattern Sequences

The figures contained in this appendix show the position of the control rods and the magnitude of core flow at each depletion point used to evaluate the BWR extended cycle core design.

Figure C.1: BWR Control Rod Sequences: 0.75 GWD/MTU to 3.00 GWD/MTU

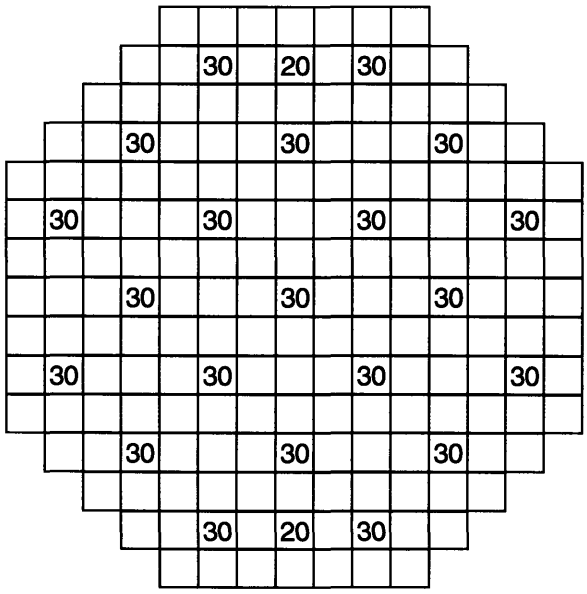

0.75 GWD/MTU
Core Flow = 100%
Rod Sequence A_2-1

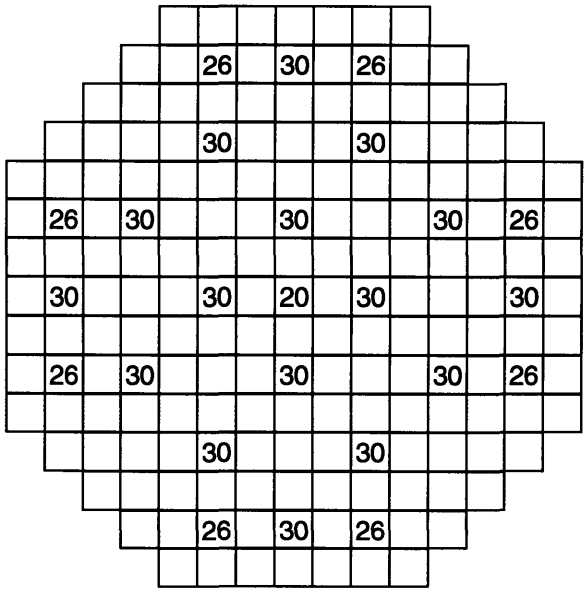

1.50 GWD/MTU
Core Flow = 100%
Rod Sequence A_2-1

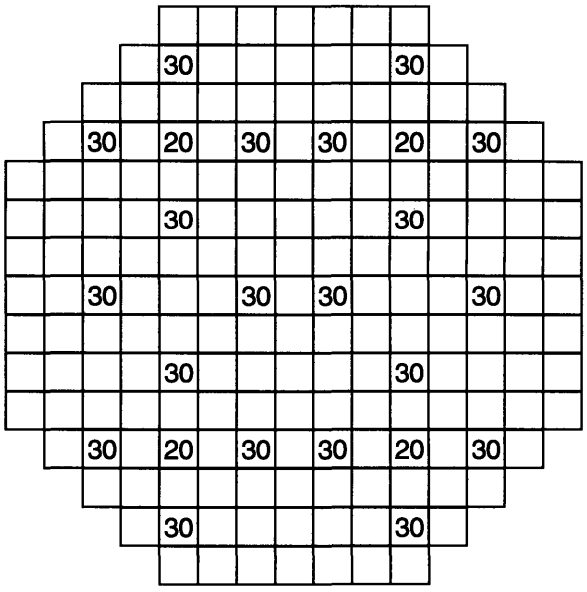

2.25 GWD/MTU
Core Flow = 100%
Rod Sequence B_2-1

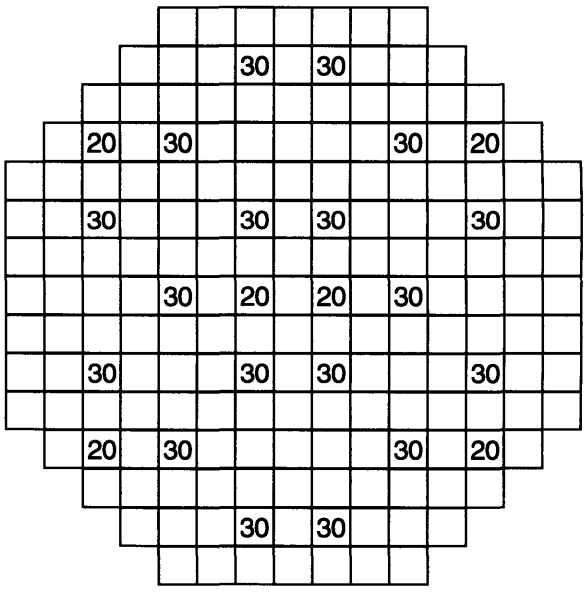

3.00 GWD/MTU
Core Flow = 100%
Rod Sequence B_2-1

[N] **N** = Number of 3 inch increments that the control blade is withdrawn from fully inserted

Figure C.2: BWR Control Rod Sequences: 3.75 GWD/MTU to 6.00 GWD/MTU

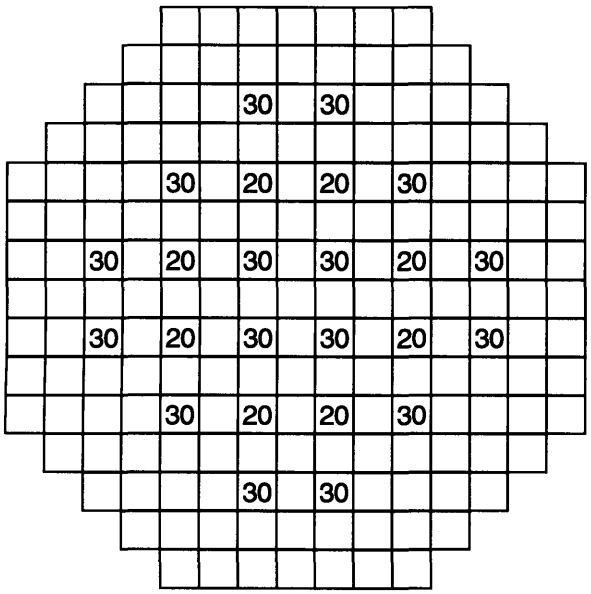

3.75 GWD/MTU
Core Flow = 100%
Rod Sequence A_1-1

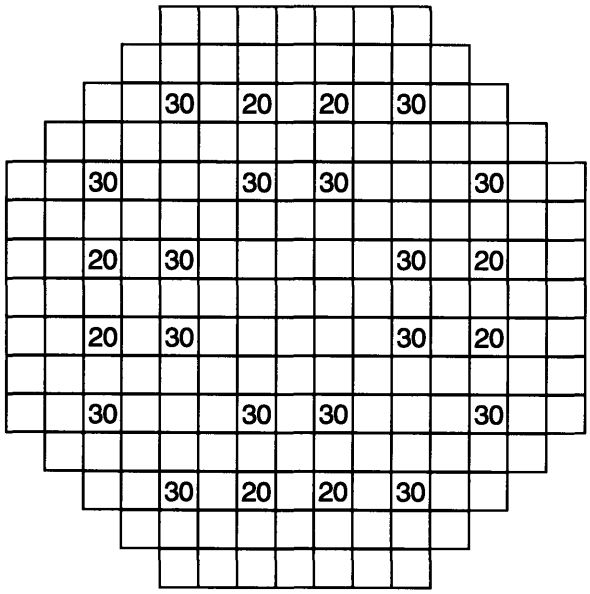

4.50 GWD/MTU
Core Flow = 100%
Rod Sequence A_1-1

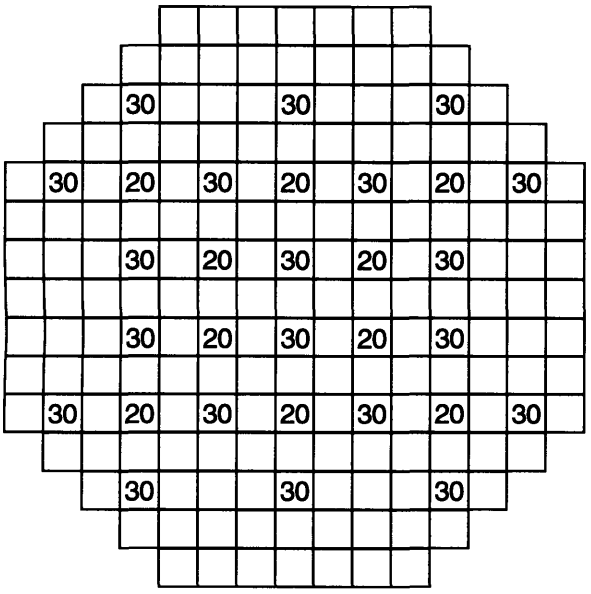

5.25 GWD/MTU
Core Flow = 100%
Rod Sequence B_1-1

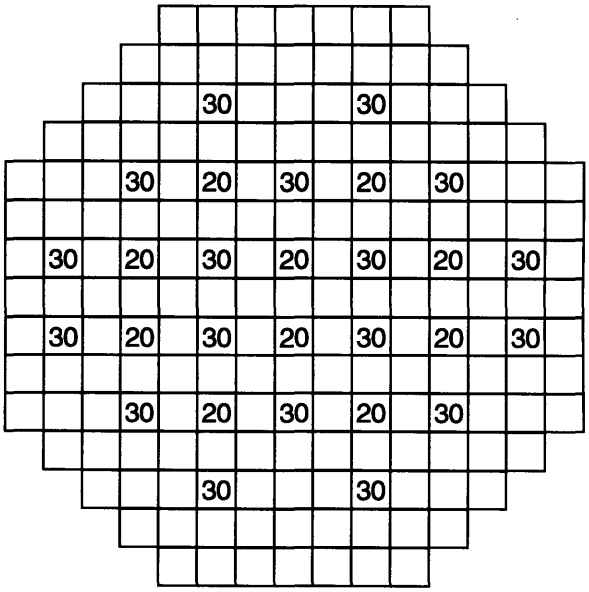

6.00 GWD/MTU
Core Flow = 100%
Rod Sequence B_1-1

N = Number of 3 inch increments that the control blade is withdrawn from fully inserted

Figure C.3: BWR Control Rod Sequences: 6.75 GWD/MTU to 9.00 GWD/MTU

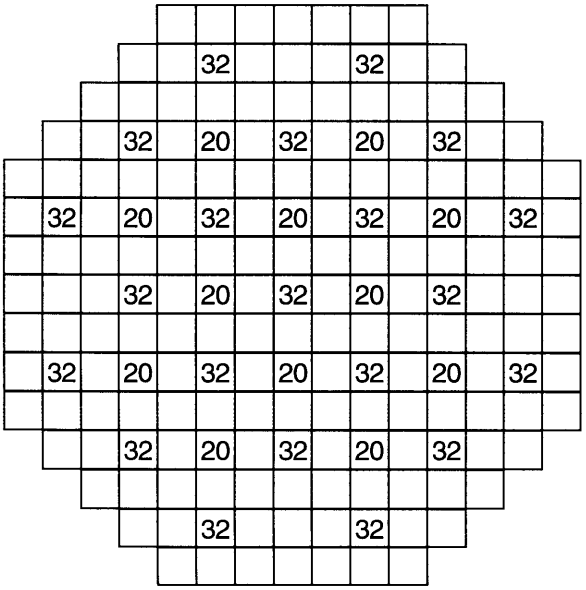

6.75 GWD/MTU
Core Flow = 100%
Rod Sequence A_2-2

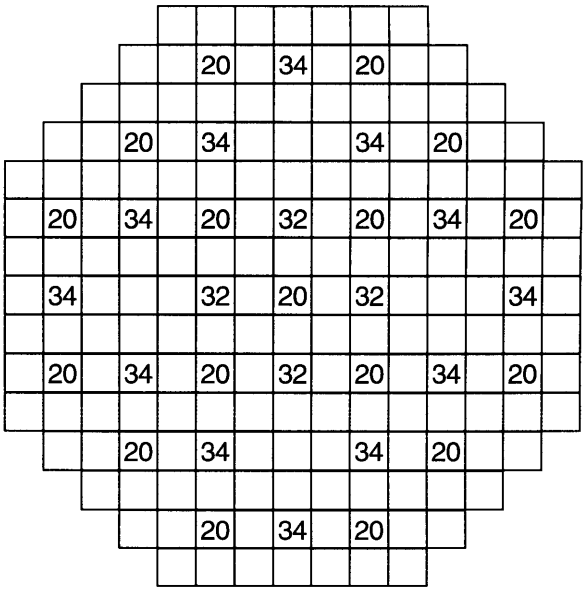

7.50 GWD/MTU
Core Flow = 100%
Rod Sequence A_2-2

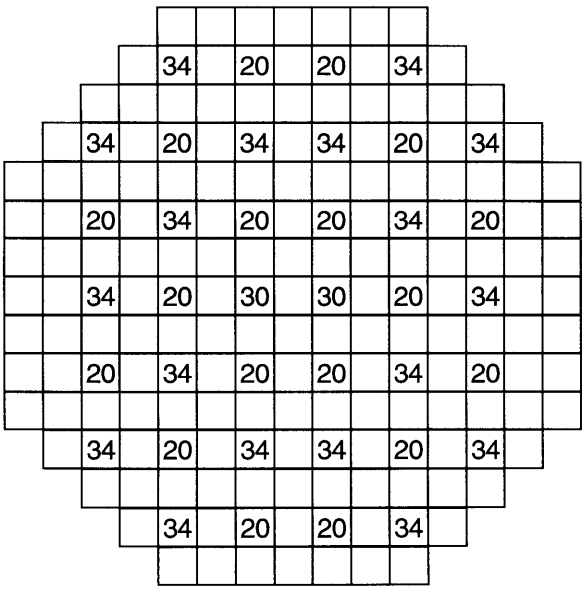

8.25 GWD/MTU
Core Flow = 98%
Rod Sequence B_2-2

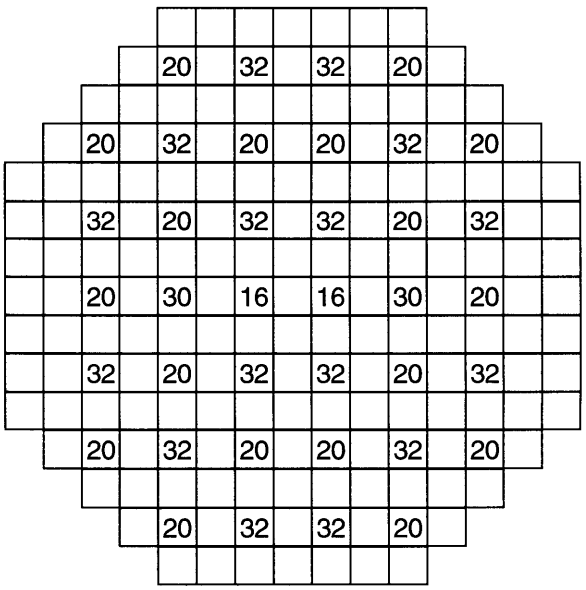

9.00 GWD/MTU
Core Flow = 100%
Rod Sequence B_2-2

N = Number of 3 inch increments that the control blade is withdrawn from fully inserted

Figure C.4: BWR Control Rod Sequences: 9.75 GWD/MTU to 12.00 GWD/MTU

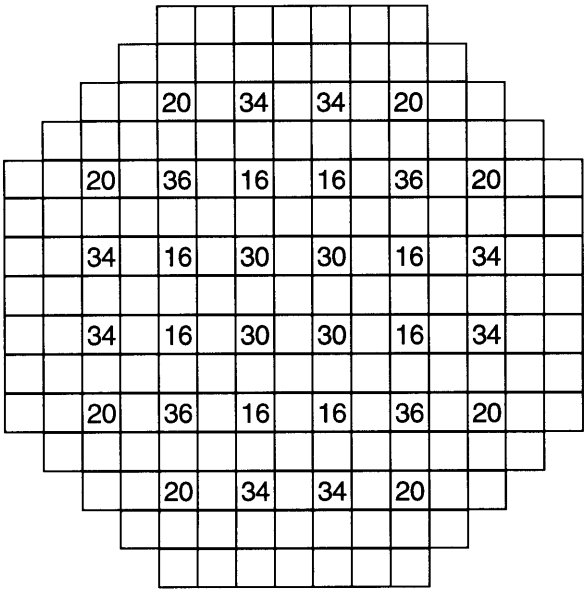

9.75 GWD/MTU
Core Flow = 94%
Rod Sequence A_1-2

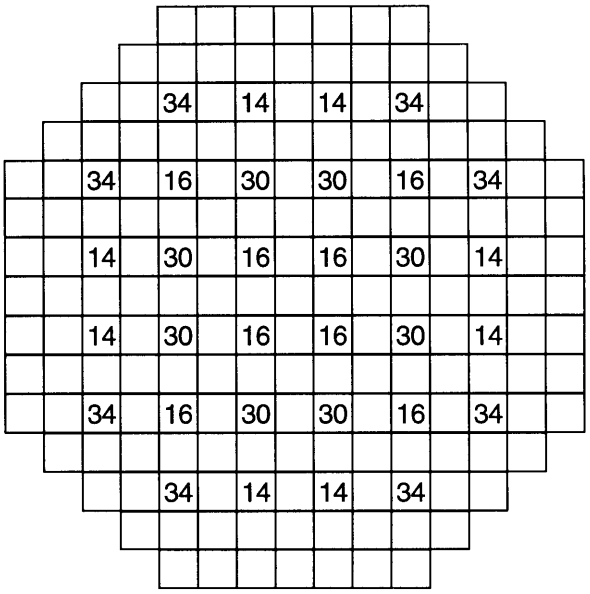

10.50 GWD/MTU
Core Flow = 100%
Rod Sequence A_1-2

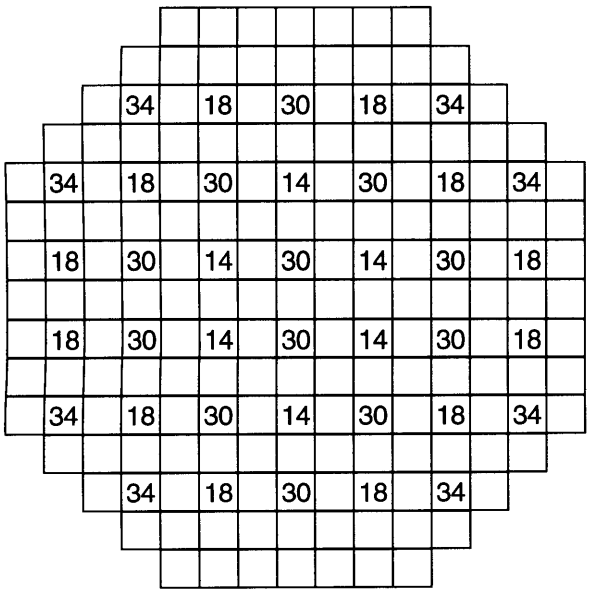

11.25 GWD/MTU
Core Flow = 94%
Rod Sequence B_1-2

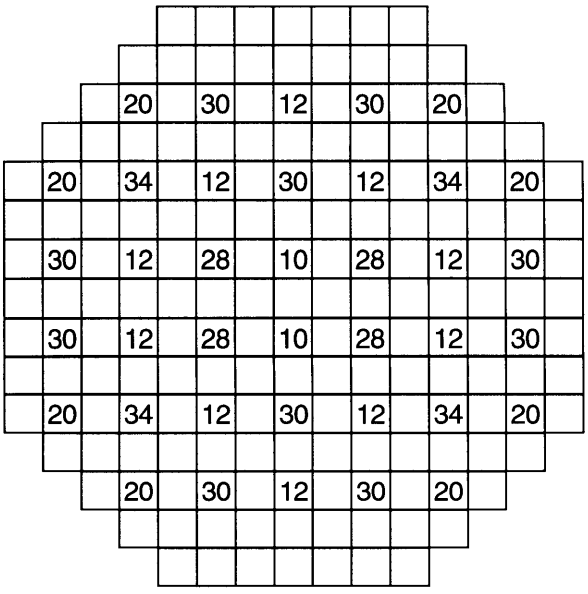

12.00 GWD/MTU
Core Flow = 100%
Rod Sequence B_1-2

N = Number of 3 inch increments that the control blade is withdrawn from fully inserted

Figure C.5: BWR Control Rod Sequences: 12.75 GWD/MTU to 15.00 GWD/MTU

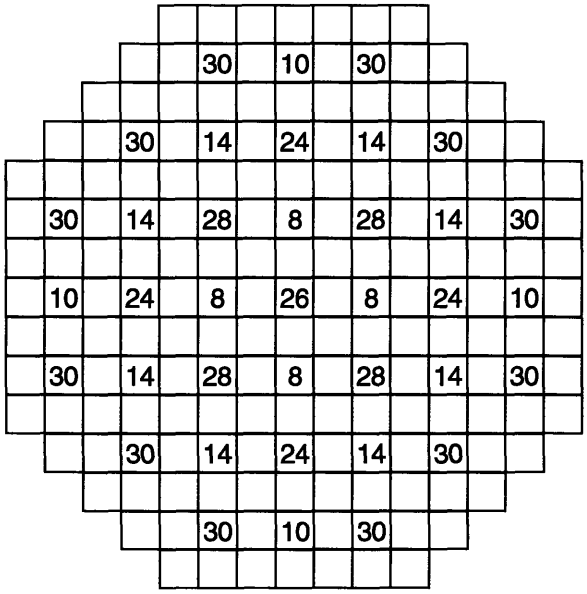

12.75 GWD/MTU
Core Flow = 100%
Rod Sequence A_2-3

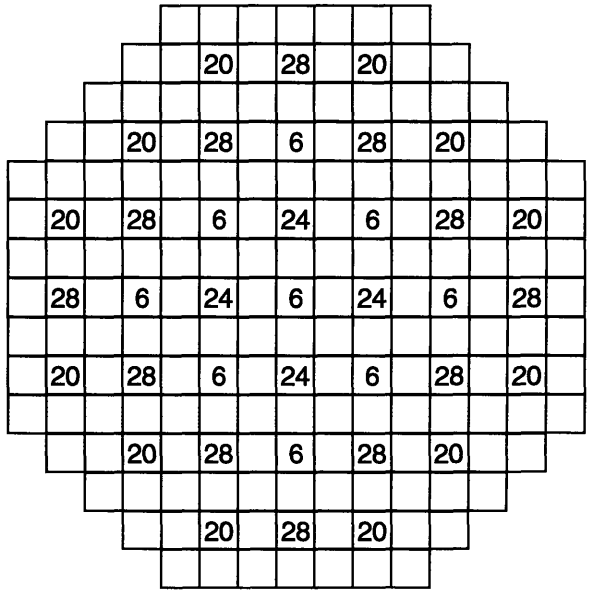

13.50 GWD/MTU
Core Flow = 100%
Rod Sequence A_2-3

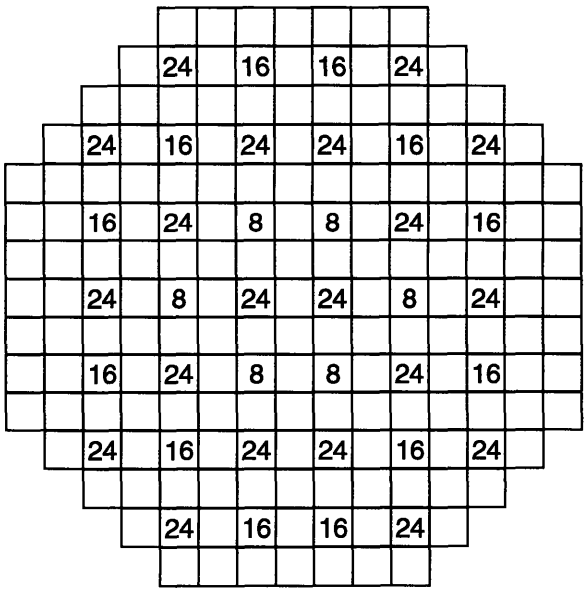

14.25 GWD/MTU
Core Flow = 100%
Rod Sequence B_2-3

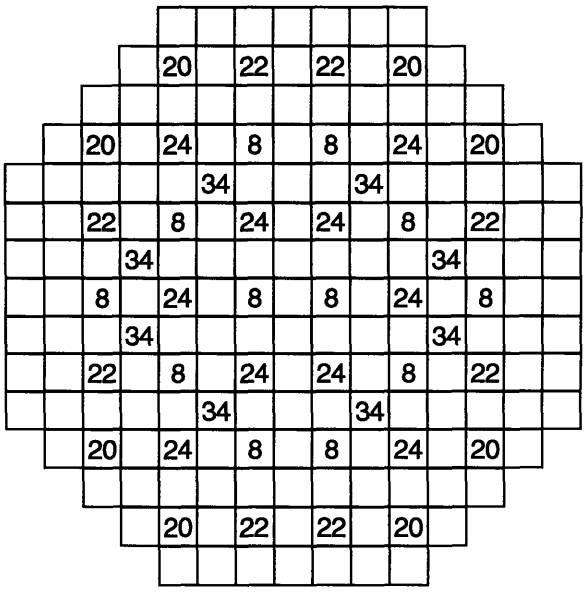

15.00 GWD/MTU
Core Flow = 100%
Rod Sequence B_2-3

[N] **N** = Number of 3 inch increments that the control blade is withdrawn from fully inserted

Figure C.6: BWR Control Rod Sequences: 15.75 GWD/MTU to 18.00 GWD/MTU

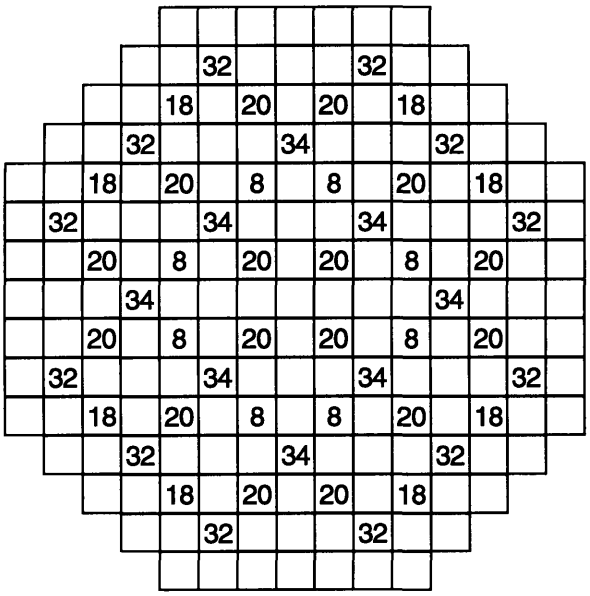

15.75 GWD/MTU
Core Flow = 90%
Rod Sequence A_1-3

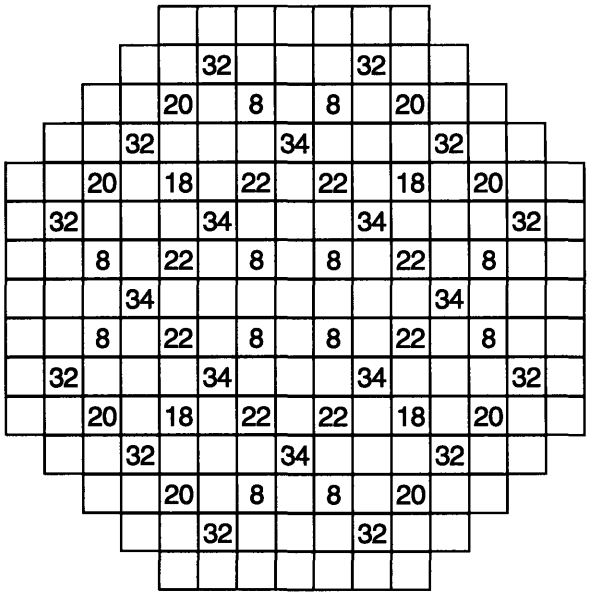

16.50 GWD/MTU
Core Flow = 82%
Rod Sequence A_1-3

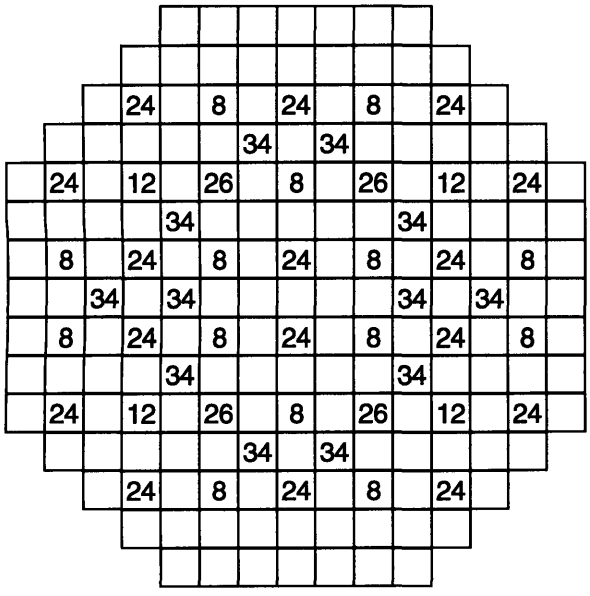

17.25 GWD/MTU
Core Flow = 82%
Rod Sequence A_1-3

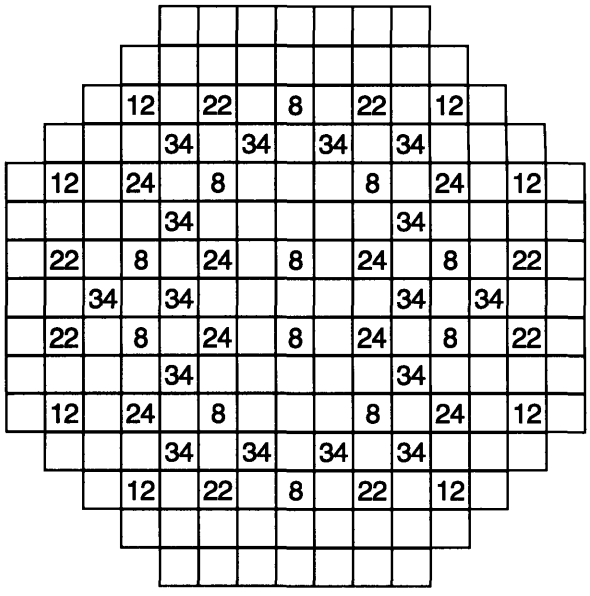

18.00 GWD/MTU
Core Flow = 80%
Rod Sequence B_1-3

[N] N = Number of 3 inch increments that the control blade is withdrawn from fully inserted

Figure C.7: BWR Control Rod Sequences: 18.75 GWD/MTU to 21.00 GWD/MTU

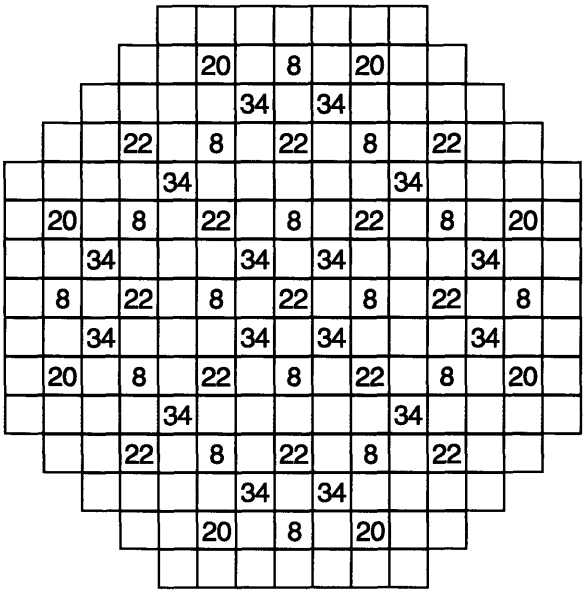

18.75 GWD/MTU
Core Flow = 80%
Rod Sequence A_2-4

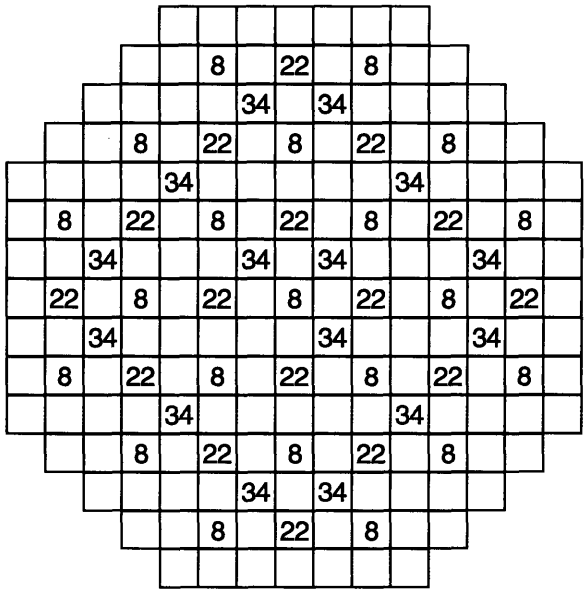

19.50 GWD/MTU
Core Flow = 80%
Rod Sequence A_2-4

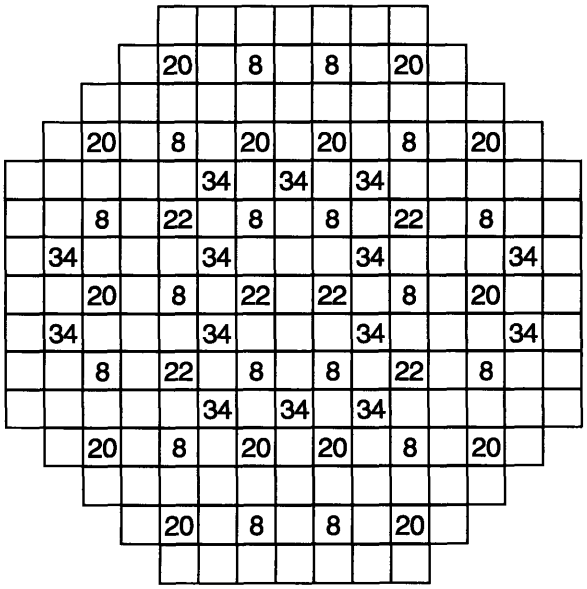

20.25 GWD/MTU
Core Flow = 80%
Rod Sequence B_2-4

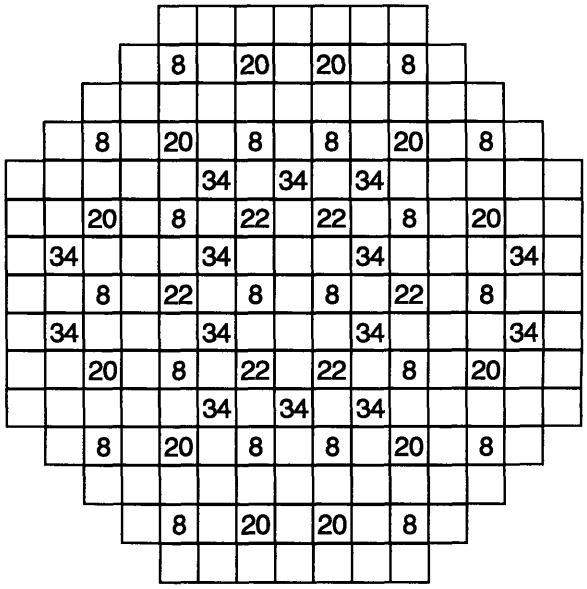

21.00 GWD/MTU
Core Flow = 80%
Rod Sequence B_2-4

N = Number of 3 inch increments that the control blade is withdrawn from fully inserted

Figure C.8: BWR Control Rod Sequences: 21.75 GWD/MTU to 24.00 GWD/MTU

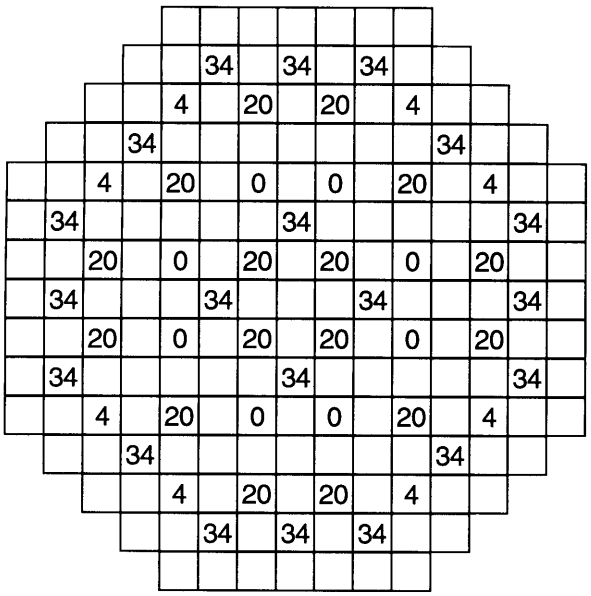

21.75 GWD/MTU
Core Flow = 80%
Rod Sequence A_1-4

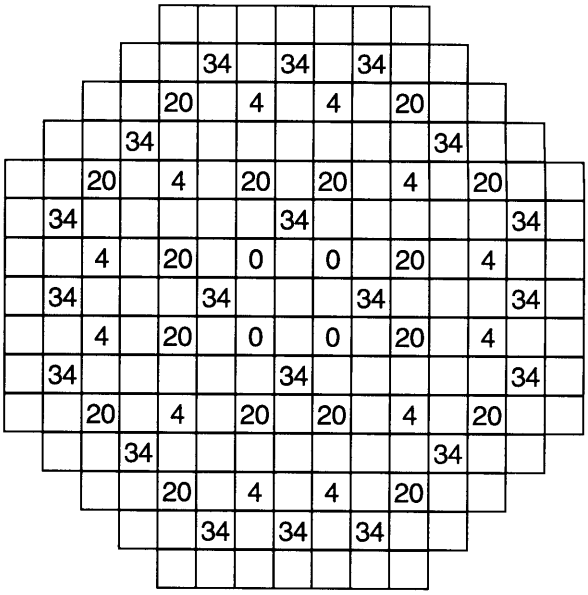

22.50 GWD/MTU
Core Flow = 80%
Rod Sequence A_1-4

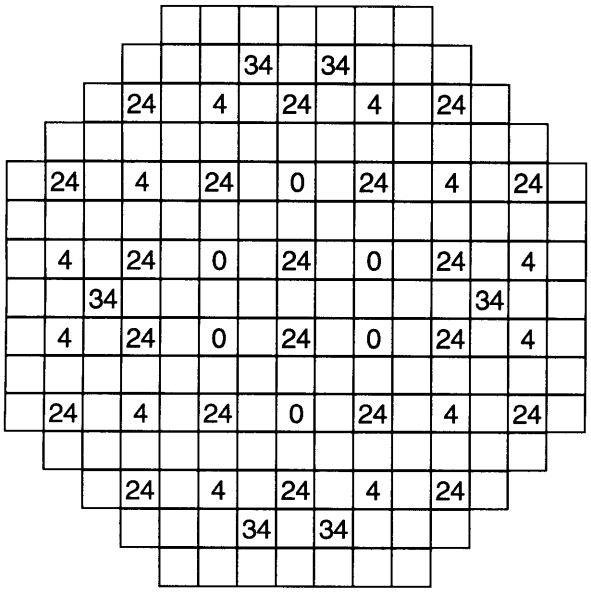

23.25 GWD/MTU
Core Flow = 80%
Rod Sequence B_1-4

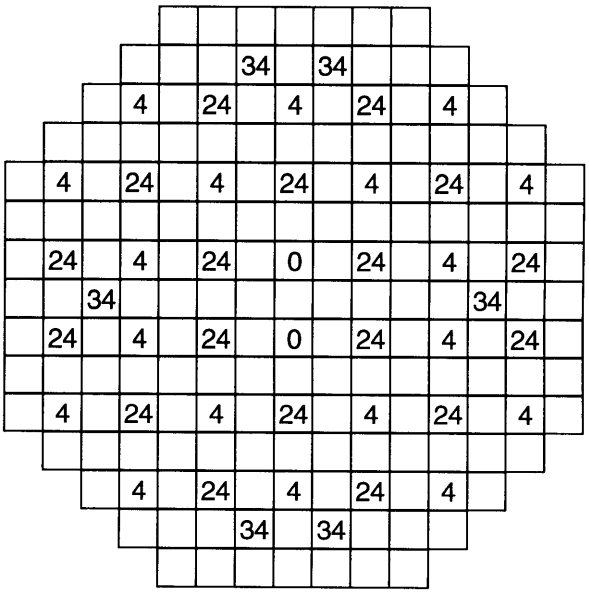

24.00 GWD/MTU
Core Flow = 80%
Rod Sequence B_1-4

N **N** = Number of 3 inch increments that the control blade is withdrawn from fully inserted

Figure C.9: BWR Control Rod Sequences: 24.75 GWD/MTU to 27.00 GWD/MTU

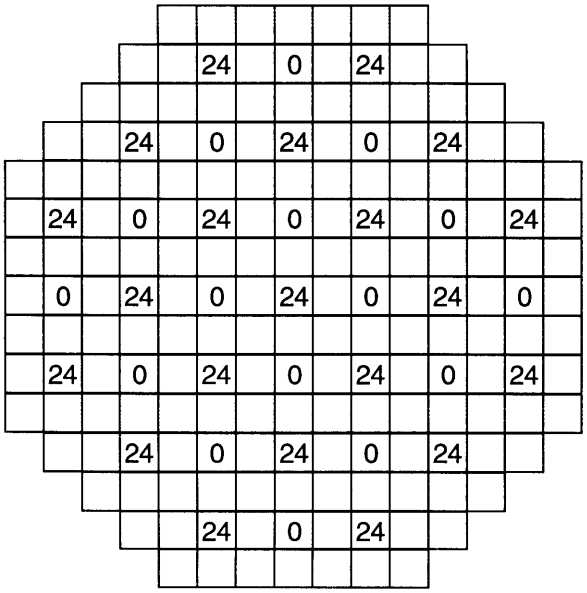

24.75 GWD/MTU
Core Flow = 80%
Rod Sequence A_2-5

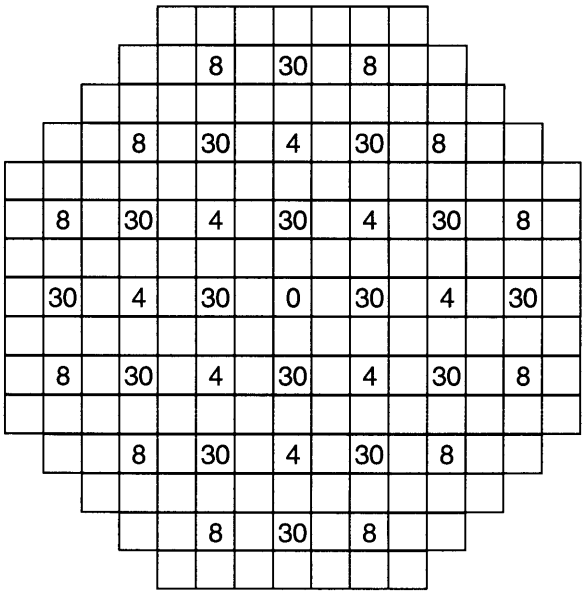

25.50 GWD/MTU
Core Flow = 80%
Rod Sequence A_2-5

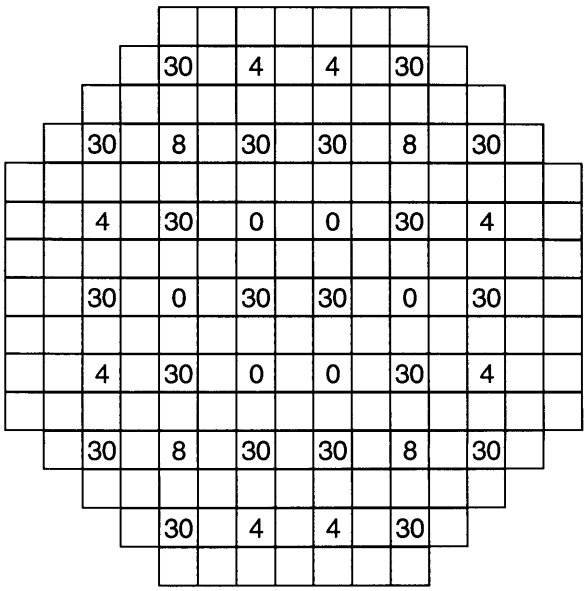

26.25 GWD/MTU
Core Flow = 80%
Rod Sequence B_2-5

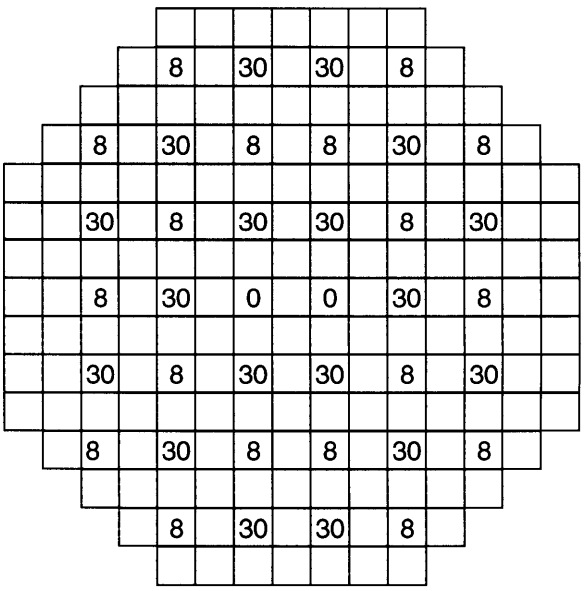

27.00 GWD/MTU
Core Flow = 80%
Rod Sequence B_2-5

N **N** = Number of 3 inch increments that the control blade is withdrawn from fully inserted

Figure C.10: BWR Control Rod Sequences: 27.75 GWD/MTU to 30.00 GWD/MTU

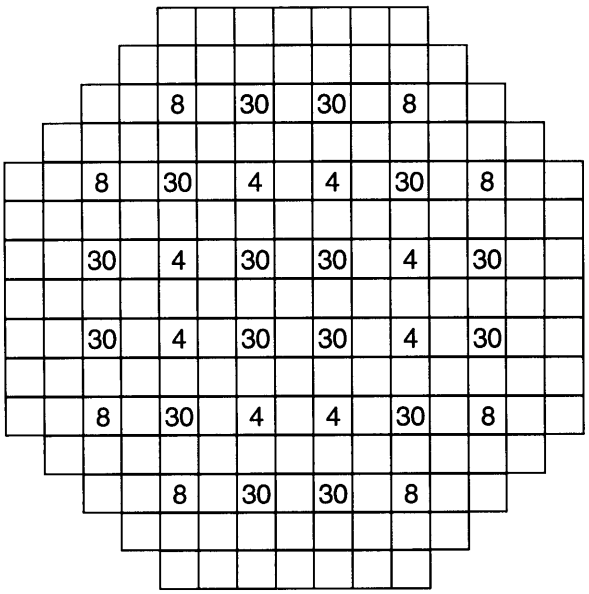

27.75 GWD/MTU
Core Flow = 80%
Rod Sequence A_1-5

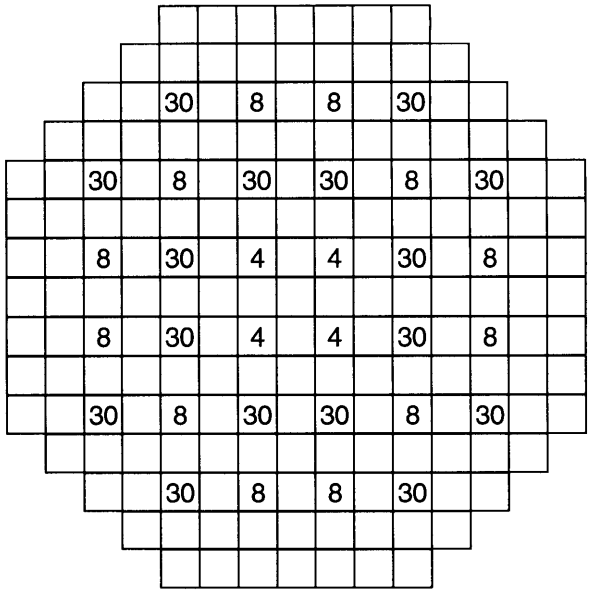

28.50 GWD/MTU
Core Flow = 84%
Rod Sequence A_1-5

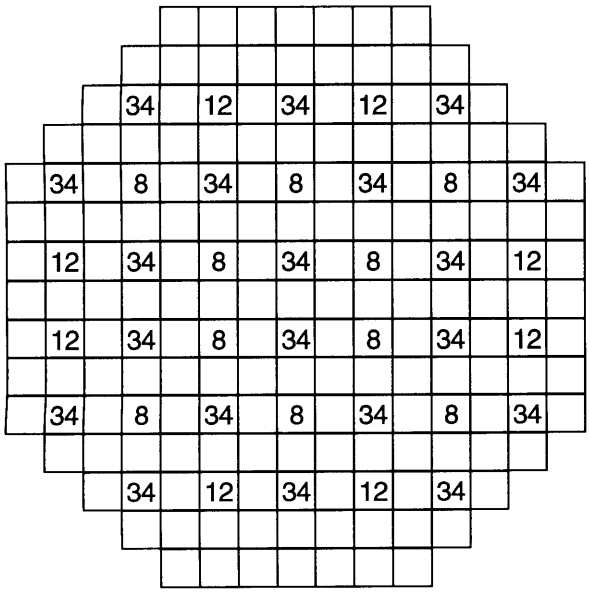

29.25 GWD/MTU
Core Flow = 80%
Rod Sequence B_1-5

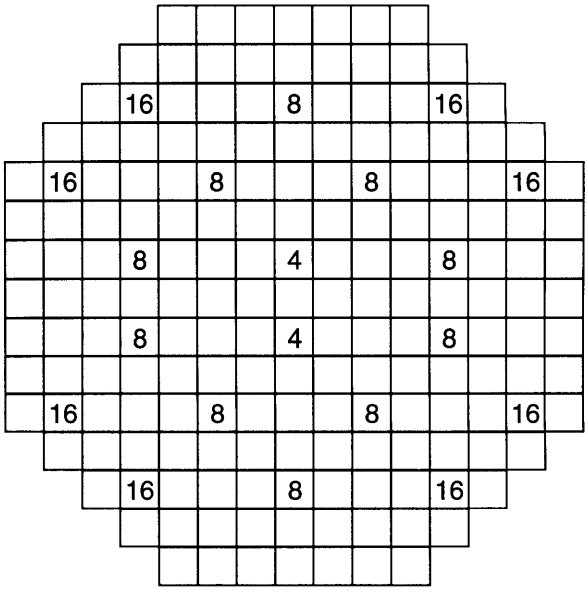

30.00 GWD/MTU
Core Flow = 94%
Rod Sequence B_1-5

[N] **N** = Number of 3 inch increments that the control blade is withdrawn from fully inserted

Figure C.11: BWR Control Rod Sequences: 30.75 GWD/MTU to 33.00 GWD/MTU

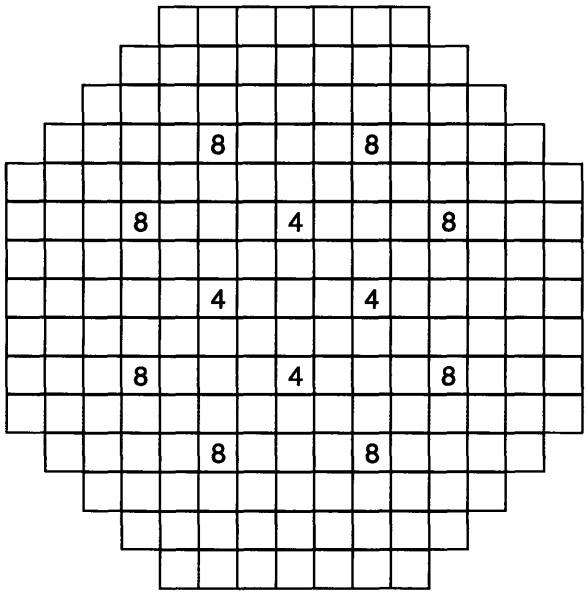

30.75 GWD/MTU
Core Flow = 90%
Rod Sequence A_2-6

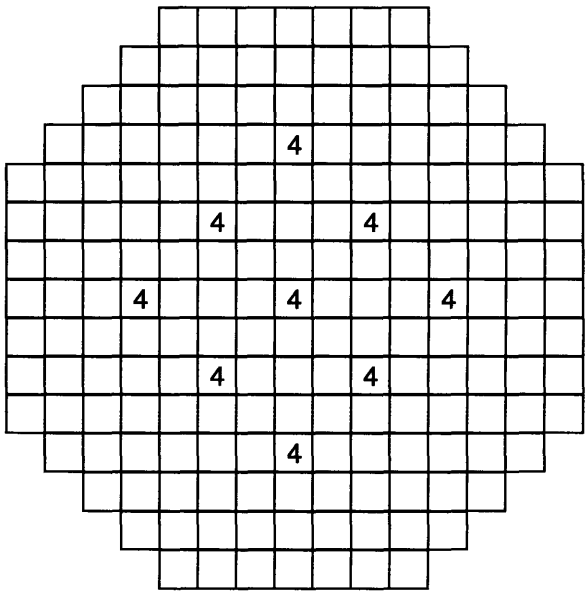

31.50 GWD/MTU
Core Flow = 94%
Rod Sequence A_2-6

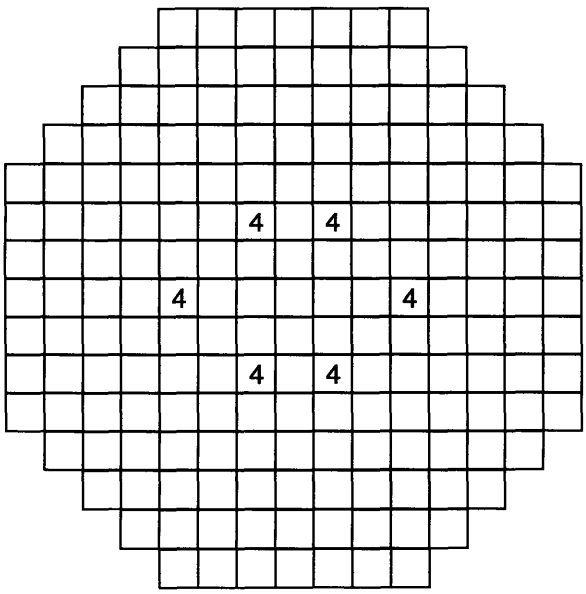

32.25 GWD/MTU
Core Flow = 90%
Rod Sequence B_2-6

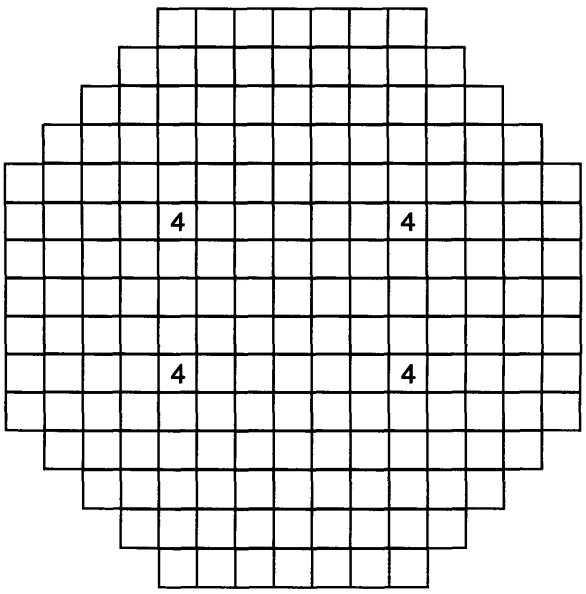

33.00 GWD/MTU
Core Flow = 90%
Rod Sequence B_2-6

[N] N = Number of 3 inch increments that the control blade is withdrawn from fully inserted

Figure C.12: BWR Control Rod Sequences: 33.75 GWD/MTU to 34.20 GWD/MTU

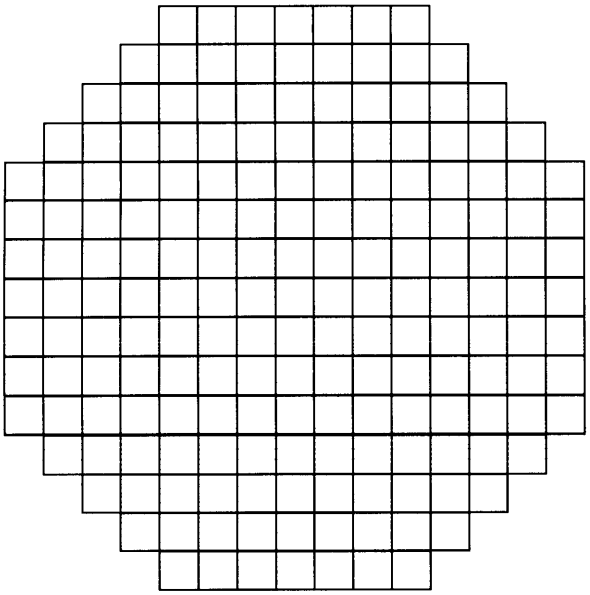

33.75 GWD/MTU
Core Flow = 82%
All Rods Withdrawn

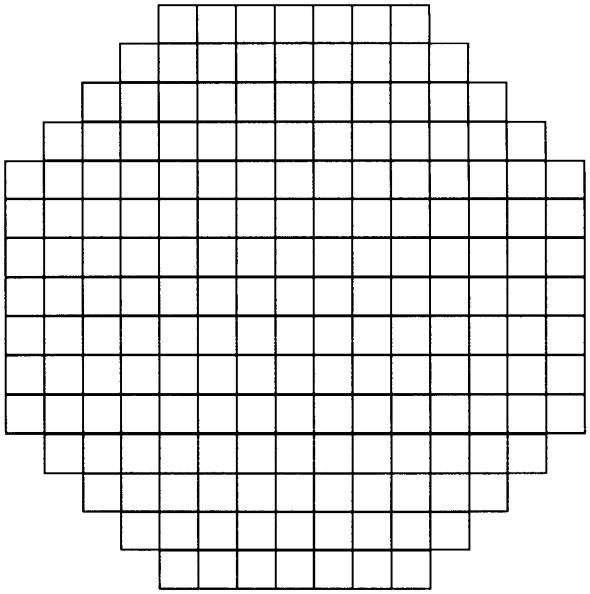

34.20 GWD/MTU
Core Flow = 88%
All Rods Withdrawn

[N] **N** = Number of 3 inch increments that the control blade is withdrawn from fully inserted

6X10-3Y